ADVENTURES IN HIGH ENERGY THEORY AND PHENOMENOLOGY

A Dissertation

Presented to the Faculty of the Graduate School

of Cornell University

in Partial Fulfillment of the Requirements for the Degree of

Doctor of Philosophy

by

Dean Jonathan Robinson

May 2013

ADVENTURES IN HIGH ENERGY THEORY AND PHENOMENOLOGY

Dean Jonathan Robinson, Ph.D.

Cornell University 2013

Various studies of high energy theory and phenomenology are presented.

We first present a mechanism that naturally produces light Dirac neutrinos. The central idea is that the right-handed neutrinos are composite. Any realistic composite model must involve 'hidden flavor' chiral symmetries. In general some of these symmetries may survive confinement, and in particular, if a U(1) survives it must imply an exact $B - L$ symmetry at low energies. Dirac neutrinos are therefore produced, which are naturally light due to compositeness.

In general, elementary keV sterile Dirac neutrinos can be a natural ingredient of this composite neutrino scenario. For a certain class of composite neutrino theories, these sterile neutrinos naturally have the appropriate mixing angles to be resonantly produced warm dark matter (WDM). Alternatively, we show these sterile neutrinos can be WDM produced by an entropy-diluted thermal freeze-out, with the necessary entropy production arising not from an out-of-equilibrium decay, but rather from the confinement of the composite neutrino sector, provided there is sufficient supercooling.

We next present a formalism for the flavor oscillation of unstable particles that relies only upon the analytic structure of the time Fourier-transformed two-point function. We derive exact oscillation probability and integrated oscillation probability formulae, and verify that our results reproduce the known results for both neutrino and neutral meson oscillation in the expected regimes of parameter space. The generality of our approach permits us to investigate flavor oscillation

in exotic parameter regimes, and present the corresponding oscillation formulae.

Kinematic edges in cascade decays provide a probe of the masses of new particles. In some new physics scenarios the decay chain involves intermediate particles of different flavors that can mix and oscillate. We discuss the implication of such oscillation, and in particular its interplay with the non-zero widths of the particles. We derive explicit formulae for differential decay rates involving both non-zero widths and oscillation, and show that in the case where the mass difference between the intermediate particles is of the order of their widths, both oscillation and width effects are important. An examination of the physical observables contained in these differential decay rates is also provided. We calculate differential decay rates for cases in which the intermediate particles are either scalars or fermions.

Finally, we present flavor SU(3) sum rules for $D \to PP$ and $D \to PV$ decay amplitudes, that are valid to second order in symmetry breaking by the strange quark mass spurion. Decay rate sum rules are also computed to this order. Particular attention is given to sum rules arising from the isospin and U-spin subgroups, the former providing sensitive tests for alternative sources of SU(3) breaking. We apply the latter together with the postulated $\Delta U = 0$ rule for the large penguin picture to predict the ratio and difference of the direct CP asymmetries for $D \to KK^*$ and $D \to \pi\rho$.

BIOGRAPHICAL SKETCH

Dean J. Robinson is a native of Sydney, Australia. Educated at the Sydney Grammar School, Dean completed his undergraduate studies at the University of New South Wales (UNSW), Sydney, majoring in both physics and pure mathematics. He graduated from UNSW in 2006 with first class honours and the university medal in physics.

Dean began his graduate studies at Cornell in the Fall of 2007, first working with Prof. André LeClair on formal aspects of quantum field theory, before joining the research group of Prof. Yuval Grossman in 2009. There he worked with Yuval and various talented collaborators in a broad area of high energy theory and phenomenology. After receiving his degree, he will join the Department of Physics at UC Berkeley as a postdoctoral associate.

Dean has been married to his wife, Lauren, since 2009.

For Lauren, and Allan and Elizabeth

ACKNOWLEDGEMENTS

I thank my parents, Allan and Elizabeth, for their ever-present and innumerable support in all that I've done and chosen to do, and I thank them together with my siblings, Jocelyn and Stuart, and all my nephews and nieces, for letting me live so far away from home. Thank you also to Sarah and Bob for being ever-supportive parents-in-law.

I owe a great debt of gratitude to my adviser, Yuval Grossman, for not only continually teaching me new ways to think about the physics of Nature, and teaching me a lot of physics too, but also for showing me how to be an effective physicist. Thank you, Yuval, for all the guidance, advice and opportunities. I also thank André LeClair for the opportunity to work on several projects together, which were invariably enjoyable and educational, and Lawrence Gibbons for providing a valuable and genial experimental presence on my thesis committee.

I wish to thank Fady Bishara, Roni Harnik, Eliot Kapit, Mario Martone, Jing Shu, Yuhsin Tsai, and Jure Zupan for being wonderful collaborators. I also thank Nima Arkani-Hamed, Kfir Blum, Josh Berger, David Curtin, Iftah Galon, Roni Harnik, Ben Heidenreich, Maxim Perelstein, Yael Shadmi, Bibhushan Shakya, João P. Silva, Philip Tanedo, Yuhsin Tsai, Tomer Volansky and Jure Zupan for various and multiple helpful discussions concerning the research presented herein. I am very grateful to Andrew Hanes and Michael Bishop, and to both my undergraduate honours advisers Gary Morriss and Michael Kuchiev for helping me on my way towards a doctorate in physics and beyond. A very special thanks to Nima Arkani-Hamed and Kfir Blum for generously arranging and providing me a space to work at the Institute for Advanced Study, and always being available to discuss my work and theirs. The works contained in this thesis are supported by the U.S. National Science Foundation and by the United States-Israel Binational Science

Foundation.

The LEPP theory group at Cornell is a superb, warm and stimulating place to conduct research and to learn. Thank you to all the LEPP theory faculty, postdocs and grad students for making it so! Thank you especially to my fellow grad students, Johannes, Mathieu, Ben, Jack, Nick, Thomas, Sohang, Itay, Yang, Dan, Gang, Mike, Mike, John, David, Mario, Riccardo, and Bibhushan, and in particular the (re)founding members of the Beyond SM journal club, Josh, David, Flip and Yuhsin, for creating a wonderfully collegial peer-learning environment.

Finally, to my lovely wife Lauren, thank you for putting up with a husband in grad school with such patience and support, and for readily agreeing to all the sacrifices it entailed. There's no one better to share an adventure with than you.

TABLE OF CONTENTS

LIST OF TABLES

LIST OF FIGURES

CHAPTER 1

INTRODUCTION

1.1 Overview

The Standard Model (SM) of particle physics, first outlined in the 1970s, has for the most part withstood more than four decades of precision experiments. However, even though the SM was never intended to be a holistic description of Nature, there is substantial evidence that the SM is an incomplete description of the physics of elementary particles and fields.

This evidence takes the form of open theoretical problems and unexpected experimental observations, some of which are very well-known, and others which are more obscure; some of which are motivated by contrast with empirical observations, and others by our theoretical aesthetic preferences. A very incomplete list of these includes, in no particular order: the large hierarchy between the Planck, electroweak and cosmological vacuum scales – respectively the hierarchy problem and the cosmological constant problem; the stability of mass of the recently observed scalar [1, 2] – a candidate Higgs boson – under quantum corrections, and the mechanism of electroweak symmetry breaking; the horizon problem; the physical realization, if any, of supersymmetry; the nature of dark matter; the origin of the light neutrino masses, implied by their flavor oscillations; the mechanism of baryogenesis and leptogenesis; the hierarchy of the SM fermion masses and the structure of the Cabibbo-Kobayashi-Maskawa (CKM) matrix – the flavor puzzle; the large muon magnetic moment; and the strong CP problem.

The research studies presented in this thesis are all motivated by consideration

of one or more of these open problems. In the following, we present a brief overview and the theoretical context for each study.

1.2 Composite Neutrinos and Warm Dark Matter

The resolution of the solar neutrino problem – the observation of active neutrino oscillations – has provided strong evidence that the active neutrinos have masses at scales $\sim 10^{-12}$ below the electroweak scale ($\sim 10^2$ GeV). At present it is unknown whether the neutrinos are Majorana or Dirac in structure, and the mechanism which is responsible for these light masses is unclear. The most popular mechanism is the well-known seesaw mechanism, and its variants, but these are far from unique. In particular, it has long been known that confining theories can incorporate a natural dynamical mechanism for producing fermion mass hierarchies. Very briefly, beginning with a gauge and chiral flavor group, this dynamical framework constructs a cascade of chiral symmetry breaking, called tumbling, over a series of scales, Λ_i. At each Λ_i scale, a condensate breaks the chiral flavor symmetry to a subgroup, creating massive fermions with masses $\sim \Lambda_i$, and leaving a massless remainder that may gain masses at a yet lower scale. The end result is a hierarchy of massive fermions, whose multiplicity and flavor structure is well-defined by the pattern of chiral symmetry breaking. If some chiral symmetry survives the confinement, then there are necessarily massless composite states in the final spectrum.

This mechanism has been used in Extended Technicolor (ETC) theories to generate the quark and lepton masses at loop-level – they cannot be generated at tree level in such theories, since there is no elementary scalar. The conceit is

that the quarks and leptons are elementary degrees of freedom necessary to cancel the electroweak anomalies, but interact with the confining sector only through irrelevant interactions. It is worth mentioning that it is extremely difficult to reconcile ETC theories with both precision flavor constraints and the SM fermion mass spectrum [3]. For example, to name but a few constraints, generic ETC predicts contributions to flavor-changing neutral currents, $\mu \to e\gamma$, or the $K_{L,S}$ mass splitting. Precision electroweak contraints on these processes then imply a lower bound $\Lambda_{\rm ETC} > 10^4$ TeV (not to mention the proton decay bound, generically now $\sim 10^{15}$ TeV), which renders the SM fermions far too light. As a consequence technicolor theories are mostly considered to be ruled out as the mechanism of electroweak symmetry breaking. However, unlike for the quarks, light neutrinos are desirable, so one may ask: Can we use this tumbling structure to generate the light neutrino masses?

In Chapters 2 and 3 we present two studies, which expropriate this dynamical framework into the leptonic sector of the SM. The central idea, first proposed in Ref. [4], is that the right-handed neutrino is a composite formed in a hidden confining sector, and this compositeness is responsible for the light neutrino masses. In Chapter 2 we explore the general structure of the preonic theories that may generate composite right-handed neutrinos and some of their phenomenology. Particularly interesting are theories in which some of the 'hidden flavor' chiral symmetries survive confinement. In particular, if a U(1) flavor symmery survives it must imply an exact $B - L$ symmetry, such that naturally light Dirac neutrinos are therefore produced.

Similar to the generation of quark masses in ETC, elementary sterile neutrino states with loop generated masses may be necessarily present in some composite

neutrino theories. Whenever a sterile state is featured in a theory, it is usually of interest to determine its cosmological history, in particular whether it can be (a component of) dark matter. Not only must a dark matter candidate be long-lived and produced with the correct relic abundance – approximately 26% of the critical energy density [5] – but it also must satisfy several other constraints. These include: the Lyman-α bounds – i.e. the scale of the structure formation – which place an upper bound on the DM free-streaming length, and hence its temperature; Big-Bang Nucleosynthesis (BBN) bounds, which constrain the temperature of the DM during the BBN epoch; x-ray flux bounds, arising from observations of dwarf galaxies that are thought to be mostly DM, which constrain the DM coupling to photons; and for fermions, the Tremaine-Gunn bound, arising from the density of the same dwarf galaxies, which constrain the DM mass. DM theories that also account for baryo- or leptogenesis are further preferred.

The standard cosmology at present includes cold dark matter (CDM), in the form of weakly interacting massive particles (WIMPs). Together with dark energy, this is called the Λ-CDM model. These WIMPs feature free-streaming lengths well below that of dwarf galaxies, and as is well-known, WIMPs that interact at the electroweak scale happen to have the correct DM relic abundance: the WIMP 'miracle'. In the last decade, a competing DM candidate has emerged in the form of a keV sterile neutrino, among others. With appropriate active-sterile mixing angles, these sterile neutrinos can be warm dark matter (WDM). That is, a DM candidate warmer than CDM, with a free-streaming length no greater than the typical dwarf galaxy scale. In Chapter 3 we show that for a certain class of composite neutrino theories, the sterile neutrinos with loop generated masses naturally have the appropriate active-sterile mixing angles and masses to be resonantly produced keV-scale WDM. Particularly interesting is the observation that the simplest such

theory requires a confinement scale near to the electroweak scale, and a interaction scale at 10^4 TeV, conveniently evading the current flavor bounds. In a novel alternate approach, we also show these sterile neutrinos can be WDM produced by an entropy-diluted thermal freeze-out, with the necessary entropy production arising not from an out-of-equilibrium decay, but rather from the confinement of the composite neutrino sector, provided there is sufficient supercooling.

1.3 Oscillation and Collider Kinematic Edges

The formalism of flavor oscillation has a long history. Flavor oscillation is in essence just an interference effect between propagation amplitudes, and as a result there are many competing formalisms of flavor oscillation, that can be constructed from slightly different axiomatic assumptions. For example, the plane wave formalism simply constructs the oscillation as interference between time-evolved stationary states, but the price is an ambiguity of the reference frame in which the evolution time is defined, since different plane waves travel at different speeds.

In Chapter 4 we present a purely field-theoretic formalism for the flavor oscillation of (un)stable particles. We show that, provided there are no decoherence effects, the exact flavor oscillation probabilities depend only upon the simple poles of the exact time Fourier-transformed two-point function, as defined in a laboratory frame. These poles – and thus the oscillation formulae themselves – are fully defined by just the physical masses, m_j, and decay rates, Γ_j, of the propagating degrees of freedom, which are physical observables. The advantage of this approach is that there is no ambiguity of reference frame, and the general results are applicable to both stable (e.g. neutrino) and unstable (e.g. neutral meson)

degrees of freedom. Moreover, particle-like propagation becomes just one limiting behavior of the correlation functions in the limit $m_j \gg \Gamma_j$. That is, the generality of our approach permits us to extend our results into exotic parameter regimes – for example the manifestly non-particle-like regime $m_j \ll \Gamma_j$ – and present the corresponding oscillation formulae.

The oscillation of unstable particles may play an important role in current experimental searches for new degrees of freedom, for example the supersymmetry searches at the Large Hadron Collider (LHC). It is expected that new physics (NP) degrees of freedom may be detectable through cascade decays to SM particles. This is a sequence of decays, e.g. $A \to XB \to XYC$, in which A, B and C are NP, and X, Y are SM. It has long been known that the distribution of the invariant mass $(p_X + p_Y)^2$ features a sharp cut-off called a kinematic edge, or endpoint. Measurement of this endpoint permits us to constrain the NP masses in the chain, because it is a function of only the NP masses themselves.

It is natural to expect that the sharpness of this edge depends on the width of the intermediate state B, and if multiple B intermediate states are possible, we expect an edge corresponding to each one. However, even more interesting is to consider NP scenarios for which the intermediate B particles not only exist in multiple flavors but can mix and oscillate. In this case the question becomes: How are the edges smeared, and under what conditions can the different edges be resolved?

In Chapter 5 we discuss the consequences of such oscillation, and in particular its interplay with the non-zero widths of the particles. We derive explicit formulae for differential decay rates involving both non-zero widths and oscillation for both scalar and fermionic intermediate particles, and an examination of the physical

observables contained in these differential decay rates is presented. For example, we show how the masses and widths of NP particles could be extracted from the shape, smearing and heights of the kinematic edges. Furthermore we develop an edge resolution criterion, and show that in the case where the mass difference between the intermediate particles, Δm, is less than their average widths, $\bar{\Gamma}$, multiple edges cannot be resolved. Even more interesting, if the splitting of the geometric and arithmetic means of the intermediate masses is of the order of the mass splitting itself, the resolution criterion requires $\Delta m \gg \bar{\Gamma}$. This implies that the kinematic edge method cannot distinguish multiple intermediate NP degrees of freedom in this narrow region of parameter space.

1.4 Sum Rules in Charm Decays

The experimental verification of the unitarity of the CKM matrix [3] is one of the triumphs of the Standard Model. Nonetheless, precision tests of flavor physics provide a rich ground for the detection of new physics phenomena. In general, the precision flavor results imply that NP effects may only arise at loop-level. The most sensitive NP tests therefore probe the rare – i.e. loop level – SM processes that can be significantly enhanced by NP contributions. For example, tests of flavor-changing neutral currents, such as $B \to \mu\mu$, or GIM suppressed processes like $b \to s\gamma$, have received much attention. In a similar vein, direct CP violation arising from the decay of neutral mesons is also studied. Where anomalous results are found, our inability to precisely compute QCD amplitudes below the QCD confinement scale often makes us uncertain whether these anomalous results arise from the SM or from NP effects.

Over the last decade, larger than expected direct CP violation was detected in the non-leptonic charm decays $D^0 \to K^+K^-$ and $D^0 \to \pi^+\pi^-$. The difference of the direct CP violation between these two modes happens to be a useful observable. It has been reported by Belle, BaBar, CDF and LHCb to be ~ 2.5 standard deviations from zero, and approximately ten times larger than expected by comparison with the B system or naïve estimation.[1] This result was initially thought to be a clear signal of NP. However, further consideration suggested the anomaly may instead arise from non-perturbative enhancement of particular penguin amplitudes: The D meson decay amplitudes furnish representations of the approximate flavor SU(3) symmetry, whose SM sources of breaking are well-understood; It has been shown that the approximate flavor SU(3) symmetry admits a pattern of enhanced penguins consistent with the data to first order in SU(3) breaking. One notable phenomenological scheme for penguin enhancement is the $\Delta U = 0$ rule – the U is U-spin, an SU(2) flavor subgroup – which is broadly analogous to the established $\Delta I = 1/2$ isospin rule in kaon physics.

If the D^0 direct CP anomaly is due to SM effects – that is, if there are no NP effects – then the D meson decay modes must also satisfy SU(3) sum rules. These are group theoretic relations among amplitudes that can be computed to arbitrary order in symmetry breaking, provided the sources of breaking are known. Sum rules are particularly valuable relations, because they permit us to test the known SM pattern of flavor SU(3) symmetry breaking independently of our ability to compute QCD amplitudes. Not only are such tests necessary conditions for enhancement schemes like the $\Delta U = 0$ rule, but they may also be probes of NP in their own right, because they are necessary conditions of the SM pattern of SU(3) breaking itself.

[1] Recent LHCb results [6] have significantly reduced this deviation from zero. At present it is unclear whether the anomaly has been ameliorated.

In Chapter 6, we present flavor SU(3) sum rules for $D \to PP$ and $D \to PV$ decay amplitudes – P (V) denotes a pseudoscalar (vector) meson – that are valid to second order in symmetry breaking by the strange quark mass spurion. This spurion is the dominant source of SU(3) breaking in the SM, and sum rules valid to second order in SU(3) breaking by this spurion are expected to hold at the $\sim 4\%$ level. We also compute decay rate sum rules to this order, which have the advantage being independent from strong phases, and therefore easier to measure. We pay particular attention to sum rules arising from the isospin and U-spin subgroups. The former provide sensitive tests for alternative sources of SU(3) breaking, which is a possible NP signal. The latter permit us to predict the unmeasured $D^0 \to \rho^- K^+$ branching fraction, and within the $\Delta U = 0$ rule framework, the ratio and difference of the direct CP asymmetries for $D \to KK^*$ and $D \to \pi\rho$.

CHAPTER 2

COMPOSITE DIRAC NEUTRINOS

Based on the 2010 article "Composite Dirac Neutrinos", written in collaboration with Yuval Grossman and published in JHEP 01 (2011) 132.

2.1 Introduction

The possibility that various fields of the Standard Model (SM) are composite has been considered in depth (see e.g. Refs [3, 7, 8]). Apart from potentially resolving the hierarchy problem, one of the key features of composite theories is that they usually include a natural mechanism to produce large fermion mass hierarchies. Put simply, the bound-states, which form the degrees of freedom of the effective low-energy theory, may acquire masses over a large range of scales via a 'tumbling' pattern of confinement-induced spontaneous chiral symmetry breaking [9, 10, 11].

Compositeness can therefore explain the very small scale of the neutrino masses. One particularly simple scenario was proposed in Ref. [4] and discussed in Refs. [12, 13]. The idea is to assume that the right-handed neutrinos are massless chiral bound states produced via the confinement of a hidden sector at a scale Λ. These states acquire very small masses via interactions with the SM at a much higher scale, $M \gg \Lambda$. The scale M may be the confinement scale of a yet more fundamental theory that condenses into the SM and hidden sectors. After Higgs-induced electroweak spontaneous symmetry breaking, the neutrino masses arise via irrelevant operators that are suppressed by powers of Λ/M, and hence the neutrino masses are very light. In general one finds that both light Dirac and Majorana mass terms can be produced for the neutrinos in this manner.

A more popular mechanism used to produce light neutrino masses is the see-saw mechanism, which requires the existence of heavy, sterile Majorana neutrinos and produces light Majorana masses for the neutrinos. As an alternative, it is interesting to consider whether one can find a theory that naturally produces light *Dirac* neutrinos instead. Apart from compositeness, there are several known mechanisms which can produce Dirac mass terms for the neutrinos. For example, light Dirac

masses can be produced via schemes involving supersymmetry breaking [14, 15, 16], supergravity [17], extra dimensions [18, 19, 20, 21, 22], discrete gauge symmetries [23, 24], extra U(1) symmetries [25, 26], or unparticles with large anomalous dimensions [27]. In some of these cases Dirac neutrinos naturally arise, whereas in others, Dirac neutrinos are obtained by an *ad hoc* imposition of lepton number.

In this chapter, we explore the above mentioned compositeness scenario further by considering the role of the symmetries of the hidden sector, which naturally arise from the pattern of confinement-induced spontaneous symmetry breaking of the preonic theory. Previous analyses have not taken into account the fact that if one assumes that the right-handed neutrinos are the chiral bound states in a confined hidden sector, then the right-handed neutrinos must be non-trivially charged under some chiral 'hidden flavor' symmetry. These extra hidden flavor symmetries must feature in the structure of the neutrino mass terms. In particular, we show that there exists a mechanism based on this hidden flavor symmetry that naturally produces Dirac neutrinos. This mechanism arises in the following case: the hidden flavor symmetry is a U(1) symmetry; the chiral bound states – the right-handed neutrinos – all have the same hidden flavor charge; the SM Higgs, ϕ, is charged under this hidden flavor symmetry such that the right-handed neutrinos may couple to the left-handed SM; and ϕ is the only scalar in the low-energy theory with a non-trivial vacuum expectation value (vev). The main result is that the U(1) axial combination of the SM hypercharge and hidden flavor symmetries, which is unbroken by $\langle\phi\rangle$, plays the role of lepton number, guaranteeing that there are no Majorana masses. In other words, instead of lepton number being either an accidental symmetry or imposed *ad hoc*, the hidden flavor symmetry – necessarily arising in our compositeness scenario from the chirality of the right-handed neutrinos – ensures that only Dirac neutrinos are produced.

The paper is organized as follows. In Sec. 2.2, we first review the general mechanism through which composite right-handed neutrinos may naturally produce light neutrino masses. In Sec. 2.3 we present a simple extension of the SM with composite, chiral right-handed neutrinos and a U(1) hidden flavor symmetry. Intriguingly, we show that once the right-handed SM fields are also assigned an extra hidden flavor charge, then the theory is non-anomalous. Moreover, after spontaneous symmetry breaking, the unbroken axial symmetry for this theory is isomorphic to $B - L$. The theory therefore produces the usual SM Dirac fermions, along with Dirac neutrinos that have heavily suppressed masses. Finally, in Sec. 2.4 we examine the phenomenology of our low energy theory. The general structure of the neutrino mass spectrum and the PMNS leptonic mixing matrix is presented. We also discuss non-unitarity effects and possible dark matter candidates among the heavier sterile neutrinos.

2.2 Compositeness and Chiral Symmetry

2.2.1 General dynamical framework

We first provide a brief review of the underlying features and assumptions inherent to composite neutrino models. More details can be found, for example, in Ref. [28, 29, 7, 8].

In the study of composite theories, one generally posits the existence of an ultraviolet theory of chiral fermions, called preons, which has a chiral gauge $\otimes$ flavor symmetry. This theory undergoes confinement to produce a low-energy effective theory whose degrees of freedom are bosonic and fermionic bound states.

These bound states are singlets of the original gauge group, but may have non-trivial flavor symmetries.

The formation of such singlets is just a mathematical exercise that is subject to the 't Hooft anomaly matching conditions [28, 29]. The main difficulty in composite theories is to determine the dynamics of confinement, which in turn determines the physical bound states, the symmetries of the effective theory, and the scales at which confinement occurs. For example, confinement could occur at just one scale. Alternatively one could conceive of a preonic theory which first condenses into an effective theory with weak, asymptotically-free effective couplings, so that at some lower scale it further condenses into a yet lower energy effective theory. At each scale, scalar condensates could induce spontaneous symmetry breaking, so that the final unbroken symmetries and physical degrees of freedom for these two cases may be different.

One approach determines this dynamical information via the complementarity principle. In brief, the complementarity principle is the idea that the pattern of confinement-induced symmetry breaking and the chiral bound states can be determined from a dynamical symmetry breaking scheme for the preonic theory in the absence of confinement. An exposition of this principle and other necessary assumptions can be found elsewhere (see e.g. Refs [9, 10, 11]). For our purposes it is sufficient to note the following:

(i) Confinement may occur in stages at successively lower energy scales. At each scale, bound states with non-trivial gauge and flavor charges may be produced, and there may exist a scalar condensate with a non-trivial vacuum expectation value, which leads to spontaneous symmetry breaking of the chiral symmetry. The original gauge $\otimes$ flavor symmetries are thus said to

'tumble' down through these stages to a final unbroken subgroup. Tumbling and confinement ceases when one ends up with a low-energy effective field theory for which the chiral bound states are all confining gauge singlets.

(ii) The original chiral symmetry may or may not be completely spontaneously broken by confinement. At any stage of confinement, if the chiral symmetry is not completely broken, then the 't Hooft anomaly matching constraints imply that there must be chiral, massless bound states in the effective theory produced below the corresponding confinement scale.

(iii) At a confinement scale Λ, fermionic bound states furnishing real representations may acquire either Majorana or Dirac masses, with masses typically at the confinement scale.

(iv) However, if these fermionic bound states are gauge singlets and interact with scalar condensates only via the heavy gauge bosons or scalars produced at some higher scale $\Lambda' \gg \Lambda$, then their mass will be generated at loop level, and will be suppressed by at least a factor $(\Lambda/\Lambda')^2$. This is the so-called secondary mass generation mechanism [9, 7], which is the similar to the mechanism by which the fermions acquire masses in extended technicolor theories.

2.2.2 Generation of light masses

This section recapitulates the ideas of Ref. [4]. The general approach of composite neutrino models is to suppose that the right-handed neutrinos are the chiral bound states of a hidden sector, which condenses at scale Λ but couples to the SM via some higher scale $M \gg \Lambda$. The idea is that the compositeness of the right-handed neutrinos suppresses their effective Yukawa coupling to the SM by powers of Λ/M.

Let us suppose that there exists a preonic theory which undergoes confinement at a scale M, such that the gauge $\otimes$ flavor symmetry groups of the theory spontaneously break down to a subgroup $G_{\rm c} \otimes G_{\rm F} \otimes G_{\rm SM}$, where $G_{\rm c}$ ($G_{\rm F}$) is a confining gauge (flavor) symmetry and $G_{\rm SM}$ is the usual $\mathrm{SU}(3)_c \otimes \mathrm{SU}(2)_L \otimes \mathrm{U}(1)_Y$ symmetry of the Standard Model. For the sake of clarity later on, we will henceforth call the degrees of freedom of the original preonic theory *UV preons*.

Let us suppose that below the confinement scale M we have an effective theory with: (1) the usual left-handed leptonic SM fields, L_L, which are $G_{\rm c} \otimes G_{\rm F}$ singlets; (2) chiral bound states q, which are SM singlets but furnish non-trivial $G_{\rm c} \otimes G_{\rm F}$ representations; (3) a scalar condensate ϕ which is a $G_{\rm c}$ singlet, but has non-trivial $G_{\rm F}$ charges and otherwise has the charges of the SM Higgs. The chiral bound states q act as preons for the $G_{\rm c} \otimes G_{\rm F}$ theory, so henceforth we refer to them as *effective preons*. As they are SM singlets, we say that the effective preons q comprise a hidden sector. It follows from this hypothesis that the SM and hidden sectors may only interact via the exchange of heavy messengers at scale M.

Now let us suppose that there exists a combination of n effective preons, crudely denoted by q^n, that contains a right-handed spin-1/2 Lorentz representation, and has precisely the correct flavor charges such that $\phi^* q^n$ is a $G_{\rm F}$ singlet. Note that since q^n is spin-1/2, then n is odd and $n \geq 3$. Integrating out heavy degrees of freedom, we have an effective irrelevant vertex

$$\mathcal{L}_{\rm yuk} = \frac{\lambda}{M^{3(n-1)/2}} \bar{L}_L \tilde{\phi} q^n \ , \tag{2.1}$$

where λ is an $\mathcal{O}(1)$ number and as usual $\tilde{\phi}_a = \epsilon_{ab} \phi^{b*}$ with respect to $\mathrm{SU}(2)_L$ indices. Well below confinement scale M, the hidden sector suffers further confinement, possibly over multiple scales

$$M \gg \ldots \gg \Lambda_i \gg \ldots \gg \Lambda \ , \tag{2.2}$$

such that confinement ceases below the Λ scale. For the sake of simplicity, hereafter we assume that the hidden sector suffers confinement as just one scale Λ. Therefore, at scale Λ, q^n condenses into a right-handed spin-1/2 bound state N_R

$$q^n \to N_R \Lambda^{3(n-1)/2}, \tag{2.3}$$

and we end up with low-energy effective Yukawa

$$\mathcal{L}_{\rm yuk} = \lambda \left(\frac{\Lambda}{M}\right)^{\frac{3(n-1)}{2}} \bar{L}_L \tilde{\phi} N_R \ , \tag{2.4}$$

where λ is some redefined $\mathcal{O}(1)$ coupling. As advertised, the compositeness of N_R has suppressed the Yukawa coupling in Eq. (2.4) by powers of

$$\epsilon \equiv \frac{\Lambda}{M} \ll 1 \ . \tag{2.5}$$

After ϕ acquires a non-trivial vev, then neutrino masses are produced from Eq. (2.4). Since $n \geq 3$, such masses will be at most of the order $\langle\phi\rangle\epsilon^3$. For sufficiently small ϵ, the neutrino Dirac masses will be suppressed compared to those of the charged leptons. Note also that the larger the number of effective preons in N_R, the greater the suppression.

The Yukawa term in Eq. (2.4) is not the only possible mass generating term. As yet there is no symmetry which prevents the formation of Majorana mass terms from higher dimensional operators. As an example, the operator

$$\frac{1}{M}(L_L \tilde{\phi})^T \sigma^2 L_L \tilde{\phi} \ , \tag{2.6}$$

produces a Majorana mass for the left-handed neutrinos. In summary so far, in this class of composite neutrino models, one finds both light Dirac and Majorana mass terms.

2.2.3 Renormalization Effects

In our discussion so far we have omitted possible effects due to renormalization group (RG) running. For example, Eq. (2.4) involves vevs evaluated at the two different scales: The first is due to the condensation of the UV preons that breaks the UV preonic theory down to $G_{\rm c} \otimes G_{\rm F} \otimes G_{\rm SM}$ at scale M; the second arises from the condensation of the effective preons in the hidden sector at scale Λ. To be consistent in choice of renormalization scale, it is therefore necessary to run the operator (2.1) from scale M down to scale Λ, so we should expect that RG effects will modify Eq. (2.4). However, the tumbling scenario outlined in Sec. 2.2.1 implictly assumes that the effective theory between scales M and Λ, of which (2.1) is an operator, is asymptotically free. As a result, we expect RG effects to introduce power-logarithmic corrections to Eq. (2.4).

An alternative is to consider the possibility that the effective theory of effective preons q is approximately conformal and strongly coupled between scales M and Λ. In this case we can contemplate large, constant anomalous dimensions for operators such as (2.1) or for the loop-generated masses produced by the secondary mass generation mechanism. This is similar to the well-known walking technicolor scenario (see e.g. Ref. [30] for a review). However, this strong, conformal scenario is inconsistent with the tumbling scenario, because the confinement scale of the effective preons becomes badly defined if they have strong, approximately conformal dynamics above Λ. (We note that the idea of conformal right handed neutrinos that couple to the SM through irrelevant operators has been recently considered in Ref. [27].)

We expect the power-logarithmic RG effects in the asymptotically free, tumbling scenario will lead to $\mathcal{O}(1)$ or smaller corrections to Eq. (2.4), depending on

the details of the effective preonic theory in the hidden sector. In this chapter, we seek to describe only the model-independent effects of the hidden sector on mass and coupling scales (up to assumptions about its symmetry breaking pattern), so these corrections can be absorbed into the parameter λ, which we assumed was just an $\mathcal{O}(1)$ number. In other words, while RG effects could lead to important corrections in a specific model, they do not change the scale of the Yukawa coupling to the right-handed neutrinos, and we therefore need not consider RG effects henceforth in this chapter.

2.2.4 Role of chiral symmetry

The confinement down to the scale Λ generally results in the spontaneous symmetry breaking of $G_{\rm c} \otimes G_{\rm F} \to G'_{\rm c} \otimes G'_{\rm F}$. Since we assumed that confinement stops below Λ, it must be that any chiral bound states are $G'_{\rm c}$ singlets, but furnish complex $G'_{\rm F}$ representations.

Crucial to the above analysis leading to Eq. (2.4) is the implicit assumption that the N_R are a subset of these chiral bound states. If this was not the case, then they would acquire Dirac or Majorana mass terms at scale Λ or higher. Hence, if the N_R are to be chiral, then some chiral flavor symmetry $G'_{\rm F}$ must survive confinement. Henceforth we call $G'_{\rm F}$ the hidden flavor symmetry. Note that the 't Hooft anomaly matching conditions require that the $G'_{\rm F}$ anomalies of the chiral bound states match those of the original UV preons.

This chiral hidden flavor symmetry has two important consequences. First, as in the 't Hooft formalism, the chiral symmetry ensures that there must be elementary spectator fermions, whose $G'_{\rm F}$ anomalies cancel those of the chiral bound

Field	$\mathrm{SU}(2)_L$	$\mathrm{U}(1)_Y$	$\mathrm{U}(1)_\mathrm{F}$	$\mathrm{U}(1)_a$
ϕ	$\square$	$\frac{1}{2}$	γ	0
L_L	$\square$	$-\frac{1}{2}$	0	$-\gamma/2$
N_R	$\mathbf{1}$	0	γ	$-\gamma/2$

Table 2.1: SM, hidden flavor, and axial representations of the $\mathrm{U}(1)_\mathrm{F}$ model of section 2.2.5.

states. The second consequence is that the scalar ϕ must also have hidden flavor charges: since $\phi^* N_R$ is a G'_F singlet, and since N_R transforms under a complex representation of G'_F, then it follows that ϕ transforms non-trivially under G'_F too.

2.2.5 Dirac neutrinos

Let us now present a toy model that produces light Dirac neutrinos. The main idea is that inclusion of the chiral hidden flavor symmetry together with some special choices will result in an unbroken lepton number.

Suppose G'_F is just a U(1) symmetry

$$G'_\mathrm{F} \equiv \mathrm{U}(1)_\mathrm{F} \ , \tag{2.7}$$

so that N_R and ϕ both have the same non-zero $\mathrm{U}(1)_\mathrm{F}$ charge, which we denote hereafter by γ. We then have $\mathrm{SU}(2)_L \otimes \mathrm{U}(1)_Y \otimes \mathrm{U}(1)_\mathrm{F}$ group structure as shown in Table 2.1. Now, observe that ϕ is uncharged under the U(1) axial combination of the $\mathrm{U}(1)_Y$ and $\mathrm{U}(1)_\mathrm{F}$, which has charge $a \equiv \gamma Y - F/2$ and is denoted by $\mathrm{U}(1)_a$. (Here and henceforth Y (F) denotes the $\mathrm{U}(1)_Y$ ($\mathrm{U}(1)_\mathrm{F}$) charge of the field in question.) The axial symmetry $\mathrm{U}(1)_a$ is therefore unbroken by $\langle\phi\rangle$, and so it remains a symmetry of the spontaneously broken theory. Moreover both L_L and N_R have axial charge $a = -\gamma/2$. Hence for the field content of Table

2.1, global $\mathrm{U}(1)_a$ is isomorphic to lepton number. It immediately follows if ϕ is the only scalar which gets a vev, then Majorana masses cannot be produced by spontaneous symmetry breaking: only Dirac masses are produced, and these are light due to compositeness, as in Eq. (2.4). Note that there may be other higher dimensional operators apart from the Yukawa term in Eq. (2.4) that also produce contributions to the Dirac masses. However, these contributions will be further suppressed by powers of $\langle\phi\rangle/M$ and ϵ.

2.3 A U(1) hidden flavor model

2.3.1 Field Content

We now seek to exploit the above result to produce a realistic extension of the SM with light Dirac neutrinos. Following from the above, we choose $G'_{\mathrm{F}} \equiv \mathrm{U}(1)_{\mathrm{F}}$. This choice has the added advantage that ϕ has the same number of field degrees of freedom as the SM Higgs. Let us now suppose the effective preonic $G_{\mathrm{c}} \otimes G_{\mathrm{F}}$ theory can be chosen such that there are exactly three chiral right-handed bound states, N_R^i, all with the same $\mathrm{U}(1)_{\mathrm{F}}$ charge, γ. Examples of such theories are presented in Appendix A.1.

We assume that ϕ has the same charges as in Table 2.1 and is the only scalar which acquires a vev. It follows from this assumption that in order for the usual SM mass structure to be produced, we must have Yukawa terms of the form

$$\mathcal{L}_{\mathrm{yuk}} = \bar{L}_L^i \phi E_R^j + \bar{L}_L^i \tilde{\phi} N_R^j + \bar{Q}_L^i \phi D_R^j + \bar{Q}_L^i \tilde{\phi} U_R^j + \mathrm{h.c.}\ , \tag{2.8}$$

where E_R, D_R, U_R and Q_L are the right-handed charged leptons, down and up quarks and left-handed quark doublets respectively. (We henceforth refer to E_R,

Field	$\mathrm{SU}(3)_c$	$\mathrm{SU}(2)_L$	$\mathrm{U}(1)_Y$	$\mathrm{U}(1)_\mathrm{F}$	$\mathrm{U}(1)_a$
ϕ	$\mathbf{1}$	$\square$	$\frac{1}{2}$	γ	0
L_L^i	$\mathbf{1}$	$\square$	$-\frac{1}{2}$	0	$-\frac{\gamma}{2}$
E_R^{*i}	$\mathbf{1}$	$\mathbf{1}$	1	γ	$\frac{\gamma}{2}$
N_R^{*I}	$\mathbf{1}$	$\mathbf{1}$	0	$-\gamma$	$\frac{\gamma}{2}$
N_L^α	$\mathbf{1}$	$\mathbf{1}$	0	γ	$-\frac{\gamma}{2}$
Q_L^i	$\square$	$\square$	$\frac{1}{6}$	0	$\frac{\gamma}{6}$
U_R^{*i}	$\overline{\square}$	$\mathbf{1}$	$-\frac{2}{3}$	$-\gamma$	$-\frac{\gamma}{6}$
D_R^{*i}	$\overline{\square}$	$\mathbf{1}$	$\frac{1}{3}$	γ	$-\frac{\gamma}{6}$

Table 2.2: Scalar and left-handed fermionic field content for the $U(1)$ hidden flavor model describes in section 2.3.1. As above, the axial charge $a = \gamma Y - F/2$. It is clear that $\mathrm{U}(1)_a \simeq \mathrm{U}(1)_{B-L}$.

U_R and D_R as the right-handed SM fields.) Assuming that the left-handed SM fields have no hidden flavor charges, then in order for such terms to exist the right-handed SM fields must also have $\mathrm{U}(1)_\mathrm{F}$ charges. The only possible hidden flavor charge assignments are shown in Table 2.2, along with the usual SM charges.

It is intriguing that the unbroken axial symmetry in this theory is isomorphic to $B - L$. Hence $B - L$ remains an unbroken symmetry in this theory, and only Dirac fermions are produced by the spontaneous symmetry breaking induced by $\langle\phi\rangle$. This is one of the main results of this chapter.

Before proceeding, several comments are in order. First, there may be an arbitrary number of right-handed bound states with the hidden flavor charge γ: we have denoted these as N_R^I. In line with the above supposition, a subset of three of these bound states, denoted by N_R^i, are chiral. The remainder, denoted N_R^α, must form massive Dirac fermions with left-handed bound states N_L^α, which must therefore have $\mathrm{U}(1)_\mathrm{F}$ charge γ. These Dirac neutrinos will typically have masses at the Λ confinement scale. (It is possible, however, that some of these

masses are suppressed via the secondary mass generation mechanism.) We have implicitly adopted here the following index notation, which we will continue to use throughout the remainder of this chapter: Upper case Roman indices denote all spin-1/2 bound states of a particular $\mathrm{U}(1)_{\mathrm{F}}$ charge; lower case Roman indices denote chiral bound states and leptonic flavor; lower case Greek indices denote massive spin-1/2 bound states.

Second, the $\mathrm{U}(1)_{\mathrm{F}}$ charges in Table 2.2 are clearly commensurate, which permits this U(1) to be embedded in a semi-simple Lie group. This must be the case, since $\mathrm{U}(1)_{\mathrm{F}}$ was generated by spontaneous symmetry breaking of a larger group.

Finally, note that in principle there may be various other SM sterile spin-1/2 bound states in the theory with hidden flavor charge $F \neq \pm\gamma$. By hypothesis none of these are chiral, so they must be heavy with masses generally at scale Λ. More significantly, these bound states necessarily have axial charge $a \neq \mp\gamma/2$, so that they cannot form Dirac mass terms with the neutrinos. We therefore neglect them henceforth.

2.3.2 Anomaly cancellation

A crucial issue is the cancellation of the anomalies. It is clear that there are no anomalies in the SM sector, but there may be non-trivial anomalies involving $\mathrm{U}(1)_{\mathrm{F}}$. Let us therefore examine all these anomalies. Clearly there is no $\mathrm{SU}(2)_{\mathrm{L}}^2\mathrm{U}(1)_{\mathrm{F}}$ anomaly since the left-handed SM is not charged under $\mathrm{U}(1)_{\mathrm{F}}$. Let N be the number of physical right-handed neutrinos, i.e. let $I = 1, \ldots, N$, so that

$\alpha = 4, \ldots, N$. Then we have anomalies

$$\begin{aligned}
&\mathcal{A}\big[\mathrm{U}(1)_{\mathrm{F}}^3\big] \propto \big[3 - N + (N-3) + 3 - 3\big]\gamma^3 = 0 \ , \\
&\mathcal{A}\big[\mathrm{gravity}^2\mathrm{U}(1)_{\mathrm{F}}\big] \propto \big[3 - N + (N-3) + 3 - 3\big]\gamma = 0 \ , \\
&\mathcal{A}\big[\mathrm{SU}(3)_c^2\mathrm{U}(1)_{\mathrm{F}}\big] \propto (3\gamma - 3\gamma) = 0 \ , \\
&\mathcal{A}\big[\mathrm{U}(1)_Y^2\mathrm{U}(1)_{\mathrm{F}}\big] \propto \gamma - 3\gamma\bigg(-\frac{2}{3}\bigg)^2 + 3\gamma\bigg(\frac{1}{3}\bigg)^2 = 0 \ , \\
&\mathcal{A}\big[\mathrm{U}(1)_Y\mathrm{U}(1)_{\mathrm{F}}^2\big] \propto \gamma^2 - 3\frac{2}{3}\gamma^2 + 3\frac{1}{3}\gamma^2 = 0 \ .
\end{aligned} \tag{2.9}$$

So with the above hidden flavor assignments all the anomalies involving $\mathrm{U}(1)_{\mathrm{F}}$ cancel. We have thus shown that the theory presented in Table 2.2 is a consistent extension of the SM with composite Dirac neutrinos.

2.3.3 Right-handed SM

So far we have not discussed the compositeness of the right-handed SM. In our model the right-handed SM is charged under $\mathrm{U}(1)_{\mathrm{F}} \subseteq G_{\mathrm{F}}$, so we would naïvely expect these fields to be composite at scales Λ (or Λ_i). The SM Yukawa couplings would then be suppressed by ϵ (or Λ_i/M, which might account for inter-family mass splittings, but we do not consider this possibility further in this chapter).

It is also conceivable that the field content and group structure of the UV preonic theory can be chosen such that these fields are composite only at scale M. In this scenario the right-handed SM Yukawa couplings are not suppressed by compositeness. The reason is that these Yukawa terms now depend on only one compositeness scale, M, which must cancel by naïve dimensional analysis. In comparison, the compositeness of the neutrinos at scale Λ suppresses their Yukawa couplings to the left-handed leptons by powers of ϵ, as in Eq. (2.4). As a result,

the large mass hierarchy between the neutrinos and the rest of the SM fermions is achieved.

With reference to the 't Hooft anomaly matching formalism, another possibility is to identify the right-handed SM as spectators, that is, as the elementary fields which are uncharged under any of the confining gauge groups, but which precisely cancel the 'flavor' $\mathrm{SU}(3)_c \otimes \mathrm{U}(1)_Y \otimes \mathrm{U}(1)_\mathrm{F}$ anomalies. In this case, the SM Yukawa couplings are similarly not suppressed by compositeness. A further advantage of this scenario is that the compositeness contributions to e.g. the anomalous magnetic moment are suppressed, such that the strong bounds on M due to the electron $g-2$ are evaded.

2.3.4 Symmetry breaking pattern and gauge bosons

Let us now proceed to further examine the pattern of symmetry breaking for this theory. Since gauge symmetries are not violated by quantum gravity effects, we assume $\mathrm{U}(1)_\mathrm{F}$ is a weakly gauged symmetry. This assumption also follows from the usual 't Hooft prescription.

The effective Higgs ϕ has the same number of degrees of freedom and same scalar potential $V(\phi)$ as in the SM. We are therefore free to choose the usual unitarity gauge defined by $\langle\phi\rangle = (0, v)^T$. In this gauge it is clear that the electromagnetic symmetry $U(1)_\mathrm{EM}$, with generator $Q = T^3 + Y$, remains a gauge symmetry of the theory. Further, it is clear that $\mathrm{U}(1)_a \simeq \mathrm{U}(1)_{B-L}$ is a gauge symmetry too.

Apart from the $\mathrm{SU}(3)_c$ generators, there are two unbroken generators after spontaneous symmetry breaking. These generators must correspond to two U(1)s,

whose generators must be linearly independent combinations of Q and $B-L$. We may therefore write the electroweak symmetry breaking pattern for this theory as

$$\mathrm{SU}(2)_L \otimes \mathrm{U}(1)_Y \otimes \mathrm{U}(1)_\mathrm{F} \to U(1)_\mathrm{EM} \otimes U(1)' \,, \tag{2.10}$$

where the generator of $U(1)'$ is a linear combination of Q and $B-L$, and its gauge boson, A'_μ, is orthonormal to the photon A_μ. An explicit presentation of the gauge boson mass basis and couplings is presented in Appendix A.2.

Let us now suppose that $\mathrm{U}(1)_\mathrm{F}$ is weakly gauged compared to the SM. That is, we define

$$\kappa \equiv \frac{2\gamma g_\mathrm{F}}{\sqrt{g^2 + g'^2 + (2\gamma g_\mathrm{F})^2}} \tag{2.11}$$

where g_F is the gauge coupling of the $\mathrm{U}(1)_\mathrm{F}$, and we assume $\kappa \ll 1$. This is a reasonable assumption if $\mathrm{U}(1)_\mathrm{F}$ is a subgroup of the UV preonic flavor group, while G_SM has generators arising from the UV preonic confining gauge group. For our present purposes, it is sufficient to note that in the $g_F \ll g$ limit we recover the usual SM gauge boson structure along with a A'_μ gauge boson that is weakly coupled to all fields. In particular, the covariant derivative in this limit (A.19) is

$$\begin{aligned} iD_\mu \simeq i\partial_\mu - gT^\pm W^\pm_\mu - eQA_\mu - \frac{g}{c_W}\left[\left(T^3 - Qs_W^2\right) - \frac{\kappa^2}{2}\left(Qc_W^2 + Y - B - L\right)\right] Z_\mu \\ - \frac{g\kappa}{c_W}\left[Qc_W^2 - \frac{B-L}{2}\right] A'_\mu \,, \end{aligned} \tag{2.12}$$

for which all terms are defined in Appendix A.2. Note that the couplings of the A'_μ to both the SM and hidden sector is suppressed by a factor κ, while the coupling of the hidden sector to the Z is even more strongly suppressed by a factor κ^2. In general, the phenomenological consequences of this extra gauge boson are suppressed by κ, which we can always choose small enough to satisfy experimental bounds.

In principle, kinetic mixing between the photon and A'_μ can occur in this theory. However, any such mixing is suppressed by κ. Moreover, by construction the gauge group of this theory embeds into the gauge $\otimes$ flavor groups of a fundamental UV preonic theory. If one assumes the UV preonic theory contains only a single U(1) factor, then the underlying symmetry of the UV preonic theory prevents kinetic mixing between orthonormal U(1) gauge bosons in the full quantum low energy theory.

2.4 Phenomenology

We now proceed to examine some phenomenological aspects of our U(1) hidden flavor model. The parameters characterizing compositeness are just Λ and ϵ. We emphasis that, by construction, this model is an effective low-energy theory, which is well-defined only at scales well below the Λ confinement scale. Hence the phenomenology presented in the following section holds only at scales much less than Λ.

Cosmological and in particular big-bang nucleosythesis constraints on Λ are presented in Ref. [13]. In the case that the hidden sector undergoes chiral symmetry breaking, as we have assumed throughout, one requires $\Lambda \gtrsim r^{1/3}$ GeV, where r is the ratio of right and left handed neutrino number densities. It is therefore expected, though not necessary, that Λ should be greater than the GeV scale.

In general, the phenomenology of this model is the same as that of the well-known SM with Dirac neutrinos, up to corrections due to compositeness and the A'_μ coupling. The former results in non-diagonal couplings of the neutrinos to the Z and Higgs as well as a non-unitary PMNS matrix. The latter amounts to

a rescaling of the couplings. However, all these corrections prove to be strongly suppressed by v/M, ϵ and/or κ factors. That is, so long as these factors are sufficiently small, the phenomenology of exotic processes is indistinguishable from the SM with Dirac neutrinos within current experimental precision. The spirit of this section is to verify this suppression explicitly.

2.4.1 Baryon and lepton number violation

Since only $B - L$ is an exact symmetry of our theory, higher dimensional B and L violating operators are in principle permitted in the low energy theory. Hence proton decay and deuterium decay can occur, although neutrinoless double-β decay is forbidden. The exact structure of any particular B violating operator depends on the details of the UV preonic theory. However, we can estimate upper bounds on any particular B or L violating process from the low energy effective field theory, by assuming any such operator exists at the lowest possible mass dimension. Note that since we assumed that the SM was composite at scale M, then any B violating process must be mediated by heavy gauge bosons at scale M or higher.

For example, the simplest operator which produces the proton decay $p \to e^+\gamma$ has the form $uude/M^2$ by naïve dimensional analysis. Hence in our theory the proton decay rate is suppressed by at least $(\Lambda_{\rm QCD}/M)^4$. Similarly, we expect any B violating process to be suppressed by powers of $\Lambda_{\rm QCD}/M$. The current proton decay bound [31] implies that $M \gtrsim 10^{15}$ GeV. In contrast, $M \gtrsim 10^3$ TeV is well-motivated by suppression of flavor changing neutral currents in extended technicolor models (see e.g. Ref. [30]), while bounds from four-Fermi contact interactions typically require $M \gtrsim 10$ TeV [31]. Generally, these discrepancies are resolved by detailed consideration of the structure of the UV preonic theory, which

is beyond the scope of the present paper. (A detailed generic discussion regarding bounds on the SM compositeness scale can be found in e.g. Ref. [7].) For the purposes of this chapter, we will henceforth assume just that $M \gtrsim 10$ TeV, and that tighter experimental bounds are satisfied by the details of the UV preonic theory.

2.4.2 Yukawa terms

The leading order (in v/M) mass generating terms for the leptonic sector of the U(1) hidden flavor theory are simply the Yukawa terms

$$\lambda^{\ell}_{ij}\bar{L}^i_L\phi E^j_R + \lambda_{iI}\epsilon^{3(n_I-1)/2}\bar{L}^i_L\tilde{\phi}N^I_R + \bar{N}^\alpha_L\Lambda_\alpha N^\alpha_R \ , \tag{2.13}$$

where n_I is the number of effective preons comprising N^I_R, λ and λ^ℓ are $\mathcal{O}(1)$ matrices, and we have written the massive spin-1/2 bound states in their mass basis, with masses $\Lambda_\alpha \sim \Lambda$ (or $\sim \Lambda\epsilon^2$ if there is any secondary mass generation).

Let us now suppose that there are in total N spin-1/2 bound states which correspond to physical right-handed neutrinos, of which three are chiral and $K \equiv N-3$ are massive. Further, let us also redefine

$$\epsilon^{3(n_I-1)/2}\lambda_{iI} \equiv \epsilon^{\tilde{n}}\tilde{\lambda}_{iI} \tag{2.14}$$

where $\tilde{n} = \min_I[3(n_I-1)/2]$ and $\tilde{\lambda}$ absorbs the remaining powers ϵ. That is, we factored out the largest possible power of ϵ to form a $3\times N$ matrix, $\tilde{\lambda}$, with at least one $\mathcal{O}(1)$ column: The remaining entries are suppressed by powers of ϵ. After spontaneous symmetry breaking we write the mass terms as

$$\mathcal{L}_{\rm m} = v\lambda^{\ell}_{ij}\bar{E}^i_L E^j_R + \Lambda\begin{pmatrix}\bar{N}^i_L & \bar{N}^\alpha_L\end{pmatrix} A \begin{pmatrix}N^i_R \\ N^\alpha_R\end{pmatrix} + \text{h.c.}, \tag{2.15}$$

where A is an $N \times N$ square matrix

$$A \equiv \begin{pmatrix} \theta\tilde{\lambda}_3 & \theta\tilde{\lambda}_K \\ 0 & d_K \end{pmatrix} \ . \tag{2.16}$$

Here the parameter

$$\theta \equiv \frac{v}{\Lambda}\epsilon^{\tilde{n}} \ , \tag{2.17}$$

the subscripts denote the number of columns, and d_K is diagonal with entries Λ_α/Λ. We assume that mostly $[d_K]_{\alpha\alpha} \sim \mathcal{O}(1)$, but there may exist some entries of d_K which are suppressed by ϵ^2 due to secondary mass generation.

2.4.3 Leptonic mixing matrix

In general, both λ^ℓ and A have biunitary decompositions of the form

$$\lambda^\ell = V^\ell d^\ell W^{\ell\dagger} \ , \quad \text{and } A = V d W^\dagger \ , \tag{2.18}$$

where d^ℓ (d) is a 3×3 ($N \times N$) diagonal matrix and V^ℓ and W^ℓ (V and W) are 3×3 ($N \times N$) unitary matrices. As usual we define the lepton mass basis by

$$\begin{aligned} e_L &= V^{\ell\dagger} E_L & \qquad e_R &= W^{\ell\dagger} E_R \\ \nu_L &= V^\dagger N_L & \qquad \nu_R &= W^\dagger N_R \ . \end{aligned} \tag{2.19}$$

A notable difference from the SM is that here there are 3 charged lepton mass eigenstates, but N neutrino mass eigenstates.

In the neutrino mass basis the W couplings are non-diagonal, as usual. Since the N_L^i and N_L^α have different Z couplings, as can be seen in Eq. (2.12), Z neutrino couplings in the mass basis are non-diagonal too. To order $\mathcal{O}(\kappa^2)$, one finds that

non-diagonal neutrino currents are

$$\mathcal{J}_W^{\mu-} = \frac{g}{\sqrt{2}}\bar{e}_L U\gamma^\mu\nu_L \ , \tag{2.20}$$

$$\mathcal{J}_Z^{\mu} = \frac{g}{2c_W}\left(1+\frac{\kappa^2}{2}\right)\bar{\nu}_L U^\dagger U\gamma^\mu\nu_L - \frac{g\kappa^2}{2c_W}\bar{\nu}_L\gamma^\mu\nu_L \ , \tag{2.21}$$

where we have defined the $3\times N$ leptonic mixing matrix, U, by

$$U^{iI} = [V^{\ell\dagger}]^{ij}[V^n]^{jI} \ . \tag{2.22}$$

In Eq. (2.21) we have applied the identity $(V^\dagger)^{I\alpha}V^{\alpha J} = \delta^{IJ} - (V^\dagger)^{Ii}V^{iJ}$ and then inserted $V^\ell V^{\ell\dagger} = 1$ to write the non-diagonal Z current in terms of $U^\dagger U$. It is worthwhile noting here that the unitarity of V^l and V implies

$$[UU^\dagger]_{ij} = [V^{\ell\dagger}]_{ik}[V]_{kI}[V^\dagger]_{Im}[V^\ell]_{mj} = \delta_{ij} \ , \tag{2.23}$$

whereas

$$[U^\dagger U]_{IJ} = [V^\dagger]_{Ik}[V]_{kJ} \neq \delta_{IJ} \ . \tag{2.24}$$

Hence the mixing matrix is only unitary from the right.

The Higgs couplings to the neutrinos are also non-diagonal in the mass basis. Explicitly, writing the massive Higgs as h, from Eqs. (2.13) and (2.19) we have

$$\mathcal{L}_h = h^\dagger\bar{N}_L^i\epsilon^{\tilde{n}}\tilde{\lambda}_{iI}N_R^I = h^\dagger\bar{\nu}_L^I(V^\dagger)^{Ii}\epsilon^{\tilde{n}}\tilde{\lambda}_{iJ}W^{JK}\nu_R^K \ . \tag{2.25}$$

From Eqs. (2.16) and (2.18) it follows that $(\theta\tilde{\lambda}W)^{iI} = (Vd)^{iI}$, so then

$$\mathcal{L}_h = h^\dagger\bar{\nu}_L\left(U^\dagger U\frac{m}{v}\right)\nu_R + \text{h.c} \ , \tag{2.26}$$

where m is the diagonal neutrino mass matrix, $m \equiv \Lambda d$.

2.4.4 Neutrino mass spectrum and eigenstates

Let us now determine the neutrino mass spectrum, as well as the general structure of V. We are particularly interested in determining V since this matrix is a

Eigenstate	Mass	Composition
ν_L^l	$\lesssim \theta\Lambda = v\epsilon^{\tilde{n}}$	$a_j N_L^j + \theta a_\alpha N_L^\alpha$
ν_L^H	$\sim \Lambda$ or $\sim \epsilon^2\Lambda$	$a_j \theta N_L^j + a_\alpha N_L^\alpha$

Table 2.3: Neutrino mass spectrum and composition of left-handed neutrino mass eigenstates. The coefficients a_j and a_α are $\mathcal{O}(1)$ numbers.

component of the leptonic mixing matrix U. The general structure of the unitary matrix V can be determined simultaneously with the mass spectrum by diagonalizing $AA^\dagger$. Details of this diagonalization are presented in Appendix A.3. One finds that the leading order general structure of V is (A.24)

$$V = \begin{pmatrix} X_3 & \theta W_K \\ \theta Y_3 & Z_K \end{pmatrix} , \tag{2.27}$$

where the matrices X_3, Y_3, W_K and Z_K have either $\mathcal{O}(1)$ entries or entries suppressed by powers of ϵ. As a result of Eq. (2.27), the neutrino mass basis is a weak mixing between the SM fields N_L^i and the heavy bound states N_L^α, with mixing angle of order θ. A summary of the mass spectrum and corresponding eigenstates is presented in Table 2.3. Here and henceforth we denote the three light ($N-3$ heavier) neutrinos by $\nu_{L,R}^l$ ($\nu_{L,R}^H$).

2.4.5 Charged and neutral currents

The most significant consequence of this analysis is that since V^ℓ has $\mathcal{O}(1)$ entries or smaller, then by Eqs. (2.22) and (2.27) the mixing matrix has the structure

$$U = \begin{pmatrix} V^{\ell\dagger} X_3 & \theta V^{\ell\dagger} W_K \end{pmatrix} \equiv \begin{pmatrix} U_3 & \theta U_K \end{pmatrix} , \tag{2.28}$$

where $U_{3,K}$ entries are either $\mathcal{O}(1)$ or suppressed by powers of ϵ. In the mass basis the non-diagonal charged and neutral currents involving neutrinos in Eqs. (2.20)

and (2.21) are respectively

$$
\begin{aligned}
J_W^{\mu-} &= \frac{g}{\sqrt{2}}\Big(\bar{e}_L\gamma^\mu U_3\nu_L^l + \theta\big[\bar{e}_L\gamma^\mu U_K\nu_L^H\big]\Big)\ , \\
J_Z^\mu &= \frac{g}{2c_W}\Bigg[\bar{\nu}_L^l\gamma^\mu\Big(U_3^\dagger U_3(1+\kappa^2/2)-\kappa^2\Big)\nu_L^l + \theta(1+\kappa^2/2)\big[\bar{\nu}_L^l\gamma^\mu U_3^\dagger U_K\nu_L^H + \text{h.c.}\big] \\
&\quad + \bar{\nu}_L^H\gamma^\mu\Big(\theta^2 U_K^\dagger U_K(1+\kappa^2/2)-\kappa^2\Big)\nu_L^H\Bigg]\ . \qquad (2.29)
\end{aligned}
$$

It is clear that the coupling of the heavy left-handed neutrinos ν_L^H to the W and Z is suppressed by either a θ or κ^2 factor. Similarly, writing $m = \text{diag}\{m_\nu, m_H\}$, the Higgs coupling (2.26) becomes

$$
\mathcal{L}_h = h^\dagger\Bigg[\bar{\nu}_L^l U_3^\dagger U_3\frac{m_\nu}{v}\nu_R^l + \epsilon^{\tilde{n}}\bar{\nu}_L^l U_3^\dagger U_K\frac{m_H}{\Lambda}\nu_R^H + \epsilon^{\tilde{n}}\bar{\nu}_L^H U_K^\dagger U_3\frac{m_\nu}{\Lambda}\nu_R^l + \theta\epsilon^{\tilde{n}}\bar{\nu}_L^H U_K^\dagger U_K\frac{m_H}{\Lambda}\nu_R^H\Bigg], \qquad (2.30)
$$

all the terms of which are suppressed by at least $\epsilon^{\tilde{n}}$, due to both the weak mixing with heavy mass eigenstates and the light neutrino masses.

2.4.6 Scales and dark matter candidates

Before continuing any further, let us examine possible scales for ϵ. First, note from Table 2.3 that the light neutrino masses $m_\nu \lesssim v\epsilon^{\tilde{n}}$. It must be that $\tilde{n} \geq 3$, and in particular let us assume one of the light neutrinos is comprised of three effective preons, so $\tilde{n} = 3$ and $m_\nu \sim v\epsilon^3$. The other two light neutrinos may be comprised of more effective preons, in which case their masses are further suppressed. For $m_\nu \sim 0.1$ eV we then have

$$
\epsilon^3 \sim \frac{m_\nu}{v} \sim 10^{-13} \implies \epsilon \lesssim 10^{-4}\ . \qquad (2.31)
$$

Further, from Eq. (2.17) it follows that the upper bound on the mixing between the light and heavy neutrinos

$$
\theta \lesssim \frac{m_\nu}{\Lambda}\ , \qquad (2.32)
$$

and the secondary mass generation scale (if any) is, by Eq. (2.31)

$$M_{\rm 2MG} \sim \epsilon^2 \Lambda \sim \left(\frac{m_\nu}{v}\right)^{2/3} \Lambda \sim 10^{-26/3} \Lambda \ . \tag{2.33}$$

A particularly interesting scenario is to consider $\Lambda \sim 1$ TeV, which is in line with the cosmological bounds mentioned in Ref. [13]. As a result, from Eq. (2.32) the light-heavy mixing is $\theta \lesssim 10^{-13}$ and then the secondary mass generation scale

$$M_{\rm 2MG} \sim \text{KeV} \ . \tag{2.34}$$

If there is secondary mass generation, then the mass and lifetime scales of such 'intermediate' neutrinos, which we will denote ν^m, suggest they may be warm dark matter candidates [32, 33, 34, 35]. Evidence for the decay of such warm dark matter with a KeV mass scale has been potentially observed in the Willman 1 dwarf galaxy [36], although we note that the heavy light mixing angle for the intermediate neutrinos is much smaller than the claimed mixing in Ref. [36], which is $\sim 10^{-5}$.

Explicitly, the ν^m are lighter than any massive content of the SM, so kinematically they may only decay into the light neutrinos. The leading order contribution to this decay is through the tree-level neutral current $\nu^m \to 3\nu^l$ in Eq. (2.29). From naïve dimensional analysis the lifetime of these neutrinos is $\sim 10^{29}$ years. Note also that these intermediate neutrinos could be produced in a W or Z decay, but the contribution to the decay rate is suppressed by at least $\theta^2 \sim 10^{-26}$ compared to the contribution of the three light neutrinos, satisfying experimental bounds on a fourth generation light neutrino coupled to the massive SM gauge bosons [31]. We also note from Eqs. (2.29) and (2.30) that since the coupling of the ν^H to the SM is generally suppressed by at least $\epsilon^{\tilde{n}} \sim 10^{-13}$ or κ, and they have masses $\sim$ TeV, then these heavy neutrinos may be candidate 'feebly interacting massive particles' [37].

2.4.7 Non-unitarity and neutrino oscillations

The large mass scale for the heavy neutrinos means that in a process such as β-decay, production of heavy neutrino mass eigenstates ν_L^H is kinematically forbidden. As a consequence, the physical flavor states produced in experiments will consist of combinations of only the light ν_L^i. That is, the neutrino flavor basis is defined by

$$n_L^f \equiv U_3^{fi} \nu_L^i \ . \tag{2.35}$$

Here the non-unitary U_3 replaces the 3×3 unitary PMNS matrix found in the standard treatment of neutrino mixing (see e.g. [31]). We henceforth call U_3 the effective PMNS matrix. Note that intermediate neutrinos may also be produced, in which case the physical flavor states Eq. (2.35) have further components suppressed by θ: We can alternatively think of Eq. (2.35) as defining the leading order terms of the flavor basis.

The consequences of a non-unitary PMNS matrix have been previously examined in depth (see Refs [38, 39, 40], and references therein). For example, non-unitarity of the PMNS matrix means that the flavor states $|n_L^f\rangle$ are no longer orthogonal. In the context of neutrino oscillations, the probability $P_{f\to g}$ for a transition between states $|n_L^f\rangle$ and $|n_L^g\rangle$ is modified, and in particular there is a non-zero probability for a flavor transition at the source of a neutrino beam - a so-called zero distance effect. Other consequences are e.g. modified charged and neutral current cross-sections.

In general, all modifications from the standard treatment due to non-unitarity arise from factors involving either $U_3 U_3^\dagger$ or $U_3^\dagger U_3$. However, from Eqs. (2.23) and

(2.28) and the unitarity of V (2.27), we have

$$U_3 U_3^\dagger = 1 - \theta^2 U_K U_K^\dagger \ ,$$
$$U_3^\dagger U_3 = 1 - \theta^2 Y_3^\dagger Y_3 \ , \tag{2.36}$$

so that the unitarity of U_3 is only very weakly broken. That is, for our present low-energy theory the non-unitarity of U_3 only weakly modifies the standard formalism, including that of neutrino oscillations. For example, the probability associated with the zero distance effect

$$P_{f\to g}(L=0) = \frac{|(U_3 U_3^\dagger)_{fg}|^2}{(U_3 U_3^\dagger)_{ff}(U_3 U_3^\dagger)_{gg}} \simeq \theta^4 |(U_K U_K^\dagger)_{fg}|^2 \sim 10^{-54} \tag{2.37}$$

if $\Lambda \sim$ TeV, which is well below experimental threshold sensitivities. Similarly, the general expression for neutrino oscillation probabilities is the same as in the standard treatment, up to non-unitarity corrections at most $\mathcal{O}(\theta^2)$.

2.5 Conclusion

We have presented a mechanism through which light Dirac neutrinos may be naturally generated. An essential ingredient is the hidden flavor $\mathrm{U(1)_F}$ charge assigned to the Higgs scalar ϕ, which produces an unbroken axial U(1) when combined with hypercharge. With particular hidden charge assignments to the fermionic fields, this axial symmetry forbids the production of Majorana masses during the spontaneous symmetry breaking induced by $\langle\phi\rangle$ alone.

We have shown in this chapter that a simple assignment of $\mathrm{U(1)_F}$ charges, which is motivated in part by the need to reproduce the SM Yukawas involving ϕ, is non-anomalous and produces an unbroken axial symmetry that is isomorphic to $B-L$, guaranteeing that only Dirac fermions are produced. In all this, the

compositeness plays a key role: it naturally produces a pattern of chiral symmetry breaking that incorporates this extra symmetry into the theory and allows us to produce very light Dirac masses in comparison to the rest of the SM fields. Further, compositeness also naturally produces an arbitrary number of heavier neutrinos, which are weakly coupled to the SM.

Our U(1) hidden flavor model predicts observable effects beyond the SM, though the effects in question are not unique to our model. First, since it predicts Dirac neutrinos, no neutrino-less double beta decay will be observed in our model. Baryon and lepton number violating processes, the unitarity breaking of the effective PMNS matrix and the mixing between the light and heavy neutrino mass eigenstates are all strongly suppressed by compositeness, such that the effects associated with these features may be small enough to satisfy current experimental bounds. Phenomenology due to the extra gauge boson is similarly suppressed by its small coupling. Finally, the intermediate neutrinos, whose masses may be produced by secondary mass generation, are potential warm dark matter candidates, while the weakly coupled heavier neutrinos could be so-called feebly interacting massive particles.

CHAPTER 3

KEV WARM DARK MATTER AND COMPOSITE NEUTRINOS

Based on the 2012 article "KeV Warm Dark Matter and Composite Neutrinos", written in collaboration with Yuhsin Tsai and published in JHEP 08 (2012) 161.

3.1 Introduction

Sterile neutrinos with masses at the keV scale are a popular warm dark matter (WDM) candidate [41, 42, 43, 44, 45, 46, 47, 48, 49, 50, 51, 52, 53, 54, 35, 55, 56, 57, 58, 59, 60, 61], that may potentially account for small-scale structure formation (see e.g [62, 63, 56]) and possibly explain large pulsar kick velocities [64, 35]. Sterile neutrino WDM can be produced non-thermally via (non)-resonant oscillations from the active neutrinos [42, 43, 44, 65, 66, 52, 35, 54, 67, 68], by decays from the inflaton [69, 70], or thermally with subsequent entropy dilution (see e.g. [71, 72]). Typically, the parameter space spanned by the mass (hereafter m_d) and active-sterile mixing angle (hereafter θ_d) for sterile neutrino WDM is most tightly constrained by Lyman-α [66, 71] and x-ray flux [73, 74, 65, 57, 68] bounds, along with free-streaming, Tremaine-Gunn and big-bang nucleosynthesis bounds, too (see e.g. [35, 67]). The aggregate effect of these bounds depends on the production mechanism of the sterile neutrino WDM. In particular, at present purely non-resonant production is disfavored, while windows exist for resonant production, production from inflaton decay, or from entropy-diluted thermal freeze out [65, 66, 54, 35].

In this chapter, we show that elementary keV *Dirac* sterile neutrinos can be a natural feature of the composite neutrino scenario [4, 13, 12, 75, 76], in the same way that the light fermions of the standard model (SM) can arise naturally in the extended technicolor framework [77]. Briefly, the composite neutrino scenario is a class of theories in which the right-handed neutrinos are composite bound states of a confining hidden sector (CHS).

The possibility of such keV sterile neutrinos was first mentioned briefly in Ref. [78], and some of its x-ray flux bounds were investigated in [79]. In this chapter,

we present a more generalized discussion of this mechanism that is independent of the precise details of the confining sector, and then proceed to investigate the possible cosmological histories for this WDM candidate. We show certain classes of CHS's can naturally produce keV sterile neutrinos with active-sterile mixing angle in the resonant production window, and a freeze out temperature $\gtrsim$ TeV. Provided the post-inflation reheating temperature is below the TeV scale, then these keV sterile neutrinos could be WDM produced non-thermally via the usual resonant production mechanism [42, 43, 44, 65, 66, 52, 35, 54, 67, 68], or by a combination of inflaton decay and subsequent non-resonant production [69, 70].

As mentioned above, an alternative to non-thermal WDM production is ultra-relativistic thermal production followed by entropy dilution (see e.g. [71]). This has the advantage of producing colder WDM than resonant production and can better evade the Lyman-α bounds. Usually the diluting entropy is produced by the out-of-equilibrium decay of a sufficiently long-lived heavy particle. In this chapter we examine another compelling possibility: The first-order phase transition induced by the confinement of the hidden sector can also produce significant entropy if there is sufficient supercooling. This results in thermal keV WDM. We will discuss the details of this mechanism.

3.2 The Composite Dirac Neutrino Model

3.2.1 Setup

The generic theory of interest is a low-energy effective field theory below a scale M. Its group structure is $G_{\rm c} \otimes G_{\rm F} \otimes G_{\rm SM}$, with $G_{\rm c}$ a confining group called ν-color,

$G_{\rm SM}$ the SM gauge groups (or a UV extension), and $G_{\rm F}$ a global (or weakly gauged) hidden flavor group. The theory consists of three sectors

$$\chi \sim G_{\rm c} \otimes G_{\rm F} \ , \qquad \xi \sim G_{\rm F} \ , \qquad q \sim G_{\rm SM} \otimes G_{\rm F} \ , \tag{3.1}$$

and which interact only via M-scale irrelevant operators. We call χ 'preons' and say they belong to the CHS. Here q denote the SM fields extended to also carry hidden flavor $G_{\rm F}$, and we say ξ comprise the 'extended hidden sector' (EHS). We assume that the χ and ξ are purely chiral fermions, but we emphasise that like the SM sector, the χ and ξ may consist of various different irreps.

The ν-color group confines at a confinement scale $\Lambda \ll M$. Necessarily $M \gg v$, the electroweak scale, so it is convenient to define two parameters

$$\epsilon \equiv \Lambda/M \ll 1 \ , \qquad \theta \equiv v/M \ll 1 \ . \tag{3.2}$$

Confinement of the CHS produces preonic bound states, which we shall crudely denote as χ^p: The superscript denotes the number of preons participating in the bound state. Formation of a scalar condensate χ^m with $\langle \chi^m \rangle \neq 0$ generically induces a spontaneous breaking of the hidden flavor group $G_{\rm F} \to G'_{\rm F} \subset G_{\rm F}$. This produces a new sub-Λ effective field theory, which consists of: preonic bound states; ξ and q decomposed into $G'_{\rm F}$ irreps; and also light 'hidden pions'. There are three crucial ideas:

(i) If the CHS has non-trivial $G'_{\rm F}$ anomalies, then anomaly matching of the CHS to its confined phase, with ξ and q acting as chiral spectators, implies that there are *massless* fermionic bound states after confinement. The remaining bound states generically have masses $\sim \Lambda$, except for the hidden pions, which can be massless or have arbitrarily small masses, depending on the nature of the $G_{\rm F}$ symmetry breaking. We assume the pion masses are sufficiently small that they make negligible contributions to the DM energy fraction.

Hereafter we shall assume $G'_{\rm F} = {\rm U}(1)_{\rm F}$, and that there are precisely three massless bound states all with the same ${\rm U}(1)_{\rm F}$ charge [1]. For simplicity we assume the massless bound states have the same number of preons, hereafter denoted n, necessarily an odd integer. We shall suggestively denote these bound states as n_R^i, $i = 1, 2, 3$ with ${\rm U}(1)_{\rm F}$ charge $F(n_R) = +1$. Explicit examples of preonic theories capable of producing such spectra are presented in Ref. [78]. The corresponding sub-Λ EFT that we shall consider hereafter is shown in Table 3.1. In producing this EFT, we require that the mechanisms of $G_{\rm F} \to {\rm U}(1)_{\rm F}$ breaking and electroweak symmetry breaking are independent, at least to a good approximation.

	ϕ	L_L^c	E_R	Q_L^c	U_R	D_R	n_R
F	$+1$	0	-1	0	1	-1	$+1$

Table 3.1: ${\rm U}(1)_{\rm F}$ charge assignments to the massless bound states n_R and the SM fields $q = \{\phi, Q, U, D, L, E\}$, which also have the usual SM charges (not shown). The n_R are SM sterile by construction.

One can check $2Y - F = B - L$, so ${\rm U}(1)_{\rm F}$ is nonanomalous, and the electroweak symmetry breaking (EWSB) pattern is

$$ {\rm SU}(2)_{\rm L} \otimes {\rm U}(1)_Y \otimes {\rm U}(1)_{\rm F} \to {\rm U}(1)_{\rm EM} \otimes {\rm U}(1)_{B-L} \ . \tag{3.3} $$

That is, one obtains Dirac neutrinos, with the n_R acting as right-handed neutrinos. Note ${\rm U}(1)_{\rm F}$ may be gauged, but we assume its gauge coupling and kinetic mixing with the photon are sufficiently small that they can be neglected.

(ii) For the sub-Λ EFT in Table 3.1, there exist irrelevant operators that couple the preons of the massless n_R – i.e. the $G_{\rm c}$ singlets χ^n – to the SM singlet $\bar{L}_L \tilde{\phi}$.

[1] In this case decomposition of q under $G_{\rm F} \to {\rm U}(1)_{\rm F}$ could result in multiple copies of SM irreps, also with the same ${\rm U}(1)_{\rm F}$ charges, which could be the source of flavor.

Such an operator is generically of form

$$\frac{1}{M^{3(n-1)/2}}\bar{L}_L\tilde{\phi}\chi^n \to \epsilon^{3(n-1)/2}\bar{L}_L\tilde{\phi}n_R \ , \tag{3.4}$$

after confinement. That is, this operator produces a suppressed Yukawa in the sub-Λ EFT. Since n_R are massless and there is $B-L$ symmetry (3.3), this operator leads to light Dirac neutrino masses after EWSB, compared to the electroweak scale.

There may also be other vector-like right-handed fermionic bound states N_R and N_L^c, with $F(N_{R,L}) = +1$ We shall again assume for simplicity they contain n preons. Such bound states must form Dirac fermions with Λ scale masses, and the N_R will generically also have operators of form (3.4). $N_{R,L}$ are therefore Λ-scale sterile Dirac neutrinos.

(iii) Under decomposition into $\mathrm{U}(1)_\mathrm{F}$ irreps, the chiral EHS fields ξ may form real $\mathrm{U}(1)_\mathrm{F}$ representations and acquire masses. However, because the EHS couples only irrelevantly to the condensate vev $\langle\chi^m\rangle$ responsible for $G_\mathrm{F} \to \mathrm{U}(1)_\mathrm{F}$, the mass terms must be suppressed. This is the same mechanism which suppresses the quark and lepton masses in Extended Technicolor theories [77]. Explicitly, for a Dirac fermion $\xi_{R,L}$, such mass terms arise from operators of the form

$$\frac{1}{M^{(3m-2)/2}}\xi\chi^m\xi \to \Lambda\epsilon^{(3m-2)/2}\bar{\xi}_L\xi_R \ , \tag{3.5}$$

after confinement [2]. If also $F(\xi_{R,L}) = +1$, then there may exist irrelevant operators that couple the corresponding G_c singlet $\chi^m\xi$ to $\bar{L}_L\tilde{\phi}$, noting any renormalizable coupling of ξ directly to $\bar{L}_L\tilde{\phi}$ is forbidden by the G_F chiral structure. That is, we

[2]There may also be mass cross terms involving $\xi_L N_R$, for example. However, we assume that such cross-terms, i.e involving composite and elementary states, are suppressed by the details of the UV theory above M. An analogous assumption must also be made for the proton decay operator $uude/M^2$.

could have

$$\frac{1}{M^{3m/2}}\bar{L}_L\tilde{\phi}\chi^m\xi \to \epsilon^{3m/2}\bar{L}_L\tilde{\phi}\xi_R \ . \tag{3.6}$$

Consequently, such a $\xi_{R,L}$ forms an *elementary* sterile Dirac neutrino with naturally suppressed mass term $\sim \Lambda\epsilon^{(3m-2)/2}$ and coupling to the active sector $\sim \epsilon^{3m/2}$. In principle, there may be several species of such a Dirac neutrino, as well as other EHS fermions with $F \neq \pm 1$ that acquire Dirac or even Majorana masses of the same size.

3.2.2 Spectrum

We may classify the sub-Λ EFT by a tuple (n, m), where n (odd ≥ 3) is the number of preons in the sterile neutrino bound states, and m (even ≥ 2) is the number of preons in the symmetry breaking condensate. After EWSB, from eqs. (3.4)–(3.6) a (n, m) theory has neutrino mass term,

$$\Lambda \begin{pmatrix} \nu_L \\ \xi_L \\ N_L \end{pmatrix}^T \begin{pmatrix} \theta\epsilon^{\frac{3n-5}{2}} & \theta\epsilon^{\frac{3m-2}{2}} & \theta\epsilon^{\frac{3n-5}{2}} \\ 0 & \epsilon^{\frac{3m-2}{2}} & 0 \\ 0 & 0 & 1 \end{pmatrix} \begin{pmatrix} n_R \\ \xi_R \\ N_R \end{pmatrix} \ , \tag{3.7}$$

where ν_L is the SM active neutrino. Each entry of this mass matrix denotes the prefactor of an $\mathcal{O}(1)$ sub-block, whose dimensions depends on the number of species of each type of sterile neutrino. For example, the upper left entry must be 3×3.

For $m \leq n-1$, the mass spectrum can be determined by expansions in ϵ and θ. One obtains at leading order

$$m_l \sim v\epsilon^{\frac{3(n-1)}{2}} \ , \qquad m_d \sim \Lambda\epsilon^{\frac{3m-2}{2}} \ , \qquad m_h \sim \Lambda \ . \tag{3.8}$$

Here the superscripts l, d and h denote 'light', 'dark' and 'heavy'. The left-handed

mass basis is, at leading order in ϵ and θ,

$$\begin{pmatrix} \nu_L^l \\ \nu_L^d \\ \nu_L^h \end{pmatrix} \sim \begin{pmatrix} 1 & \theta & \theta\epsilon^{\frac{3n-5}{2}} \\ \theta & 1 & \theta^2\epsilon^{\frac{3n+6m-9}{2}} \\ \theta\epsilon^{\frac{3n-5}{2}} & \theta^2\epsilon^{\frac{3n-5}{2}} & 1 \end{pmatrix} \begin{pmatrix} \nu_L \\ \xi_L \\ N_L \end{pmatrix} , \tag{3.9}$$

and the right-handed mass basis is

$$\begin{pmatrix} \nu_R^l \\ \nu_R^d \\ \nu_R^h \end{pmatrix} \sim \begin{pmatrix} 1 & \theta^2\epsilon^{\frac{3(n-m-1)}{2}} & \theta^2\epsilon^{3n-5} \\ \theta^2\epsilon^{\frac{3(n-m-1)}{2}} & 1 & \theta^2\epsilon^{\frac{3n+3m-7}{2}} \\ \theta^2\epsilon^{3n-5} & \theta^2\epsilon^{\frac{3n+3m-7}{2}} & 1 \end{pmatrix} \begin{pmatrix} n_R \\ \xi_R \\ N_R \end{pmatrix} . \tag{3.10}$$

We emphasise that eqs. (3.9) and (3.10) denote only sub-block prefactors; the entries of the sub-blocks themselves are generically $\mathcal{O}(1)$ numbers multiplied by the appropriate prefactor.

It is clear from eq. (3.9) that the dark-active mixing angle $\theta_d \sim \theta$. One can then rearrange eqs. (3.8) and (3.9) into

$$m_d\theta_d \sim v\left(\frac{m_l}{v}\right)^{\frac{m}{n-1}} , \quad \frac{\Lambda}{m_d} \sim \left(\frac{m_l}{v}\right)^{\frac{2-3m}{3n-3}} , \tag{3.11}$$

in which the right-hand sides are fully specified by (n, m) and the requirement that $m_l \sim 0.05$ eV, $v \simeq 174$ GeV. Figure 3.1 shows $\sin^2(2\theta_d)$ up to $\mathcal{O}(1)$ uncertainty as a function of m_d, with $m = n - 1$. Theories with $m < n - 1$ have much larger mixing angles, and are therefore ruled out by x-ray flux constraints, so we consider only $(n, n-1)$ theories henceforth. For such theories $M \sim 2\times10^4(m_d/5\text{ keV})$ TeV, and we provide the corresponding Λ and ϵ in Table 3.2.

It is amusing to note that for the $(n, n-1)$ theories $m_d \sim 5$ keV implies $\sin^2(2\theta_d) \sim 3\times10^{-10}$, which matches the (as yet unconfirmed) *Chandra* results in the Willman I dwarf galaxy [36].

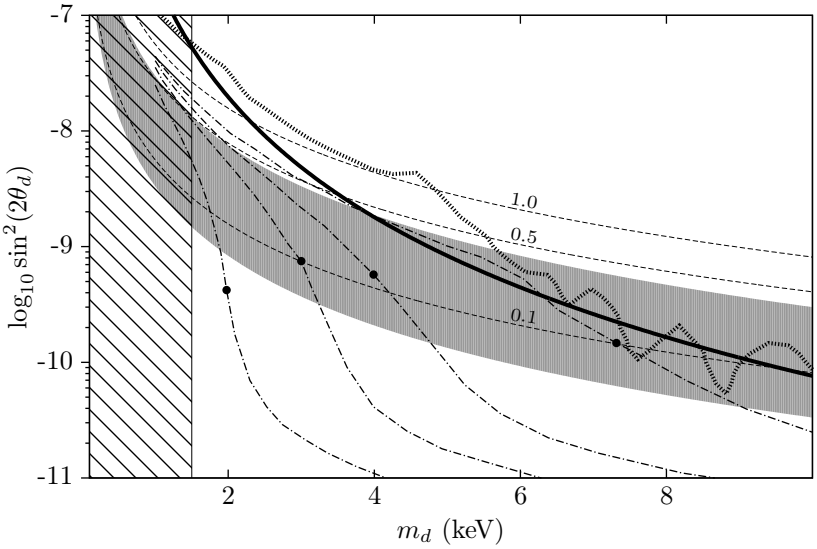

Figure 3.1: Mixing angle $\sin^2(2\theta_d)$ up to $\mathcal{O}(1)$ uncertainty (light gray) as a function of m_d, for $(n, n-1)$ theories. Also shown: Non-resonant production contours (dashed lines), labelled by the ratio of ν^d and DM energy fractions, $\Omega_d/\Omega_{\rm DM}$ [49, 54, 35]; resonant total DM production contours (dash-dotted lines) for lepton asymmetries $Y_{\Delta L} = 8,\ 12,\ 16,\ 25 \times 10^{-6}$ (resp. top to bottom), and their corresponding Lyman-α lower bounds on the WDM mass (black dots) [54]; the Lyman-α exclusion for thermally produced WDM with subsequent entropy dilution (hatched region, see e.g. [66, 35] and eq. (3.21) below) assuming 100% ν^d WDM; the x-ray flux exclusion for 100% ν^d WDM fitted from most stringent archival data (heavy black line, see e.g. [65, 54]) and from the most recent observations of dwarf spheriodal galaxies [80] (heavy broken line).

3.2.3 Dirac vs Majorana

The keV sterile neutrinos in this chapter are Dirac, in contrast with the Majorana sterile neutrinos often considered in other WDM scenarios. The WDM production mechanisms that we consider below produce dominantly symmetric DM – the resonant production mechanism requires an asymmetry in the proper number density $(n_\nu - n_{\bar\nu})/n_\nu < 10^{-2}$ [44, 52] – so that the DM particles and antiparticles are present in the same abundances to a very good approximation. The x-ray flux bounds due to sterile neutrinos are therefore insensitive to the mass structure, since

(n,m)	$\Lambda \times (5\text{ keV}/m_d)$ (TeV)	$\epsilon \times (5\text{ keV}/m_d)$
$(3,2)$	1	7×10^{-5}
$(5,4)$	10^2	8×10^{-3}
$(7,6)$	7×10^3	9×10^{-2}

Table 3.2: Confinement scale Λ and ϵ for $(n, n-1)$ theories. Such theories with $n > 7$ have $\epsilon \not\ll 1$, and are not considered further.

decay modes to the active neutrino and antineutrino are present in both cases: I.e, the x-ray flux is due to either $N \to \nu\gamma$ and $N \to \nu^c\gamma$ for a Majorana neutrino N, or $\nu^d \to \nu\gamma$ and $\bar{\nu}^d \to \bar{\nu}\gamma$ for the present scenario. Similarly, (non)-resonant production by conversion from the left-handed active neutrinos will produce the same sterile neutrino energy fraction, Ω_d, regardless of the Dirac or Majorana nature of the masses. In Fig. 3.1 we therefore use the existing results for both the x-ray bounds and production processes, without any alteration for the Dirac mass structure.

The x-ray bounds could also be altered by exotic $\nu^d \to X\gamma$ decay channels, that might arise from M-scale irrelevant operators. We emphasize that the chiral and composite structure of the composite neutrino framework ensures any such operators are of sufficiently high dimension that the corresponding decay rates are negligible. For example, in the $(3,2)$ theory $\nu^d \to \gamma\nu^l$ or $\nu^d \to \gamma\Pi\nu^l$ could also arise from $\chi^3\chi^2 F_{\mu\nu}\sigma^{\mu\nu}\xi/M^7$ which confines to $(\Lambda^5/M^7)n_R(\Lambda+\Pi)F_{\mu\nu}\sigma^{\mu\nu}\xi_L$. This respectively produces decay rates $\sim \epsilon^{12}m_d^3/M^2$ or $\sim \epsilon^{10}m_d^5/M^4$, that are negligible compared to the decay through mixing with the active neutrinos.

3.2.4 Decoupling

Our knowledge of the generic structure of the non-renormalizable operators permits us to consider the cosmological histories of the CHS and EHS, and therefore determine whether the ν^d sterile neutrinos can be a WDM candidate: satisfying the (m_d, θ_d) bounds is necessary but not sufficient for this. For the $(n, n-1)$ theories, we now enumerate various important processes and their freeze out temperatures, $T_{\rm fr}$. We assume the effective degrees of freedom at the TeV scale $g_* \sim 10^2$.

(i) $\bar{X}X \leftrightarrow \bar{Y}Y$, where $X, Y \in \{q, \xi, \chi\}$. These processes couple the SM, CHS and EHS. The dimension-5 operator $\phi^\dagger \phi \bar{X} X$ is heavily suppressed, since X are all chiral. The leading operators are then the dimension-6

$$\frac{1}{M^2} \bar{X} \gamma^\mu X \bar{Y} \gamma_\mu Y \ ; \ T_{\rm fr} \sim \left[\frac{g_*^{\frac{1}{2}} M^4}{M_{\rm pl}} \right]^{1/3} \sim \ {\rm TeV} \ , \tag{3.12}$$

and similarly for $\phi^\dagger \partial_\mu \phi \bar{X} \gamma^\mu X / M^2$. Note that the current collider constraint on the dark matter - quark interaction is insensitive to the coupling due to the large mediator mass, M [81, 82].

(ii) $\bar{\xi}_R \xi_L \leftrightarrow 2\Pi$, where Π denotes the hidden pions. This process is generated by the non-linear sigma operator

$$m_d \bar{\xi}_R \xi_L e^{i\Pi/\Lambda} \ ; \ T_{\rm fr} \sim \left[\frac{g_*^{\frac{1}{2}} \Lambda^4}{(m_d)^2 M_{\rm pl}} \right] \sim \ {\rm TeV} \ , \tag{3.13}$$

for the $(3, 2)$ theory, and much larger for $(5, 4)$ and $(7, 6)$.

(iii) $\bar{\nu}_L^d \nu_L^d \leftrightarrow \bar{q} q$. This can occur also through W and Z exchange, and must freeze out before BBN. The pertinent operators are

$$\frac{g(\theta_d)^2}{2 c_W} \bar{\nu}_L^d \not{Z} \nu_L^d \ , \ \frac{g \theta_d}{\sqrt{2}} \bar{\nu}_L^d \not{W} \ell_L \ ; \ T_{\rm fr} \sim \left[\frac{g_*^{\frac{1}{2}} m_W^4}{(\theta_d)^4 M_{\rm pl}} \right]^{1/3} \sim \ {\rm TeV} \ .$$

(iv) $\bar{\nu}_L^l \nu_R^l \leftrightarrow 2\Pi$. This must also freeze out before the BBN epoch. The non-linear sigma coupling of $\nu_{L,R}^l$ to the hidden pions is suppressed by both the left and right mixing between active and sterile sectors. From eqs. (3.9) and (3.10) this leads to an extra prefactor of $(\theta_d)^3$ for the non-linear sigma operator in eq. (3.13), and therefore a decoupling much larger than the TeV scale.

(v) $2h \leftrightarrow 2\Pi$. This is generated by the operator $\phi^\dagger\phi(\chi^m)^\dagger\chi^m/M^{3m-2}$ which confines to the dimension-4 operator $\epsilon^{3m-2}\phi^\dagger\phi\Pi\Pi$. This becomes efficient only *below*

$$T_{\rm fr} \sim \epsilon^{6m-4} M_{\rm pl}/g_*^{\frac{1}{2}} \lesssim 10^{-7} \text{ eV} , \tag{3.14}$$

for $(n, n-1)$ theories, and therefore does not produce significant recoupling.

3.3 Warm Dark Matter

3.3.1 Non-Thermal WDM

The moral of the above analysis is that approximately below the TeV scale, the SM, CHS and EHS are decoupled. From Table. 3.2, confinement of the CHS also occurs at latest at the TeV scale. As a result, we may imagine a scenario in which the post-inflation reheating temperature $T_{\rm rh} <$ TeV. In this case, the sterile Dirac neutrinos ν^d might never be in thermal contact with the SM plasma, and therefore be produced non-thermally through the (non)-resonant production mechanism [42, 43, 44, 52], forming the WDM.

As can be seen in Fig. 3.1, the predicted (m_d, θ_d) values fall outside the $\Omega_d > \Omega_{\rm DM}/2$ non-resonant production region, which itself is ruled out by the combination

of Lyman-α [83, 66] and x-ray flux bounds [65, 54]. However the (m_d, θ_d) ranges still overlap an allowed window for full WDM resonant production if there is a sufficiently large lepton asymmetry [44, 51, 52, 35, 54]. Alternatively, in this low reheat scenario, coupling of the sterile neutrinos to the inflaton – an SM singlet – could result in significant non-thermal WDM production from its decay [69, 70], with the remaining fraction (if any) produced by non-resonant production.

Just as for exotic x-ray decay channels, the chiral structure of the SM, CHS and EHS generically suppresses the operators that may produce non-thermal sterile neutrino WDM from SM decays. For example, from eqs. (3.6) and (3.8) it is clear that Higgs to sterile neutrino decay rate is suppressed by $\epsilon^{3m} \sim (m_l/v)^2$ for $(n, n-1)$ theories, so there is no significant production from the Higgs decay channel. Along similar lines to the inflaton scenario, one might putatively extend the Higgs sector with a SM singlet that can decay to the EHS without such suppression (see e.g. [84, 85]), however we do not make any such assumptions about the SM Higgs sector here.

One might also consider production via lepton or hadron decays such as $\tau \to e\xi\xi$ or $B \to K\xi\xi$ respectively. The chiral structure ensures such processes can only be mediated by operators of the form

$$\frac{\lambda_{ij}}{M^2}\bar{q}^i\gamma^\mu q^j\bar{\xi}\gamma_\mu\xi \ . \tag{3.15}$$

This type of operator necessarily produces FCNCs, too, but the large mediator scale M easily evades the present bounds for quark FCNCs [3]. One finds for the dominant top decay process $\Gamma/H(m_t) \lesssim 10^{-4}$. For semi-relativistic tops in thermal equilibrium, this produces a sterile neutrino energy fraction $\Omega_d \sim 1\%\ \Omega_{\rm DM}$, so that this production channel can be neglected. Similarly, production from spin-1 bound state decays like $\rho_0 \to \xi\xi$ is negligible due to suppression of the rate by a $(\Lambda_{\rm qcd}/M)^4$

factor.

3.3.2 Thermal WDM

The $(3, 2)$ theory exhibits the interesting feature that the decoupling temperature of the EHS, T_d, the confinement temperature of the CHS, $T_c \sim \Lambda$, and decoupling of temperature the CHS, T_χ, all occur at the TeV scale. In contrast to the non-thermal resonant scenario, for a $(3, 2)$ theory one may plausibly consider a scenario in which all three sectors are initially in thermodynamic equilibrium, the lepton asymmetry is small, and

$$T_d > T_c > T_\chi \ . \tag{3.16}$$

In this scenario, the EHS fermions ξ freeze-out ultra-relativisitically before confinement, and there is no subsequent resonant production: from Fig. 3.1 we see that fractional non-resonant production at the 10% $\Omega_{\rm DM}$ level may still occur, but we shall neglect this henceforth as it is a subdominant contribution. Defining $Y \equiv n/s$ – the ratio of the comoving number density and entropy density – then for each *Dirac* ξ species

$$Y_\xi = \frac{135\zeta(3)}{2\pi^4}\frac{1}{g^d_{*\rm S}} \ , \tag{3.17}$$

where $g^d_{*\rm S}$ is entropic effective equilibrium number of degrees of freedom at freeze-out.

Even if only one species of ξ – the Dirac $\xi_{R,L}$ – obtains a mass m_d, which we assume henceforth, such a Y_ξ leads to over-closure unless $g^d_{*\rm S} \sim 10^4$. This is unnaturally large since $g_{*\rm S} \sim 10^2$ for the SM at this scale. However, if after freeze-out the entropy increases by a factor γ, then the frozen out species are diluted, $Y_\xi \to Y_\xi/\gamma$. The present-day energy fraction for the Dirac ν^d, which are

an admixture dominantly composed of $\xi_{R,L}$, is then

$$\frac{\Omega_d}{\Omega_{\rm DM}} \simeq \frac{Y_\xi m_d s_0}{\rho_c \Omega_{\rm DM}} = \frac{1.1\times 10^4}{g^d_{*\rm S}\gamma}\left(\frac{m_d}{5\ {\rm keV}}\right)\ , \tag{3.18}$$

in which we used $s_0 \simeq 2.89\times 10^3\ {\rm cm}^{-3}$, $\rho_c \simeq 10.5h^2{\rm cm}^{-3}{\rm keV}$, and $\Omega_{\rm DM} = 0.105h^{-2}$. It is clear that we need $g^d_{*\rm S}\gamma \gtrsim 10^4$ for a DM candidate.

3.3.3 Supercooled Confinement

The ordering (3.16) permits us to consider the confinement of the CHS as the source of entropy that dilutes Y_ξ after freeze-out. The entropy production from a confinement-induced first-order phase transition can be significant if it occurs suddenly after supercooling [86, 87]. That is, if the confinement phase transition (CPT) begins at a cooler temperature $T_i < T_c$, and the duration of the transition $\tau_c \ll 1/H(T_i)$, the Hubble time at temperature T_i.

Before confinement – at temperature T_i – and after confinement – at temperature $T_f > T_\chi$ –, we suppose that we have equilibrium plasmas. By construction

$$\begin{aligned} g_{*\rm S}(T_i) &\equiv g^i_{*\rm S} = g^{\rm SM}_{*\rm S} + g^{\rm c}_{*\rm S} \simeq 2\times 10^2\ , \\ g_{*\rm S}(T_f) &\equiv g^f_{*\rm S} \equiv g^{\rm SM}_{*\rm S} + g^{\rm bs}_{*\rm S} \simeq 10^2\ . \end{aligned} \tag{3.19}$$

Here $g^{\rm SM}_{*\rm S}$, $g^{\rm c}_{*\rm S}$ and $g^{\rm bs}_{*\rm S}$ denote the effective equilibrium relativistic degrees of freedom in the SM, CHS and the bound states. By construction, for three n_R we have $g^{\rm bs}_{*\rm S} = 2\cdot 3\cdot (7/8) + N_\Pi$ with N_Π the number of hidden pions. We have assumed $g^{\rm bs}_{*\rm S} \sim 10$ and $g^{\rm SM}_{*\rm S},\ g^{\rm c}_{*\rm S} \simeq 10^2$. Note that since the frozen out $\xi_{L,R}$ have only four degrees of freedom, then $g^d_{*\rm S} \simeq g^i_{*\rm S}$.

Since $T_f > T_\chi$, then such entropy production leads to reheating of *both* the CHS and SM, because they only decouple later at T_χ. This mutual reheating means the

present DM temperature, T_d^0, compared to that of the active neutrinos, T_ν^0, is just

$$\frac{T_d^0}{T_\nu^0} = \left(\frac{g_{*_S}^f}{\gamma g_{*_S}^d}\frac{g_{*_S}^\nu}{g_{*_S}^{\rm SM}}\right)^{1/3} \simeq \left(\frac{10.75}{1.1\times 10^4 (m_d/5\text{ keV})}\right)^{1/3} , \tag{3.20}$$

from eq. (3.18) and since $g_{*_S}^f \simeq g_{*_S}^{\rm SM}$. Equation (3.20) implies the entropy-diluted thermal WDM is red-shifted compared to the active neutrino plasma. The Lyman-α bounds [83, 66, 71] require non-resonantly produced WDM – at present temperature T_ν^0 – to satisfy $m_{\rm nrp} > 10$ keV. Since the free-streaming length $\lambda_{\rm FS} \propto T/m$ (see e.g. [35]), this Lyman-α bound translates to $m_d > 10(T_d^0/T_\nu^0)$ keV. Together with eq. (3.20) we find that thermally produced ν^d may safely avoid the Lyman-α bound, provided

$$m_d > 1.5 \text{ keV} . \tag{3.21}$$

This is the Lyman-α bound displayed in Fig. 3.1.

Note also that the n_R and hidden pion contribution to the effective number of neutrino degrees of freedom, $\delta N_\nu^{\rm eff}$, at the big-bang nucleosynthesis (BBN) epoch is

$$\delta N_\nu^{\rm eff} = (8/14) g_{*_S}^{\rm bs} \left(g_{*_S}^\nu / g_{*_S}^{\rm SM}\right)^{4/3} \lesssim 0.26 (g_{*_S}^{\rm bs}/10) . \tag{3.22}$$

It is amusing to note that the right-handed neutrinos together with the hidden pions can supply sufficient effective degrees of freedom at the BBN epoch to significantly contribute to the observed $\delta N_\nu^{\rm eff} \sim 1$ excess (see e.g [88, 89]). In contrast, this is difficult to achieve with seesaw models, or even ad hoc Dirac neutrino models.

3.3.4 Entropy Production Estimate

The massive bound states typically have masses $x\Lambda$, with $x \gtrsim 1$, so they are non-relativistic. Their corresponding widths are generically also $\Gamma \sim \Lambda$. This

leads to $\Gamma/H(T_i) \sim M_{\rm pl}\Lambda/T_i^2 \ggg 1$. In contrast, the longest-lived heavy bound state we could contemplate decays only via exchange of an M-scale boson, like the electroweak decay of the Λ^0 baryon of QCD. In this case, the decay rate is $\Gamma \sim \Lambda x^5 \epsilon^4$. For the $(3,2)$ theory $\epsilon \sim 10^{-4}$, so that $\Gamma/H(T_i) \gtrsim x^5\epsilon^4 M_{\rm pl}\Lambda/T_i^2 \gg 1$. This means that even for a sudden CPT, the heavy bounds states all decay within τ_c and generically, predominantly produce hidden pions and n_R with energies $\sim T_c$. It seems reasonable, then, to treat the CPT as a quasiequilibrium process, in which the non-relativistic heavy bound states have exponentially suppressed number and energy densities, while pions and n_R are thermal with temperature T_c.

With this in mind, one can estimate the amount of entropy production by treating the CPT as a first-order phase transition in $g_{*\rm S}$, as a function of $\zeta \equiv (RT)^3$. Here R is the universe scale factor and T the equilibrium temperature. The picture is that confinement begins at supercooled plasma temperature T_i, and suddenly produces the relativistic pions and n_R at temperature T_c, so that $g_{*\rm S}$ undergoes a jump at $\zeta_i = (R_i T_i)^3$ from $g^i_{*\rm S}$ to

$$g^{f\prime}_{*\rm S} = g^{\rm SM}_{*\rm S} + g^{\rm bs}_{*\rm S}\big(T_c/T_i\big)^3 \ . \tag{3.23}$$

This expression for $g^{f\prime}_{*\rm S}$ follows just from the definition $g_{*\rm S}(T) \equiv \sum_\alpha g^\alpha_{*\rm S}(T_\alpha/T)^3$, a sum over species at different temperatures. After the phase transition, the plasma undergoes an adiabatic thermalization until $g_{*\rm S} = g^f_{*\rm S}$ and $T = T_f$. SM-CHS decoupling at T_χ follows thereafter. Figure 3.2 shows this history.

Provided $(T_c/T_i)^3 \gg g^{\rm SM}_{*\rm S}/g^{\rm bs}_{*\rm S} \sim 10$, the entropy production estimate from eq. (3.23) is then

$$\gamma \equiv \frac{S_f}{S_i} = \frac{g^{f\prime}_{*\rm S}\zeta}{g^i_{*\rm S}\zeta} \simeq \frac{g^{\rm bs}_{*\rm S}}{g^i_{*\rm S}}\left(\frac{T_c}{T_i}\right)^3 \ . \tag{3.24}$$

The important feature of this naïve estimate is the $(T_c/T_i)^3$ dependence of the

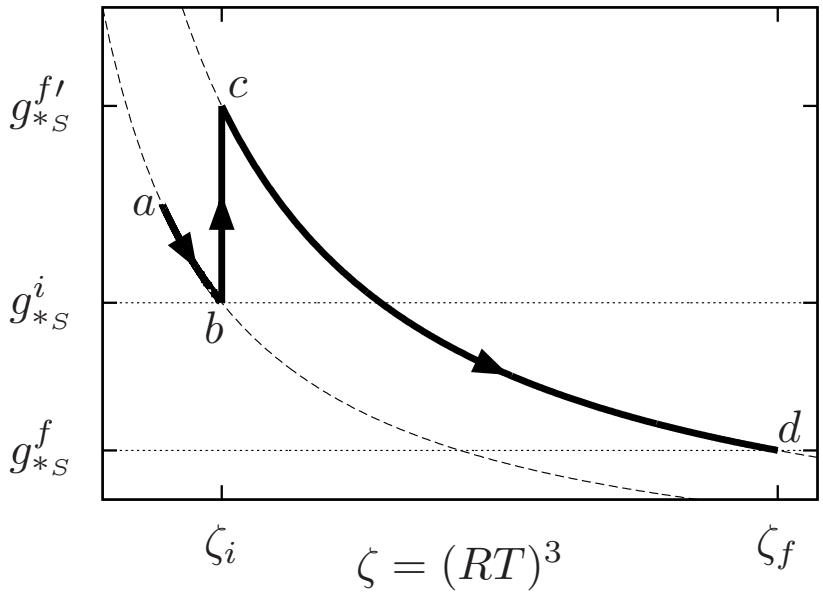

Figure 3.2: A sketch of the thermal history. Species freeze-out (a-b) along the S_i adiabat (lower dashed), is followed by the CPT (b-c), which is a first-order $g_{*\mathrm{S}}$ phase transition in ζ. The CPT is followed by thermalization (c-d) along the S_f adiabat (upper dashed) until $g_{*\mathrm{S}} = g^f_{*\mathrm{S}}$ at which $T = T_f$. Once $T = T_\chi$, the CHS and SM decouple.

entropy production. A more careful treatment in Ref. [86] produces the result

$$\gamma \simeq \frac{1}{r}\left(\frac{r-1}{3}\right)^{3/4}\left(\frac{T_c}{T_i}\right)^3 , \qquad r \equiv \frac{g^i_{*\mathrm{S}}}{g^f_{*\mathrm{S}}} . \tag{3.25}$$

One also finds $T_f = [(r-1)/3]^{1/4} T_c$. Using this result and eq. (3.18), and fixing $r = 2$, it follows that for $\Omega_d \leq \Omega_{\mathrm{DM}}$ (i.e. $\gamma g^d_{*\mathrm{S}} \geq 1.1 \times 10^4 m^d/5$ keV) we require

$$\frac{T_c}{T_i} \geq 6.3\left(\frac{2\times 10^2}{g^d_{*\mathrm{S}}}\right)^{1/3}\left(\frac{m_d}{5\text{ keV}}\right)^{1/3} . \tag{3.26}$$

Note $T_f = 0.76 T_c$ here, so it is plausible that $T_f > T_\chi$. By comparison to eq. (3.26), the QCD maximal supercooling is $T_c/T_i \simeq 1.7$ [86]. However, given that this upper bound will be sensistive e.g. to the tunneling probabilities between the metastable (G_{F} symmetric) and stable (G'_{F} symmetric) vacua, the degree of supercooling required in this estimate is not implausible.

3.4 Conclusions

Within the composite neutrino framework, we have shown in this chapter that keV sterile Dirac neutrinos can be naturally produced with mixing angles appropriate for non-thermal resonant production, provided the composite neutrinos are all comprised of n preons and the scalar condensate vev has $n-1$ of them. Alternatively, for a $(3,2)$ theory, a single keV sterile Dirac neutrino species could be WDM produced by entropy-diluted ultrarelativistic freeze-out. In this latter case the entropy can be provided by a supercooled confinement-induced phase transition.

CHAPTER 4

FLAVOR OSCILLATION FROM THE TWO-POINT FUNCTION

Based on the 2011 article "Flavor Oscillation from the Two-Point Function", written in collaboration with Mario Martone and published in Phys. Rev. D 85, 045006 (2012).

4.1 Introduction

The phenomenon of flavor oscillation plays an important role in the physics of neutral meson and neutrino systems. In particular, flavor oscillation provides the only means to measure the extremely small mass and decay rate splittings among the neutral mesons, and also provides convincing evidence for the existence of non-zero neutrino masses. The theoretical descriptions of flavor oscillation fall into several categories, including the basic plane wave Pontecorvo formalism [90, 91], intermediate [92, 93, 94, 95, 96, 97, 98, 99, 100, 101, 102] and external [103, 104, 105, 106, 107, 108, 109, 110] wavepacket approaches and quantum field theoretic results [111, 112, 113, 114, 115, 116, 117, 118, 119, 120]. Some detailed reviews of these approaches, their underlying assumptions, results and difficulties can be found in Refs. [121, 91, 122, 123] (and references therein). To be very brief: In the first, one assumes the flavor states are unitary combinations of plane-wave mass eigenstates that follow spacetime worldlines, and one must carefully define the proper times of the mass eigenstates in order to obtain the well-known Pontecorvo oscillation formula. The intermediate wavepacket approach treats the oscillating degrees of freedom as a linear combination of one-particle states, while the external wavepacket approach treats the oscillating particles as quantum fields, whose propagator is convolved with wavepackets at the source and detector.

A large amount of Literature has been devoted to deriving, studying and comparing oscillation formulae within these different approaches. Particular care has been taken to include important effects such as measurement uncertainties, coherence effects, the finite size of the detector and source, all of which together lead to somewhat complicated formulae. Our goal in this paper is less ambitious: Using a quantum field theoretic approach, we present a simple formalism of oscillation

based entirely on the properties of the *spatially* Fourier transformed propagator. We call this the spatial two-point function. The resulting oscillation formulae are particularly elegant, and precisely reproduce both the Pontecorvo neutrino result and (CP violating) neutral meson mixing results (see e.g. Ref. [124, 125]) in appropriate parameter regimes.

To construct this formalism, we assume that the oscillation experiment measures the exchanged energy E and source-detector displacement $\boldsymbol{L}$ to infinite precision, along with flavor at both the source and detector. This is possible because E, $\boldsymbol{L}$ and flavor are commuting observables, so that an amplitude which depends exclusively on these quantities is well-defined. The key idea is that the spatial two-point function $\Delta(E, \boldsymbol{L})$ in the flavor basis is a well-defined amplitude which encodes flavor oscillation over a displacement $\boldsymbol{L}$ at energy E. We therefore assume that the experiment amplitude is proportional to $\Delta(E, \boldsymbol{L})$ and explore the resulting oscillation formulae. The advantages of this description are: There is no ambiguity in the choice of reference frame - all computations are done in the lab frame and one never needs to introduce proper times into the formalism; the oscillation probabilities can be computed exactly; and one obtains formulae whose physical meaning can be easily discerned in various limits. Since we do neglect several real physical effects mentioned above — in particular the physics of the source and detector are neglected — the limits of the applicability of our theoretical description to actual oscillation experiments should be carefully examined. Nonetheless, we believe this approach provides an instructive, leading order description of the physics of oscillation in real experiments.

In terms of the previous Literature on this subject, our approach is best categorized as a special case of the above-mentioned external wavepacket formalism

with stationary states [105]. However, to our knowledge, the oscillation physics contained just in the two-point function has not been thoroughly investigated and the resulting general oscillation formulae for unstable particles obtained by our approach have not been previously presented. One exception is Ref. [111], whose amplitudes for stable fermions agree with our results for the special case of stable particles.

This paper is structured as follows. In Section 4.2 we present the oscillation formalism. In Section 4.3 the exact spatial two-point function $\Delta(E, \boldsymbol{L})$ for unstable fields is presented, and the exact oscillation probabilities and integrated oscillation probabilities are computed. In Section 4.4 we examine our results in several different parameter regimes and recover both the neutral meson-mixing results and Pontecorvo neutrino oscillation results in appropriate limits.

4.2 Formalism

4.2.1 Experiment Amplitude

Our starting point is to consider an experiment which involves the propagation between a source and a detector of a set of fields $\{\phi^\alpha\}$, which are allowed to mix. As usual, α is an experimentally measurable label called the flavor, which is henceforth always denoted by a Greek index. The set $\{\phi^\alpha\}$ is called the flavor field basis.

In this paper we assume the $\alpha \to \beta$ oscillation experiment measures the exchanged energy E and source-detector displacement $\boldsymbol{L}$ to infinite precision in the

lab frame. The amplitude for the experiment must then have the form

$$\mathcal{M} = \mathcal{M}_{\alpha\beta}(E, \boldsymbol{L}) \ . \tag{4.1}$$

This is a well-defined amplitude since E, $\boldsymbol{L}$ and flavor are commuting observables. Note that as a consequence of the infinitely precise E and $\boldsymbol{L}$ measurement neither the time of travel nor the three-momentum between the source and detector is well-defined, because these observables do not commute with E and $\boldsymbol{L}$ respectively. In other words the initial and final states of this amplitude must be energy-spatial eigenstates, rather than momentum-time eigenstates.

The key idea of this paper rests on the observation that the time Fourier-transformed time-ordered exact two-point function — the spatial two-point function — defined by

$$\Delta_{\alpha\beta}(E, \boldsymbol{L}) \equiv \int dt \Big\langle T\Big\{\phi^{\beta}(t, \boldsymbol{L})\phi^{\alpha\dagger}(0, \boldsymbol{0})\Big\}\Big\rangle e^{iEt} \ , \tag{4.2}$$

is the field theoretic object which encodes the oscillation of flavor $\alpha \to \beta$ over a displacement $\boldsymbol{L}$ with energy E. (As usual $\langle T\{\phi^{\beta}(x)\phi^{\alpha\dagger}(y)\}\rangle \equiv \Delta_{\alpha\beta}(x-y)$ is a function of $x-y$ due to translation invariance.) It is therefore natural to write

$$\mathcal{M}_{\alpha\beta}(E, \boldsymbol{L}) = \mathcal{A}_{\rm S}^{\alpha}\mathcal{A}_{\rm D}^{\beta}\Delta_{\alpha\beta}(E, \boldsymbol{L}) \ , \tag{4.3}$$

(no sum over α, β) where $\mathcal{A}_{\rm S,D}^{\alpha}$ encode the physics of the source and detector, which we have assumed factorizes out of the amplitude[1]. Assuming $\mathcal{A}_{\rm S,D}^{\alpha}$ are known, the implication of Eq. (4.3) is that $|\Delta_{\alpha\beta}(E, \boldsymbol{L})|^2$ is a measurable quantity, from which we may proceed to construct oscillation probabilities.

So far we have not specified the spin of ϕ^{α}. As is well-known, if ϕ^{α} are massive they must create spin-j particles, with j a half-integer, which have $2j+1$ spin

[1]The general criteria under which such a factorization may be possible in real oscillation experiments has been examined previously in detail (see e.g. Ref. [123]). Foregoing such a discussion, our intent here is that the physics of the source and detector can be neglected up to their ability to distinguish flavor.

degrees of freedom. We assume that these spin degrees of freedom decouple, so that we need only consider scalar propagators henceforth.

4.2.2 Oscillation Probability

Having written down the amplitude for the experiment, we now define the flavor oscillation probability via

$$P_{\alpha\to\beta}(E,\boldsymbol{L}) \equiv \frac{\left|\Delta_{\alpha\beta}(E,\boldsymbol{L})\right|^2}{\sum_\gamma \left|\Delta_{\alpha\gamma}(E,\boldsymbol{L})\right|^2} \ . \tag{4.4}$$

Here $P_{\alpha\to\beta}$ forms a well-defined probability distribution, since $P_{\alpha\beta} \geq 0$ and $\sum_\beta P_{\alpha\beta} = 1$. In some experiments, measurement of $|\Delta_{\alpha\beta}|^2$ at a precise $\boldsymbol{L}$ is replaced by a volume-averaged measurement,

$$\mathcal{A}^{\rm I}_{\alpha\beta}(E) \equiv \int d^3\boldsymbol{L} \left|\Delta_{\alpha\beta}(E,\boldsymbol{L})\right|^2 \ . \tag{4.5}$$

This is equivalent to the time-averaged amplitudes measured in e.g. meson mixing experiments, in which the initial and final flavor states are determined by tagging via decay products (see e.g. Ref. [124, 125]). We can correspondingly define an integrated oscillation probability

$$P^{\rm I}_{\alpha\to\beta}(E) \equiv \frac{\mathcal{A}^{\rm I}_{\alpha\beta}(E)}{\sum_\gamma \mathcal{A}^{\rm I}_{\alpha\gamma}(E)} = \frac{\int d^3\boldsymbol{L} \left|\Delta_{\alpha\beta}(E,\boldsymbol{L})\right|^2}{\sum_\gamma \int d^3\boldsymbol{L} \left|\Delta_{\alpha\gamma}(E,\boldsymbol{L})\right|^2} \ . \tag{4.6}$$

This is also a well-defined probability distribution.

4.2.3 Propagator and 1PI Basis

So far in this paper we have formulated a description of flavor oscillation in terms of just the exact quantum amplitude $\Delta(E,\boldsymbol{L})$, which is equivalently defined as the

spatial Fourier transform of the exact propagator, $\Delta(p^2)$. Explicitly,

$$\Delta_{\alpha\beta}(E, \boldsymbol{L}) = \int \frac{d^3\boldsymbol{p}}{(2\pi)^3} \Delta_{\alpha\beta}(p^2) e^{i\boldsymbol{p}\cdot\boldsymbol{L}} \ . \tag{4.7}$$

Applying external field methods to the path-integral formulation of quantum field theory, it is a well-known result (see e.g. [126, 127]) that for a set of N fields $\{\phi^\alpha\}$ the exact two-point function is the inverse of the exact two-point one-particle-irreducible (1PI) function: $\Delta_{\alpha\beta}(x-y) = -\Pi^{-1}_{\alpha\beta}(x-y)$. The Fourier transform of this result is

$$\Delta_{\alpha\beta}(p^2) = \left[\frac{i}{p^2\mathbf{1} - M^2(p^2)}\right]_{\alpha\beta} \ . \tag{4.8}$$

Henceforth we shall call the $N \times N$ matrix of functions $M^2(p^2)$ the exact two-point 1PI function.

In general, one cannot compute the exact propagator $\Delta(p^2)$ exactly for all p^2. However, the combination of Eqs (4.7) and (4.8) suggests that the exact spatial two-point function is sensitive only to the pole structure of $\Delta(p^2)$. As we shall see below, with suitable assumptions this pole structure depends only on physical masses and rest frame decay rates, permitting us to construct exact oscillation probabilities in terms of just these measureable quantities, E, $\boldsymbol{L}$, and a mixing matrix, despite our incomplete knowledge of the exact propagator.

Now, the exact propagator (4.8) is generally not diagonal in flavor space — there would be no oscillation if this were the case — but the analytic structure of $\Delta(p^2)$ is greatly simplified if the exact propagator can be diagonalized. Ultimately, we want to be able to write

$$\Delta_{\alpha\beta}(p^2) = U^{\alpha j}(U^{-1})^{j\beta}\Delta_j(p^2) \ , \qquad \Delta_j(p^2) \equiv \frac{i}{p^2 - M_j^2(p^2)} \ , \tag{4.9}$$

so that

$$\Delta_{\alpha\beta}(E,\boldsymbol{L}) = U^{\alpha j}(U^{-1})^{j\beta}\Delta_j(E,\boldsymbol{L}) \ , \qquad \Delta_j(E,\boldsymbol{L}) \equiv \int \frac{d^3p}{(2\pi)^3}\frac{ie^{i\boldsymbol{p}\cdot\boldsymbol{L}}}{p^2 - M_j^2(p^2)} \ . \tag{4.10}$$

In Eq. (4.9), U is the constant and possibly unitary matrix that diagonalizes $\Delta(p^2)$ (equivalently $M^2(p^2)$), and $M_j^2(p^2)$ are the N eigenvalues of $M^2(p^2)$. Below we'll see that the $M_j(p^2)$ determine the physical masses and rest frame decay rates of the particles propagating in $\Delta_{\alpha\beta}(p^2)$.

In constrast to the usual diagonalization of the classical Lagrangian mass terms, diagonalization of the exact propagator may be non-trivial. In Appendix B.1 we discuss the details of the diagonalization of $\Delta(p^2)$, the properties of U and how this exact quantum formalism both relates to and differs from the usual classical mixing matrix formalism. For our purposes here, we assume $\Delta(p^2)$ is diagonalizable in the manner of Eq. (4.9). Unless otherwise stated, we also assume U is unitary. An immediate consequence of unitarity is that spatial two-point function can now be written as

$$\Delta_{\alpha\beta}(E,\boldsymbol{L}) = U^{\alpha j}U^{\beta j*}\Delta_j(E,\boldsymbol{L}) \ . \tag{4.11}$$

Let us now define the 1PI basis. This basis is a generalization of the mass basis derived in the classical formalism, that may accommodate both unstable particles and a description of CP violation for two flavors. In particular, if U is constant (but not necessarily unitary), then there exists a well-defined second basis of fields $\{\phi^j\}$, henceforth denoted by a Latin index, which are defined via the linear transformations

$$\phi^{\alpha\dagger} = U^{\alpha j}\phi^{j\dagger} \ . \tag{4.12}$$

Note that $\phi^\dagger$ creates a particle state, while ϕ creates an anti-particle state: We have chosen this definition of basis change by U in order that it coincides with

the usual definition in terms of one-particle quantum states. We call ϕ^j the 1PI basis for the following reason. If U is unitary, then observe that not only $M^2(p^2)$ but also the two-point function is diagonal, i.e. $\langle T\{\phi^i(x)\phi^{j\dagger}(y)\}\rangle = \delta_{ij}\Delta_j(x-y)$. This implies that $M_j^2(p^2)$ is the 1PI function for ϕ^j, whence the name. In contrast, if U is not unitary, then even though $M^2(p^2)$ is still diagonalized by U, we have $\langle T\{\phi^i(x)\phi^{j\dagger}(y)\}\rangle \neq \delta_{ij}\Delta_j(x-y)$. Therefore $M_j^2(p^2)$ is no longer the 1PI function for ϕ^j. Nonetheless, we shall always refer to the field basis defined by Eq. (4.12) to be the 1PI basis, and often call $\phi^{j\dagger}$ the 1PI states.

Tying the diagonalization of the exact propagator and the definition of 1PI basis together, we can now explain why we have taken care to consider the case of non-unitary U: We do so to accommodate CP-violating two-flavor neutral meson oscillations (for three or more flavors, even unitary U may have a CP-violating phase), which we consider in Sec. 4.3.4. The idea is that the Hamiltonian for such a system is diagonalized by a constant non-unitary matrix [125, 124], so we therefore expect U to be non-unitary too. In this context the flavor field basis (1PI basis) then corresponds to the CP conjugate states (evolution eigenstates). One deduces U is a particular constant 2×2 non-unitary matrix, from which we can immediately derive the usual oscillation formulae.

4.2.4 Exact Propagator Analytic Structure

Let us finally examine the analytic structure of $\Delta_j(E, \boldsymbol{L})$, which is explicitly

$$\Delta_j(E, \boldsymbol{L}) = \int \frac{d^3p}{(2\pi)^3} \frac{ie^{i\boldsymbol{p}\cdot\boldsymbol{L}}}{p^2 - M_j^2(p^2)} \ . \tag{4.13}$$

If ϕ^j is unstable, then the propagator $\Delta_j(p^2)$ will have a unique Breit-Wigner or resonance pole, which by convention is a simple pole located at

$$p^2 = m_j^2 - im_j\Gamma_j \ . \tag{4.14}$$

Here m_j is the physical mass and $\Gamma_j \geq 0$ is the rest frame decay rate. The non-zero imaginary part for this pole enforces the usual Feynman pole prescription and associated time-ordering, so that we need not add the usual $i\epsilon$ convergence term in the denominator of Eq. (4.13), provided we assume $\Gamma_j \neq 0$. Consequently, taking the $\Gamma_j \to 0^+$ limit, which corresponds to ϕ^j being stable, can only be performed after all integrations and other limits are evaluated.

By definition there are no higher order poles in $\Delta_j(p^2)$ and the residue at the pole (4.14) is unity: Eq. (4.14) and this latter condition are equivalent to $M_j^2(m_j^2 - im_j\Gamma_j) = m_j^2 - im_j\Gamma_j$ and $M_j^{2\prime}(m_j^2 - im_j\Gamma_j) = 0$ respectively.

4.3 Exact Oscillation Probability

4.3.1 Spatial Two-Point Function

Computation of the oscillation probabilities (4.4) and (4.6) boils down to computing the spatial two-point function $\Delta_j(E, \boldsymbol{L})$. As shown in Appendix B.2, the integral (4.13) can be performed exactly, with final result (B.12)

$$\Delta_j(E, L) = \frac{i}{4\pi L} \exp\left\{ \frac{i}{\sqrt{2}}\left[\sqrt{R_j^2 + A_j^2} + R_j\right]^{1/2} L - \frac{1}{\sqrt{2}}\left[\sqrt{R_j^2 + A_j^2} - R_j\right]^{1/2} L \right\} . \tag{4.15}$$

in which

$$R_j \equiv E^2 - m_j^2 \ ,$$
$$A_j \equiv m_j \Gamma_j \ . \tag{4.16}$$

Note that the exact result in Eq. (4.15) is independent of the orientation of $\boldsymbol{L}$.

4.3.2 Exact Probabilities

We may now compute the exact oscillation probability via application of Eqs. (4.4), (4.10) and (4.15), and the exact integrated oscillation probability via Eqs. (4.6), (4.10) and (4.15). It is convenient to define the wavenumber and characteristic inverse decay lengths

$$\omega_j \equiv \frac{1}{\sqrt{2}} \left[\sqrt{R_j^2 + A_j^2} + R_j \right]^{1/2} \ ,$$
$$\zeta_j \equiv \frac{1}{\sqrt{2}} \left[\sqrt{R_j^2 + A_j^2} - R_j \right]^{1/2} \ , \tag{4.17}$$

along with

$$\Delta\omega_{jk} \equiv \omega_j - \omega_k \ , \qquad \Delta\zeta_{jk} \equiv \zeta_j - \zeta_k \ , \qquad \bar{\zeta}_{jk} \equiv \zeta_j + \zeta_k \ . \tag{4.18}$$

We call $\Delta\omega_{jk}$ the oscillation wavenumber.

Exploiting the unitarity of U, one finds the exact oscillation probability

$$P_{\alpha\to\beta}(E,L) = \left\{ \sum_j |U^{\alpha j}|^2 |U^{\beta j}|^2 e^{-2\zeta_j L} + 2 \sum_{j<k} \mathrm{Re}\left[U^{\alpha j} U^{\beta j *} U^{\alpha k *} U^{\beta k} e^{i\Delta\omega_{jk} L} e^{-\bar{\zeta}_{jk} L} \right] \right\}$$
$$\times \left[\sum_j |U^{\alpha j}|^2 e^{-2\zeta_j L} \right]^{-1} \ . \tag{4.19}$$

For $\zeta_j \to 0^+$, this has the exact form of the Pontecorvo oscillation formula [90, 121]. We will show below that within a certain parameter regime, $\Delta\omega_{jk} \simeq (m_k^2 - m_j^2)/2E$,

recovering the usual result. The exact integrated oscillation probability is similarly

$$P^{\rm I}_{\alpha\to\beta}(E) = \left\{\sum_j |U^{\alpha j}|^2|U^{\beta j}|^2/2\zeta_j + 2\sum_{j<k}{\rm Re}\left[U^{\alpha j}U^{\beta j*}U^{\alpha k*}U^{\beta k}\frac{\bar\zeta_{jk}+i\Delta\omega_{jk}}{\bar\zeta^2_{jk}+\Delta\omega^2_{jk}}\right]\right\} \times\left[\sum_j |U^{\alpha j}|^2/2\zeta_j\right]^{-1}. \tag{4.20}$$

(The Δ_j normalization $i/4\pi L$ plays an important role in computing the integrals in Eq. (4.6).) Note that for both Eqs. (4.19) and (4.20) we have not assumed CP conservation.

4.3.3 Two-Flavor Formulae

It is particularly illuminating to present the oscillation probability and integrated oscillation probability for the case that there are just two flavors. In this case we can choose U to be real, orthogonal: The only physical parameter is the mixing angle and there is no CP violation. We adopt the convention for two flavors that $\alpha = +,-$ and $j = 1,2$. One obtains oscillation probability

$$\begin{aligned} P_{\alpha\to\beta}(E,L) = &\left\{|U^{\alpha1}|^2|U^{\beta1}|^2\right\}\left[|U^{\alpha1}|^2+|U^{\alpha2}|^2e^{-2\Delta\zeta_{21}L}\right]^{-1} \\ &+\left\{|U^{\alpha2}|^2|U^{\beta2}|^2\right\}\left[|U^{\alpha1}|^2e^{+2\Delta\zeta_{21}L}+|U^{\alpha2}|^2\right]^{-1} \\ &+\left\{2U^{\alpha1}U^{\beta1}U^{\alpha2}U^{\beta2}\cos(\Delta\omega_{12}L)\right\}\left[|U^{\alpha1}|^2e^{+\Delta\zeta_{21}L}+|U^{\alpha2}|^2e^{-\Delta\zeta_{21}L}\right]^{-1}. \end{aligned} \tag{4.21}$$

Assuming without loss of generality that $\Delta\zeta_{21} > 0$, then for $\Delta\zeta_{21}L \gg 1$, the first term is asymptotically constant, the second decays to zero while the third term produces a damped oscillation decaying to zero, with oscillation wavenumber $\Delta\omega_{12}$. In particular, for $\Delta\zeta_{21}L \gg 1$,

$$P_{\alpha\to\beta}(E,L) \simeq |U^{\beta1}|^2\ . \tag{4.22}$$

If we adopt the notation that $(\phi^\beta)^\dagger$ creates $|\beta\rangle$ and $(\phi^j)^\dagger$ creates $|j\rangle$, then the right side of Eq. (4.22) is nothing but $|\langle\beta|1\rangle|^2$. This is the probability of the β flavor state being measured as the $j = 1$ 1PI state, which has the longer decay length $1/\zeta_1 > 1/\zeta_2$. This behavior is familiar to that found in the K neutral meson system: Since the K_L eigenstate has a much longer decay length than the K_S, then the K_L will be exponentially more abundant at large distances from the source compared to the K_S state. As a result, at large distances there is no more oscillation and the oscillation probabilities $K \to K$ or $\overline{K} \to K$ both collapse to $|\langle K|K_L\rangle|^2$. This is exactly the behavior in Eq. (4.22).

Before presenting the two-flavor integrated oscillation probability, for convenience we first define

$$x \equiv \frac{\Delta\omega_{12}}{\bar{\zeta}_{12}} , \qquad y \equiv \frac{\Delta\zeta_{21}}{\bar{\zeta}_{12}} . \tag{4.23}$$

In Sec. 4.4.2 below we shall verify that x and y reduce to their usual definitions $x \simeq \Delta m/\bar{\Gamma}$ and $y \simeq \Delta\Gamma/2\bar{\Gamma}$ within a certain regime of the parameters E, $m_{1,2}$ and $\Gamma_{1,2}$. With the definitions (4.23), Eq. (4.20) reduces to

$$P^{\rm I}_{\alpha\to\beta}(E) = \left\{ |U^{\alpha1}|^2|U^{\beta1}|^2(1+y) + |U^{\alpha2}|^2|U^{\beta2}|^2(1-y) + 2U^{\alpha1}U^{\beta1}U^{\alpha2}U^{\beta2}\left[\frac{1-y^2}{1+x^2}\right]\right\} \times \left[1 + y\big(|U^{\alpha1}|^2 - |U^{\alpha2}|^2\big)\right]^{-1} . \tag{4.24}$$

4.3.4 CP Violation and Non-Unitary Diagonalization for Two Flavors

The above oscillation probabilities (4.19) and (4.20) (or (4.4) and (4.6)) may be generalized to the case that U is constant and non-unitary, which is applicable to the study of CP violation in two-flavor neutral meson mixing. In this context, we

identify the flavor fields $(\phi^{\pm})^\dagger$ as the creation operators of the CP conjugate states $|P^0\rangle$ and $|\overline{P^0}\rangle$, while the 1PI basis $(\phi^{1,2})^\dagger$ create the evolution eigenstates $|P_{L,H}\rangle$ respectively. Comparing Eq. (4.12) with the usual notation for $|P^0\rangle$ and $|\overline{P^0}\rangle$ in terms of $|P_{L,H}\rangle$ (assuming CPT symmetry)

$$\begin{aligned} |P^0\rangle &= \frac{1}{2p}\big(|P_L\rangle + |P_H\rangle\big) \ , \\ |\overline{P^0}\rangle &= \frac{1}{2q}\big(|P_L\rangle - |P_H\rangle\big) \ , \end{aligned} \tag{4.25}$$

then leads to the identification

$$U = \frac{1}{2pq} \begin{matrix} {\scriptstyle +} \\ {\scriptstyle -} \end{matrix} \overset{\begin{matrix} \quad 1 & \quad 2 \end{matrix}}{\begin{pmatrix} q & q \\ p & -p \end{pmatrix}} \ , \tag{4.26}$$

which is non-unitary for $|p/q| \neq 1$. As $|p/q| \neq 1$ is sufficient for CP violation in Eq. (4.25), the consequence of the identification (4.26) is that CP violation in two-flavor mixing is manifested as non-unitary diagonalization of the two-point function. Note also that if U is non-unitary then the 1PI states are no longer orthogonal, as expected for the evolution eigenstates $|P_{L,H}\rangle$. That is $\langle T\phi^i(x)\phi^{j\dagger}(y)\rangle \neq \delta_{ij}\Delta_j(x-y)$. From Eq. (4.9) we have for non-unitary U

$$\Delta_{\alpha\beta}(E,L) = U^{\alpha j}(U^{-1})^{j\beta}\Delta_j(E,L) \ , \tag{4.27}$$

and from Eqs. (4.15) and (4.17) one then finds exact amplitudes

$$\begin{aligned} \big|\Delta_{\pm\pm}(E,L)\big|^2 &= \frac{1}{32\pi^2 L^2} e^{-\bar{\zeta}_{12}L}\Big[\cosh(\Delta\zeta_{12}L) + \cos(\Delta\omega_{12}L)\Big] \ , \\ \big|\Delta_{+-}(E,L)\big|^2 &= \frac{|q|^2}{|p|^2}\frac{1}{32\pi^2 L^2} e^{-\bar{\zeta}_{12}L}\Big[\cosh(\Delta\zeta_{12}L) - \cos(\Delta\omega_{12}L)\Big] \\ &= \frac{|q|^4}{|p|^4}\big|\Delta_{-+}(E,L)\big|^2 \ . \end{aligned} \tag{4.28}$$

These strongly resemble the amplitudes found from the usual meson mixing quantum mechanical analysis (see below), except that here a spatial dependence has

replaced the usual time dependence and $\Delta\omega_{jk}$, $\Delta\zeta_{jk}$ and $\bar{\zeta}_{jk}$ have the form presented in Eq. (4.18). One finds exact integrated oscillation probabilities

$$\begin{aligned} P^{\rm I}_{+\to+} &= \frac{2+x^2-y^2}{2+x^2-y^2+\left|q/p\right|^2(x^2+y^2)} \ , \\ P^{\rm I}_{+\to-} &= \frac{x^2+y^2}{x^2+y^2+\left|p/q\right|^2(2+x^2-y^2)} \ , \end{aligned} \tag{4.29}$$

and one can also contemplate measuring the ratio of the amplitudes for oscillation into either flavor state

$$\begin{aligned} F \equiv \frac{\mathcal{A}^{\rm I}_{+-}(E)}{\mathcal{A}^{\rm I}_{++}(E)} &= \frac{\int {\rm d}L |\Delta_{+-}(E,L)|^2}{\int {\rm d}L |\Delta_{++}(E,L)|^2} \\ &= \left|\frac{q}{p}\right|^2 \frac{x^2+y^2}{2+x^2-y^2} \ . \end{aligned} \tag{4.30}$$

Let us compare the exact results in Eqs. (4.29) and (4.30) with the analogous formulae obtained via the usual quantum mechanical treatment of neutral meson oscillations. Following Refs. [124, 125] we can write down the time evolution for an initial pure $|P^0\rangle$ and $|\overline{P^0}\rangle$ state

$$\begin{aligned} |P^0(t)\rangle &= g_+(t)|P^0\rangle + \frac{q}{p}\, g_-(t)|\overline{P^0}\rangle \\ |\overline{P^0}(t)\rangle &= \frac{p}{q}\, g_-(t)|P^0\rangle + g_+(t)|\overline{P^0}\rangle \ , \end{aligned} \tag{4.31}$$

where

$$|g_\pm(t)|^2 = \frac{e^{-\bar{\Gamma}t}}{2}\Big[\cosh(\Delta\Gamma t/2) \pm \cos(\Delta m t)\Big] \ . \tag{4.32}$$

In the standard notation

$$x = \Delta m/\bar{\Gamma} \ , \qquad y = \Delta\Gamma/2\bar{\Gamma} \ , \tag{4.33}$$

where $\bar{\Gamma} = (\Gamma_1+\Gamma_2)/2$, the two formulae in Eqs. (4.29) should be compared with

$$\frac{\int_0^\infty {\rm d}t\ |\langle P^0|P^0(t)\rangle|^2}{\int_0^\infty {\rm d}t\ \Big[|\langle P^0|P^0(t)\rangle|^2 + |\langle\overline{P^0}|P^0(t)\rangle|^2\Big]} = \frac{2+x^2-y^2}{2+x^2-y^2+|q/p|^2(x^2+y^2)} \tag{4.34}$$

and

$$\frac{\int_0^\infty \mathrm{d}t\ |\langle\overline{P^0}|P^0(t)\rangle|^2}{\int_0^\infty \mathrm{d}t\ \left[|\langle P^0|P^0(t)\rangle|^2 + |\langle\overline{P^0}|P^0(t)\rangle|^2\right]} = \frac{x^2+y^2}{x^2+y^2+|p/q|^2(2+x^2-y^2)}\ . \quad (4.35)$$

Finally Eq. (4.30) should be compared to

$$\frac{\int_0^\infty \mathrm{d}t\ |\langle\overline{P^0}|P^0(t)\rangle|^2}{\int_0^\infty \mathrm{d}t\ |\langle P^0|P^0(t)\rangle|^2} = \left|\frac{q}{p}\right|^2 \frac{x^2+y^2}{2+x^2-y^2}\ . \quad (4.36)$$

Our exact results are in perfect agreement with those of the usual analysis, except that in Eqs. (4.29) and (4.30), the parameters x and y have the more general definitions encoded in Eqs. (4.16), (4.17) and (4.23). Once again, in Sec. 4.4.2 below we shall verify that x and y reduce to their usual definitions $x \simeq \Delta m/\bar{\Gamma}$ and $y \simeq \Delta\Gamma/2\bar{\Gamma}$ within a certain regime of the parameters E, $m_{1,2}$ and $\Gamma_{1,2}$.

Before proceeding, please note that the oscillation probabilities (4.19), (4.20), (4.21), (4.24) and (4.28) presented in this section are a function of only $\Delta\omega_{jk}$, $\Delta\zeta_{jk}$, $\bar{\zeta}_{jk}$ or ζ_j (of the latter three variables, only two are independent). Consequently, specifying just ω_j and ζ_j is sufficient to specify the oscillation probabilities. This shall be our practice throughout the remainder of this paper.

4.4 Regimes

The results presented in Sec. 4.3 are elegant and concise, but their physical interpretation is not obvious. However, in various regimes of the parameters E, m_j and Γ_j, our exact results for the wavenumber and characteristic inverse decay lengths ω and ζ reduce to simpler expressions with clear physical meanings. In this section we explore several different regimes of physical interest, and show that in certain regimes our results reproduce the well-known neutrino and neutral meson oscillation formulae.

4.4.1 Particle Regime

The first regime of interest is the case

$$R_j \gg A_j \ , \quad \text{i.e.} \quad E^2 - m_j^2 \gg m_j \Gamma_j \ . \tag{4.37}$$

It is straightforward to expand Eq. (4.17) about $A_j = 0$, and to leading order in A_j/R_j one obtains the wavenumber and characteristic inverse oscillation lengths

$$\omega_j \simeq \sqrt{E^2 - m_j^2} \ , \qquad \zeta_j \simeq \frac{m_j \Gamma_j}{2\sqrt{E^2 - m_j^2}} \ . \tag{4.38}$$

The oscillation probabilities (4.19) and (4.20) follow immediately from this and Eqs. (4.18), as do their two-flavor versions (4.21) and (4.24). In particular, in this regime we have to leading order in A_j/R_j

$$x \simeq 2\frac{\sqrt{R_1} - \sqrt{R_2}}{A_1/\sqrt{R_1} + A_2/\sqrt{R_2}} \ , \qquad y \simeq \frac{A_1/\sqrt{R_1} - A_2/\sqrt{R_2}}{A_1/\sqrt{R_1} + A_2/\sqrt{R_2}} \ . \tag{4.39}$$

In this regime, the spatial two-point function for a 1PI state

$$\Delta_j(E, L) \simeq \frac{i}{4\pi L} \exp\left\{ i\sqrt{E^2 - m_j^2} L - \frac{m_j \Gamma_j}{2\sqrt{E^2 - m_j^2}} L \right\} \ . \tag{4.40}$$

For $\Gamma_j \to 0^+$, this looks precisely like the propagator of an on-shell one-particle state with momentum $p = (E^2 - m_j^2)^{1/2}$. We therefore call the regime (4.37) the particle regime. The resemblance of the amplitude (4.40) to that of a particle suggests that we should obtain both the neutrino and meson mixing oscillation formula within the particle regime. We explicitly verify this in the next two sections.

The physical meaning of the spatial two-point function perhaps becomes more clear if we define analogous Lorentz factors and proper time

$$\gamma_j = E/m_j \ , \qquad \beta_j = \sqrt{1 - m_j^2/E^2} \ , \qquad \tau_j = L/\gamma_j \beta_j \ . \tag{4.41}$$

Substituting these into Eq. (4.40) we obtain the spatial two-point function in terms of τ_j instead of L, which we can interpret as a 'rest frame' propagator. Explicitly,

$$\Delta_j(\tau_j) \simeq \frac{i}{4\pi L} \exp\left\{ im_j(\gamma_j^2 - 1)\tau_j - \frac{\Gamma_j \tau_j}{2} \right\} . \tag{4.42}$$

The second term in the exponential looks like the usual rest frame decay of an unstable particle, and in particular it is clear that Γ_j can be interpreted as the rest frame decay rate. The first term looks like the usual proper time evolution of a particle, except for the $\gamma^2 - 1$ factor. This factor arises because pL is not a Lorentz invariant, but rather $E\gamma\tau - pL = m\tau$ is. It is a consequence of the experiment measure E rather than the time of transit between the source and detector.

Let us now proceed to verify that the usual neutrino and neutral meson mixing oscillation formulae are obtained in this particle regime.

4.4.2 Small Mass Splitting: Neutral Meson Oscillation

In all known neutral meson systems, the mass difference between the two mass eigenstates is extremely small in comparison with their masses. For the K, D, B_d and B_s neutral meson systems one finds [121]

$$\left(\frac{\Delta m}{m}\right)_K \sim \left(\frac{\Delta m}{m}\right)_D \sim 10^{-14} , \qquad \left(\frac{\Delta m}{m}\right)_{B_d} \sim 10^{-13} , \qquad \left(\frac{\Delta m}{m}\right)_{B_s} \sim 10^{-12} . \tag{4.43}$$

It seems then, that the appropriate regime for neutral meson oscillation is the particle regime with the additional constraint that the mass splitting is small. We define the mean mass m and mass splitting Δm via $m_1 = m + \Delta m/2$ and $m_2 = m - \Delta m/2$, so the small mass splitting limit is $\Delta m/m \ll 1$. We also define $y_0 \equiv \Delta\Gamma/2\bar{\Gamma}$, in which $\bar{\Gamma} \equiv (\Gamma_1 + \Gamma_2)/2$ and $\Delta\Gamma \equiv \Gamma_2 - \Gamma_1$.

Expanding the particle regime expressions (4.39) for x and y in the small mass splitting limit is complicated by the fact that neither x nor y can be expressed as function of $\Delta m/m$ alone. However, one may show that

$$x \simeq \frac{\Delta m}{\bar{\Gamma}}\left[1 + \frac{y_0}{2\beta^2}\frac{\Delta m}{m} + \sum_{p=2}^{\infty}\frac{X_p(y_0, m, E)}{2^p\beta^{2p}}\left(\frac{\Delta m}{m}\right)^p\right]$$
$$y \simeq \frac{\Delta\Gamma}{2\bar{\Gamma}}\left[1 + \frac{1-y_0^2}{2\beta^2 y_0}\frac{\Delta m}{m} + \sum_{p=2}^{\infty}\frac{Y_p(y_0, m, E)}{2^p\beta^{2p}}\left(\frac{\Delta m}{m}\right)^p\right] , \tag{4.44}$$

for which X_p and Y_p are rational functions of y_0, m and E. The parameter β is defined as in Eqs. (4.41), but for mass m. In general, any of X_p, Y_p or $1/\beta$ could be arbitrarily large for some configuration of the parameters y_0, m and E, so the expansions (4.44) are not always well-controlled power series in $\Delta m/m$. However, it's plausible that the expansions are well-controlled in the parameter space regimes, and respective very small mass splittings (4.43), relevant to the neutral meson systems. In such regimes, we then obtain for sufficiently small mass splittings

$$x \simeq \frac{\Delta m}{\bar{\Gamma}} , \qquad y \simeq \frac{\Delta\Gamma}{2\bar{\Gamma}} . \tag{4.45}$$

These are precisely the usual definitions for the parameters x and y in the neutral meson mixing formalism. Moreover, in terms of the 'proper time' τ - defined for m in Eqs. (4.41) - the same expansion in small mass splitting renders the CP violating amplitudes (4.28)

$$\left|\Delta_{++}(E, L)\right|^2 \simeq \frac{1}{32\pi^2 L^2}\exp(-\bar{\Gamma}\tau)\Big[\cosh(\Delta\Gamma\tau/2) + \cos(\Delta m\tau)\Big] ,$$
$$\left|\Delta_{+-}(E, L)\right|^2 \simeq \frac{1}{32\pi^2 L^2}\frac{|q|^2}{|p|^2}\exp(-\bar{\Gamma}\tau)\Big[\cosh(\Delta\Gamma\tau/2) - \cos(\Delta m\tau)\Big] . \tag{4.46}$$

Up to a normalization of $1/16\pi^2 L^2$, these are exactly the time evolution amplitudes found within the usual meson mixing analysis [124, 125] as is evident in Eq. (4.32). The physical interpretation of τ is the proper time elapsed in the rest frame of a classical particle with mass m and lab frame energy E that traverses a distance L.

Since we have already verified that, in terms of x and y, our integrated oscillation probabilities match those found in the usual treatment, we have therefore recovered the well-known meson mixing amplitudes and time-integrated probabilities from the structure of the two-point function alone. Our analysis, however, also implies that the usual meson mixing results are valid *only* within the small mass splitting particle regime. Outside this regime the more general results of Sec. 4.3.4 will apply.

An immediate question is whether the regimes of validity of our derivation and the standard quantum mechanical one disagree. The standard derivation is performed in terms of time evolution, and requires a *common* proper time for the mass eigenstates [124, 125], which are one-particle states. If the energy of the oscillation experiment is fixed, as we assume throughout this paper, then this assumption is equivalent to assuming $\Delta m \to 0$. So the standard derivation is similarly applicable only in the small mass splitting limit.

4.4.3 (Ultrarelativistic) Stable Particle Regime: Neutrino Oscillation

For a neutrino oscillation experiment we expect the neutrinos to be ultrarelativistic and stable in the lab frame. The ultrarelativistic stable limit of the particle regime corresponds to $E \gg m_j$ and $\Gamma_j \to 0^+$ for all j. Expanding in this limit, the wavenumbers and characteristic inverse decay lengths (4.38) become, to leading order in m_j/E,

$$\omega_j \simeq E - \frac{m_j^2}{2E} \ , \qquad \zeta_j = 0 \ , \tag{4.47}$$

so that

$$\Delta_j(E,L) \simeq \frac{i}{4\pi L}\exp\left\{iEL - i\frac{m_j^2}{2E}L\right\} . \tag{4.48}$$

Applying Eqs. (4.19) and the unitarity of U leads immediately to

$$\begin{aligned} P_{\alpha\to\beta}(E,L) &\simeq \sum_j |U^{\alpha j}|^2|U^{\beta j}|^2 + 2\sum_{j<k}\mathrm{Re}\Big[U^{\alpha j}U^{\beta j*}U^{\alpha k*}U^{\beta k}\exp\Big\{-i\frac{\Delta m_{jk}^2}{2E}L\Big\}\Big] \\ &= \delta_{\alpha\beta} + 2\sum_{j<k}\mathrm{Im}\Big[U^{\alpha j}U^{\beta j*}U^{\alpha k*}U^{\beta k}\Big]\sin\left(\frac{\Delta m_{jk}^2}{2E}L\right) \\ &\quad - 4\sum_{j<k}\mathrm{Re}\Big[U^{\alpha j}U^{\beta j*}U^{\alpha k*}U^{\beta k}\Big]\sin^2\left(\frac{\Delta m_{jk}^2}{4E}L\right) , \end{aligned} \tag{4.49}$$

where $\Delta m_{jk}^2 \equiv m_j^2 - m_k^2$. This is precisely the Pontecorvo neutrino oscillation formula. Hence we have derived the neutrino oscillation formula in a purely quantum field theoretic formalism, involving just the structure of the spatial two-point function. Comparing Eqs. (4.38) and (4.47), it is straightforward to generalize this result to just the stable particle regime $E > m_j$, $\Gamma_j \to 0^+$ via the replacement in Eq. (4.49)

$$-\frac{\Delta m_{jk}^2}{2E} \to \sqrt{E^2 - m_j^2} - \sqrt{E^2 - m_k^2} . \tag{4.50}$$

4.4.4 (Deep) Virtual Regime

Having verified that our exacts results reduce to the expected results for both the neutral meson and neutrino systems, let us now exploit the generality of Eqs. (4.15), (4.17) and (4.19) to push E, m_j and Γ_j into non-standard, though physically relevant, regimes of parameter space. So far we have only considered regimes for which $E > m_j$, so let us now consider the case

$$-R_j \gg A_j \ , \quad \text{i.e.} \ \ m_j^2 - E^2 \gg m_j\Gamma_j \ , \tag{4.51}$$

which we call the virtual regime for reasons outlined below. If also $E \ll m_j$, then we call this the deep virtual regime. As we will investigate in Sec. 4.4.5 below, the

virtual regime is particularly interesting if one 1PI state is very heavy compared to another.

In the virtual regime, the wavenumber and characteristic inverse decay lengths become to leading order in $A_j/|R_j|$

$$\omega_j \simeq \frac{m_j \Gamma_j}{2\sqrt{m_j^2 - E^2}} , \qquad \zeta_j \simeq \sqrt{m_j^2 - E^2} . \tag{4.52}$$

Again, the oscillation probabilities (4.19) and (4.20) follow immediately from this and Eqs. (4.18). Within this regime, two flavors with a sufficiently small mass splitting have integrated oscillation probability described by the parameters

$$x \simeq \frac{\Delta\Gamma}{2\bar{\Gamma}} , \qquad y \simeq \frac{\Delta m}{\bar{\Gamma}} . \tag{4.53}$$

These are, of course, just a swap of the usual parameters one sees in the particle regime.

In the virtual regime Eq. (4.15) becomes

$$\Delta_j(E, L) \simeq \frac{i}{4\pi L} \exp\left\{ i \frac{m_j \Gamma_j}{2\sqrt{m_j^2 - E^2}} L - \sqrt{m_j^2 - E^2} L \right\} . \tag{4.54}$$

The spatial two-point function no longer looks like that of a one-particle state. This is especially clear in the stable virtual case $m_j > E$ and $\Gamma_j \to 0^+$, for which $\Delta_j(E, L)$ is just an exponential decay: This was noticed previously in Ref. [111]. Note also that for the unstable case, the wavenumber is determined by the decay rate, rather than by a momentum $(E^2 - m_j^2)^{1/2}$, and vice versa for the characteristic inverse decay length.

Let us briefly comment on the physical interpretations of the virtual regime results, from which we derive its name. As explained in Sec. 4.2.1, the spatial two-point function $\Delta_j(E, L)$ does not encode the propagation of just a single particle

with a definite momentum. Rather, as suggested by Eq. (4.13), we may think of the spatial two-point function as the continuous sum of a set of propagators, each corresponding to the propagation of a momentum eigenstate. The condition $E < m_j$ then implies all these momentum eigenstates must be off-shell, so in this case $\Delta_j(E, L)$ includes no on-shell propagating particles. That is they are virtual particles, whence the regime name. Alternatively, $E < m_j$ is analogous to the usual quantum mechanical tunnelling condition, with the mass acting as the potential barrier. From either point of view, we emphasize that we should expect $\Delta(E, L)$ to be exponentially suppressed in the stable case, precisely as we see in Eq. (4.54).

4.4.5 Mixed Regime

It is interesting to consider the case that different 1PI states occupy different regimes. For example, we could consider a two-flavor oscillation in the case that one 1PI state is in the particle regime, while the other is in the virtual regime. We call such a case the mixed regime. This scenario doesn't occur for the neutral meson or neutrino systems because the mass splitting between 1PI states is very small compared to E. However, the large mass hierarchy of the quark sector combined with the possibility of quark oscillations [128, 129], provides a natural setting in which we may contemplate a mixed regime oscillation.

For concreteness, let us suppose there is a fourth quark doublet (t', b'), with masses much larger than the top quark mass. The existence of a fourth quark family is strongly constrained by the electroweak weak precision measurements [130, 131, 132], but nonetheless phenomenologically still perfectly viable (see Ref. [121] for mass bounds). A quark oscillation experiment could then involve a top quark decaying to a final state $t \to X_\beta$ via intermediate b or b' down-type quarks.

The generic diagrammatic form of such an experiment is shown in Fig. 4.1.

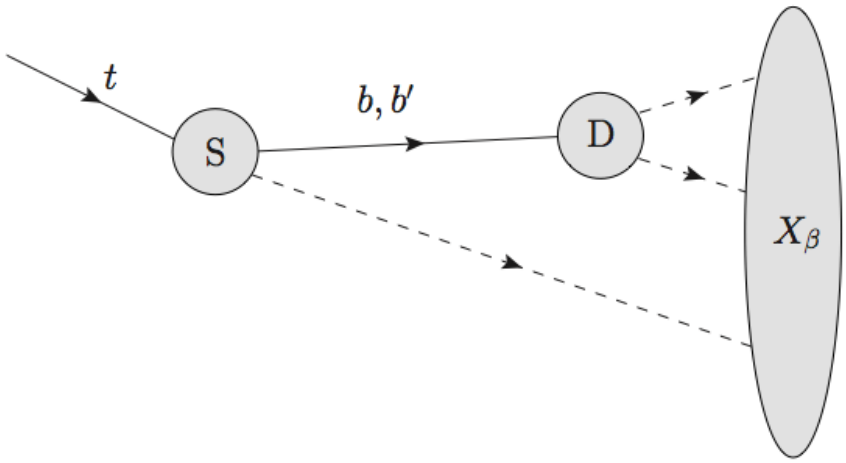

Figure 4.1: Quark oscillation experiment $t \to X_\beta$.

Let us adopt the following notation. The flavor of the down-type quarks is determined by their up-type partner, so we denote the down-type flavor quarks by b_t and $b_{t'}$. That is, $\alpha = t, t'$. Correspondingly the 1PI states are denoted b and b', so $j = b, b'$. The idea here is that the top quark produces the flavor quark b_t at the source vertex, S, while the generic final state X_β in the detector can tag the flavor at vertex D. In order to describe the physics of this experiment using our formalism, and for simplicity, we also assume the following:

i) The amplitude of the experiment is described by Eq. (4.3).

ii) We neglect the presence of the other two down-type quarks d and s, and consider an effective two-flavor mixing between the third and fourth quark generations. Consequently, the final state X_β only measures flavors $\beta = t, t'$.

iii) The b is in the stable particle regime ($E > m_b$ and $\Gamma_b \to 0^+$), while b' in the stable virtual regime ($E < m_{b'}$ and $\Gamma_{b'} \to 0^+$).

iv) The energy, E, exchanged between S and D can be precisely measured.

v) The 2×2 mixing matrix U, which diagonalizes the 1PI function, is unitary.

The extent to which these assumptions are applicable to an actual quark oscillation experiment is questionable. Our intent is merely to demonstrate that with such assumptions, we can perhaps gain insight into the physics of quark oscillations by use of our formalism.

With these assumptions, we have wavenumber and characteristic inverse decay lengths

$$\omega_b = \sqrt{E^2 - m_b^2}\ , \qquad \omega_{b'} = 0\ , \qquad \zeta_b = 0\ , \qquad \zeta_{b'} = \sqrt{m_{b'}^2 - E^2}\ , \tag{4.55}$$

so that the oscillation wavenumbers

$$\Delta\omega_{bb'} = \sqrt{E^2 - m_b^2}\ , \qquad \Delta\zeta_{b'b} = \sqrt{m_{b'}^2 - E^2}\ . \tag{4.56}$$

The oscillation probabilities follow immediately from Eqs. (4.21) and (4.24), while the corresponding spatial two-point functions

$$\begin{aligned} \Delta_b(E,L) &= \frac{i}{4\pi L}\exp\left\{ i\sqrt{E^2 - m_b^2}L \right\}\ , \\ \Delta_{b'}(E,L) &= \frac{i}{4\pi L}\exp\left\{ -\sqrt{m_{b'}^2 - E^2}L \right\}\ . \end{aligned} \tag{4.57}$$

In particular, note that the b' two-point function is exponentially suppressed, as we expect for a virtual particle. Further, the integrated probability has parameters

$$x = \sqrt{\frac{E^2 - m_b^2}{m_{b'}^2 - E^2}}\ , \qquad y = 1\ , \tag{4.58}$$

so that in the two-flavor integrated oscillation probability (4.24) there is no longer any interference term — and hence no oscillation — between the two mass eigenstates. From Eq. (4.20) one finds integrated oscillation probability

$$P^{\mathrm{I}}_{t\to\beta}(E) = 2\frac{|U^{tb}|^2|U^{\beta b}|^2}{1 + |U^{tb}|^2 - |U^{tb'}|^2}\ . \tag{4.59}$$

(Note that convergence of the integrated amplitude with $\zeta_b = 0$ is ensured by the usual $i\epsilon$ term, which is taken to zero after integration. Equivalently, since $m_b\Gamma_b$ acts as the ϵ throughout this paper, the stable limit is determined by taking $\Gamma_b \to 0^+$ after integration over L.) As expected, the probability is controlled purely by the mixing of the flavor states with the particle-like 1PI state b which is in the stable particle regime.

4.4.6 Threshold Regime

One last regime of interest, which to the knowledge of the authors has not been previously discussed, is the case

$$|R_j| \ll A_j \ , \quad \text{i.e.} \ \ |E^2 - m_j^2| \ll m_j\Gamma_j \ . \tag{4.60}$$

We call this the threshold regime, since $E \simeq m_j$. To zeroth order in $|R_j|/A_j$, the wavenumber and characteristic inverse lengths reduce to

$$\omega_j = \zeta_j \simeq \sqrt{\frac{m_j\Gamma_j}{2}} \ , \tag{4.61}$$

and the oscillation probabilities follow as usual. This time (4.15) becomes

$$\Delta_j(E,L) \simeq \frac{i}{4\pi L} \exp\left\{(i-1)\sqrt{\frac{m_j\Gamma_j}{2}}L\right\} \ . \tag{4.62}$$

Here, curiously, the inverse decay length and wavenumber both depend on the geometric mean of the decay rate and mass, and coincide. We are unaware of an intuitive physical reason why they should coincide at threshold. There is, however, a limited particle analog to this behavior. If we were to interpret ω_j as the momentum, as we did in the particle regime, then we would have

$$p_j^2 \simeq m_j^2 - m_j\Gamma_j/2 \ . \tag{4.63}$$

That is, the 1PI states can be thought of as virtual particles slightly perturbed from the mass shell if $\Gamma_j \ll m_j$.

In the threshold regime, a small mass splitting for two flavors results in

$$x = y \simeq \frac{\sqrt{\Gamma_1} - \sqrt{\Gamma_2}}{\sqrt{\Gamma_1} + \sqrt{\Gamma_2}} \tag{4.64}$$

while if also the decay rates have a small splitting, $\Gamma_{1,2} = \Gamma \mp \Delta\Gamma$, $\Delta\Gamma \ll \Gamma$, then

$$x = y \simeq -\Delta m/m - \Delta\Gamma/\Gamma \ll 1 \ . \tag{4.65}$$

A well-motivated example of oscillation in which the threshold regime is applicable to both 1PI states is unknown to the authors. Despite this, we do wish to emphasize that the generality of Eqs. (4.19) and (4.20) permits exploration of parameter regimes in which a quantum mechanical treatment might be unfeasible.

4.5 Conclusions

In this paper we have used only the structure of the spatial two-point function $\Delta_{\alpha\beta}(E, L)$ to derive general flavor oscillation probability formulae for unstable fields. We have not only shown that this structure reproduces the usual Pontecorvo neutrino oscillation formulae and time-integrated (CP violating) neutral meson mixing formulae, but we have also found generalized exact expressions with natural physical interpretations in several different parameter regimes. Our results for the stable particle and stable virtual regimes agree with the results of Ref. [111] for stable fermions. However, our exact oscillation probabilities for unstable fields and the analysis of the unstable particle, threshold and virtual regimes has not been previously presented.

The advantages of the formalism we have employed in this paper are several. The exact computability and integrability of $\Delta_{\alpha\beta}(E, L)$ permitted us to obtain exact, elegant probability oscillation formulae. Moreover, the choice of reference frame throughout this paper is the unambiguous laboratory frame: There is no need in our approach to contemplate mass eigenstate rest frames and proper times. To the extent that complicating effects such as coherence, finite detector and source size, non-trivial source and detector physics, and measurement uncertainty can be neglected, our results provide an instructive leading order description of the physics of flavor oscillation, that is valid over the entire E, m, Γ parameter space.

In terms of future work, keeping in mind the large existing Literature on this subject, perhaps the most interesting avenue left to explore is the analogous formalism for flavor oscillation in matter, that is, the Mikheyev-Smirnov-Wolfenstein effect.

CHAPTER 5

KINEMATIC EDGES AND FLAVOR OSCILLATION

Based on the 2011 article "Kinematic Edges and Flavor Oscillation", written in collaboration with Yuval Grossman and Mario Martone and published in JHEP 10 (2011) 127.

5.1 Introduction

Many new physics scenarios predict cascade decays of new heavy degrees of freedom into Standard Model (SM) particles. A canonical example is the cascade decay of a squark into a quark plus two leptons and a neutralino $\tilde{q} \to q\tilde{\chi}_2^0 \to ql\tilde{l} \to qll\tilde{\chi}_1^0$. It is well-known that for a cascade decay of the general form

$$A \to XB \to XYC \ , \tag{5.1}$$

where X and Y are massless SM particles and $m_A > m_B > m_C$, the differential decay rate, $d\Gamma_A/ds$, possesses a kinematic edge located at [133, 134, 135, 136, 137, 138]

$$s = \frac{(m_A^2 - m_B^2)(m_B^2 - m_C^2)}{m_B^2}, \qquad s \equiv (p_X + p_Y)^2 \ . \tag{5.2}$$

This kinematic edge is in essence a step function in the differential decay rate distribution, and it arises due to kinematic upper bounds on the on-shellness of the intermediate exchanged particle, B. The location of the kinematic edge provides an indirect means to either measure or constrain the masses of the A, B and C particles involved in the cascade. This mass measurement technique is called kinematic edge or endpoint method [139, 140, 141, 142, 143, 144, 145]. It is particularly important in the case that C is invisible, in which case the particle masses cannot be measured directly.

In order to derive the kinematic edge in Eq. (5.2), one must assume that B is an on-shell mass eigenstate. This is a natural and plausible assumption to make, but it neglects the fact that B must also have a non-zero width, $\Gamma_B > 0$. One expects a non-zero width for B to smear the kinematic edge, because such a width smears out the invariant mass range within which B can be on-shell. However, for all phenomenologically important scenarios $\Gamma_B \ll m_B$, so this smearing effect is

considered to be small, and for this reason the role of Γ_B has been usually neglected. In some previous analyses, Γ_B has been incorporated into the differential decay rate by convolving the kinematic edge with a Breit-Wigner distribution [146].

In many well-motivated theories the field B has not one but several flavors, which means that B is a superposition of multiple mass eigenstates that may mix together and oscillate. For example, this scenario is predicted in various SUSY theories [147, 148, 149, 150, 151], and many proposals of ways to measure mass splittings, mixing and oscillation have been presented previously [152, 153, 154, 155, 156]. For just two flavors, it is well-known that the importance of the interference — the oscillation — between the mass eigenstates, denoted B_1 and B_2, is characterized by the dimensionless parameter

$$x \equiv \frac{\Delta m}{\bar{\Gamma}} \ , \tag{5.3}$$

that is the ratio of the $B_{1,2}$ mass splitting to their average decay rate. In the case that $x \ll 1$ or $x \gg 1$, oscillation is respectively unimportant because the oscillation length scale is too long or the oscillation is washed out. Oscillation effects, however, are significant in the case that $x \sim 1$. Due to the dependence of x on both the mass splitting and the decay rates, non-zero width and flavor oscillation effects cannot be independently considered. In other words, analysis of flavor oscillation requires the incorporation of the non-zero B widths into the computation of the differential decay rates.

If the flavors do not oscillate significantly, or if interference is negligible due to $x \gg 1$, then we simply expect $d\Gamma_A/ds$ to feature multiple, distinct kinematic edges, each corresponding to a single mass eigenstate, and the role of the widths should be unimportant. A detailed analysis of the physical information contained in the differential decay rates for the limit $x \to \infty$, in which oscillation and widths are

negligible, has been conducted in Ref. [157]. However, if oscillation is significant, then we not only expect interference terms to become important, but we also expect the form of $d\Gamma_A/ds$ to be smeared by the non-negligible widths.

The purpose of this chapter is to examine this prediction and its consequences in detail. We do this for the case of two-flavor mixing, with $B_{1,2}$ either scalars or spin-1/2 fermions that interact with the external particles A, C, X, and Y via Yukawa-type interactions. In Sec. 5.2 we first redevelop the kinematic edge formalism via a field theoretic approach, accounting for the finite width with a Breit-Wigner propagator for B. For the simple case of a scalar ϕ^3 interaction with a single intermediate B, we show explicitly how the kinematic edge arises in the $\Gamma_B \to 0$ limit. We also show that the kinematic edges have their own well-defined 'edge width' that is a function of Γ_B/m_B, permitting us to quantify how much the kinematic edge is smeared for a given B width.

In Sec. 5.3 we introduce two-flavor mixing for both the scalar and fermion cases, and present the corresponding explicit results for $d\Gamma_A/ds$ in detail. As expected, we find that interference between the mass eigenstates is important only for the regime $x \sim 1$. We also rederive the result that in the fermion case, spin correlations between X and Y alter the shape of $d\Gamma_A/ds$ dramatically compared to the scalar B case, and verify that in the case of a vectorial coupling, the two-flavor fermionic case corresponds to the scalar one (see e.g. [158]). We present the explicit and detailed derivations of the results presented in Sec. 5.3 in Appendix C.1.

Finally, in Sec. 5.4 we briefly explore the physical observables contained in the differential decay rates with oscillation, and how these may be used to constrain or measure the oscillation parameters, the masses, and the decay rates. We also propose a kinematic edge resolution criterion, which specifies under what condi-

tions the two kinematic edges can be distinguished. We show that in most regions of parameter space the edge resolution criterion is simply $x > 1$, which aligns with our expectation that the edges should be resolvable when interference is negligible. We consider as an example in Sec. 5.4 the special case that B consists of two flavors of sleptons, with oscillation parameters as motivated by gauge mediation SUSY breaking theories. Along with the kinematic edge constraints, we show that: the degree of oscillation — the magnitude of x — can be determined directly from the widths of the edges; the ratio of the kinematic edge step heights provides three observables, which uniquely constrain a parameter subspace involving x, the mass splitting and the mixing angle; and that the $s = 0$ intercepts provide two other physical observables, which are measurable even if the edges cannot be resolved. Lastly, we show that for the alternative case that the Bs are fermions, the parameter space is constrained by these observables in an identical fashion to the scalars, the only difference being that the fermion parameter space is enlarged by one extra dimension compared to the scalar case.

5.2 Non-Zero Width

In this section, we examine the role of a non-zero width Γ_B, and how it affects the sharp kinematic edge of Eq. (5.2). The usual derivation of Eq. (5.2) requires three assumptions: X and Y are massless; energy-momentum conservation; and, crucially, that B is on-shell. One may then derive Eq. (5.2) from kinematics alone. To include the finite width, we must instead perform an explicit field-theoretic computation of the differential decay rate $d\Gamma_A/ds$.

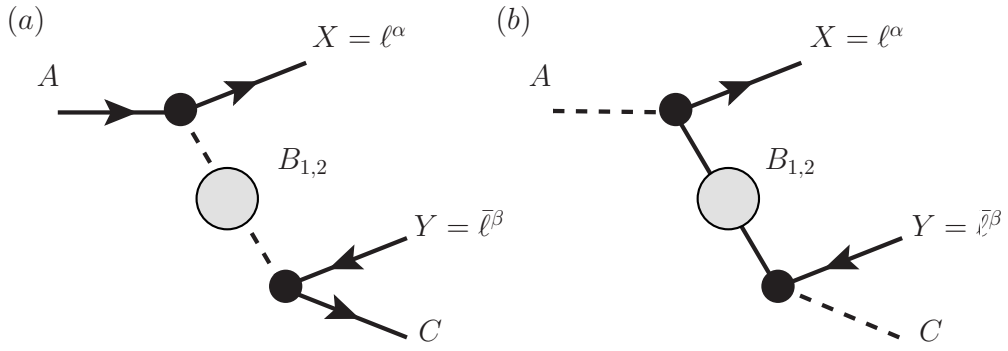

Figure 5.1: Decay amplitudes for the particle A in the case that the intermediate states $B_{1,2}$ are either (a) scalars or (b) fermions.

5.2.1 Breit-Wigner Approximation

In this chapter, we will be mainly concerned with the differential decay rates associated with the two amplitudes shown in Fig. 5.1, in which the intermediate exchanged particles $B_{1,2}$ are respectively either scalars or fermions, and have Yukawa-type couplings to the external fields A, X, Y and C. We assume that X and Y are both leptons, which are denoted by the fields ℓ^α. We also assume, unless stated otherwise, that X and Y are massless

$$m_X = m_Y = 0 \ , \tag{5.4}$$

while the particles A, $B_{1,2}$ and C have cascade-ordered masses

$$m_A > m_{1,2} > m_C \ . \tag{5.5}$$

To simplify notation we drop henceforth the subscript A from the decay rate, so that $\Gamma_A \equiv \Gamma$.

Let us consider the propagator for B in the field-theoretic approach. Throughout the paper we shall always assume that

$$\Gamma_B / m_B \ll 1 \ . \tag{5.6}$$

It is well-known that in the small width regime (5.6), and provided $p_B^2 \simeq m_B^2$, the exact propagator for an unstable particle is well-approximated by the Breit-Wigner propagator. (In a formal way, this approximation amounts to the leading order term of the propagator's Laurent series expanded around the pole $p^2 = m^2 - im\Gamma$.) In the same spirit as the saddle point approximation, integrals of amplitudes involving the propagator — precisely the objects with which we are concerned in this chapter — are well-approximated by the Breit-Wigner function, *provided* the domain of phase space integration includes the Breit-Wigner maximum $p_B^2 = m_B^2$. The reason is that the dominant contribution to such integrals is then due to an interval containing $p_B^2 = m_B^2$, and the Breit-Wigner is the leading order approximation within this interval. Outside this interval, the contribution to the integral by both the propagator and the Breit-Wigner are negligible, so we can approximate the propagator by the Breit-Wigner for all p_B^2, even though the Breit-Wigner tails may be poor approximations to the exact propagator tails. This argument extends naturally to objects involving sums of different propagators, that is, the differential decay rate for multiple flavors.

Inclusion of the Breit-Wigner maximum $p_B^2 = m_B^2$ within the domain of integration is guaranteed by assumption (5.5). Hence for any number of flavors, finite width effects in the differential decay rate are approximated to leading order in Γ_B/m_B by use of the Breit-Wigner propagators.

For just two flavors, note that this result holds for all values of x. In particular, it is well-known that if the maxima are well-separated such that only the propagator tails overlap — i.e. x is large — then the Breit-Wigner approximation is a poor approximation to the corresponding interference term. However, we emphasize that if only the tails of the propagators overlap, then the corresponding

interference term is also always negligible compared to the other terms contributing to the differential decay rate. As a result the failure of the Breit-Wigner approximation in the interference term for large x results in a negligible correction to the overall differential decay rate. So the Breit-Wigner approximation is a valid leading order approximation for all x.

For the scalar, the Breit-Wigner approximation is

$$D_{\rm sc}(p^2) = \frac{i}{p^2 - m^2 + im\Gamma} \ , \tag{5.7}$$

while for a fermion

$$D_{\rm f}(\not{p}) = i\frac{\not{p} + \sqrt{m^2 - im\Gamma}}{p^2 - m^2 + im\Gamma} \simeq i\frac{\not{p} + m - i\Gamma/2}{p^2 - m^2 + im\Gamma} \ , \tag{5.8}$$

due to Eq. (5.6). Note that we keep the $i\Gamma/2$ term as it is not necessarily small compared to $\not{p} + m$, and in fact it produces leading order contributions in the case of intermediate particle oscillation.

5.2.2 ϕ^3 Interaction

To study the smearing of the kinematic edge due to $\Gamma_B \neq 0$, it is instructive to first consider a toy ϕ^3 interaction calculation in which all the particles involved in the cascade are scalars and computational technicalities are therefore simplified. For further simplicity, we assume B is just a single scalar mass eigenstate.

Consider such a ϕ^3 scalar interaction, of the form

$$\mathcal{L} = g_X \phi_A \phi_B \phi_X + g_Y \phi_C \phi_B \phi_Y \ . \tag{5.9}$$

The amplitude for the decay of A is

$$i\mathcal{M} = \frac{i g_X g_Y}{p_B^2 - m_B^2 + i m_B \Gamma_B} \ . \tag{5.10}$$

Squaring this amplitude and integrating over phase space, one finds

$$\frac{d\Gamma}{ds} = \frac{g_X^2 g_Y^2}{32(2\pi)^3 m_A^3} \frac{1}{m_B \Gamma_B} \tan^{-1}\left(\frac{m_B}{\Gamma_B}\eta\right)\Bigg|_{\eta=\eta_-(s)}^{\eta=\eta_+(s)} , \tag{5.11}$$

where

$$\begin{aligned} \eta_\pm(s) &\equiv 1 + \xi(s) \pm \sqrt{\xi(s)^2 - m_A^2 m_C^2/m_B^4} \\ \xi(s) &\equiv \frac{s - (m_A^2 + m_C^2)}{2m_B^2} \ . \end{aligned} \tag{5.12}$$

We report the details of this calculation in Appendix C.1.

It is important to note that $\Gamma_B \propto g_Y^2/m_B$ ($g_{X,Y}$ have mass dimension one here), so in the limit $\Gamma_B/m_B \to 0$, $g_Y^2/m_B\Gamma_B$ is finite. This means that Eq. (5.11) has a well-defined normalization in the $\Gamma_B/m_B \to 0$ limit. To encode this explicitly, we therefore write

$$\frac{g_Y^2}{m_B \Gamma_B} = \tilde{g}_Y^2 \ , \tag{5.13}$$

which is dimensionless. Adopting this convention, Eq. (5.11) becomes

$$\frac{d\Gamma}{ds} = \frac{g_X^2 \tilde{g}_Y^2}{32(2\pi)^3 m_A^3} \tan^{-1}\left(\frac{m_B}{\Gamma_B}\eta\right)\Bigg|_{\eta=\eta_-(s)}^{\eta=\eta_+(s)} , \tag{5.14}$$

which is manifestly finite in the limit $\Gamma_B/m_B \to 0$. We will employ similar redefinitions of the coupling at the Y vertex throughout the paper.

Overall momentum conservation in the A rest frame requires that $s = m_A^2 + m_C^2 - 2E_C m_A^2$, so it must always be that

$$s \leq \left(m_A - m_C\right)^2 \equiv s_{\max} \ . \tag{5.15}$$

Observe that $\eta_-(s_{\max}) = \eta_+(s_{\max})$, and $\eta_\pm(s)$ become complex for $s > s_{\max}$, so the differential decay rate is always precisely zero for $s \geq s_{\max}$ as expected. We emphasize that this maximum is not related to the kinematic edge, but is a distinct kinematic constraint.

Let us now extract the kinematic edge from the differential decay rate. Expanding Eq. (5.14) in $\Gamma_B/m_B \ll 1$ we have

$$\frac{d\Gamma}{ds} \propto \frac{\pi}{2}\big\{\mathrm{sgn}\big[\eta_+(s)\big] - \mathrm{sgn}\big[\eta_-(s)\big]\big\} - \left(\frac{1}{\eta_+(s)} - \frac{1}{\eta_-(s)}\right)\frac{\Gamma_B}{m_B} + \dots \ . \tag{5.16}$$

The leading order term produces a step function in s: For $\mathrm{sgn}[\eta_+(s)] = -\mathrm{sgn}[\eta_-(s)]$ the leading order term is π, while for $\mathrm{sgn}[\eta_+(s)] = \mathrm{sgn}[\eta_-(s)]$, the leading order term is zero. The location of this step, s_0, must therefore satisfy either

$$\eta_+(s_0) = 0 \ , \qquad \text{or} \qquad \eta_-(s_0) = 0 \ . \tag{5.17}$$

(The ratio of m_B to the geometric mean of m_A and m_C determines which function is zero in Eqs. (5.17). If $m_A m_C/m_B^2 < 1$ then $\eta_-(s_0) = 0$ and $\eta_+(s_0) > 0$; if $m_A m_C/m_B^2 > 1$ then $\eta_+(s_0) = 0$ and $\eta_-(s_0) < 0$; while if $m_A m_C/m_B^2 = 1$ then both $\eta_\pm(s_0) = 0$.)

Using the definitions (5.12), one may verify that the solution to Eqs. (5.17) is always

$$s_0 = \frac{(m_A^2 - m_B^2)(m_B^2 - m_C^2)}{m_B^2} \ , \tag{5.18}$$

which is precisely the expected kinematic edge (5.2). We have therefore shown that the zeroth order contribution in Γ_B/m_B to Eq. (5.16) produces the kinematic edge, while terms of the order Γ_B/m_B and higher smear the edge into Eq. (5.14). A plot of the differential decay rate for different Γ_B/m_B is shown in Fig. 5.2.[1] Notice that if $m_B^2 = m_A m_C$, then $s_0 = s_{\max}$, so the kinematic edge collides with the overall kinematic constraint. For all other cases $s_0 < s_{\max}$. Note also that the terms of the order Γ_B/m_B and higher in Eq. (5.16) each diverge at the kinematic edge, while

[1]Readers expert in the kinematic edge method may wonder why the differential decay rate in Fig. 5.2 is rectangular in shape, rather than the usual triangle. The reason is that we have plotted here $d\Gamma/ds$ rather than $d\Gamma/d\sqrt{s}$, the latter convention being common in the Literature because the background is usually flat in $\sqrt{s}$. However, the former convention is also used (see e.g. [158]). Throughout this chapter we shall always consider $d\Gamma/ds$.

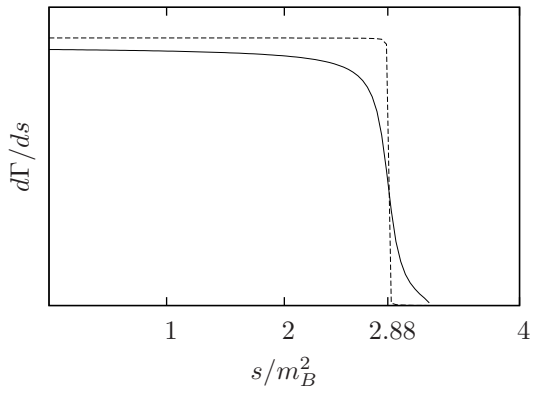

Figure 5.2: Differential decay rate with parameter choice $m_A/m_B = 2$, $m_C/m_B = 0.2$ and $\Gamma_B/m_B = 10^{-1}$ (solid) or $\Gamma_B/m_B = 10^{-3}$ (dashed). The kinematic edge $s_0/m_B^2 = 2.88$ clearly emerges as $\Gamma_B/m_B \to 0$.

the resummed expression in Eq. (5.14) is finite. This occurs because the formal expansion of the Breit-Wigner propagator in powers of Γ_B/m_B does not converge. Hence, even though expanding Eq. (5.14) provides us insight into the kinematic edge structure, nonetheless the full expression (5.14) is itself the leading order differential decay rate in Γ_B/m_B. Similarly, throughout this chapter we will not expand the closed form functions produced by the Breit-Wigner approximation, although we will expand their prefactors.

That the kinematic edge arises from the $\Gamma_B/m_B \to 0$ limit of an arctangent function is the main result of this section. We will see below that these functions, and their associated kinematic edges, are a general feature of the differential decay rates considered in this chapter.

5.2.3 On-shellness of B

It is also instructive at this point to consider how the on-shellness of B is encoded in this field-theoretic derivation of the kinematic edge. The amplitude squared can be written as

$$|\mathcal{M}|^2 = \frac{g_X^2 g_Y^2}{(p^2 - p_0^2)(p^2 - p_0^{*2})} = \frac{g_X^2 g_Y^2}{p_0^2 - p_0^{*2}} \left[\frac{1}{p^2 - p_0^2} - \frac{1}{p^2 - p_0^{*2}} \right] , \tag{5.19}$$

where $p_0^2 = m_B^2 - i m_B \Gamma_B$ and the * indicates complex conjugation. The key observation is that if one takes the $\Gamma_B/m_B \to 0$ limit before rather than after computation of $d\Gamma/ds$, one finds that the amplitude squared is

$$|\mathcal{M}|^2 = \lim_{\Gamma_B \to 0} \frac{g_X^2 g_Y^2}{m_B \Gamma_B} \mathrm{Im} \left[\frac{1}{p^2 - m_B^2 - i m_B \Gamma_B} \right] = \frac{2\pi}{m_B^2} g_X^2 \tilde{g}_Y^2 \delta(p^2 - m_B^2) \ . \tag{5.20}$$

We then see that the differential decay rate in the limit $\Gamma_B/m_B \to 0$ is simply a phase space integral of a delta function that forces B to be on-shell. This integral yields a step function as expected, with the edge occurring at the value of s for which B can no longer be on-shell.

5.2.4 Edge Width

Let us now specify how the smearing of the kinematic edge is related to non-zero Γ_B/m_B. In order to characterize the amount of smearing of the kinematic edge, one may show that the gradient of the differential decay rate, $d^2\Gamma/ds^2$, is of the form

$$d^2\Gamma/ds^2 = \frac{f(s)}{(s - s_0)^2 + \sigma^2} \ , \tag{5.21}$$

where $f(s)$ is a smooth function of s that is slowly varying compared to the Breit-Wigner factor near the kinematic edge. Hence near the edge

$$d^2\Gamma/ds^2 \simeq \frac{f(s_0)}{(s - s_0)^2 + \sigma^2} \ , \tag{5.22}$$

in the same spirit as the saddle point approximation. This Breit-Wigner is clearly maximal at the kinematic edge and has full width at half-maximum (FWHM)

$$\sigma \simeq 2m_B^2 \frac{\Gamma_B}{m_B} \left| \left(\Gamma_B/m_B\right)^2 + 1 - m_A^2 m_C^2/m_B^4 \right| . \tag{5.23}$$

We call σ the edge width. Note that in general $(\Gamma_B/m_B)^2$ is not necessarily small compared to $1 - m_A^2 m_C^2/m_B^4$. For the examples shown in Fig. 5.2, we have $\sigma/m_B^2 \simeq 0.2$ or 2×10^{-3} respectively, which match the naïvely expected orders of magnitude. The FWHM of $d^2\Gamma/ds^2$ is in principle a measurable quantity: Measurement of σ provides constraints on the size of the ratio Γ_B/m_B, rendering Eq. (5.23) as an important results.

5.2.5 Non-zero Width of A

So far in this discussion we have treated A as an on-shell external state. In practice, however, A itself is an intermediate state of a yet larger cascade that started with a heavier mother particle, denoted A'. In such a scenario, one measures $d\Gamma_{A'}/ds$ instead of $d\Gamma_A/ds$, and since A has a non-zero width, then the amplitude corresponding to this differential decay rate has the form

$$\left(\frac{i}{p_A^2 - m_A^2 + i m_A \Gamma_A}\right)\left(\frac{i}{(p_A - p_X)^2 - m_B^2 + i m_B \Gamma_B}\right) . \tag{5.24}$$

Here the smearing due to Γ_A convolves with that of Γ_B: If Γ_A is sufficiently large then we expect the B kinematic edge structure to be lost — i.e. smeared away — by this convolution. For non-zero Γ_A, not only does this convolution generally further smear the kinematic edge, but it also means we cannot generally distinguish the smearing effects of Γ_A from Γ_B in the differential decay rate. That is, the results of Sec. 5.2.2, which account for smearing due to non-zero Γ_B alone, would be invalid.

Our analysis of non-zero Γ_B effects in this section implies that smearing due to Γ_A vanishes as the parameter $\Gamma_A/m_A \to 0$. In particular, from the amplitude (5.24) we expect the Γ_A smearing to be negligible if

$$\Gamma_A/m_A \ll \Gamma_B/m_B \ . \tag{5.25}$$

For multiple flavors we require $\Gamma_A/m_A \ll \Gamma_j/m_j$ for all j. In this regime, the effect of A's non-zero width on each kinematic edge is negligible compared to the effects of the respective non-zero B widths.

From Eq. (5.14), we have

$$\frac{\Gamma_A}{m_A} \sim \frac{g_X^2 \tilde{g}_Y^2}{m_A^2} \frac{s_0}{m_A^2} \lesssim \frac{g_X^2 \tilde{g}_Y^2}{m_A^2} \ , \tag{5.26}$$

since $s_0/m_A^2 < 1$. So smearing due to A's non-zero width is negligible provided the coupling g_X is sufficiently small. For the remainder of this chapter, we shall always assume Eq. (5.25) is satisfied for all flavors, so that smearing due to A is negligible.

We shall now use the insight we have gained into finite width effects from this simple ϕ^3 theory to study the kinematic edge with flavor oscillation.

5.3 Flavor Oscillation

In this section we present results for the cases that $B_{1,2}$ are scalars or fermions, which we call the intermediate scalar and intermediate fermion cases respectively.

5.3.1 Oscillation Parameters and Small Width Regime

Before proceeding, let us define the following usual oscillation parameters in terms of the $B_{1,2}$ mass and decay rates, $m_{1,2}$ and $\Gamma_{1,2}$:

$$m \equiv \frac{m_2 + m_1}{2} \ , \qquad \Delta m \equiv m_2 - m_1 \ , \qquad \bar{\Gamma} \equiv \frac{\Gamma_2 + \Gamma_1}{2} \ , \qquad \Delta\Gamma \equiv \Gamma_2 - \Gamma_1 \ , \tag{5.27}$$

where $m_2 \geq m_1$ and

$$x \equiv \frac{\Delta m}{\bar{\Gamma}} \ , \qquad y \equiv \frac{\Delta\Gamma}{2\bar{\Gamma}} \ , \qquad z \equiv \frac{\Delta m}{2m} \ . \tag{5.28}$$

Note that $x \geq 0$ is unbounded, while $-1 \leq y \leq 1$ and $0 \leq z \leq 1$. The small width regimes for each mass eigenstate are defined, as usual, by $\Gamma_j/m_j \ll 1$. It is convenient to define the parameters

$$\epsilon_j \equiv \Gamma_j/m_j \ , \qquad \epsilon \equiv \bar{\Gamma}/m = \frac{m_1\epsilon_1 + m_2\epsilon_2}{m_1 + m_2} \ .$$

Just as before, we shall always assume small widths $\epsilon_j \ll 1$. Observe that since $m_{1,2}$ and $\epsilon_{1,2}$ are positive definite quantities, then this assumption implies $\epsilon \ll 1$.

The four parameters m, x, y and z are independent so they uniquely specify $m_{1,2}$, $\Gamma_{1,2}$ and $\epsilon_{1,2}$, viz.

$$m_{1,2} = m(1 \pm z) \ , \qquad \Gamma_{1,2} = \frac{2mz}{x}(1 \pm y) \ , \qquad \epsilon = \frac{2z}{x} \ , \qquad \epsilon_{1,2} = \frac{2z}{x}\left(\frac{1 \pm y}{1 \pm z}\right) \ . \tag{5.29}$$

It is clear that in the small width approximation

$$z \ll x. \tag{5.30}$$

Ideally, we may present all the differential decay rates just in terms of the oscillation parameters m, x, y and z alone. However, for the sake of compactness and clarity, we shall instead present our results in terms of a mixture of both m, x, y and

z as well as $m_{1,2}$, $\Gamma_{1,2}$, ϵ and $\epsilon_{1,2}$ with the understanding that the latter may be expressed in terms of the former via Eqs. (5.29).

Finally, we assume CP conservation. Thus, for two flavors the mixing matrix U, as defined in what follows (cf. Eqs. (5.32) and (5.42)), is real orthogonal and has a single physical mixing angle, θ. We write

$$U = \begin{array}{c} \alpha \backslash^{i} \\ 1 \\ 2 \end{array} \begin{array}{c} \begin{array}{cc} 1 & 2 \end{array} \\ \begin{pmatrix} \cos\theta & \sin\theta \\ -\sin\theta & \cos\theta \end{pmatrix} \end{array} . \tag{5.31}$$

5.3.2 Intermediate Scalars

First consider the differential decay rate due to the amplitude in Fig. 5.1a. Here B is a superposition of two mass eigenstates with B_1 and B_2 scalars of two different flavors, while A, X, Y and C are fermions, with Yukawa-type vertices defined by

$$\mathcal{L}^{\mathrm{s}} = \bar{\psi}_A\big(g_L^X P_L + g_R^X P_R\big)\ell^\alpha U^{\alpha i *}\phi_B^i + \bar{\psi}_C\big(g_L^Y P_L + g_R^Y P_R\big)\ell^\alpha U^{\alpha i *}\phi_B^i \, . \tag{5.32}$$

We will not report here the study of a single intermediate scalar for this interaction. As shown in Appendix C.1, this case does not differ considerably from the ϕ^3 case studied in details in Section 5.2.2. The only difference is the presence of linear and logarithmic terms in s, which are suppressed by factors of ϵ.

We write the differential decay rate as

$$\left.\frac{d\Gamma^{\alpha\beta}}{ds}\right|_{\mathrm{sc}} = \big[(g_L^X)^2 + (g_R^X)^2\big]\big[(\tilde{g}_L^Y)^2 + (\tilde{g}_R^Y)^2\big]\left(\left.\frac{d\Gamma_1^{\alpha\beta}}{ds}\right|_{\mathrm{sc}} + \left.\frac{d\Gamma_2^{\alpha\beta}}{ds}\right|_{\mathrm{sc}} + \left.\frac{d\Gamma_{12}^{\alpha\beta}}{ds}\right|_{\mathrm{sc}}\right) . \tag{5.33}$$

The first two terms come respectively from the squared single B_1 and B_2 contributions. The final term is the interference term for the two different flavors. The

subscript 'sc' denotes an internal scalar. Note also that just as for the ϕ^3 case in Eq. (5.13), the combination $(g^Y_{L,R})^2 m/\bar{\Gamma}$ is finite in the zero width limit (the couplings are now dimensionless), so we write,

$$\left(g^Y_{L,R}\right)^2 \frac{m}{\bar{\Gamma}} = \left(\tilde{g}^Y_{L,R}\right)^2 , \tag{5.34}$$

in which $\tilde{g}^Y_{L,R}$ are finite. In Eq. (5.33) we have already removed the $1/\epsilon = m/\bar{\Gamma}$ factor absorbed by $g^Y_{L,R}$ and replaced it with $\tilde{g}^Y_{L,R}$.

To leading order in ϵ the square terms are

$$\left.\frac{d\Gamma_j^{\alpha\beta}}{ds}\right|_{\rm sc} = \frac{|U^{\alpha j}|^2|U^{\beta j}|^2}{(2\pi)^3}\frac{s_0^j}{m_A^3}\left(\frac{1+(-)^j z}{1+(-)^j y}\right)\tan^{-1}\left[\frac{\eta}{\epsilon_j}\right]\Bigg|_{\eta=\eta_-^j}^{\eta=\eta_+^j} , \tag{5.35}$$

in which we have defined (cf. Eqs. (5.12) and (5.18))

$$\begin{aligned} s_0^j &\equiv \frac{(m_A^2-m_j^2)(m_j^2-m_C^2)}{m_j^2} , \\ \xi_j(s) &\equiv \frac{s-(m_A^2+m_C^2)}{2m_j^2} , \\ \eta_\pm^j &\equiv 1+\xi_j(s) \pm \sqrt{\xi_j^2(s) - m_A^2 m_C^2/m_j^4} . \end{aligned} \tag{5.36}$$

In Eq. (5.35) we have discarded terms whose coefficients are subleading order in ϵ or ϵ_j, but just as for the ϕ^3 example we have not expanded the arctangent function itself, in order to avoid creating artificial divergences at the kinematic edges.

The interference term is

$$\left.\frac{d\Gamma_{12}^{\alpha\beta}}{ds}\right|_{\rm sc} = \frac{m^2}{(2\pi)^3 m_A^3}\left[\frac{U^{\alpha 1}U^{\beta 1}U^{\alpha 2}U^{\beta 2}}{x^2+1}\right]\sum_{j=1,2}\left\{\mathcal{A}^j_{\rm sc}\tan^{-1}\left[\frac{\eta}{\epsilon_j}\right] + \mathcal{B}^j_{\rm sc}\log\left[\eta^2+\epsilon_j^2\right]\right\}\Bigg|_{\eta=\eta_-^j}^{\eta=\eta_+^j} . \tag{5.37}$$

with coefficients that are to leading order given by

$$\begin{aligned} \mathcal{A}^j_{\rm sc} &= \frac{(m_A^2-m^2)(m^2-m_C^2)}{m^4} , \\ \mathcal{B}^j_{\rm sc} &= -(-1)^j\frac{x}{2}\mathcal{A}^j_{\rm sc} . \end{aligned} \tag{5.38}$$

Several comments are necessary concerning the interference term and coefficients presented in Eqs. (5.37) and (5.38). We emphasize first that the coefficients are valid only to leading order in ϵ. We have also dropped contributions of $\mathcal{O}(z)$ and higher to the interference term prefactors, because their contributions are always suppressed. To see this, note that the interference terms can be written generally in the form

$$\left.\frac{d\Gamma_{12}^{\alpha\beta}}{ds}\right|_{\text{sc}} \sim \frac{a+bz}{x^2+1} \,, \tag{5.39}$$

where a and b are arbitrary linear combinations of the arctangent and logarithm functions and $a/b \sim 1$. It is clear that the denominator ensures the interference term is relevant only for $x \lesssim 1$: If instead $x \gg 1$, then the denominator suppresses the entire interference term, so the $\mathcal{O}(z)$ terms are certainly unimportant. In the case that $x \lesssim 1$, then $z \ll 1$ by Eq. (5.30). Hence the $\mathcal{O}(z)$ terms are always negligible. We emphasize, however, that we have not discarded the z dependence of the arctangent and logarithm arguments, only that of their prefactors. The ability to drop the $\mathcal{O}(z)$ contributions in the interference term prefactors applies similarly to the intermediate fermion case. The full expressions, including $\mathcal{O}(z)$ terms are reported in Appendix C.1.2.

The square terms in Eq. (5.35) bear obvious similarities to the ϕ^3 result in Eq. (5.14). The same analysis applies. Each square term becomes a step function in the zero width limit, producing a kinematic edge at

$$s = s_0^j \equiv \frac{(m_A^2 - m_j^2)(m_j^2 - m_C^2)}{m_j^2} \,, \tag{5.40}$$

respectively, but these edges are smeared out by non-zero ϵ_j. Eq. (5.29) implies that for a fixed z and y, the smaller x is, the larger the ϵ_j become. Hence in the oscillation regime, $x \sim 1$, the kinematic edges are more smeared compared to the $x \gg 1$ case. Similarly, the arctangent contributions to the interference term

have edges which are smeared according to the size of the ϵ_j parameters, with edge widths given by Eq. (5.23). As expected, *strong flavor oscillation smears the kinematic edges.* An example of this smearing of the kinematic edges is shown in Fig. 5.3 for fixed z but varying x. In this figure we have chosen $z = 0.1$, a relatively large value, in order that the edges are visually distinct.

As mentioned above, the interference term has a $1/(1 + x^2)$ prefactor, which means that for $x \gg 1$ the entire interference term is suppressed. Since $x \gg 1$ corresponds to no interference due to flavor oscillation 'wash-out', this is precisely the expected behavior. In Fig. 5.3 an example of the relative importance of the interference term contribution is shown graphically for the case that $x \sim 1$. As can be seen, for the chosen parameters the interference terms appear to slightly enhance the sharpness of the edges. Obviously, as x becomes smaller, the role of the interference term becomes more significant.

Another new feature of the interference term are the logarithm terms. These logs do not contain kinematic edges. Instead, in terms of ϵ for fixed z, and being careful to include the $1/(x^2 + 1)$ and $\mathcal{B}_{\rm sc} \sim x$ prefactors, the log terms are of form

$$\left.\frac{d\Gamma_{12}^{\alpha\beta}}{ds}\right|_{\rm sc,log} \sim \frac{z\epsilon}{\epsilon^2 + z^2} \log\left(\eta^2 + \epsilon^2\right)\Big|_{\eta_-}^{\eta_+} . \tag{5.41}$$

From Eq. (5.17), at a kinematic edge we have either $\eta_\pm = 0$, so the log terms are largest at a kinematic edge. However, in the $\epsilon \to 0$ (or $x \to \infty$) limit these log terms manifestly vanish. Notice also that for $z \to 0$ with x fixed, the large logs at the kinematic edge cancel due to the different signs of $\mathcal{B}_{\rm sc}^j$.

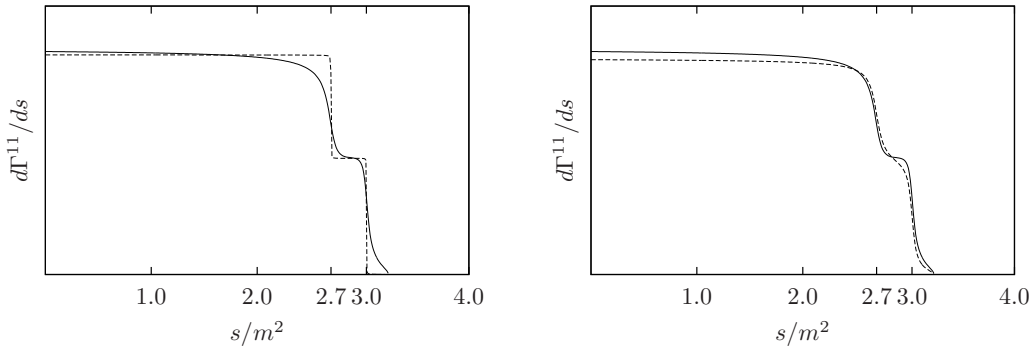

Figure 5.3: Left: Intermediate scalar differential decay rate for $\alpha = \beta = 1$, with the parameter choices $\theta = \pi/4$, $m_A/m = 2$, $m_C/m = 0.2$, $z = y = 0.1$, and $x = 4$ (solid) or $x = 4 \times 10^2$ (dashed). These correspond to $\epsilon = 5 \times 10^{-2}$, 5×10^{-4} respectively. The kinematic edges at $s_0^1/m^2 = 2.7$ and $s_0^2/m^2 = 3.0$ are smeared as ϵ becomes larger. Right: Intermediate scalar differential decay rate for the same parameter choices and $x = 4$ with (solid) and without (dashed) the interference terms.

5.3.3 Single Intermediate Fermion

In contrast to the intermediate scalar case, a single intermediate fermion case presents novelties which are worth discussing. In particular, since the B is now a spin-1/2 particle, we expect spin correlations between X and Y. These correlations lead to a differential decay rate with triangular or trapezoidal envelope rather than the square envelope found for the intermediate scalar case.

Consider the following interactions for a single intermediate fermionic B,

$$\mathcal{L}^{\rm f} = \bar{\psi}_B \big(g_L^X P_L + g_R^X P_R\big) \ell_X \phi_A^\dagger + \bar{\psi}_B \big(g_L^Y P_L + g_R^Y P_R\big) \ell_Y \phi_C^\dagger \ . \tag{5.42}$$

Squaring the amplitude in Fig. 5.1b, summing (averaging) over final (initial) spins, and integrating over phase space, one finds differential decay rate of the form

$$\left.\frac{d\Gamma}{ds}\right|_{\rm f} = \big[(g_L^X \tilde{g}_L^Y)^2 + (g_R^X \tilde{g}_R^Y)^2\big] \left.\frac{d\Gamma}{ds}\right|_- + \big[(g_L^X \tilde{g}_R^Y)^2 + (g_R^X \tilde{g}_L^Y)^2\big] \left.\frac{d\Gamma}{ds}\right|_+ \ . \tag{5.43}$$

The subscript 'f' denotes an internal fermion. The couplings $\tilde{g}_{L,R}^Y$ are defined as in Eqs. (5.13) and (5.34), and the m_B/Γ_B factor has already been similarly factored

out of the decay rates $d\Gamma/ds|_\pm$. The two terms in Eq. (5.43) arise from two purely chiral interactions: i.e. the cases $g_L^X = g_R^Y = 0$ or $g_R^X = g_R^Y = 0$ respectively. We therefore call $d\Gamma/ds|_\pm$ the chiral differential decay rates. The chiral differential decay rates turn out to have respectively a positive or negative slope in s, whence the subscript (see Appendix C.1 for details).

One finds to leading order in $\Gamma_B/m_B \ll 1$,

$$\begin{aligned}\left.\frac{d\Gamma}{ds}\right|_- &= \frac{s_0 - s}{(2\pi)^3 m_A^3}\mathrm{Tan}^{-1}\left[\frac{m_B}{\Gamma_B}\eta\right]\Bigg|_{\eta=\eta_-(s)}^{\eta=\eta_+(s)} \\ \left.\frac{d\Gamma}{ds}\right|_+ &= \frac{s}{(2\pi)^3 m_A^3}\ \mathrm{Tan}^{-1}\left[\frac{m_B}{\Gamma_B}\eta\right]\Bigg|_{\eta=\eta_-(s)}^{\eta=\eta_+(s)}\ ,\end{aligned} \tag{5.44}$$

where $\eta_\pm$ and s_0 are defined in Eqs. (5.12) and (5.18) respectively.

A few remarks about Eqs. (5.43) and (5.44) are in order. First, obviously the linear s dependence of the arctangent prefactors in Eqs. (5.44) changes the overall shape of the chiral differential decay rates from a rectangle into a triangle of either positive or negative slope. Second, just as for the intermediate scalar case, the arctangent functions produce a kinematic edge at $s = s_0$ which is smeared by non-zero Γ_B. Note, however, that the negatively sloped differential decay rate is precisely zero at the kinematic edge. Finally, from Eqs. (5.44) and (5.43), we see that in $d\Gamma/ds|_\mathrm{f}$ the linear s dependent piece of the arctangent prefactor is proportional to

$$\left[(g_L^X \tilde{g}_L^Y)^2 + (g_R^X \tilde{g}_R^Y)^2\right] - \left[(g_L^X \tilde{g}_R^Y)^2 + (g_R^X \tilde{g}_L^Y)^2\right]\ . \tag{5.45}$$

This s dependence disappears if either the X or Y vertex has a vectorial coupling, i.e $g_L^X = g_R^X$ or $g_L^Y = g_R^Y$ respectively. In this case we obtain a square envelope for the differential decay rate. In other words, if at least one coupling is vectorial then there are no spin correlations between X and Y, provided one averages over their initial and final spins. This means that for such vectorial coupling, one cannot

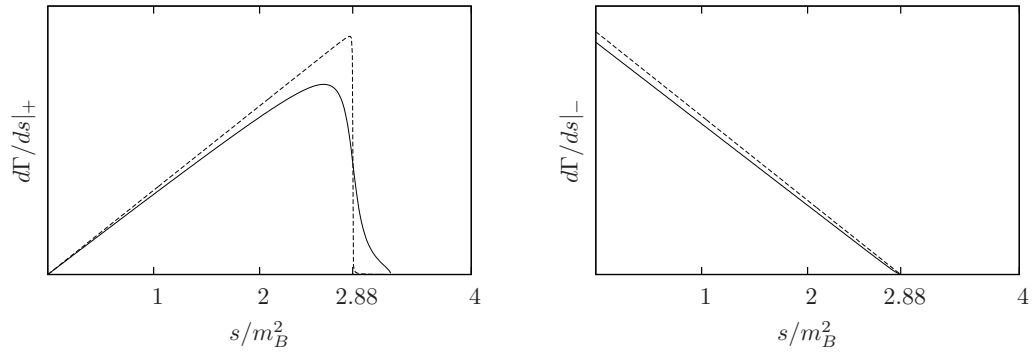

Figure 5.4: Chiral differential decay rates for the cases $g_L^X = g_R^Y = 0$ (left) and $g_R^X = g_L^Y = 0$ (right) with parameter choice $m_A/m_B = 2$, $m_C/m_B = 0.2$ and $\Gamma_B/m_B = 10^{-1}$ (solid) or $\Gamma_B/m_B = 10^{-3}$ (dashed). For the positive slope distribution, the kinematic edge $s_0/m_B^2 = 2.88$ clearly emerges as $\Gamma_B/m_B \to 0$, while the negative slope is always precisely zero at the kinematic edge.

distinguish a single intermediate fermion from an intermediate scalar using the shape of the differential decay rate. This is a well-known result (see e.g. [158]). Plots of the chiral differential decay rates are shown in Fig. 5.4.

5.3.4 Intermediate Fermion with Flavor Oscillation

Let us next consider the differential decay rate for the amplitude in Fig. 5.1b with two-flavor mixing. This time there are two intermediate fermions B_1 and B_2, with Yukawa-type vertices

$$\mathcal{L}^{\mathrm{f}} = \bar{\psi}_B^i \big(g_L^X P_L + g_R^X P_R\big) U^{\alpha i *} \ell^\alpha \phi_A^\dagger + \bar{\psi}_B^i \big(g_L^Y P_L + g_R^Y P_R\big) U^{\alpha i *} \ell^\alpha \phi_C^\dagger \,. \tag{5.46}$$

Just as for the single intermediate fermion, the differential decay rate is of the form

$$\left.\frac{d\Gamma^{\alpha\beta}}{ds}\right|_{\mathrm{f}} = \big[(g_L^X \tilde{g}_L^Y)^2 + (g_R^X \tilde{g}_R^Y)^2\big] \left.\frac{d\Gamma^{\alpha\beta}}{ds}\right|_- + \big[(g_L^X \tilde{g}_R^Y)^2 + (g_R^X \tilde{g}_L^Y)^2\big] \left.\frac{d\Gamma^{\alpha\beta}}{ds}\right|_+ . \tag{5.47}$$

Again the subscript 'f' denotes an internal fermion. The chiral differential decay rates, $d\Gamma/ds|_\pm$, now have both square and interference terms, so we write

$$\left.\frac{d\Gamma^{\alpha\beta}}{ds}\right|_\pm = \left.\frac{d\Gamma_1^{\alpha\beta}}{ds}\right|_\pm + \left.\frac{d\Gamma_2^{\alpha\beta}}{ds}\right|_\pm + \left.\frac{d\Gamma_{12}^{\alpha\beta}}{ds}\right|_\pm . \tag{5.48}$$

The square terms are similar to Eqs. (5.44). To leading order in ϵ, they are

$$\begin{aligned}
\left.\frac{d\Gamma_j^{\alpha\beta}}{ds}\right|_+ &= \frac{|U^{\alpha j}|^2|U^{\beta j}|^2}{(2\pi)^3}\left[\frac{s}{m_A^3}\right]\left(\frac{1+(-)^j z}{1+(-)^j y}\right)\tan^{-1}\left[\frac{\eta}{\epsilon_j}\right]\Bigg|_{\eta=\eta_-^j}^{\eta=\eta_+^j}, \\
\left.\frac{d\Gamma_j^{\alpha\beta}}{ds}\right|_- &= \frac{|U^{\alpha j}|^2|U^{\beta j}|^2}{(2\pi)^3}\left[\frac{s_0^j - s}{m_A^3}\right]\left(\frac{1+(-)^j z}{1+(-)^j y}\right)\tan^{-1}\left[\frac{\eta}{\epsilon_j}\right]\Bigg|_{\eta=\eta_-^j}^{\eta=\eta_+^j} .
\end{aligned} \tag{5.49}$$

The interference terms are similar to Eq. (5.37)

$$\left.\frac{d\Gamma_{12}^{\alpha\beta}}{ds}\right|_\pm = \frac{m^2}{(2\pi)^3 m_A^3}\left[\frac{U^{\alpha 1}U^{\beta 1}U^{\alpha 2}U^{\beta 2}}{x^2+1}\right]\sum_{j=1,2}\left\{\mathcal{A}_\pm^j \tan^{-1}\left[\frac{\eta}{\epsilon_j}\right] + \mathcal{B}_\pm^j \log\left[\eta^2+\epsilon_j^2\right]\right\}\Bigg|_{\eta=\eta_-^j}^{\eta=\eta_+^j}, \tag{5.50}$$

except that the coefficients (to leading order in ϵ) are

$$\begin{aligned}
\mathcal{A}_+^j &= \frac{s}{m^2} , \\
\mathcal{B}_+^j &= -(-)^j \frac{x}{2}\frac{s}{m^2} , \\
\mathcal{A}_-^j &= \mathcal{A}_{\rm sc}^j - \frac{s}{m^2} , \\
\mathcal{B}_-^j &= \mathcal{B}_{\rm sc}^j + (-)^j \frac{x}{2}\frac{s}{m^2} .
\end{aligned} \tag{5.51}$$

We have again dropped the $\mathcal{O}(z)$ terms, as discussed in Sec. 5.3.2. Notice that the square terms $d\Gamma_j/ds|_-$ are precisely zero at their kinematic edges and thereafter. As a result, rather than a double edge, the $d\Gamma/ds|_-$ rate has two kinks, which are smeared as ϵ increases. Plots of the chiral differential decay rates $d\Gamma/ds|_\pm$ and summed differential decay rates (5.43) are presented in Fig. 5.5.

Our analysis in Sec. 5.3.2 concerning the role of the logarithms, arctangents and $1/(x^2+1)$ factors in the interference terms for scalars applies equally to our

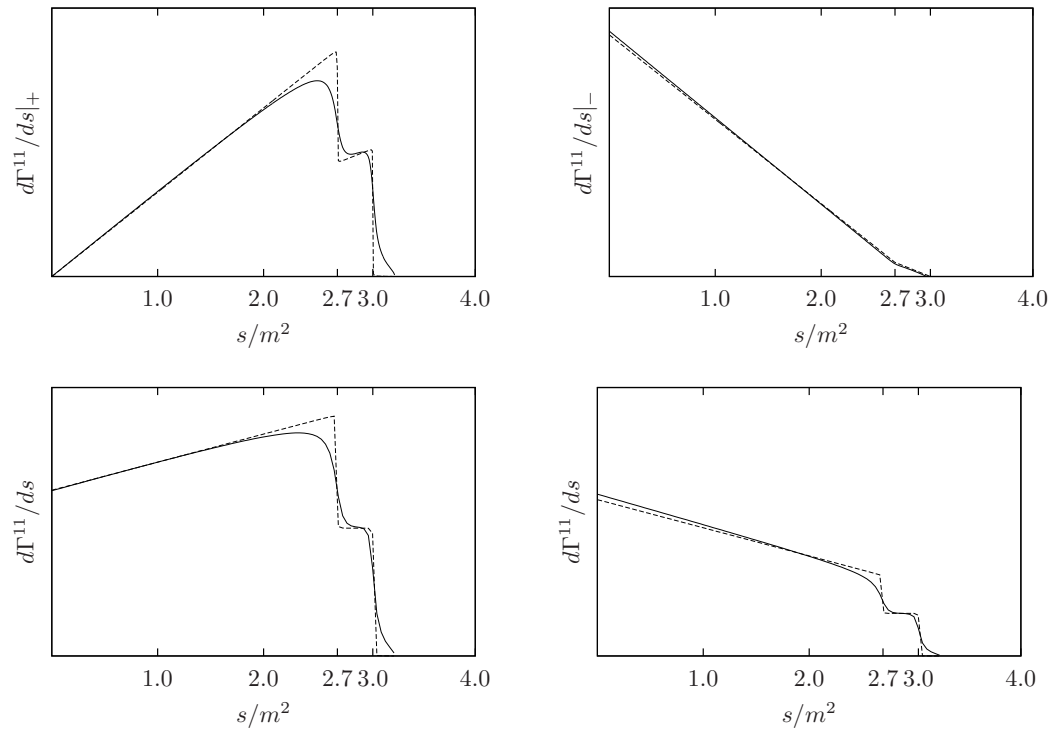

Figure 5.5: Internal fermion chiral differential decay rates $d\Gamma^{11}/ds|_+$ (upper left), $d\Gamma^{11}/ds|_-$ (upper right), and summed differential decay rates $d\Gamma^{11}/ds$ (lower left and right). The parameter choices are $\theta = \pi/4$, $m_A/m = 2$, $m_C/m = 0.2$, $z = y = 0.1$, and $x = 4$ (solid) or $x = 4 \times 10^2$ (dashed), which correspond to $\epsilon = 5 \times 10^{-2}$ and 5×10^{-4} respectively. For the summed rates we choose couplings such that $(g_L^X \tilde{g}_L^Y)^2 + (g_R^X \tilde{g}_R^Y)^2 = 1/2$, $(g_L^X \tilde{g}_R^Y)^2 + (g_R^X \tilde{g}_L^Y)^2 = 3/2$ (lower left) and vice-versa (lower right). The kinematic edges in $d\Gamma/ds|_+$ at $s_0^1/m^2 = 2.7$ and $s_0^2/m^2 = 3.0$ are evident as x becomes large, while in $d\Gamma/ds|_-$ we see instead two kinks. The trapezoidal shape and kinematic edges of the summed rates $d\Gamma^{11}/ds$ are manifest.

results for the intermediate fermions. As mentioned above, the main difference between the intermediate scalar and intermediate fermion results are the linear s prefactors, along with the fact that there are twice as many terms corresponding to the two chiral coupling cases. Finally, note that in the case a coupling is vectorial, both the square and interference terms reduce to the intermediate scalar case: The linear s dependence in the prefactors manifestly cancels and the fermion and scalar couplings coincide, just as for a single mass eigenstate.

This cancellation does not, however, persist in the log interference terms at higher ϵ order (see Appendix C.1.3 for details). This non-cancellation may be an artifact of the Breit-Wigner approximation [159, 160] and is certainly negligible here. Yet, it is worth pointing out that such a difference could open possibilities for intermediate particle spin determination in the vectorial coupling case. A possible physical origin of the difference between the bosonic and the fermionic cases may be off-shellness effects in the interference term: When the intermediate particles are far off-shell, e.g. in the $m_{1,2} \gg m_A > m_C$ regime, the differential decay rate is very different depending on the spin of the intermediate particle. Since off-shellness is parametrized by ϵ, to compute such off-shell spin effects would require analysis of higher order ϵ terms. This is beyond the scope of this chapter, and thus we do not exploit this possible avenue for spin determination any further here.

5.4 Observables

Having presented the differential decay rates for the intermediate fermion and scalar cases with flavor oscillation in Sec. 5.3, we now examine what physical observables can in principle be measured from these distributions. We emphasize that we do not study the feasibility of such measurements. A detailed analysis of the physical information contained in the differential decay rates for the limit $x \to \infty$, in which oscillation and widths are negligible, has been conducted in Ref. [157].

For the purposes of this discussion, in this section we will focus on the canonical example of cascade decay with an intermediate slepton (that is, a scalar)

$$\tilde{\chi}_1^0 \to \ell\tilde{\ell} \to \ell\ell\tilde{\chi}_2^0 \,. \tag{5.52}$$

In line with our discussion so far, we shall assume that there are only two flavors of slepton which mix significantly. We shall also assume they couple to the neutralino χ_1 (χ_2) and the electron e (muon μ) via CP preserving interactions of the form in Eq. (5.32). We adopt the notation

$$\psi_{A,C} \equiv \chi_{1,2} \ , \qquad \ell^{1,2} \equiv e, \mu \ . \tag{5.53}$$

In contrast to the notation defined in Eq. (5.31), for the sake of clarity in this section we will henceforth assign the flavor indices of the mixing matrix to be $\alpha = e, \mu$.

The SUSY spectrum depends on the mechanism of SUSY breaking. If the breaking is mediated in a flavor-universal manner then the mass splitting is small. For example, gauge mediation in SUSY breaking theories naturally gives mass splittings and decay widths for sleptons of the order GeV. Since existing bounds on the slepton masses imply $m_{\tilde{\ell}} > 10^2$ GeV, then for this decay we consider oscillation parameters

$$m \sim 10^2 \text{ GeV} \ , \qquad y \simeq 0 \ , \qquad z \sim 10^{-2} \ , \qquad x \sim 1 \ . \tag{5.54}$$

These parameters satisfy the small width condition $\epsilon_{1,2} \ll 1$, and flavor oscillation is strong.

5.4.1 Parameter Counting: Kinematic Edges

As explained in Sec. 5.3.1, measurement of the four oscillation parameters m, x, y and z uniquely determines the slepton masses and widths. The other physical parameters we wish to measure are the mixing angle θ, the neutralino masses m_{χ_1} and m_{χ_2}, and the couplings $g^X_{L,R}$ and $g^Y_{L,R}$, so we have eleven physical parameters

of interest in total. However, from Eq. (5.33) only the combination

$$\tilde{g} \equiv \left[(g_L^X)^2 + (g_R^X)^2\right]\left[(\tilde{g}_L^Y)^2 + (\tilde{g}_R^Y)^2\right] , \tag{5.55}$$

appears in the differential decay rate, so only $\tilde{g}$ can be measured. Thus we have an eight dimensional parameter space.

In the case of two-flavor mixing and with CP conservation, the differential decay rates are symmetric in flavor indices, as can be seen from Eqs. (5.35) and (5.37). That is, $d\Gamma^{\alpha\beta}/ds = d\Gamma^{\beta\alpha}/ds$. As a result, there are three independent differential decay rate distributions which can be measured, namely

$$\frac{d\Gamma^{ee}}{ds} , \qquad \frac{d\Gamma^{e\mu}}{ds} = \frac{d\Gamma^{\mu e}}{ds} , \qquad \frac{d\Gamma^{\mu\mu}}{ds} . \tag{5.56}$$

Note that in the most general case U can be complex, and the interference prefactors then generally contain $U^{\alpha i}U^{\beta i*}U^{\alpha j*}U^{\beta j}$. As a result $d\Gamma^{\alpha\beta}/ds \neq d\Gamma^{\beta\alpha}/ds$, and then each final state provides an independent differential decay rate.

The positions of the kinematic edges (5.40) are obviously lepton flavor independent, and therefore are the same for these three distributions. The edges therefore yield two independent constraints on the four-dimensional parameter subspace $\{m_{\chi_1}, m_{\chi_2}, m, z\}$, constraining it to a two-dimensional surface. The full parameter space is constrained by the edges to a six-dimensional surface. We now must seek other observables to further constrain the parameter space.

5.4.2 Direct Measurement of the Widths and Oscillation

In Sec. 5.2.4 we established that the smearing of the edges is characterized by the edge width σ, defined in Eq. (5.23). The edge width approximates the full width at half maximum of the derivative of the differential decay rate, $d\Gamma^2/ds^2$, and is

therefore a measurable quantity. Assuming that $1 - m_{\chi_1}^2 m_{\chi_2}^2/m^4 \sim \mathcal{O}(1)$ and since $y \simeq 0$, $z \sim 10^{-2} \ll 1$, then for the intermediate slepton cascade the edge width reduces simply to

$$\sigma \simeq 2\epsilon \frac{m^4 - m_{\chi_1}^2 m_{\chi_2}^2}{m^2} = \frac{4m^2 z}{x}\left(1 - \frac{m_{\chi_1}^2 m_{\chi_2}^2}{m^4}\right) , \tag{5.57}$$

for both kinematic edges. Since this is lepton flavor independent, all three differential decay rates feature two kinematic edges with the same edge width, yielding one independent further constraint on the parameter space.

Significantly, since the magnitudes of m and z are fixed by other theoretical considerations (as in Eq. (5.54)), and provided $1 - m_{\chi_1}^2 m_{\chi_2}^2/m^4 \sim \mathcal{O}(1)$, then measurement of σ provides the magnitude of x. As a consequence, the measurement of the smearing of the edges — the edge width — measures the degree of flavor oscillation.

5.4.3 Edge Resolution Criterion

So far in this discussion we have assumed that it is possible to distinguish the two edges, that is to say, it is possible to resolve them. But if the separation of the edges is of similar or smaller size than their widths, $\sigma_{1,2}$, then it is reasonable to assume that one may not resolve the two edges. This leads to a natural edge resolution criterion. For two kinematic edges to be resolvable, we require the separation of the edges to be greater than their average width, that is

$$\left|s_0^1 - s_0^2\right| > \frac{\sigma_1 + \sigma_2}{2} . \tag{5.58}$$

For $z \ll 1$ and $1 - m_{\chi_1}^2 m_{\chi_2}^2/m^4 \sim \mathcal{O}(1)$, this criterion reduces to just a simple restriction on x,

$$x > 1 . \tag{5.59}$$

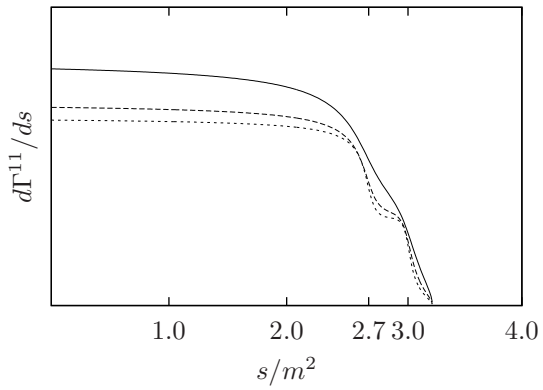

Figure 5.6: Intermediate scalar differential decay rate, with the parameter choices $\theta = \pi/4$, $m_A/m = 2$, $m_C/m = 0.2$, $y = 0$, $z = 0.1$, and $x = 1$ (solid), $x = 2$ (dashed) or $x = 3$ (dotted). These correspond to $\epsilon = 0.2$, $\epsilon = 0.1$ and $\epsilon = 0.02$ respectively.

This is an interesting result, because the resolvability depends on both the separation and the widths of the edges, so naïvely we would expect the resolution criterion to depend on both x and z. That said, this result implies that oscillation and edge resolvability are inversely correlated, which aligns with our expectation that the edges should be resolvable when interference is negligible. For the intermediate slepton cascade we have $x \sim 1$, so the edges may not always be resolvable, but they are if we restrict our attention to $x > 1$, which is often the regime of interest. A graphical demonstration of the sensitivity of this criterion is provided in Fig. 5.6. For $x = 2$ the edges are already visibly resolvable. Note that the parameters have been chosen in this figure to match our prior discussion, while still satisfying $z, \epsilon \ll 1$ and $1 - m_{\chi_1}^2 m_{\chi_2}^2/m^4 \sim \mathcal{O}(1)$, and do not arise from the slepton cascade.

5.4.4 Edge Degeneracy and the Geometric Mean

Before continuing, we wish to point out that kinematic edges can be irresolvable even in the absence of strong oscillation. That is, there are special points in parameter space at which two kinematic edges (5.40) are degenerate, i.e. $s_0^1 = s_0^2$. This occurs not only for the obvious case that $m_1 = m_2$, but also if

$$m_1 m_2 = m_A m_C \ , \tag{5.60}$$

that is, if the geometric means of $m_{1,2}$ and $m_{A,C}$ are the same. In terms of the parameter z, this condition corresponds to

$$z = \sqrt{1 - \frac{m_A m_C}{m^2}} \ . \tag{5.61}$$

If we require $z \ll 1$, then it follows that $1 - m_{\chi_1}^2 m_{\chi_2}^2 / m^4 \ll 1$, too. So Eq. (5.60) is satisfied in a different regime of parameter space to that considered in Sec. 5.4.3.

The physical origin of this degeneracy can be understood by observing that if X and Y are massless, then the invariant mass $s = 2(|\vec{p}_X||\vec{p}_Y| - \vec{p}_X \cdot \vec{p}_Y) \leq 4|\vec{p}_X||\vec{p}_Y|$. One derives the kinematic edge, s_0^j, from kinematics by maximizing s subject to B_j being on-shell. It is clear that a given value of s can be obtained from many configurations of $\vec{p}_X$ and $\vec{p}_Y$. For instance, s has the symmetry $|\vec{p}_X| \to \lambda |\vec{p}_Y|$, $|\vec{p}_Y| \to |\vec{p}_X|/\lambda$, $\forall \lambda \in \mathbb{R}$. It is therefore not surprising that there exist different on-shell B masses with correspondingly different $p_{X,Y}$ configurations, but with s_0 the same. In particular, it can be shown that $m_1 \to m_A m_C / m_1 = m_2$ is equivalent to $\lambda = m_A / m_C$. So if $m_1 m_2 = m_A m_C$, then the two kinematic edges are degenerate.

When Eq. (5.60) is satisfied, the kinematic edges collide, so that one may not determine the number of intermediate mass eigenstates from the differential decay rate $d\Gamma/ds$. There may, of course, still be oscillation between the two B's in this

case or none at all. The moral of this section and Sec. 5.4.3 is that the observation of a certain number of kinematic edges provides only a lower bound on the number of intermediate degrees of freedom.

5.4.5 Step Height Ratios

If the edges are resolvable, the ratio of the heights of the step functions that form the kinematic edges is another observable. For $y \simeq 0$ and $z \ll 1$, using the results of Sec. 5.3.2 one may show that this step height ratio is to leading order in z

$$R^{\alpha\beta} = \frac{|U^{\alpha 1}|^2|U^{\beta 1}|^2 + U^{\alpha 1}U^{\beta 1}U^{\alpha 2}U^{\beta 2}[1 + (x/\pi)\log\epsilon]/(x^2+1)}{|U^{\alpha 2}|^2|U^{\beta 2}|^2 + U^{\alpha 1}U^{\beta 1}U^{\alpha 2}U^{\beta 2}[1 - (x/\pi)\log\epsilon]/(x^2+1)} \ . \tag{5.62}$$

The step height ratio is lepton flavor dependent, yielding three constraints on the three dimensional $\{z, x, \theta\}$ parameter space. Consequently, the step height ratios probe z, x and θ. Reversing the parameter counting above, measurement of σ now constrains m uniquely, while the two kinematic edges are left to constrain m_{χ_1} and m_{χ_2}. With $y \simeq 0$, only the coupling combination $\tilde{g}$ is left unconstrained by these observables.

5.4.6 $s = 0$ Intercepts

We now consider the value of the decay rate at $s = 0$, which we call the $s = 0$ intercept. These intercepts are another three physical observables. Since they depend on overall normalization, they permit measurement of $\tilde{g}$, and moreover, they are measurable even if the edges cannot be resolved. Explicitly, for the three

independent differential decay rates, these intercepts are to leading order

$$I^{\alpha\beta} = \tilde{g}\frac{(m_{\chi_1}^2 - m^2)(m^2 - m_{\chi_2}^2)}{8\pi^2 m_A^3 m^2}\left[|U^{\alpha 1}|^2|U^{\beta 1}|^2 + |U^{\alpha 2}|^2|U^{\beta 2}|^2 + \frac{2U^{\alpha 1}U^{\beta 1}U^{\alpha 2}U^{\beta 2}}{x^2+1}\right] . \tag{5.63}$$

Unlike the step height ratios, not only does $I^{e\mu} = I^{\mu e}$, but also $I^{ee} = I^{\mu\mu}$, so the intercepts actually provide just two independent observables. The kinematic edges, edge width, step height ratios and $s = 0$ intercepts thus provide eight physical observables for the original eight-dimensional parameter space. Alternatively, if we set $y \simeq 0$, then the seven-dimensional parameter space is over-constrained. Note also that the single independent *ratio* of these intercepts is normalization independent, and therefore constrains just the $\{x, \theta\}$ parameter subspace.

5.4.7 Intermediate Fermion Observables

Let us now consider the physical observables for the case of two-flavor mixing with intermediate fermions. It is convenient to define

$$\tilde{g}_+ \equiv (g_L^X \tilde{g}_L^Y)^2 + (g_R^X \tilde{g}_R^Y)^2 , \qquad \tilde{g}_- \equiv (g_L^X \tilde{g}_R^Y)^2 + (g_R^X \tilde{g}_L^Y)^2 , \tag{5.64}$$

which are the measurable coupling combinations analogous to $\tilde{g}$ above. The parameter space for fermions is therefore enlarged by one dimension compared to the scalar case. We assume the same oscillation parameter structure as in Eqs. (5.54).

Just as for the intermediate scalar case above, there are still three independent differential decay distributions (5.56); the kinematic edges and edge width still provide respectively two and one physical observables that constrain the parameter space; and the edge resolution criterion (5.59) is the same. Apart from the dimensionalities of their parameter spaces, the only other difference between the scalar and fermionic cases is that for the latter, rather than step height ratios one must

instead measure the ratio of trapezoid apex heights. That is, one must extrapolate the smeared edges into sharp corners — the solid to the dotted lines in Fig. 5.5 — and measure the ratio of the trapezoid apex heights so formed. This is obviously possible, but will presumably introduce more error into the experimental results. At leading order in ϵ and z these apex height ratios are identical to the step height ratios in Eq. (5.62), and the leading order contribution is due to $d\Gamma/ds|_+$ only.

The $s = 0$ intercepts are similarly the same as in Eq. (5.63) but with $\tilde{g}$ replaced by just $\tilde{g}_-$, since $d\Gamma/ds|_+$ is manifestly zero at $s = 0$, so the intercepts depend only on $\tilde{g}_-$. One can constrain $\tilde{g}_+$ by measuring the apex heights themselves, rather than their ratio, which depend only on $\tilde{g}_+$ to leading order in z.

5.5 Conclusion

In this chapter we have presented explicit differential decay rates for cascade decays of the form (5.1) as a function of the XY invariant mass, s, including the effects of both finite particle widths and flavor oscillation. In particular, we considered both scalar and spin-1/2 intermediate particles with Yukawa-type vertices. Our results successfully reproduce the usual kinematic edge results in zero width, zero oscillation limit, and we have shown how to quantify the degree of kinematic edge smearing for finite widths.

The main results of this chapter, however, involve the analysis of the interplay between non-zero width and flavor oscillation effects, as characterized by the parameters $x \equiv \Delta m/\bar{\Gamma}$ and $z \equiv \Delta m/2m$. Not only does x control the degree of oscillation or interference between the two B mass eigenstates, it also plays an important role in the degree of smearing of the two kinematic edges and their re-

solvability. In general, the larger x, the smaller the smearing and interference, and the greater the resolvability.

We have also shown how various physical observables of the differential decay rates can be used to constrain the oscillation parameter space, mainly for the special case of a slepton cascade with parameters motivated by gauge mediation SUSY breaking theories. In particular, apart from the kinematic edges, these observables include the edge widths, step height ratios and the $s = 0$ intercepts. Building on the special case considered in Sec. 5.4, a subject of future work may be to apply our explicit results to more realistic, more complicated or more general scenarios.

Another avenue of study may be to extend the current two-flavor treatment to the three or more flavors. Furthermore, one might lift the CP conservation assumption which we have made throughout this chapter. Such CP violation will produce CP violating interference terms, which may have interesting physical effects. We plan to address these issues in the future.

CHAPTER 6

SU(3) SUM RULES FOR CHARM DECAY

Based on the 2012 article "SU(3) Sum Rules for Charm Decay", written in collaboration with Yuval Grossman and published in JHEP 04 (2013) 67.

6.1 Introduction

The origin of the unexpectedly large direct CP asymmetry $\Delta\mathcal{A}_{\rm CP} \equiv \mathcal{A}_{\rm CP}[D^0 \to K^-K^+] - \mathcal{A}_{\rm CP}[D^0 \to \pi^-\pi^+]$ [161, 162, 163, 164, 165, 166, 167] is yet to be explained. Any explanation of this result relying upon new physics [168, 169, 170, 171, 172, 173, 174, 175, 176, 177, 178, 179] must first properly determine the contribution from the Standard Model (SM). To this end, several studies [180, 181, 182, 183, 184, 185, 186, 187, 188] have produced consistent pictures in which the large CP asymmetry may solely originate in the SM, via enhancement of the penguin amplitudes. These studies exploit the approximate flavor SU(3) or U-spin symmetries and show that they admit patterns of penguin enhancement consistent with experimental results. In some approaches [185, 186, 187], it can be shown that enhanced penguins can be consistently globally fitted to the data, to first order in the flavor SU(3) breaking. Moreover, it can be shown that large non-perturbative 'penguin contraction' final state interactions [182, 183, 180, 181, 184] can sufficiently enhance the penguins, such that the data can be explained. One approach in particular [182] has demonstrated that penguin contraction contributions to the $\Delta U = 0$ penguin reduced matrix elements – the so-called $\Delta U = 0$ rule for large broken penguins – yields a consistent picture for the U-spin subgroup irreps.

Explanations of the direct CP asymmetry excess by particular patterns of flavor SU(3) breaking (hereafter just SU(3), unless otherwise indicated) are complicated by the simultaneous empirical observation of both large SU(3) breakings *and* SU(3) sum rules. Generically, one expects the scale of SU(3) (or U-spin) breaking at the amplitude level to be comparable to the splitting of the kaon and pion decay

constants, i.e.,

$$\varepsilon \equiv f_K/f_\pi - 1 \sim 0.2 \ , \tag{6.1}$$

and therefore all SU(3) relations are expected to be violated at this order. However, measuring the reduced square amplitude, defined to be

$$|(D|f)|^2 \equiv \Gamma[D \to f] m_D^2/p_f \ , \tag{6.2}$$

in which p_f is the center-of-mass momentum of the final state, one finds empirically the Cabibbo-weighted amplitude relation

$$\left| \frac{(D^0|K^+K^-)/V_{cs}^* V_{us}}{(D^0|\pi^+\pi^-)/V_{cd}^* V_{ud}} \right| - 1 = 0.82 \pm 0.02 \ , \tag{6.3}$$

together with the U-spin amplitude sum rule

$$\frac{|(D^0|K^+K^-)/V_{cs}^* V_{us}| + |(D^0|\pi^+\pi^-)/V_{cd}^* V_{ud}|}{|(D^0|K^+\pi^-)/V_{cd}^* V_{us}| + |(D^0|\pi^+K^-)/V_{cs}^* V_{ud}|} - 1 = 0.040 \pm 0.016 \ . \tag{6.4}$$

That is, the former is comparable to $\mathcal{O}(1)$ and the latter to $\mathcal{O}(\varepsilon^2)$, rather than the expected $\mathcal{O}(\varepsilon)$.

Sum rules such as eq. (6.4) are actually a generic consequence of flavor SU(3) breaking. They may exist to arbitrary orders in the SU(3) breaking, although there may be no such sum rules once the order of breaking is sufficiently high, depending on the pattern of symmetry breaking. Commonly, one assumes large SU(3) breaking by the spurion associated with the strange quark mass (see e.g. [189, 190, 191, 182, 185, 186]). Hereafter we call this spurion the s-mass spurion. For example, in the $\Delta U = 0$ rule approach [182], certain enhanced U-spin breaking penguins significantly contribute to relations such as eq. (6.3) or $\Delta\mathcal{A}_{\rm CP}$, but the particular U-spin sum rule (6.4) is preserved under the s-mass spurion pattern of breaking to $\mathcal{O}(\varepsilon^2)$, yielding a consistent picture of the experimental results.

One can naturally extend the s-mass spurion breaking pattern to the full SU(3). An immediate programme is to find the consequent sum rules, which compared

to (6.4) involve the many other D meson decay modes that furnish the SU(3) irreps. Verifying such sum rules is a generic test of any picture of charm decays that invokes this pattern of SU(3) breaking. In this paper we compute the SU(3) sum rules that are valid to $\mathcal{O}(\varepsilon^2)$ in the SU(3) breaking by the s-mass spurion. We further compute the square amplitude sum rules to this order, which have the added advantage of not depending on strong phases. We call these rate sum rules, due to their dependence only on decay rates. Particular attention is given to sum rules which arise from isospin or U-spin. The former are expected to have parametrically smaller breakings, providing sensitive tests of alternate source of SU(3) breaking. The latter produce square amplitude sum rules to $\mathcal{O}(\epsilon^2)$, and are therefore easier to verify. Where feasible, we shall also discuss current experimental verification of these broken SU(3) sum rules, or predictions arising from them.

This paper is structured as follows. We first briefly recapitulate the construction of the D meson decay amplitudes in terms of reduced matrix elements using the Wigner-Eckart theorem, and the decomposition of the effective Hamiltonian into SU(3) irreps. We then proceed to compute the $D \to PP$ and $D \to PV$ amplitudes – P (V) denotes pseudoscalar (vector) – in terms of their reduced matrix elements to $\mathcal{O}(\varepsilon^2)$, explicit results being provided in appendices. In doing so, we emphasize that unlike Refs. [189, 191, 185, 186] we do not assume SU(3) breaking arises only from the lowest SU(3) irreps, nor do we neglect doubly Cabbibo-suppressed (DCS) amplitudes. From these results, we extract both amplitude and rate sum rules, valid to $\mathcal{O}(\varepsilon^2)$. We briefly discuss current experimental measurements of the novel sum rules, and use existing data to predict the as-yet-unmeasured $D^0 \to \rho^- K^+$ rate. We emphasise that this prediction is group theoretic in origin. Finally, we proceed to predict ratio and difference of the direct CP asymmetries for $D \to KK^*$ and $D \to \pi\rho$ under the $\Delta U = 0$ rule [182]. We also show in an appendix how to

derive the zeroth order sum rules without computing the reduced matrix elements explicitly.

6.2 Framework

6.2.1 Amplitudes and Notation

We write the in-state D-meson SU(3) triplet and out-state pseudoscalar and vector SU(3) octets and singlets in the usual tensor coefficient notation

$$
\begin{aligned}
[D_3]^i &= \begin{pmatrix} D^0 \\ D^+ \\ D_s^+ \end{pmatrix} \ , \qquad [P_1] = \eta_1 \ , \qquad [V_1] = \phi_1 \ , \\
[P_8]^i_j &= \begin{pmatrix} \frac{1}{\sqrt{2}}\pi_0 + \frac{1}{\sqrt{6}}\eta_8 & \pi^+ & K^+ \\ \pi^- & -\frac{1}{\sqrt{2}}\pi_0 + \frac{1}{\sqrt{6}}\eta_8 & K^0 \\ K^- & \bar{K}^0 & -\sqrt{\frac{2}{3}}\eta_8 \end{pmatrix} \ , \\
[V_8]^i_j &= \begin{pmatrix} \frac{1}{\sqrt{2}}\rho_0 + \frac{1}{\sqrt{6}}\omega_8 & \rho^+ & K^{*+} \\ \rho^- & -\frac{1}{\sqrt{2}}\rho_0 + \frac{1}{\sqrt{6}}\omega_8 & K^{*0} \\ K^{*-} & \bar{K}^{*0} & -\sqrt{\frac{2}{3}}\omega_8 \end{pmatrix} \ .
\end{aligned}
\tag{6.5}
$$

Hereafter Latin indices are SU(3) tensor indices, while Greek indices label a particular state, so that for $M \in \{D_3, P_8, P_1, V_8, V_1\}$, then $(M_\alpha)^i_j = \partial M^i_j / \partial M_\alpha$ is the tensor corresponding to state M_α.

In general, for a Hamiltonian H – presumed to be an SU(3) tensor operator –

we are interested in constructing decay amplitudes of the form

$$A_{\mu\to\alpha\beta} \equiv \left\langle M_\alpha N_\beta \middle| H \middle| [D_3]_\mu \right\rangle \ . \tag{6.6}$$

The Wigner-Eckart theorem ensures that

$$A_{\mu\to\alpha\beta} = \sum_w X_w (C_w)_{\alpha\beta\mu} \ , \quad (C_w)_{\alpha\beta\mu} = \frac{\partial^3}{\partial M_\alpha \partial N_\beta \partial [D_3]_\mu} \left[M_j^i N_l^k H^{p_1\cdots p_n}_{q_1\cdots q_m} [D_3]^r \right]_w \ . \tag{6.7}$$

Here the square brackets indexed by w denote a linearly independent contraction of the SU(3) indices, X_w is the reduced matrix element for each such contraction, M, $N \in \{P_{1,8}, V_{1,8}\}$, and $H^{p_1\cdots p_n}_{q_1\cdots q_m}$ are the tensor components of the effective Hamiltonian. Each contraction C_w is a Wigner-Eckart invariant, and note that eq. (6.7) implies the Hamiltonian can be written as

$$H = \sum_w X_w C_w \ . \tag{6.8}$$

The amplitudes $A_{\mu\to\alpha\beta}$ are therefore fully specified by partial derivatives of the Wigner-Eckart invariants and the reduced matrix elements. Note that in the case that $M_\alpha = N_\beta$, the partial derivatives in (6.7) naturally encode an extra factor of 2, which is the expected combinatoric factor. However, in comparison to the reduced amplitude $(D|M_\alpha M_\alpha)$ defined in eq. (6.2), we have for mass eigenstates M_α

$$(D|M_\alpha M_\alpha) = \frac{1}{\sqrt{2}} A_{D\to M_\alpha M_\alpha} \tag{6.9}$$

due to the symmetry factor of 1/2 appearing in the decay rate.

6.2.2 Effective Electroweak Hamiltonian

In the SM, $\Delta C = -1$ decays arise at leading order from an effective electroweak Hamiltonian with respectively tree and penguin terms of form [192]

$$\frac{G_F}{\sqrt{2}} V_{uq_1} V^*_{cq_2} (\bar{u} q_1)_L (\bar{q}_2 c)_L \ , \quad -\frac{G_F}{\sqrt{2}} V_{ub} V^*_{cb} (\bar{q} q)_{L,R} (\bar{u} c)_L \ , \tag{6.10}$$

in which $q_{1,2}$ ($\bar{q}_{1,2}$) are (anti)-quark operators u, d, s as appropriate and V is the Cabbibo-Kobayashi-Maskawa (CKM) matrix. The brackets denote Lorentz and color structure, such that $(\bar{q}_1 q_2)_{L,R} \equiv (\bar{q}_{1a})_{L,R} \gamma_\mu (q_2^b)_{L,R}$, with color indices a and b contracted either together or with the adjacent bracket. That is, the operator

$$(\bar{q}_1 q_2)(\bar{q}_3 q_4) = C_1 (\bar{q}_{1a} q_2^b)(\bar{q}_{3b} q_4^a) + C_2 (\bar{q}_{1a} q_2^a)(\bar{q}_{3b} q_4^b) \ , \tag{6.11}$$

where C_i are Wilson coefficients, and the former color contraction arises from the color SU(3) completeness relation applied to QCD final or initial state interactions. Hereafter we drop the chiral labels L and R, as they are implied by context.

In the SU(3) picture, the operators (6.10) embed into the SU(3) four-quark Hamiltonian, which is the tensor operator

$$H = H^k_{ij} (\bar{q}^i q_k)(\bar{q}^j c) \ . \tag{6.12}$$

This tensor decomposes as $\bar{\mathbf{3}} \otimes \mathbf{3} \otimes \bar{\mathbf{3}} = \bar{\mathbf{3}}_{\boldsymbol{p}} \oplus \bar{\mathbf{3}}_{\boldsymbol{t}} \oplus \mathbf{6} \oplus \bar{\mathbf{15}}$. Adopting the tensor coefficient notation $H^k_{ij} \equiv (\bar{q}_i q^k)(\bar{q}_j c)$, one finds explicitly the decomposition

$$H^k_{ij} = \delta^k_j \left(\frac{3}{8} [\bar{\mathbf{3}}_{\boldsymbol{t}}]_i - \frac{1}{8} [\bar{\mathbf{3}}_{\boldsymbol{p}}]_i \right) + \delta^k_i \left(\frac{3}{8} [\bar{\mathbf{3}}_{\boldsymbol{p}}]_j - \frac{1}{8} [\bar{\mathbf{3}}_{\boldsymbol{t}}]_j \right) + \varepsilon_{ijl} [\mathbf{6}]^{lk} + [\bar{\mathbf{15}}]^k_{ij} \ , \tag{6.13}$$

in which the QED-preserving independent components of the H irreps are

$$
\begin{aligned}
[\bar{\mathbf{3}}_{\boldsymbol{p}}]_1 &= (\bar{u}u)(\bar{u}c) + (\bar{d}d)(\bar{u}c) + (\bar{s}s)(\bar{u}c) \\
[\bar{\mathbf{3}}_{\boldsymbol{t}}]_1 &= (\bar{u}u)(\bar{u}c) + (\bar{u}d)(\bar{d}c) + (\bar{u}s)(\bar{s}c) \\
[\mathbf{6}]^{22} &= \frac{1}{2}[(\bar{s}d)(\bar{u}c) - (\bar{u}d)(\bar{s}c)] \\
[\mathbf{6}]^{23} &= \frac{1}{4}[(\bar{u}d)(\bar{d}c) - (\bar{d}d)(\bar{u}c) + (\bar{s}s)(\bar{u}c) - (\bar{u}s)(\bar{s}c)] \\
[\mathbf{6}]^{33} &= \frac{1}{2}[(\bar{u}s)(\bar{d}c) - (\bar{d}s)(\bar{u}c)] \\
[\bar{\mathbf{15}}]^3_{12} &= \frac{1}{2}[(\bar{u}s)(\bar{d}c) + (\bar{d}s)(\bar{u}c)] \\
[\bar{\mathbf{15}}]^2_{13} &= \frac{1}{2}[(\bar{s}d)(\bar{u}c) + (\bar{u}d)(\bar{s}c)] \\
[\bar{\mathbf{15}}]^2_{12} &= \frac{3}{8}[(\bar{u}d)(\bar{d}c) + (\bar{d}d)(\bar{u}c)] - \frac{1}{4}(\bar{u}u)(\bar{u}c) - \frac{1}{8}[(\bar{u}s)(\bar{s}c) + (\bar{s}s)(\bar{u}c)] \\
[\bar{\mathbf{15}}]^3_{13} &= \frac{3}{8}[(\bar{u}s)(\bar{s}c) + (\bar{s}s)(\bar{u}c)] - \frac{1}{4}(\bar{u}u)(\bar{u}c) - \frac{1}{8}[(\bar{u}d)(\bar{d}c) + (\bar{d}d)(\bar{u}c)] \ . \qquad (6.14)
\end{aligned}
$$

All other components are set to zero due to charge conservation. Eqs. (6.10) imply that the tensor components of the electroweak Hamiltonian may be obtained at leading order from the map $(\bar{u}q_1)(\bar{q}_2 c) \mapsto V_{uq_1}V^*_{cq_2}$, $(\bar{q}q)(\bar{u}c) \mapsto -V_{ub}V^*_{cb}$ and other terms zero. Unitarity of the CKM matrix and its Wolfenstein parametrization yields finally the independent H components, to leading order in λ

$$
\begin{gathered}
[\bar{\mathbf{3}}_{\boldsymbol{p}}]_1 \simeq -2\lambda^5 A^2(\rho - i\eta) \ , \qquad [\bar{\mathbf{3}}_{\boldsymbol{t}}]_1 \simeq -\lambda^5 A^2(\rho - i\eta) \ , \\
[\mathbf{6}]^{22} \simeq -\frac{1}{2} \ , \qquad [\mathbf{6}]^{23} \simeq -\frac{\lambda}{2} \ , \qquad [\mathbf{6}]^{33} \simeq -\frac{\lambda^2}{2} \ , \\
[\bar{\mathbf{15}}]^3_{12} \simeq -\frac{\lambda^2}{2} \ , \qquad [\bar{\mathbf{15}}]^2_{13} \simeq \frac{1}{2} \ , \qquad [\bar{\mathbf{15}}]^2_{12} \simeq -\frac{\lambda}{2} \ , \qquad [\bar{\mathbf{15}}]^3_{13} \simeq \frac{\lambda}{2} \ . \qquad (6.15)
\end{gathered}
$$

It is apparent from the CKM structure that $\bar{\mathbf{3}}_{\boldsymbol{p,t}}$ will produce penguin-like contributions to an amplitude, with a CP violating phase – i.e. $\propto \lambda^5 A^2(\rho - i\eta)$ – while the $\mathbf{6}$ and $\bar{\mathbf{15}}$ produce tree-like CF, SCS and DCS terms.

Finally, note that in this parameterization the two $\bar{\mathbf{3}}$ irreps of eq. (6.13) are linear combinations of $\bar{\mathbf{3}}_{\boldsymbol{p,t}}$ and hence always proportional to one another at leading

order in λ; they are not linearly independent. This means we need only consider a single $\bar{\mathbf{3}}$ when computing amplitudes from the invariants and reduced matrix elements. Henceforth, without loss of generality we consider just $\bar{\mathbf{3}}_{\boldsymbol{p}}$ for this purpose, multiplying it by a factor of 3/8 to match the first $\bar{\mathbf{3}}$ irrep of eq. (6.13), and we hereafter call the resulting irrep simply $\bar{\mathbf{3}}$.

6.2.3 SU(3) Breaking

Under the assignment of eqs. (6.15), the electroweak Hamiltonian, H, itself may be thought of as an SU(3) violating spurion. We assume further SU(3) breaking is produced by the s-mass spurion, which in traceless tensor form is

$$m_s = \varepsilon \begin{pmatrix} 1 & 0 & 0 \\ 0 & 1 & 0 \\ 0 & 0 & -2 \end{pmatrix} \quad , \quad \varepsilon \sim 0.2 \ . \tag{6.16}$$

The Hamiltonian becomes $H + Hm_s$ at first order in the spurion, i.e. at order $\mathcal{O}(\varepsilon)$. By eq. (6.7) the corresponding amplitudes are

$$\begin{aligned} A_{\mu\to\alpha\beta} &= \langle M_\alpha M_\beta | H | D_\mu \rangle + \langle M_\alpha M_\beta | H m_s | D_\mu \rangle \\ &\equiv \sum_w X_w (C_w)_{\alpha\beta\mu} + \varepsilon \sum_w X_{w,s} (C_{w,s})_{\alpha\beta\mu} \ , \end{aligned} \tag{6.17}$$

the subscript 's' denoting the first order s-mass spurion contributions. Since we expect $X_{w,s} \sim \mathcal{O}(1)$, then corrections arising from the nth order Hm_s^n spurion term are expected to be $\mathcal{O}(\varepsilon^n)$.

A second, parametrically smaller, source of SU(3) breaking arises from the u-d mass splitting. That is, isospin breaking due to the spurion

$$m_I = \delta \begin{pmatrix} 1 & 0 \\ 0 & -1 \end{pmatrix} \quad , \quad \delta = (m_u - m_d)/\Lambda_{\rm qcd} \sim 1\% \ , \tag{6.18}$$

which we have written in the adjoint representation of the isospin subgroup, rather than as a SU(3) tensor. This spurion similarly introduces Hm_I^n corrections at $\mathcal{O}(\delta^n)$, the first order correction being $\delta \sum X_{w,I} C_{w,I}$, whose invariants can be computed similarly to those of m_s.

In this language, the key idea of the large broken penguin picture is that certain X_w and $X_{w,s}$ are enhanced. For example, under the $\Delta U = 0$ rule of Ref. [182], the reduced matrix elements associated with exclusively $\Delta U = 0$ operators are enhanced. One might propose an extension of this rule to the SU(3) picture, which would enhance the reduced matrix elements associated with contractions involving the $\Delta U = 0$ components $[\bar{\mathbf{3}}]_1$, $[\mathbf{6}]^{23}$, $[\mathbf{1\bar{5}}]^2_{12}$ and $[\mathbf{1\bar{5}}]^3_{13}$. We will discuss the implications of this idea briefly below, but a full global fit of this proposed picture to the data is beyond the scope of the present paper.

6.2.4 Formal Sum Rules

A key feature of SU(3) breaking, and the focus of this paper, is the set of associated sum rules, which can be computed to arbitrary order in ε. To be precise, a sum rule is a symbol $\mathcal{S}$, such that

$$\mathcal{S}^{\alpha\beta\mu} \mathcal{A}_{\mu \to \alpha\beta} = 0 \tag{6.19}$$

which is equivalent to

$$\mathcal{S}^{\alpha\beta\mu} (C_w)_{\alpha\beta\mu} = 0 \ , \quad \forall w \ , \tag{6.20}$$

noting that w labels the invariants. In general, a sum rule may be found to $\mathcal{O}(\varepsilon^n)$ by computing the appropriate invariants to that order, and solving the linear equations (6.20), that is, finding the kernel of $(C_w)_{\alpha\beta\mu}$. The number of sum

rules is a non-increasing function of n, and the number of sum rules may be zero once n is sufficiently high, depending on the pattern of symmetry breaking.

Alternatively, as we show in Appendix D.1, the symmetries of the Hamiltonian H may be sometimes used to compute sum rules directly, without needing to first compute the invariants. The key idea is that if there exists an operator T under which H is invariant, that is $TH = 0$, then it follows that

$$T^{\rho\sigma\gamma}_{\alpha\beta\mu}(C_w)_{\rho\sigma\gamma} = 0 \ , \tag{6.21}$$

where the indices here are the indices of the corresponding final and initial state irreps, rather than tensor indices. For example, if T is an operator that changes electric charge by ΔQ, then choosing α, β and μ corresponding to an amplitude which violates QED by $-\Delta Q$ produces a sum rule of QED preserving amplitudes. That is $\mathcal{S} = T_{\alpha\beta\mu}$. In Appendix D.1 we compute the zeroth order in m_s sum rules for $D \to PP$ by this alternate method.

On a presentational note, we emphasize that a linear combination of sum rules is also a sum rule, so that there is an arbitrarily large way to write any set of m linearly independent sum rules. In particular, in finding the kernel of C_w, one may often find short (long) sum rules involving a small (large) number of amplitudes. In writing the sum rules, we have adopted the preference that the longest sum rules have as minimal length as possible, while well-known sum rules, in particular the U-spin and the isospin sum rules, are also explicitly presented. There exists no algorithm that achieves this preference. Instead we have employed an approximate computational method in which the m-dimensional kernel is computed repeatedly under random permutations of the amplitude basis, forming a large list of dependent sum rules. After extracting well-known sum rules from this list, we then extract the shortest remaining linearly independent set of sum rules that will span

– together with the well-known ones – the m-dimensional kernel.

6.2.5 Rate Sum Rules

Amplitude sum rules can only be verified if the strong phases of each amplitude are known. Sum rules involving square amplitudes – rate sum rules – are therefore particularly useful, since these correspond to sum rules of branching ratios or decay rates, provided the corresponding phase spaces are not zero. We may similarly compute the rate sum rules by observing that

$$\left|\mathcal{A}_{\mu\to\alpha\beta}\right|^2 = \sum_w \sum_{w'} X_w X^*_{w'} (C_w)_{\alpha\beta\mu} (C_{w'})^*_{\alpha\beta\mu} \equiv \sum_u X_u (C_u)_{\alpha\beta\mu} \tag{6.22}$$

where $u = \{w, w'\}$, $X_u = X_w X^*_{w'}$ and $C_u = C_w C_{w'}$; C_w are real. Eq. (6.22) implies that one need only solve the linear equations $\mathcal{S}^{\alpha\beta\mu}(C_u)_{\alpha\beta\mu} = 0$, $\forall u$ in order to obtain the sum rules at the desired order.

It should be carefully noted that we have defined SU(3) breaking in eq. (6.1) in terms of decay constants, which themselves are proportional to amplitudes, rather than decay rates. Hence we should generically expect an SU(3) amplitude relation to be valid to $\sim \epsilon$ while a square amplitude relation should be valid to $\sim 2\epsilon$. In the present context, we similarly expect a rate sum rule to be twice as imprecise compared to an amplitude sum rule. That is, rate sum rules valid to the pth order in SU(3) breaking should be $\sim 2\epsilon^p$, while amplitude sum rules are $\sim \epsilon^p$. It is for this reason that a normed-amplitude sum rule like eq. (6.4) is an appropriate relation to compare to the naïve SU(3) breaking scale. We will discuss the origin of normed-amplitude sum rules in Secs. 6.3.4 and 6.4.5.

6.2.6 Isospin and U-spin Sum Rules

So far we have embedded the electroweak Hamiltonian into flavor SU(3) irreps, such that it is an SU(3) spurion. The effective Hamiltonian itself then generates invariants and SU(3) sum rules; a subspace of these sum rules holds once nth order s-mass spurion terms are added. We may, however, alternatively embed the effective Hamiltonian into SU(3) subgroups, in particular U-spin and isospin, and construct invariants involving only those initial and final states which furnish irreps of these subgroups. The Hamiltonian is then a spurion of these subgroups, and in this manner we may obtain sum rules, which we call the U-spin or isospin sum rules respectively. Of course, these isospin and U-spin sum rules necessarily also arise in the full SU(3) picture itself, but generally in linear combinations with other pure SU(3) sum rules.

Returning to the full SU(3) picture, while the electroweak Hamiltonian itself necessarily breaks isospin, observe the s-mass spurion m_s does not; it breaks SU(3) down to isospin $\times$ strangeness (or equivalently QED). One therefore expects isospin sum rules obtained from the electroweak Hamiltonian itself to be preserved to all orders in m_s, even though isospin itself is already broken by H. One can verify this expectation explicitly with the language of eq. (6.21): In the isospin picture, if T is an isospin tensor operator that generates isospin sum rules, i.e. $TH = 0$, then since m_s is an isospin singlet, $Tm_s = 0$. This result naturally embeds into the full SU(3) picture, thereby showing that isospin sum rules are unbroken to all orders in m_s.

This result is particularly useful: If there is no other significant source of SU(3) breaking other than m_s and m_I, then isospin sum rules valid to second order in the *isospin* spurion m_I – i.e. valid to $\mathcal{O}(\delta^2)$ – are expected to hold to the 10^{-4}

level. Verifying such a sum rule is therefore an extremely sensitive test of the presence of other sources of SU(3) breaking, which includes new physics. We shall examine such sum rules for the $D \to PP$ and $D \to PV$ case. It should be noted that sensitive sum rule tests based on isospin have previously been proposed for charmless B decays [193], although these depended on dynamical suppression of first order isospin breaking. Here the effect is due to the pattern of symmetry breaking itself.

6.2.7 Mixing

The states furnishing the SU(3) octet and singlets do not always correspond to meson mass eigenstates. In particular, one must account for $K - K$, $\omega - \phi$ and $\eta - \eta'$ mixing. In the CP limit, which we assume for kaon mixing, the mixing of $K^0 - \bar{K}^0$ is maximal, so we define the usual mass eigenstates

$$\begin{pmatrix} K_S \\ K_L \end{pmatrix} = \frac{1}{\sqrt{2}} \begin{pmatrix} 1 & 1 \\ -1 & 1 \end{pmatrix} \begin{pmatrix} K^0 \\ \bar{K}^0 \end{pmatrix} \ . \tag{6.23}$$

Similarly, the ω-ϕ mixing is idealized such that the ϕ mass eigenstate is pure $\bar{s}s$. I.e. the mass eigenstates

$$\begin{pmatrix} \omega \\ \phi \end{pmatrix} = \frac{1}{\sqrt{3}} \begin{pmatrix} 1 & \sqrt{2} \\ -\sqrt{2} & 1 \end{pmatrix} \begin{pmatrix} \omega_8 \\ \phi_1 \end{pmatrix} \ . \tag{6.24}$$

Finally, in the case of $\eta - \eta'$ mixing, the mixing angle is neither ideal nor maximal [194, 195, 196], so one defines mass eigenstates

$$\begin{pmatrix} \eta \\ \eta' \end{pmatrix} = \begin{pmatrix} \cos\theta & -\sin\theta \\ \sin\theta & \cos\theta \end{pmatrix} \begin{pmatrix} \eta_8 \\ \eta_1 \end{pmatrix} \ . \tag{6.25}$$

Hereafter while the invariants are computed in terms of the flavor SU(3) states, we shall write the sum rules in terms of either the mass or flavor basis, depending on convenience.

6.3 $D \to PP$ Sum Rules

In this section we present the $D \to PP$ amplitude and rate sum rules that are valid to $\mathcal{O}(\varepsilon^2)$, that is, they are naïvely broken at $\mathcal{O}(\varepsilon^2)$. The corresponding SU(3) invariants are presented in detail in Appendix D.2. We emphasize that we compute the sum rules only from tree-like operators. That is, we neglect the sub-leading invariants of order $\mathcal{O}(\lambda^5)$ due to the $\bar{\mathbf{3}}$ irreps, and consider only the invariants produced by the $\mathbf{6}$ and $\bar{\mathbf{15}}$.

We note in passing that the SU(3) invariants constructed from the $\mathbf{6}$ and $\bar{\mathbf{15}}$ generally involve both $\Delta U = 0$ and $\Delta U = \pm 1$ operators, but we see from the tables that only $\Delta U = 0$ amplitudes receive corrections from

$$C^{[\mathrm{PP}]_{\mathbf{6}_s}^2}_{[88]} \ , \qquad C^{[\mathrm{PP}]_{\bar{\mathbf{15}}_s}^1}_{[88]} \ , \qquad \text{and} \qquad C^{[\mathrm{PP}]_{\bar{\mathbf{15}}_s}^7}_{[88]} \ . \tag{6.26}$$

That is, these invariants must involve exclusively $\Delta U = 0$ operators. A $\Delta U = 0$ rule could then be implemented by enhancing only those reduced matrix elements associated with these three invariants. However, we do not consider this possibility further in the present work.

6.3.1 P_1P_8 Amplitude Sum Rules

Sum rules valid at first order in the spurion can be extracted from the invariants presented in Appendix D.2. One finds that there are twelve sum rules for P_8P_8 and two for P_1P_8. The two P_1P_8 sum rules are, in the SU(3) flavor basis

i)

$$-\frac{A_{D^+\to\eta_1 K^+}}{\lambda^2}+\frac{A_{D^+\to\eta_1\pi^+}}{\lambda}-\frac{A_{D_s^+\to\eta_1 K^+}}{\lambda}+A_{D_s^+\to\eta_1\pi^+}=0$$

ii)

$$-\frac{\sqrt{3}A_{D^0\to\eta_1\eta_8}}{\lambda}+\frac{\sqrt{2}A_{D^0\to\eta_1 K^0}}{\lambda^2}+\frac{A_{D^0\to\eta_1\pi_0}}{\lambda}-\sqrt{2}A_{D^0\to\eta_1\bar{K}^0}=0\ .$$

6.3.2 Isospin Sum Rules

For the P_8P_8 sum rules, we first identify the pure isospin sum rules. Explicitly, note that we have the isospin $\times$ strangeness irreps

$$\Pi^i_j=\begin{pmatrix}\frac{\pi^0}{\sqrt{2}} & \pi^+\\ \pi^- & -\frac{\pi^0}{\sqrt{2}}\end{pmatrix}\sim 3_0\ ,\quad K^i=\begin{pmatrix}K^+\\ K^0\end{pmatrix}\sim 2_{-1}\ ,\quad \eta_{8,1}\sim 1_0\ ,$$
$$\bar{K}_i=\begin{pmatrix}K^- & \bar{K}^0\end{pmatrix}\sim 2_{+1}\ ,\quad D^i=\begin{pmatrix}D^0\\ D^+\end{pmatrix}\sim 2_0\ ,\quad D_s^+\sim 1_1\ , \tag{6.27}$$

and we expect one sum rule for each of $\Pi\Pi$, ΠK and $\Pi\bar{K}$ final states. These three sum rules are,

iii)

$$-A_{D^0\to 2\pi_0}+A_{D^0\to\pi^-\pi^+}+\sqrt{2}A_{D^+\to\pi_0\pi^+}=0$$

iv)

$$A_{D^0\to\pi_0\bar{K}^0} + \frac{A_{D^0\to K^-\pi^+}}{\sqrt{2}} - \frac{A_{D^+\to\bar{K}^0\pi^+}}{\sqrt{2}} = 0$$

v)

$$\sqrt{2}A_{D^0\to K^0\pi_0} + A_{D^0\to\pi^-K^+} + \sqrt{2}A_{D^+\to\pi_0K^+} - A_{D^+\to K^0\pi^+} = 0\ .$$

Note that isospin sum rules must involve amplitudes of the same strangeness violation – i.e. same ΔS – and therefore of the same Cabibbo order, due to the structure of the effective Hamiltonian. As a result $D^0 \to K^0\bar{K}^0$, which occurs only through penguin operators, cannot form a sum rule with the other $K\bar{K}$ processes $D^+ \to K^+\bar{K}^0$ and $D^0 \to K^+K^-$, which occur at tree level. There is therefore no sum rule for the $K\bar{K}$ final state. The CF and SCS isospin rules, respectively iii and iv, have been previously shown to hold at first order in SU(3) breaking [190].

As mentioned in Sec. 6.2.6, these isospin sum rules hold to all s-mass spurion orders, so sum rules valid to second order in isospin breaking – i.e. to $\mathcal{O}(\delta^2)$ – are a sensitive test of alternate SU(3) breaking sources. If one computes the invariants at first order in SU(3) breaking by the isospin spurion, m_I, one finds that all three isospin sum rules are broken at $\mathcal{O}(\delta)$, as expected. However, the difference sum rule v $-\ \lambda$iii is valid to $\mathcal{O}(\delta^2)$. Precisely measuring the deviation from zero of the corresponding reduced amplitude sum rule

$$\frac{(D^+|K^0\pi^+) - \sqrt{2}(D^+|\pi_0K^+) + \lambda\sqrt{2}(D^+|\pi_0\pi^+)}{\sqrt{2}(D^0|K^0\pi_0) + (D^0|\pi^-K^+) - \lambda(D^0|\pi^-\pi^+) + \lambda\sqrt{2}(D^0|2\pi_0)} - 1 \qquad (6.28)$$

could therefore be a comparatively sensitive test of new physics, even if $\Delta\mathcal{A}_{CP}$ itself is due to SM physics. While branching fractions of all seven modes in this sum rule have been measured [3], one must also know the strong phases in order to compute (6.28). Strong phases can be measured from the Dalitz plots of 3-body

charm decays (see e.g [197]), and determining the strong phases here remains an experimental goal for the future.

6.3.3 P_8P_8 Sum Rules

Now, returning to the full SU(3), we choose our sum rule basis such that the above three isospin sum rules are presented explicitly, along with the single U-spin sum rule

vi)

$$\frac{A_{D^0\to K^-K^+}}{\lambda}+\frac{A_{D^0\to \pi^-K^+}}{\lambda^2}-A_{D^0\to K^-\pi^+}-\frac{A_{D^0\to \pi^-\pi^+}}{\lambda}=0\ .$$

The remaining eight linearly independent P_8P_8 sum rules are pure SU(3) sum rules, which we find to be

vii)

$$-\frac{\sqrt{3}A_{D^0\to\eta_8K^0}}{\lambda^2}+\frac{A_{D^0\to K^0\pi_0}}{\lambda^2}-\sqrt{3}A_{D^0\to\eta_8\bar{K}^0}+A_{D^0\to\pi_0\bar{K}^0}=0$$

viii)

$$\frac{\sqrt{3}A_{D^+\to\eta_8K^+}}{\lambda^2}-\frac{A_{D^+\to\pi_0K^+}}{\lambda^2}+\sqrt{2}\frac{A_{D^+\to\bar{K}^0K^+}}{\lambda}+\sqrt{3}A_{D_s^+\to\eta_8\pi^+}$$
$$-\sqrt{2}\frac{A_{D_s^+\to K^0\pi^+}}{\lambda}=0$$

ix)

$$A_{D^+\to\bar{K}^0\pi^+}-A_{D_s^+\to\bar{K}^0K^+}-\frac{A_{D^+\to\bar{K}^0K^+}}{\lambda}+\frac{A_{D_s^+\to K^0\pi^+}}{\lambda}+\frac{A_{D^+\to K^0\pi^+}}{\lambda^2}$$
$$-\frac{A_{D_s^+\to K^0K^+}}{\lambda^2}=0$$

x)

$$\sqrt{3}\frac{A_{D^0\to\eta_8\pi_0}}{\lambda} - \frac{\sqrt{2}A_{D^0\to K^0\pi_0}}{\lambda^2} - \frac{A_{D^0\to 2\pi_0}}{\lambda} - \sqrt{\frac{3}{2}}A_{D^0\to\eta_8\bar{K}^0} + \frac{A_{D^0\to K^0\bar{K}^0}}{\lambda} + \frac{3A_{D^0\to\pi_0\bar{K}^0}}{\sqrt{2}} = 0$$

xi)

$$\frac{A_{D^0\to 2\eta_8}}{\lambda} + \frac{2A_{D^0\to\eta_8\pi_0}}{\sqrt{3}\lambda} - \frac{4\sqrt{2}A_{D^0\to K^0\pi_0}}{3\lambda^2} - \frac{A_{D^0\to 2\pi_0}}{\lambda} + 2\sqrt{\frac{2}{3}}A_{D^0\to\eta_8\bar{K}^0} + \frac{2}{3}\sqrt{2}A_{D^0\to\pi_0\bar{K}^0} = 0$$

xii)

$$\frac{\sqrt{2}A_{D^+\to\pi_0K^+}}{\lambda^2} - \frac{A_{D^+\to\bar{K}^0K^+}}{\lambda} - \frac{\sqrt{2}A_{D^+\to\pi_0\pi^+}}{\lambda} + A_{D^+\to\bar{K}^0\pi^+} + \frac{\sqrt{2}A_{D_s^+\to\pi_0K^+}}{\lambda} - A_{D_s^+\to\bar{K}^0K^+} = 0$$

xiii)

$$-\sqrt{\frac{2}{3}}A_{D_s^+\to\bar{K}^0K^+} - \frac{A_{D^+\to\eta_8\pi^+}}{\lambda} - \frac{A_{D^+\to\pi_0\pi^+}}{\sqrt{3}\lambda} + \frac{2A_{D_s^+\to\pi_0K^+}}{\sqrt{3}\lambda} + \frac{A_{D^+\to\eta_8K^+}}{\lambda^2} + \frac{A_{D^+\to\pi_0K^+}}{\sqrt{3}\lambda^2} + \sqrt{\frac{2}{3}}\frac{A_{D^+\to K^0\pi^+}}{\lambda^2} = 0$$

xiv)

$$\frac{2A_{D^+\to\pi_0K^+}}{\sqrt{3}\lambda^2} - \sqrt{\frac{2}{3}}\frac{A_{D^+\to K^0\pi^+}}{\lambda^2} - \frac{2A_{D^+\to\pi_0\pi^+}}{\sqrt{3}\lambda} + \frac{A_{D_s^+\to\eta_8K^+}}{\lambda} + \frac{A_{D_s^+\to\pi_0K^+}}{\sqrt{3}\lambda} + \sqrt{\frac{2}{3}}A_{D_s^+\to\bar{K}^0K^+} - A_{D_s^+\to\eta_8\pi^+} = 0\ .$$

Again, these sum rules can only be verified provided the corresponding strong phases for each process can be measured. Conversion to the mass basis is achieved

by the relations

$$A_{D\to fK^0} = \frac{1}{\sqrt{2}}A_{D\to fK_S} - \frac{1}{\sqrt{2}}A_{D\to fK_L}\ , \quad A_{D\to f\bar{K}^0} = \frac{1}{\sqrt{2}}A_{D\to fK_S} + \frac{1}{\sqrt{2}}A_{D\to fK_L}\ ,$$
$$A_{D\to K^0\bar{K}^0} = \frac{1}{2}A_{D\to 2K_S} - \frac{1}{2}A_{D\to 2K_L}\ ,$$
$$A_{D\to f\eta_8} = \cos\theta A_{D\to f\eta} + \sin\theta A_{D\to f\eta'}\ , \quad A_{D\to f\eta_1} = -\sin\theta A_{D\to f\eta} + \cos\theta A_{D\to f\eta'}\ , \tag{6.29}$$

applying the extra symmetry factor (6.9) as appropriate. Note that the amplitudes involving either $\eta_1\eta_8$ or $\eta_8\eta_8$ final states necessarily include a $A_{D\to\eta'\eta'}$ term, which cannot be measured due to its zero phase space. The sum rules including such amplitudes, which here are sum rules (ii) and (xi), therefore cannot be measured from decays.

6.3.4 Rate Sum Rules

We next present the rate sum rules valid to $\mathcal{O}(\varepsilon^2)$, which have the added advantage of being directly proportional to the corresponding branching ratios. Following from eq. (6.22), the invariants of the square amplitudes up to and including order $\mathcal{O}(\varepsilon)$ are found by taking all possible $\mathcal{O}(1)$ and $\mathcal{O}(\varepsilon)$ pairwise products of the amplitude invariants in Appendix D.2, taking into account the mixings of Sec. 6.2.7. Applying eq. (6.9) where appropriate, one finds the following square amplitude sum rules.

(i)

$$|(D^+|K_LK^+)|^2 = |(D^+|K_SK^+)|^2$$

(ii)

$$|(D_s^+|K_L\pi^+)|^2 = |(D_s^+|K_S\pi^+)|^2$$

(iii)

$$\frac{|(D^0|K^-K^+)|^2}{\lambda^2} + \frac{|(D^0|\pi^-\pi^+)|^2}{\lambda^2} = \frac{|(D^0|\pi^-K^+)|^2}{\lambda^4} + |(D^0|K^-\pi^+)|^2$$

(iv)

$$|(D^0|2\eta)|^2 + |(D^0|\eta\pi_0)|^2 + |(D^0|2\pi_0)|^2 + |(D^0|\eta\eta')|^2 + |(D^0|\pi_0\eta')|^2 + |(D^0|2\eta')|^2$$

$$=$$

$$\Big[|(D^0|\eta K_L)|^2 - |(D^0|\eta K_S)|^2\Big] + \Big[|(D^0|K_L\pi_0)|^2 - |(D^0|K_S\pi_0)|^2\Big]$$
$$+\Big[|(D^0|K_L\eta')|^2 - |(D^0|K_S\eta')|^2\Big]$$

(v)

$$\frac{|(D^+|\eta\pi^+)|^2}{\lambda^2} + \frac{|(D^+|\pi_0\pi^+)|^2}{\lambda^2} + \frac{|(D^+|\pi^+\eta')|^2}{\lambda^2} + \frac{|(D_s^+|\eta K^+)|^2}{\lambda^2}$$
$$+\frac{|(D_s^+|\pi_0K^+)|^2}{\lambda^2} + \frac{|(D_s^+|K^+\eta')|^2}{\lambda^2}$$

$$=$$

$$\frac{|(D^+|\eta K^+)|^2}{\lambda^4} + \frac{|(D^+|\pi_0K^+)|^2}{\lambda^4} + \frac{|(D^+|K^+\eta')|^2}{\lambda^4} + |(D_s^+|\eta\pi^+)|^2 + |(D_s^+|\pi^+\eta')|^2$$
$$+\left[\frac{|(D_s^+|K_LK^+)|^2}{\lambda^2} - \frac{|(D_s^+|K_SK^+)|^2}{\lambda^2}\right] + \left[\frac{|(D^+|K_L\pi^+)|^2}{\lambda^2} - \frac{|(D^+|K_S\pi^+)|^2}{\lambda^2}\right]$$

The first two sum rules are simply consequences of $K-K$ mixing and sum rule (iii) is the U-spin rate sum rule. Combining the latter with the amplitude U-spin sum rule vi of Sec. 6.3.3, admits the possibility that the normed amplitude sum rule (6.4) may also be valid to $\mathcal{O}(\varepsilon^2)$, as expected. To see this, let us write the rate and amplitude sum rules in the form

$$|a|^2 + |b|^2 = |c|^2 + |d|^2 + \mathcal{O}(\varepsilon^2)\ , \qquad a - b = c - d + \mathcal{O}(\varepsilon^2)\ . \tag{6.30}$$

These are (non-uniquely) satisfied by the relations

$$a = c + P\varepsilon + \mathcal{O}(\varepsilon^2) \ , \qquad b = d + P\varepsilon + \mathcal{O}(\varepsilon^2) \ , \qquad \text{and} \qquad c + d = Q\varepsilon + \mathcal{O}(\varepsilon^2) \ , \tag{6.31}$$

for some $\mathcal{O}(1)$ P and Q. One may explicitly verify from Appendix D.2 that the amplitudes in the U-spin sum rule satisfy eqs. (6.31); the desired relation $|a|+|b| = |c| + |d| + \mathcal{O}(\varepsilon^2)$ – i.e. eq. (6.4) – follows immediately. We emphasize that this normed amplitude sum rule is a consequence of the particular structure of the invariants, and in the present analysis this circumstance is unique to the U-spin sum rules.

Sum rules (iv) and (v) are novel to the broken SU(3) picture. Note that sum rule (iv) involves a $D^0 \to 2\eta'$ decay, which has zero phase space. Hence this sum rule is unfortunately not measurable. In contrast, sum rule (v) is measurable, and requires that the branching ratios and phase space of all these modes be experimentally determined.

6.4 $D \to PV$ Sum Rules

As for the $D \to PP$ case, the amplitude and rate sum rules valid to $\mathcal{O}(\varepsilon^2)$ can be extracted from the $D \to PV$ invariants of Appendix D.3 by computing the kernel in the amplitude basis. Once again, we emphasize that in computing the sum rules we neglect the sub-leading invariants of order $\mathcal{O}(\lambda^5)$ due to the $\bar{\mathbf{3}}$ irreps, and consider only the invariants produced by the $\mathbf{6}$ and $\mathbf{\bar{15}}$.

6.4.1 P_1V_8 and V_1P_8 Amplitude Sum Rules

The two P_1V_8 and two V_1P_8 sum rules valid to $\mathcal{O}(\varepsilon^2)$ are respectively in the flavor basis

i)

$$\frac{A_{D^+\to\eta_1\rho^+}}{\lambda} - \frac{A_{D^+\to\eta_1 K^{*+}}}{\lambda^2} + A_{D_s^+\to\eta_1\rho^+} - \frac{A_{D_s^+\to\eta_1 K^{*+}}}{\lambda} = 0$$

ii)

$$\frac{\sqrt{3}A_{D^0\to\omega_8\eta_1}}{\lambda} - \frac{A_{D^0\to\eta_1\rho_0}}{\lambda} - \frac{\sqrt{2}A_{D^0\to\eta_1 K^{*0}}}{\lambda^2} + \sqrt{2}A_{D^0\to\eta_1\bar{K}^{*0}} = 0$$

iii)

$$\frac{A_{D^+\to\phi_1 K^+}}{\lambda^2} - \frac{A_{D^+\to\phi_1\pi^+}}{\lambda} + \frac{A_{D_s^+\to\phi_1 K^+}}{\lambda} - A_{D_s^+\to\phi_1\pi^+} = 0$$

iv)

$$-\frac{\sqrt{2}A_{D^0\to\phi_1 K^0}}{\lambda^2} - \frac{A_{D^0\to\phi_1\pi_0}}{\lambda} + \frac{\sqrt{3}A_{D^0\to\phi_1\eta_8}}{\lambda} + \sqrt{2}A_{D^0\to\phi_1\bar{K}^0} = 0\ .$$

6.4.2 Isospin Sum Rules

As for the PP case, we now proceed to determine the P_8V_8 isospin sum rules. Similarly to eq. (6.27) the isospin $\times$ strangeness vector meson irreps are

$$\rho^i_j = \begin{pmatrix} \frac{\rho^0}{\sqrt{2}} & \rho^+ \\ \rho^- & -\frac{\rho^0}{\sqrt{2}} \end{pmatrix} \sim 3_0\ , \quad K^{*i} = \begin{pmatrix} K^{*+} \\ K^{*0} \end{pmatrix} \sim 2_{-1}\ , \quad \omega_8, \phi_1 \sim 1_0\ ,$$
$$\bar{K}^*_i = \begin{pmatrix} K^{*-} & \bar{K}^{*0} \end{pmatrix} \sim 2_{+1}\ . \tag{6.32}$$

This time there are 6 isospin sum rules; two for the $\Pi\rho$ final state, and one each for the ρK, $\rho\bar{K}$, ΠK^* and $\Pi\bar{K}^*$ final states. Explicitly, these are

v)

$$A_{D_s^+\to\rho_0\pi^+} + A_{D_s^+\to\pi_0\rho^+} = 0$$

vi)

$$\sqrt{2}A_{D^0\to\rho_0\bar{K}^0} + A_{D^0\to K^-\rho^+} - A_{D^+\to\bar{K}^0\rho^+} = 0$$

vii)

$$\sqrt{2}A_{D^0\to\pi_0\bar{K}^{*0}} + A_{D^0\to K^{*-}\pi^+} - A_{D^+\to\bar{K}^{*0}\pi^+} = 0$$

viii)

$$A_{D^0\to\pi_0 K^{*0}} + \frac{A_{D^0\to\pi^- K^{*+}}}{\sqrt{2}} - \frac{A_{D^+\to K^{*0}\pi^+}}{\sqrt{2}} + A_{D^+\to\pi_0 K^{*+}} = 0$$

ix)

$$A_{D^0\to K^0\rho_0} + \frac{A_{D^0\to\rho^- K^+}}{\sqrt{2}} + A_{D^+\to\rho_0 K^+} - \frac{A_{D^+\to K^0\rho^+}}{\sqrt{2}} = 0$$

x)

$$-\sqrt{2}A_{D^0\to\pi_0\rho_0} + \frac{A_{D^0\to\rho^-\pi^+}}{\sqrt{2}} + \frac{A_{D^0\to\pi^-\rho^+}}{\sqrt{2}} + A_{D^+\to\rho_0\pi^+} + A_{D^+\to\pi_0\rho^+} = 0\ .$$

Again, these isospin sum rules hold to all s-mass spurion orders. Computing isospin breaking invariants one finds at first order in the isospin breaking spurion that vi + vii $-\sqrt{2}$v is valid to $\mathcal{O}(\delta^2)$, as are sum rules viii, ix and x. These four sum rules thus provide further isospin tests of the pattern of SU(3) breaking, that are highly sensitive to new physics. Perhaps the easiest to measure is the Cabibbo-favored combination vi + vii $-\sqrt{2}$v, which is equivalent to measuring the deviation from zero of the reduced amplitude relation

$$\frac{\sqrt{2}(D^0|\rho_0\bar{K}^0) + (D^0|K^-\rho^+) + \sqrt{2}(D^0|\pi_0\bar{K}^{*0}) + (D^0|K^{*-}\pi^+)}{(D^+|\bar{K}^0\rho^+) + (D^+|\bar{K}^{*0}\pi^+) + \sqrt{2}(D_s^+|\rho_0\pi^+) + \sqrt{2}(D_s^+|\pi_0\rho^+)} - 1\ . \qquad (6.33)$$

At present, not all these modes have been measured [3], and moreover, one must find the strong phases.

6.4.3 P_8V_8 Sum Rules

Returning to SU(3) , the two U-spin sum rules are

xi)

$$-A_{D^0\to K^{*-}\pi^+} + \frac{A_{D^0\to K^{*-}K^+}}{\lambda} - \frac{A_{D^0\to\rho^-\pi^+}}{\lambda} + \frac{A_{D^0\to\rho^-K^+}}{\lambda^2} = 0$$

xii)

$$A_{D^0\to K^-\rho^+} + \frac{A_{D^0\to\pi^-\rho^+}}{\lambda} - \frac{A_{D^0\to K^-K^{*+}}}{\lambda} - \frac{A_{D^0\to\pi^-K^{*+}}}{\lambda^2} = 0\ .$$

Choosing a basis in which the isospin and U-spin sum rules are explicit, we find a further 15 pure SU(3) sum rules, valid to $\mathcal{O}(\varepsilon^2)$,

xiii)

$$\frac{A_{D^+\to\bar{K}^{*0}K^+}}{\lambda} - \frac{A_{D^+\to K^{*0}\pi^+}}{\lambda^2} - A_{D^+\to\bar{K}^{*0}\pi^+} + \frac{A_{D_s^+\to K^{*0}K^+}}{\lambda^2}$$
$$+ A_{D_s^+\to\bar{K}^{*0}K^+} - \frac{A_{D_s^+\to K^{*0}\pi^+}}{\lambda} = 0$$

xiv)

$$A_{D^+\to\bar{K}^0\rho^+} - A_{D_s^+\to\bar{K}^0K^{*+}} - \frac{A_{D^+\to\bar{K}^0K^{*+}}}{\lambda} + \frac{A_{D_s^+\to K^0\rho^+}}{\lambda}$$
$$+ \frac{A_{D^+\to K^0\rho^+}}{\lambda^2} - \frac{A_{D_s^+\to K^0K^{*+}}}{\lambda^2} = 0$$

xv)

$$\sqrt{\frac{3}{2}}\frac{A_{D^0\to\eta_8K^{*0}}}{\lambda^2} - \frac{A_{D^0\to\pi_0K^{*0}}}{\sqrt{2}\lambda^2} + \frac{A_{D^0\to\bar{K}^0K^{*0}}}{\lambda} + \sqrt{\frac{3}{2}}\frac{A_{D^0\to\eta_8\bar{K}^{*0}}}{\lambda}$$
$$- \frac{A_{D^0\to K^0\bar{K}^{*0}}}{\lambda^2} - \frac{A_{D^0\to\pi_0\bar{K}^{*0}}}{\sqrt{2}\lambda} = 0$$

xvi)

$$-\frac{A_{D^0\to\eta_8\omega_8}}{\lambda}+\sqrt{\frac{2}{3}}\frac{A_{D^0\to\omega_8K^0}}{\lambda^2}+\frac{A_{D^0\to\omega_8\pi_0}}{\sqrt{3}\lambda}-\sqrt{\frac{2}{3}}A_{D^0\to\omega_8\bar{K}^0}+\sqrt{\frac{3}{2}}\frac{A_{D^0\to\eta_8K^{*0}}}{\lambda^2}$$
$$-\frac{A_{D^0\to\pi_0K^{*0}}}{\sqrt{2}\lambda^2}+\frac{A_{D^0\to\bar{K}^0K^{*0}}}{\lambda}=0$$

xvii)

$$-\frac{A_{D^0\to\eta_8\omega_8}}{\lambda}+\sqrt{\frac{3}{2}}\frac{A_{D^0\to\omega_8K^0}}{\lambda^2}+\frac{A_{D^0\to\eta_8\rho_0}}{\sqrt{3}\lambda}-\frac{A_{D^0\to K^0\rho_0}}{\sqrt{2}\lambda^2}+\sqrt{\frac{2}{3}}\frac{A_{D^0\to\eta_8K^{*0}}}{\lambda^2}$$
$$-\sqrt{\frac{2}{3}}A_{D^0\to\eta_8\bar{K}^{*0}}+\frac{A_{D^0\to K^0\bar{K}^{*0}}}{\lambda}=0$$

xviii)

$$\frac{A_{D_s^+\to\omega_8K^+}}{\lambda}-\frac{A_{D_s^+\to\rho_0K^+}}{\sqrt{3}\lambda}-\sqrt{\frac{2}{3}}\frac{A_{D_s^+\to K^{*0}K^+}}{\lambda^2}+\sqrt{\frac{2}{3}}A_{D_s^+\to\bar{K}^{*0}K^+}-A_{D_s^+\to\omega_8\pi^+}$$
$$+\frac{A_{D_s^+\to\rho_0\pi^+}}{\sqrt{3}}+\sqrt{\frac{2}{3}}\frac{A_{D_s^+\to K^{*0}\pi^+}}{\lambda}=0$$

xix)

$$\frac{A_{D_s^+\to\rho_0\pi^+}}{\sqrt{3}}+A_{D_s^+\to\eta_8\rho^+}-\sqrt{\frac{2}{3}}\frac{A_{D_s^+\to K^0\rho^+}}{\lambda}-\frac{A_{D_s^+\to\eta_8K^{*+}}}{\lambda}+\sqrt{\frac{2}{3}}\frac{A_{D_s^+\to K^0K^{*+}}}{\lambda^2}$$
$$+\frac{A_{D_s^+\to\pi_0K^{*+}}}{\sqrt{3}\lambda}-\sqrt{\frac{2}{3}}A_{D_s^+\to\bar{K}^0K^{*+}}=0$$

xx)

$$\frac{A_{D^+\to\omega_8\pi^+}}{\lambda}-\frac{A_{D^+\to\rho_0\pi^+}}{\sqrt{3}\lambda}-\sqrt{\frac{2}{3}}\frac{A_{D^+\to K^{*0}\pi^+}}{\lambda^2}+\sqrt{\frac{2}{3}}A_{D^+\to\bar{K}^{*0}\pi^+}+A_{D_s^+\to\omega_8\pi^+}$$
$$-\frac{A_{D_s^+\to\rho_0\pi^+}}{\sqrt{3}}-\sqrt{\frac{2}{3}}\frac{A_{D_s^+\to K^{*0}\pi^+}}{\lambda}=0$$

xxi)

$$-A_{D_s^+\to\rho_0\pi^+}-\frac{A_{D^+\to\rho_0\pi^+}}{\lambda}+\frac{A_{D_s^+\to\rho_0K^+}}{\lambda}-\frac{A_{D_s^+\to K^{*0}\pi^+}}{\sqrt{2}\lambda}+\frac{A_{D^+\to\rho_0K^+}}{\lambda^2}$$
$$-\frac{A_{D^+\to K^{*0}\pi^+}}{\sqrt{2}\lambda^2}+\frac{A_{D_s^+\to K^{*0}K^+}}{\sqrt{2}\lambda^2}=0$$

xxii)

$$\frac{A_{D^+\to\pi_0\rho^+}}{\lambda}-\frac{A_{D^+\to\bar{K}^0\rho^+}}{\sqrt{2}}-\frac{A_{D^+\to\pi_0K^{*+}}}{\lambda^2}+\frac{A_{D^+\to\bar{K}^0K^{*+}}}{\sqrt{2}\lambda}-A_{D_s^+\to\rho_0\pi^+}$$
$$-\frac{A_{D_s^+\to\pi_0K^{*+}}}{\lambda}+\frac{A_{D_s^+\to\bar{K}^0K^{*+}}}{\sqrt{2}}=0$$

xxiii)

$$\sqrt{\frac{2}{3}}A_{D_s^+\to\bar{K}^0K^{*+}}+\sqrt{\frac{2}{3}}\frac{A_{D^+\to\bar{K}^0K^{*+}}}{\lambda}+\frac{A_{D_s^+\to\eta_8K^{*+}}}{\lambda}-\frac{A_{D_s^+\to\pi_0K^{*+}}}{\sqrt{3}\lambda}+\frac{A_{D^+\to\eta_8K^{*+}}}{\lambda^2}$$
$$-\frac{A_{D^+\to\pi_0K^{*+}}}{\sqrt{3}\lambda^2}-\sqrt{\frac{2}{3}}\frac{A_{D_s^+\to K^0K^{*+}}}{\lambda^2}=0$$

xxiv)

$$\sqrt{\frac{2}{3}}A_{D_s^+\to\eta_8\rho^+}+\sqrt{\frac{2}{3}}\frac{A_{D^+\to\eta_8\rho^+}}{\lambda}-\frac{A_{D_s^+\to K^0\rho^+}}{\lambda}-\sqrt{\frac{2}{3}}\frac{A_{D_s^+\to\eta_8K^{*+}}}{\lambda}-\frac{A_{D^+\to K^0\rho^+}}{\lambda^2}$$
$$-\sqrt{\frac{2}{3}}\frac{A_{D^+\to\eta_8K^{*+}}}{\lambda^2}+\frac{A_{D_s^+\to K^0K^{*+}}}{\lambda^2}=0$$

xxv)

$$-2A_{D^0\to\pi_0\bar{K}^{*0}}-\sqrt{6}\frac{A_{D^0\to\omega_8\pi_0}}{\lambda}+\sqrt{2}\frac{A_{D^0\to\pi_0\rho_0}}{\lambda}-\sqrt{2}\frac{A_{D^0\to K^0\bar{K}^{*0}}}{\lambda}-\sqrt{3}\frac{A_{D^0\to\omega_8K^0}}{\lambda^2}$$
$$+\frac{A_{D^0\to K^0\rho_0}}{\lambda^2}+2\frac{A_{D^0\to\pi_0K^{*0}}}{\lambda^2}=0$$

xxvi)

$$\frac{\sqrt{\frac{3}{2}}A_{D^0\to\eta_8\rho_0}}{\lambda}-\frac{A_{D^0\to K^0\rho_0}}{\lambda^2}-\frac{A_{D^0\to\pi_0\rho_0}}{\sqrt{2}\lambda}+A_{D^0\to\rho_0\bar{K}^0}-\frac{1}{2}\sqrt{3}A_{D^0\to\eta_8\bar{K}^{*0}}$$
$$+\frac{A_{D^0\to K^0\bar{K}^{*0}}}{\sqrt{2}\lambda}+\frac{1}{2}A_{D^0\to\pi_0\bar{K}^{*0}}=0$$

xxvii)

$$\sqrt{\frac{2}{3}}A_{D^+\to\bar{K}^{*0}\pi^+}-\sqrt{\frac{2}{3}}A_{D_s^+\to\bar{K}^{*0}K^+}+A_{D_s^+\to\omega_8\pi^+}-\frac{2A_{D_s^+\to\rho_0\pi^+}}{\sqrt{3}}-\frac{A_{D^+\to\rho_0\pi^+}}{\sqrt{3}\lambda}$$
$$+\frac{A_{D_s^+\to\rho_0K^+}}{\sqrt{3}\lambda}-\frac{A_{D_s^+\to K^{*0}\pi^+}}{\sqrt{6}\lambda}+\frac{A_{D^+\to\omega_8K^+}}{\lambda^2}+\frac{A_{D^+\to K^{*0}\pi^+}}{\sqrt{6}\lambda^2}-\frac{A_{D_s^+\to K^{*0}K^+}}{\sqrt{6}\lambda^2}=0\ .$$

Rotation to the mass basis follows from Sec. 6.2.7, noting that in the $D \to PV$ case there are no amplitudes requiring the symmetry factor of eq. (6.9). Unlike in the PP case, one may also measure modes involving K^{*0} and $\bar{K}^{*0}$ directly, via tagging with K or K_S, so that we need not rotate to K^* mass basis.

6.4.4 Rate Sum Rules

We finally present the $D \to PV$ rate sum rules valid to $\mathcal{O}(\varepsilon^2)$, in the mass eigenstate basis, of which there are six:

i)

$$|(D_s^+|\rho_0\pi^+)|^2 = |(D_s^+|\pi_0\rho^+)|^2$$

ii)

$$\frac{|(D^0|\rho^-K^+)|^2}{\lambda^4} + |(D^0|K^{*-}\pi^+)|^2 = \frac{|(D^0|K^{*-}K^+)|^2}{\lambda^2} + \frac{|(D^0|\rho^-\pi^+)|^2}{\lambda^2}$$

iii)

$$|(D^0|K^-\rho^+)|^2 + \frac{|(D^0|\pi^-K^{*+})|^2}{\lambda^4} = \frac{|(D^0|\pi^-\rho^+)|^2}{\lambda^2} + \frac{|(D^0|K^-K^{*+})|^2}{\lambda^2}$$

iv)

$$\begin{aligned}
&\frac{|(D^+|\eta\rho^+)|^2}{\lambda^2} + \left(\frac{|(D^+|K_S\rho^+)|^2}{\lambda^2} - \frac{|(D^+|K_L\rho^+)|^2}{\lambda^2}\right) + \frac{|(D^+|\pi_0\rho^+)|^2}{\lambda^2} \\
&+\frac{|(D^+|\rho^+\eta')|^2}{\lambda^2} + \left[\frac{|(D_s^+|K_SK^{*+})|^2}{\lambda^2} - \frac{|(D_s^+|K_LK^{*+})|^2}{\lambda^2}\right] + \frac{|(D_s^+|\eta K^{*+})|^2}{\lambda^2} \\
&+\frac{|(D_s^+|\pi_0K^{*+})|^2}{\lambda^2} + \frac{|(D_s^+|K^{*+}\eta')|^2}{\lambda^2} \\
&= \\
&\frac{|(D^+|\eta K^{*+})|^2}{\lambda^4} + \frac{|(D^+|\pi_0K^{*+})|^2}{\lambda^4} + \frac{|(D^+|K^{*+}\eta')|^2}{\lambda^4} + |(D_s^+|\eta\rho^+)|^2 \\
&+|(D_s^+|\pi_0\rho^+)|^2 + |(D_s^+|\rho^+\eta')|^2
\end{aligned}$$

v)

$$\frac{|(D^+|\bar{K}^{*0}K^+)|^2}{\lambda^2}+\frac{|(D^+|\phi\pi^+)|^2}{\lambda^2}+\frac{|(D^+|\omega\pi^+)|^2}{\lambda^2}+\frac{|(D^+|\rho_0\pi^+)|^2}{\lambda^2}$$
$$+\frac{|(D_s^+|\phi K^+)|^2}{\lambda^2}+\frac{|(D_s^+|\omega K^+)|^2}{\lambda^2}+\frac{|(D_s^+|\rho_0 K^+)|^2}{\lambda^2}+\frac{|(D_s^+|K^{*0}\pi^+)|^2}{\lambda^2}$$
$$=$$
$$\frac{|(D^+|\phi K^+)|^2}{\lambda^4}+\frac{|(D^+|\omega K^+)|^2}{\lambda^4}+\frac{|(D^+|\rho_0 K^+)|^2}{\lambda^4}+\frac{|(D^+|K^{*0}\pi^+)|^2}{\lambda^4}$$
$$+|(D^+|\bar{K}^{*0}\pi^+)|^2+\frac{|(D_s^+|K^{*0}K^+)|^2}{\lambda^4}+|(D_s^+|\bar{K}^{*0}K^+)|^2+|(D_s^+|\phi\pi^+)|^2$$
$$+|(D_s^+|\omega\pi^+)|^2+|(D_s^+|\pi_0\rho^+)|^2$$

vi)

$$\left[\frac{|(D^0|\phi K_L)|^2}{\lambda^2}-\frac{|(D^0|\phi K_S)|^2}{\lambda^2}\right]+\left[\frac{|(D^0|\omega K_L)|^2}{\lambda^2}-\frac{|(D^0|\omega K_S)|^2}{\lambda^2}\right]$$
$$+\left[\frac{|(D^0|K_L\rho_0)|^2}{\lambda^2}-\frac{|(D^0|K_S\rho_0)|^2}{\lambda^2}\right]+\frac{|(D^0|\eta K^{*0})|^2}{\lambda^4}+\frac{|(D^0|\pi_0 K^{*0})|^2}{\lambda^4}$$
$$+\frac{|(D^0|K^{*0}\eta')|^2}{\lambda^4}+|(D^0|\eta\bar{K}^{*0})|^2+|(D^0|\pi_0\bar{K}^{*0})|^2+|(D^0|\bar{K}^{*0}\eta')|^2$$
$$=$$
$$\frac{|(D^0|\eta\phi)|^2}{\lambda^2}+\frac{|(D^0|\eta\omega)|^2}{\lambda^2}+\frac{|(D^0|\phi\pi_0)|^2}{\lambda^2}+\frac{|(D^0|\omega\pi_0)|^2}{\lambda^2}+\frac{|(D^0|\eta\rho_0)|^2}{\lambda^2}$$
$$+\frac{|(D^0|\pi_0\rho_0)|^2}{\lambda^2}+\frac{|(D^0|\phi\eta')|^2}{\lambda^2}+\frac{|(D^0|\omega\eta')|^2}{\lambda^2}+\frac{|(D^0|\rho_0\eta')|^2}{\lambda^2}\ ,$$

and a further four sum rules that result just from the K-K mixing,

vii)

$$|(D^0|K_S K^{*0})|^2=|(D^0|K_L K^{*0})|^2$$

viii)

$$|(D^0|K_S\bar{K}^{*0})|^2=|(D^0|K_L\bar{K}^{*0})|^2$$

ix)

$$|(D^+|K_S K^{*+})|^2 = |(D^+|K_L K^{*+})|^2$$

x)

$$|(D_s^+|K_S \rho^+)|^2 = |(D_s^+|K_L \rho^+)|^2 \ .$$

6.4.5 PV Predictions

The rate sum rules ii and iii in Sec. 6.4.4 are the PV equivalent of the PP U-spin rate sum rules. Similarly to the PP case (see Sec. 6.3.4), combining these respectively with the U-spin amplitude sum rules xi and xii of Sec. 6.4.3, admits the possibility that the following normed amplitude sum rules also hold to $\mathcal{O}(\varepsilon^2)$:

$$|(D^0|\pi^+\rho^-)|/\lambda + |(D^0|K^+K^{*-})|/\lambda = |(D^0|K^+\rho^-)|/\lambda^2 + |(D^0|\pi^+K^{*-})| \quad (6.34)$$

$$|(D^0|\pi^-\rho^+)|/\lambda + |(D^0|K^-K^{*+})|/\lambda = |(D^0|K^-\rho^+)| + |(D^0|\pi^-K^{*+})|/\lambda^2 \ . \quad (6.35)$$

One may verify from Appendix D.3 that analogous relations to eqs. (6.31) hold, ensuring these normed amplitude sum rules are valid to $\mathcal{O}(\varepsilon^2)$. We again emphasize that these normed amplitude sum rules are a consequence of the special structure of the amplitudes in the U-spin sum rules.

The branching ratios of 6.35 have been measured, and one finds from the data[1] [3]

$$\frac{|(D^0|\pi^-\rho^+)|/\lambda + |(D^0|K^-K^{*+})|/\lambda}{|(D^0|K^-\rho^+)| + |(D^0|\pi^-K^{*+})|/\lambda^2} - 1 = 6\% \pm 17\% \ , \quad (6.36)$$

[1]Particular care must be taken with the current PDG data for modes with $K^{*\pm}$ in the final state. At present, the $D^0 \to K^{*+}K^-$ mode has only been measured for the case that K^{*+} subsequently decays to $K^+\pi^0$. The isospin Clebsch-Gordan coefficients imply this occurs one-third of the time while $K^{*+} \to K^0\pi^+$ occurs two-thirds of the time. As a result, we must multiply the current PDG rate for $D^0 \to (K^{*+})K^- \to (K^+\pi^0)K^-$ by this factor of three. Similar care must be taken with the data for $D^0 \to K^{*+}\pi^-$ and $D^0 \to K^{*-}K^+$. Both $K^{*-} \to K^-\pi^0$ and $K^{*-} \to K_S\pi^+$ decay channels have been measured for the $D^0 \to K^{*-}\pi^+$ mode, so in this case we naïvely average the rates with appropriate Clebsch-Gordan factors.

which is comparable to the PP U-spin sum rule (6.4), though less precise. The DCS process of 6.34 is yet to be measured, so from the corresponding rate sum rule we instead obtain the prediction [3]

$$\mathrm{Br}(D^0 \to \rho^- K^+) \simeq (1.7 \pm 0.4) \times 10^{-4} \ . \tag{6.37}$$

We note further that we have from the data [3]

$$\left|\frac{(D^0|\pi^+\rho^-)}{(D^0|K^+K^{*-})}\right| - 1 = 0.59 \pm 0.10 \ , \qquad \left|\frac{(D^0|\pi^-\rho^+)}{(D^0|K^-K^{*+})}\right| - 1 = 0.33 \pm 0.05 \ . \tag{6.38}$$

Compared to the PP case in eq. (6.3), this implies a slightly smaller and inverse U-spin breaking for PV. If the prediction (6.37) is satisfied, then eqs. (6.36) – (6.38) are consistent with the $\Delta U = 0$ rule proposed in Ref. [182] for U-spin irreps, just as eqs. (6.3) and (6.4) are consistent with this rule for the PP case. To be explicit, under the $\Delta U = 0$ rule one assumes a large broken penguin picture, in which

$$\begin{aligned}
(D^0|K^\pm K^{*\mp}) &\simeq \lambda[T^\pm - P_{\mathrm{b}}^\pm] - \lambda^5 e^{i(\delta^\pm - \gamma)} P^\pm \ , \\
(D^0|\pi^\pm \rho^\mp) &\simeq -\lambda[T^\pm + P_{\mathrm{b}}^\pm] - \lambda^5 e^{i(\delta^\pm - \gamma)} P^\pm \ , \\
(D^0|K^{*+}\pi^-) &\simeq \lambda^2 T^+ \ , \quad (D^0|K^{*-}\pi^+) \simeq T^- \ , \\
(D^0|\rho^+ K^-) &\simeq T^+ \ , \quad (D^0|\rho^- K^+) \simeq \lambda^2 T^- \ ,
\end{aligned} \tag{6.39}$$

where T and P are respectively U-spin tree and penguin reduced matrix elements, P_b is the so-called broken penguin – which is a U-spin breaking reduced matrix element, naïvely $\mathcal{O}(\varepsilon)$ – and $\delta^\pm$ are (γ is) the strong phases (weak phase). It is assumed that the penguins are enhanced, such that $P \sim \mathcal{O}(1/\varepsilon)$ and $P_{\mathrm{b}} \sim \mathcal{O}(1)$, while T remains $\mathcal{O}(1)$. Eqs. (6.39) are consistent both with the PV U-spin sum rules as well as $\mathcal{O}(1)$ breakings of eqs. (6.38).

Applying this U-spin picture, one may predict the ratio of the KK^* and $\pi\rho$

direct CP asymmetries,

$$\frac{\mathcal{A}_{\rm CP}(K^\pm K^{*\mp})}{\mathcal{A}_{\rm CP}(\pi^\pm\rho^\mp)} \simeq \frac{(D^0|\pi^\pm\rho^\mp)}{(D^0|K^\pm K^{*\mp})} + \mathcal{O}(\varepsilon) \ . \tag{6.40}$$

We expect $(D^0|K^\pm\rho^\mp)$ to be opposite sign to $(D^0|\pi^\pm\rho^\mp)$ in the $\varepsilon \to 0$ limit and at leading order in λ (see Appendix D.3 and eq. (6.39)), so from eqs. (6.38) we have

$$\frac{\mathcal{A}_{\rm CP}(K^+K^{*-})}{\mathcal{A}_{\rm CP}(\pi^+\rho^-)} \simeq -1.59 \pm 0.10 \ , \quad \text{and} \quad \frac{\mathcal{A}_{\rm CP}(K^-K^{*+})}{\mathcal{A}_{\rm CP}(\pi^-\rho^+)} \simeq -1.33 \pm 0.05 \ , \tag{6.41}$$

up to $\mathcal{O}(\varepsilon)$ corrections.

We may further estimate the PV $\Delta\mathcal{A}_{\rm CP}$'s, defined to be

$$\begin{aligned} \Delta\mathcal{A}^\pm_{\rm CP} &\equiv \mathcal{A}_{\rm CP}(D^0 \to K^\pm K^{*\mp}) - \mathcal{A}_{\rm CP}(D^0 \to \pi^\pm\rho^\mp) \\ &= -2\lambda^4\left(\frac{P^\pm}{T^\pm - P^\pm_{\rm b}} + \frac{P^\pm}{T^\pm + P^\pm_{\rm b}}\right)\sin\delta\sin\gamma \ . \end{aligned} \tag{6.42}$$

Let P^0, $P^0_{\rm b}$, T^0 and δ_0, be the penguin, broken penguin and tree terms and strong phase respectively of the PP system, and define $\mathcal{R}^\pm \equiv P^\pm_{\rm b}/T^\pm$ and $\mathcal{R}^0 \equiv P^0_{\rm b}/T^0$. Assuming that PP and PV have same penguin contraction enhancements, such that $P^0/P^0_{\rm b} \simeq P^\pm/P^\pm_{\rm b}$, then it follows that

$$\Delta\mathcal{A}^\pm_{\rm CP} \simeq \Delta\mathcal{A}_{\rm CP}\left[\frac{\sin\delta^\pm}{\sin\delta_0}\right]\left[\frac{(\mathcal{R}^\pm)^2}{1-(\mathcal{R}^\pm)^2}\right]\left[\frac{1-(\mathcal{R}^0)^2}{(\mathcal{R}^0)^2}\right] \ . \tag{6.43}$$

Since PV is a spin-1 final state, we expect $\sin\delta^\pm/\sin\delta_0 \sim -1$ and from the data [3]

$$\mathcal{R}^+ = 0.23 \pm 0.03 \ , \qquad \mathcal{R}^- = 0.14 \pm 0.02 \ , \qquad \mathcal{R}^0 = -0.29 \pm 0.01 \ . \tag{6.44}$$

We then estimate up to $\mathcal{O}(1)$ uncertainty

$$\Delta\mathcal{A}^\pm_{\rm CP} \sim -\Delta\mathcal{A}_{\rm CP} \ . \tag{6.45}$$

We emphasize that these predictions pertain only to $\Delta U = 0$ rule of Ref. [182], and they are independent from the SU(3) sum rule analysis of this paper. Nonetheless,

the analysis of this section is motivated by our prediction that the U-spin sum rules (6.34) and (6.35) are valid to $\mathcal{O}(\varepsilon^2)$ – and one of them appears to be valid to this order – and this prediction is consistent with the $\Delta U = 0$ rule for large broken penguin picture.

6.5 Summary

In this paper we have presented the amplitude and rate sum rules, valid to $\mathcal{O}(\varepsilon^2)$, associated with SU(3) breaking by the m_s spurion for both $D \to PP$ and $D \to PV$ decays. At the amplitude level, verifying these sum rules provides a test of this pattern of flavor SU(3) breaking. In particular, the isospin sum rules (6.28) and (6.33) that are valid to second order in m_I, provide an extremely sensitive test of new SU(3) breaking sources.

In practical terms, testing the amplitude level sum rules will prove difficult in the immediate future, because of the need to measure the strong phases. As a result, the square amplitude or rate sum rules are a better candidate for future experimental tests, in particular the PV U-spin sum rules (6.36) and (6.37). The so-far imprecise verification of (6.36) is nonetheless encouraging for the development of a large broken penguin $\Delta U = 0$ rule for the PV case, analogous to Ref. [182]. Such a rule implies the predictions for the PV direct CP asymmetries (6.41) and (6.45) that we have provided above. We have also used the U-spin normed amplitude sum rules for PV to predict the $D^0 \to \rho^- K^+$ rate.

Finally, let us briefly discuss the applicability of our $D \to PP$ results to $D \to VV$, which we have not considered explicitly in this paper. For $D \to VV$, the extra Lorentz structure of the meson tensors – that is we have $V^\mu V^\nu$ – means that

the final states can be CP even or CP odd, compared to PP in which all final states are CP even. This yields a larger number of invariants and corresponding reduced matrix elements. Put in other words, whereas in PP the symmetry of the final states restricts us to symmetrized tensor contractions, in VV there is no such restriction. Despite this complication, the small phase space available to most VV decays implies that they are dominated by the s-wave channel. As a result, simply replacing P mesons with V mesons everywhere in the PP results will provide approximately correct $D \to VV$ relations.

APPENDIX A

COMPOSITE DIRAC NEUTRINOS

A.1 Examples of Preonic Theories

In Sec. 2.3 we presented a hidden flavor theory in which we assumed that there exists a $G_{\rm c}\otimes G_{\rm F}$ preonic theory that produces three chiral baryons all with the same hidden flavor charge, but possibly composed of different numbers of preons. This assumption is non-trivial, so in this appendix we search for examples of preonic theories which possess this feature.

The $\mathrm{SU}(n+4)\otimes\mathrm{SU}(n)\otimes U(1)$ preonic theories considered in Refs [4, 9, 13] produce an effective low-energy theory after only one stage of confinement. A good place to start is therefore with a preonic theory that has the same confining group representations as these theories. Hence consider a preonic theory with symmetries $G_{\rm c}=\mathrm{SU}(n)$ and $G_{\rm F}=G\otimes\mathrm{U}(1)_{\rm F}$, and preonic content as shown in Table A.1. Here $n\geq 5$ and the group G is semi-simple but arbitrary: the representations of G furnished by the preons are specified only by their dimensions d_1 and d_2. We assume that G is spontaneously broken by confinement, so that the low energy theory has only a $\mathrm{U}(1)_{\rm F}$ flavor symmetry. As a result, only the $\mathrm{SU(n)^2U(1)_F}$ instanton and $\mathrm{U}(1)_{\rm F}^3$ anomalies need to be matched. Note that in contrast to the main text, for convenience we have switched to a right-handed chirality for the preonic representations. The anomalies in this section will be calculated with respect to the right-handed fermionic representations, and therefore differ by a sign compared to those in Sec. 2.3.

Field	SU(n)	G	U(1)$_{\rm F}$
ψ	$\square$	d_1	α
χ	$\begin{array}{c}\square\\[-4pt]\square\end{array}$	d_2	β

Table A.1: Right-handed fermionic content for a candidate $G_{\rm c}\otimes G_{\rm F}$ preonic theory.

A.1.1 Statistical, group theoretic and chiral constraints

The effective theory after confinement consists of $G_{\rm c}$ singlets. We denote a general $G_{\rm c}$ singlet by $\psi^p\chi^q$, which has U(1)$_{\rm F}$ charge

$$F(\psi^p\chi^q) = p\alpha + q\beta \ . \tag{A.1}$$

Note that in this notation, a negative power $\psi^{-|p|} \equiv (\psi^\dagger)^{|p|}$. In order for $\psi^p\chi^q$ to be both an SU(n) singlet and a fermion, the integers p and q must satisfy the respective constraints

$$p + (n-2)q \mod n = 0 \ , \tag{A.2}$$

$$p + q \mod 2 = 1 \ . \tag{A.3}$$

We also require this baryon to be right-handed, which means that the condensate $\psi^p\chi^q$ must contain an odd number of right-handed preons and an even number of left-handed ones. Since by construction ψ and χ were right-handed – so that $\psi^\dagger$ and $\chi^\dagger$ are left-handed – there are only four possibilities for the configuration of the sign and parity of p and q which satisfy this constraint. These are as shown in Table A.2 and are equivalent to the algebraic constraint

$$\big[1+\mathrm{sgn}(p)\big](p \mod 2) + \big[1+\mathrm{sgn}(q)\big](q \mod 2) = 2 \ . \tag{A.4}$$

Notably, this constraint subsumes Eq. (A.3).

Sign p	Sign q	Parity p	Parity q
$+$	$+$	odd	even
$+$	$+$	even	odd
$+$	$-$	odd	even
$-$	$+$	even	odd

Table A.2: Four possible configurations of signs and parity for p and q that produce right-handed baryons.

A.1.2 $\mathrm{U}(1)_{\mathrm{F}}$ anomaly matching

We now apply the 't Hooft anomaly matching formalism. To begin, we note that the $\mathrm{SU}(n)^3$ anomaly for this theory must cancel. This implies that

$$d_1 = (n-4)d_2 \ . \tag{A.5}$$

Further, the preonic theory must have no $\mathrm{SU}(n)^2\mathrm{U}(1)_{\mathrm{F}}$ instanton anomaly, which together with Eq. (A.5) results in

$$\alpha = \frac{2-n}{n-4}\beta \equiv g(n)\beta \ . \tag{A.6}$$

Combining Eqs. (A.5) and (A.6) we have $\mathrm{U}(1)_{\mathrm{F}}^3$ anomaly

$$\begin{aligned}\mathcal{A}[\mathrm{U}(1)_{\mathrm{F}}^3] &= \alpha^3 n d_1 + \beta^3 n(n-1)d_2/2 \\ &= \frac{n d_2 \beta^3}{(n-4)^2}\left[(2-n)^3 + \frac{(n-1)(n-4)^2}{2}\right] \\ &\equiv f(n,d_2)\beta^3 \ . \end{aligned} \tag{A.7}$$

Now, let us suppose that there are precisely three right-handed chiral baryons formed from this preonic theory, which all have hidden flavor charge γ. Then the $\mathrm{U}(1)_{\mathrm{F}}^3$ anomaly of the confined phase is simply $3\gamma^3$, so by 't Hooft anomaly matching and Eq. (A.7) we must have

$$f(n,d_2)\beta^3 = 3\gamma^3 \ . \tag{A.8}$$

If we assume that there is at least one combination of preons which forms a baryon of charge γ, then there must exist integers p and q such that $\gamma = p\alpha + q\beta$. Observe that by Eq. (A.6)

$$\gamma/\beta = p\alpha/\beta + q = pg(n) + q \ , \tag{A.9}$$

so it follows that a necessary condition for the anomaly matching constraint (A.8) to be satisfied is

$$f(n, d_2) = 3[pg(n) + q]^3 \ . \tag{A.10}$$

The reason Eq. (A.10) is not a sufficient condition is because we require there to be three chiral baryons, but it is conceivable that if p and q are small enough, then there may not be enough baryons formed from this combination alone: this depends on the multiplicities generated by both the broken group G as well as tensor products of the Lorentz indices. Interestingly, note that by Eq. (A.9) γ/β is always rational and so Eq. (A.8) also implies the severe constraint

$$\left(\frac{f(n, d_2)}{3}\right)^{1/3} \in \mathbb{Q} \ . \tag{A.11}$$

This provides a necessary constraint on the combinations of n and d_2 such that there may be three chiral baryons of the same charge for the class of preonic theories defined by Table A.1. Note that Eq. (A.10) implies Eq. (A.11), but the converse does not hold.

A.1.3 Gravitational anomaly matching

In order for a preonic theory of this class to generate three chiral baryons with the same charge, we must find integers $n \geq 5$, $d_2 \geq 1$, p and q which satisfy Eqs. (A.2), (A.4) and (A.10). One further constraint is produced by the fact that the gravitational anomaly must also match.

Preon	SU(5)	G	$\mathrm{U(1)_F}$
ψ	$\square$	$d_1 = 3$	$\alpha = 3\gamma/5$
χ	$\begin{array}{c}\overline{\square}\\ \square\end{array}$	$d_2 = 3$	$\beta = -\gamma/5$
Baryon	SU(5)		$\mathrm{U(1)_F}$
$\psi^2\chi$	$\mathbf{1}$		γ
$\psi(\chi^\dagger)^2$	$\mathbf{1}$		γ
$\psi^3\chi^4$	$\mathbf{1}$		γ
$\vdots$			

Table A.3: Preonic field content and possible chiral baryons for the candidate SU(5) preonic theory.

The gravitational anomaly for the baryons is 3γ. For the preonic theory we have

$$\mathcal{A}_{\mathrm{grav}}[\mathrm{U(1)_F}] = nd_1\alpha + n(n-1)d_2\beta/2 = \frac{nd_2}{2}(3-n)\beta \ . \tag{A.12}$$

From Eq. (A.8), simultaneous matching of the gravitational and $\mathrm{U(1)_F^3}$ anomalies then requires that

$$f(n, d_2) = 3\left[\frac{nd_2}{6}(3-n)\right]^3 \ . \tag{A.13}$$

The only integer solutions for this equation with $n \geq 5$ are $n = 5$, $d_2 = 3$ or $n = 6$, $d_2 = 1$. A computer search reveals that for these values, there exists a large number of p and q configurations which satisfy Eqs. (A.2), (A.4) and (A.10). These theories are presented in Tables A.3 and A.4, along with some possible baryonic configurations. Examples of preonic theories with such field content are respectively three copies of the $\mathrm{SU(5)} \otimes U(1)$ theory or the $\mathrm{SU(6)} \otimes \mathrm{SU(2)} \otimes U(1)$ theory that are presented in Ref. [9].

It is clear that there is sufficient p, q combinations to produce three right-handed chiral baryons with $\mathrm{U(1)_F}$ charge γ (not including multiplicities from broken G rerepresentations or tensor products of Lorentz representations). Note also that neither of these theories can exhibit secondary mass generation. The reason is that all the

Preon	SU(6)	G	$\mathrm{U}(1)_\mathrm{F}$
ψ	$\square$	$d_1 = 2$	$\alpha = 2\gamma/3$
χ	$\begin{array}{c}\square\\[-4pt]\square\end{array}$	$d_2 = 1$	$\beta = -\gamma/3$
Baryon	SU(6)		$\mathrm{U}(1)_\mathrm{F}$
$\psi^2\chi$	$\mathbf{1}$		γ
$\psi^4\chi^5$	$\mathbf{1}$		γ
$\psi^6\chi^9$	$\mathbf{1}$		γ
$\vdots$			

Table A.4: Preonic field content and possible chiral baryons for the candidate SU(6) preonic theory.

baryons of charge γ must contain a common preon with any scalar condensate: for secondary mass generation we require more sophisticated preonic content.

We have thus found two $G_\mathrm{c}\otimes G_\mathrm{F}$ preonic theories which can produce three right-handed chiral baryons of the same $\mathrm{U}(1)_\mathrm{F}$ charge. Of course, there exists many more possibilties which we have not considered here. We have also not specified here the pattern of chiral symmetry breaking, or exactly which of the above condensates correspond to the chiral baryons. These will depend on the ultraviolet completion of the theory, the broken hidden flavor symmetry G, the dynamics of confinement, and other physical assumptions, which is beyond the scope of the present paper.

A.2 Gauge boson structure and couplings

In this appendix we present the gauge boson mass basis and further detail of the gauge boson couplings.

With an extra $\mathrm{U}(1)_\mathrm{F}$ gauge symmetry we have covariant derivative

$$iD_\mu = i\partial_\mu - gT^aW^a_\mu - g'YB_\mu - g_\mathrm{F}FC_\mu \ , \tag{A.14}$$

Boson	Structure	Mass^2
$W_\mu^\pm$	$(W_\mu^1 \mp iW_\mu^2)/\sqrt{2}$	$v^2g^2/2$
Z_μ	$c_W s_F W_\mu^3 - s_W s_F B_\mu - c_F C_\mu$	$v^2g^2/2s_F^2c_W^2$
A_μ	$s_W W_\mu^3 + c_W B_\mu$	0
A'_μ	$c_W c_F W_\mu^3 - s_W c_F B_\mu + s_F C_\mu$	0

Table A.5: Gauge boson mass basis for the U(1) hidden flavor model.

where as usual T^a (W_μ^a) are the SU(2)$_L$ generators (gauge bosons), and C_μ is the U(1)$_{\rm F}$ gauge boson. Define

$$\cos\theta_F \equiv \frac{2\gamma g_{\rm F}}{\sqrt{g^2+g'^2+(2\gamma g_{\rm F})^2}}\ ,$$
$$\cos\theta_W \equiv \frac{g}{\sqrt{g^2+g'^2}}\ , \tag{A.15}$$

and let us write $\cos\theta_{F,W} = c_{F,W}$, $\sin\theta_{F,W} = s_{F,W}$. It is straightforward to find the orthonormal mass basis for the gauge bosons, which is presented in Table A.5. Note that the massless gauge bosons A_μ and A'_μ are orthonormal with respect to the $\{W^3, B, C\}$ basis.

We are generally free to choose orthonormal A_μ and A'_μ up to a unitary transformation. However, the choice of the basis for the massless gauge bosons in Table A.5 proves to be particularly convenient, because in this mass basis the covariant derivative becomes

$$iD_\mu = i\partial_\mu - gT^\pm W_\mu^\pm - eQA_\mu - \frac{g}{c_W}\left[s_F\big(T^3 - Qs_W^2\big) - \left(Y - \frac{B-L}{2}\right)\frac{c_F^2}{s_F}\right]Z_\mu$$
$$- \frac{gc_F}{c_W}\left[Qc_W^2 - \frac{B-L}{2}\right]A'_\mu\ , \tag{A.16}$$

where $e = gs_W$ and we have used the relations $F/2\gamma = Y - a/\gamma$ and $a/\gamma = (B-L)/2$ if $L = 1$ for the electron. It is clear that A_μ is the SM photon. Note that the generator of $U(1)'$, whose gauge boson is the A'_μ, is a linear combination of Q and $B - L$.

Consider now the limit $g_{\rm F} \ll g, g'$. We can redefine this limit as

$$\kappa \equiv c_F \ll 1 \ , \tag{A.17}$$

so that $s_F = 1 - \kappa^2/2 + \mathcal{O}(\kappa^4)$. To order $\mathcal{O}(\kappa^2)$, we then have mass basis gauge bosons

$$\begin{aligned} Z_\mu &\simeq (1-\kappa^2/2) Z_\mu^{\rm SM} + \kappa C_\mu \ , \\ A'_\mu &\simeq \kappa Z_\mu^{\rm SM} + (1-\kappa^2/2) C_\mu \ , \end{aligned} \tag{A.18}$$

where $Z^{\rm SM}$ is the SM Z boson, and Z_μ has mass $m_Z^2 \simeq (1+\kappa^2/2) v^2 g^2 / 2 c_W^2$. Further, the covariant derivative in this limit is simply

$$\begin{aligned} iD_\mu \simeq i\partial_\mu - g T^\pm W_\mu^\pm - eQA_\mu - \frac{g}{c_W}\left[\left(T^3 - Q s_W^2\right) - \frac{\kappa^2}{2}\left(Q c_W^2 + Y - B - L\right)\right] Z_\mu \\ - \frac{g\kappa}{c_W}\left[Q c_W^2 - \frac{B-L}{2}\right] A'_\mu \ . \end{aligned} \tag{A.19}$$

Hence at leading order in κ we have the usual SM gauge bosons, mass spectra and couplings.

A.3 Neutrino mass basis and spectrum

Consider

$$AA^\dagger = \begin{pmatrix} \theta^2(\tilde\lambda_3 \tilde\lambda_3^\dagger + \tilde\lambda_K \tilde\lambda_K^\dagger) & \theta \tilde\lambda_K d_K \\ \theta d_K \tilde\lambda_K^\dagger & d_K^2 \end{pmatrix} \ . \tag{A.20}$$

The upper left 3×3 block is Hermitian, and can be diagonalized by unitary V_3, so that we then have

$$AA^\dagger = \begin{pmatrix} V_3 & \\ & 1 \end{pmatrix} \begin{pmatrix} \theta^2 d_3^2 & \theta V_3^\dagger \tilde\lambda_K d_K \\ \theta d_K \tilde\lambda_K^\dagger V_3 & d_K^2 \end{pmatrix} \begin{pmatrix} V_3^\dagger & \\ & 1 \end{pmatrix} \ . \tag{A.21}$$

Since $\tilde{\lambda}$ contains at least one $\mathcal{O}(1)$ column, we expect at least one entry of the diagonal d_3 to be $\mathcal{O}(1)$ too, while the others may be suppressed. The exact nature of d_3, including any hierarchies therein, strongly depends on the structure and symmetries (if any) of $\tilde{\lambda}$. Determining $\tilde{\lambda}$ is beyond the scope of this chapter.

To leading order in θ, one may show that the characteristic equation for $AA^\dagger$ is

$$0 = \prod_{i=1}^{3}(\theta^2 d_i^2 - x)\prod_{\alpha=4}^{N}(d_\alpha^2 - x) - \theta^2 \sum_{j,\beta}\Big[\prod_{i\neq j}\prod_{\alpha\neq\beta}(d_\alpha^2 - x)(\theta^2 d_i^2 - x)B_{j\beta}B_{j\beta}^*\Big] \ , \quad \text{(A.22)}$$

where $B = V_3^\dagger \tilde{\lambda}_K d_K$, $d_i = [d_3]_{ii}$ and $d_\alpha = [d_K]_{\alpha\alpha}$. It follows immediately from this and Eq. (2.15) that the mass spectrum for the neutrinos is

$$\begin{aligned} m_i &= v\epsilon^{\tilde{n}} d_i\big[1 + \mathcal{O}(\theta^2)\big] \ , \\ m_\alpha &= \Lambda d_\alpha\big[1 + \mathcal{O}(\theta^2)\big] \ . \end{aligned} \quad \text{(A.23)}$$

Hence we have three light neutrinos, with masses suppressed by at least $\epsilon^{\tilde{n}}$ compared to the charged leptons, and $N-3$ neutrinos with masses $\sim \Lambda$ (or $\sim \Lambda\epsilon^2$). It follows from Eqs (A.21) and (A.22) that the leading order general structure of V must be

$$V = \begin{pmatrix} X_3 & \theta W_K \\ \theta Y_3 & Z_K \end{pmatrix} \ . \quad \text{(A.24)}$$

APPENDIX B

FLAVOR OSCILLATION FROM THE TWO-POINT FUNCTION

B.1 Diagonalization of the exact propagator

In this appendix we discuss the subtleties involved in diagonalizing the exact propagator in Eq. (4.8),

$$\Delta_{\alpha\beta}(p^2) = \left[\frac{i}{p^2\mathbf{1} - M^2(p^2)}\right]_{\alpha\beta} . \tag{B.1}$$

In general the exact propagator $\Delta(p^2)$ is not necessarily Hermitian. It is therefore not always diagonalizable by a unitary matrix and may not even be diagonalizable at all. If, however, $\Delta(p^2)$ *is* diagonalizable by some invertible matrix U, then observe that: We should generally expect U to be a function of p^2, $U = U(p^2)$, since $\Delta = \Delta(p^2)$; The diagonalizability of $\Delta_{\alpha\beta}(p^2)$ is equivalent to that of $M^2_{\alpha\beta}(p^2)$, since if one is diagonalizable by $U(p^2)$ then so is the other.

Keeping these two observations in mind, in the standard field theoretic oscillation formalism one first diagonalizes the tree-level Lagrangian mass terms, thus obtaining free propagators for the mass eigenstates, and then one can construct two-point amplitudes perturbatively. For example, the well-known PMNS (CKM) matrix diagonalizes the lepton (quark) masses in the Standard Model with right-handed neutrinos (SM + ν_R). However, in general such a diagonalization does not persist to all orders in perturbation theory. In particular, in the SM + ν_R model the flavor changing 1PI functions are zero at tree-level, but receive non-zero contributions at loop level, which are small due to the GIM mechanism. To see

this, note that the exact propagator for a left-handed neutrino in the mass basis is

$$\Delta_{ij}(\not{p}) = \frac{i\delta_{ij}}{\not{p} - m_j} + \quad \text{ 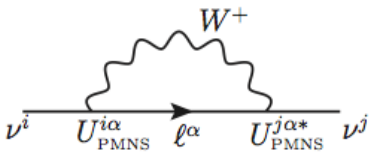 } \quad + \dots \,, \tag{B.2}$$

in which we use the usual SM notation. The mass splittings of the leptons ensure that the neutrino exact propagator is not diagonal at all loop orders in the PMNS basis. Another manifestation of this effect is that flavor changing neutral currents do not appear at tree level, but they do appear at higher loop orders. The moral is that if the propagator is diagonalizable in the exact theory, it is generally diagonalizable by a p^2-dependent matrix, which is different from the PMNS or CKM matrix at subleading order and not necessarily unitary.

Due to the GIM suppression, it is common in oscillation formalisms to neglect this effect because it occurs at subleading order in perturbation theory. Instead, one presumes that the propagator is diagonalized by the constant, unitary PMNS or CKM matrix. In this paper we make a similar assumption in Eq. (4.9) in the main text. The validity of this assumption is model dependent, and a discussion of the general circumstances under which it applies is beyond the scope of this paper. Nonetheless, as the above SM + ν_R example demonstrates, it is true at leading order in perturbation theory for certain important theories.

We emphasize finally that rather than arising from a diagonalization of the bare classical Lagrangian, the matrix U here diagonalizes the exact propagator $\Delta_{\alpha\beta}(p^2)$, which includes all quantum corrections. For the SM + ν_R example discussed above, U therefore coincides at zeroth order with the neutrino PMNS or quark CKM matrix. However, in general U acts as the mixing matrix between the flavor field basis and the 1PI basis (defined in the main text), rather than between the flavor basis and the mass basis of the classical Lagrangian.

B.2 Computation of $\Delta_j(E, \boldsymbol{L})$

In this appendix we compute the integral in Eq. (4.13):

$$\Delta_j(E, \boldsymbol{L}) = \int \frac{d^3p}{(2\pi)^3} \frac{ie^{i\boldsymbol{p}\cdot\boldsymbol{L}}}{p^2 - M_j^2(p^2)} \ . \tag{B.3}$$

First, it is convenient to partition the 3-momentum as

$$\boldsymbol{p} = p_L \boldsymbol{L}/L + \boldsymbol{p}_\perp \ , \quad \boldsymbol{p}_\perp \cdot \boldsymbol{L} = 0 \ , \tag{B.4}$$

so that $\boldsymbol{p}\cdot\boldsymbol{L} = p_L L$ and $d^3\boldsymbol{p} = d^2\boldsymbol{p}_\perp dp_L$. It is clear that the integrand of Eq. (B.3) has a p_L pole determined by Eq. (4.14), which becomes in terms of p_L

$$p_L^2 = E^2 - p_\perp^2 - m_j^2 + im_j\Gamma_j \ . \tag{B.5}$$

Since $L > 0$, one can close the p_L integration contour on the upper-half complex plane, and then only the p_L pole in the upper-half plane contributes to the integral. Let this (positively oriented) integration contour be denoted by C. (Note that a $M_j^2(p^2)$ branch cut on the p_L real axis doesn't affect the integral, since it can be rotated off the axis by an appropriate choice of the principal branch.) With the notation of Eq. (B.4) the spatial two-point function becomes

$$\Delta_j(E, \boldsymbol{L}) = \int \frac{d^2p_\perp}{(2\pi)^2} \oint_C \frac{dp_L}{2\pi} \frac{ie^{ip_L L}}{E^2 - p_\perp^2 - p_L^2 - m_j^2 + im_j\Gamma_j} \ . \tag{B.6}$$

Note that $\Delta_j(E, \boldsymbol{L})$ is independent of the orientation of $\boldsymbol{L}$, so $\Delta_j(E, \boldsymbol{L}) = \Delta_j(E, L)$. The physical consequence of the p_L contour integration is to force the 4-momentum of the integrand (4.13) to be on the 'pole shell' in the complex sense defined by Eq. (4.14). We can interpret the remaining $d^2\boldsymbol{p}_\perp$ integral to be a sum over on-pole-shell transverse 3-momenta.

Let us now perform the p_L integral. In more compact notation, the propagator has a p_L pole satisfying

$$p_L^2(p_\perp) = R_j(p_\perp) + iA_j \ , \tag{B.7}$$

with

$$R_j(p_\perp) \equiv E^2 - p_\perp^2 - m_j^2 \ ,$$
$$A_j \equiv m_j \Gamma_j \ . \tag{B.8}$$

We do not make any assumption regarding the sign of $R_j(p_\perp)$. However, for $\Gamma_j > 0$ it is clear that $\mathrm{Arg}[p_L^2] \in (0, \pi]$. Therefore, defining $z \equiv A_j / R_j(p_\perp)$, it must be that

$$\mathrm{Arg}[p_L^2] = \mathrm{Tan}^{-1}(z) \equiv \begin{cases} \tan^{-1}|z|, \ z > 0 \\ \\ \pi - \tan^{-1}|z|, \ z \leq 0 \end{cases} \ , \tag{B.9}$$

where $\tan^{-1}|\cdot| : [0, \infty) \to [0, \pi/2]$. This permits us to compactly write $p_L^2(p_\perp)$ in complex polar notation. Taking a square root is now trivial, and the p_L pole in the upper-half complex plane is

$$p_L(p_\perp) = \Big[R_j^2(p_\perp) + A_j^2\Big]^{1/4} \exp\left[\frac{i}{2}\mathrm{Tan}^{-1}\left(\frac{A_j}{R_j(p_\perp)}\right)\right] \ . \tag{B.10}$$

Applying the residue theorem to Eq. (B.6), and observing that $p_L(p_\perp)$ is only a function of the magnitude of $\boldsymbol{p}_\perp$, we now have

$$\Delta_j(E, L) = -\frac{1}{4\pi}\int_0^\infty \frac{p_\perp dp_\perp}{p_L(p_\perp)} e^{ip_L(p_\perp)L} \ . \tag{B.11}$$

Observe, furthermore, that Eq. (B.7) implies $p_\perp / p_L(p_\perp) = -p_L'(p_\perp)$. Hence

$$\begin{aligned} \Delta_j(E, L) &= \frac{1}{4\pi}\int_0^\infty dp_\perp p_L'(p_\perp) e^{ip_L(p_\perp)L} \\ &= \frac{i}{4\pi L} e^{ip_L(0)L} \ , \end{aligned}$$

as $p_L(p_\perp) \to i\infty$ when $p_\perp \to \infty$. Writing $R_j \equiv R_j(0) = E^2 - m_j^2$, we have finally

$$\begin{aligned} \Delta_j(E, L) &= \frac{i}{4\pi L} \exp\left\{ i\Big[R_j^2 + A_j^2\Big]^{1/4} \exp\left[\frac{i}{2}\mathrm{Tan}^{-1}\left(\frac{A_j}{R_j}\right)\right] L \right\} \\ &= \frac{i}{4\pi L} \exp\left\{ \frac{i}{\sqrt{2}}\Big[\sqrt{R_j^2 + A_j^2} + R_j\Big]^{1/2} L - \frac{1}{\sqrt{2}}\Big[\sqrt{R_j^2 + A_j^2} - R_j\Big]^{1/2} L \right\} \ . \end{aligned} \tag{B.12}$$

In the last line we have used several trigonometric identities along with the definition of Tan^{-1} in Eq. (B.9).

APPENDIX C

KINEMATIC EDGES AND FLAVOR OSCILLATION

C.1 Phase Space Integral and Non-Zero Width

In the following we compute the differential decay rate $d\Gamma/ds$ for a cascade decay of the general form (5.1)

$$A \to XB \to XYC \ . \tag{C.1}$$

Although some of what is reported in this appendix is already well-known, it is our hope that its recapitulation here is a useful reference to the reader.

For the three body decay (C.1) the differential decay rate is [198, 199]

$$d\Gamma = \frac{|\mathcal{M}|^2}{2(2\pi)^5 m_A} \frac{d^3\vec{p}_X}{2E_X} \frac{d^3\vec{p}_Y}{2E_Y} \frac{d^3\vec{p}_C}{2E_C} \delta^{(4)}(p_A - p_X - p_Y - p_C) \ , \tag{C.2}$$

where $E_j = (p_j^2 + m_j^2)^{1/2}$ and $|\mathcal{M}|^2$ is the amplitude-squared, to be specified later. The differential decay rate is obviously defined in the A rest frame. The amplitude-squared $|\mathcal{M}|^2$ is averaged over all spin indices (if any). As a result, note that $|\mathcal{M}|^2$ has spherical symmetry under arbitrary spatial rotations of the external momenta configuration. We consider only amplitudes of form

$$|\mathcal{M}|^2 = |\mathcal{M}|^2(s, s_1) \ , \tag{C.3}$$

where $s = (p_X + p_Y)^2$ and $s_1 = (p_A - p_X)^2$.

To obtain the differential decay rate, $d\Gamma/ds$, we must integrate out all other variables except for the Lorentz invariant $s = (p_X + p_Y)^2$. To do this, we first integrate out $\vec{p}_Y$ using the momentum conserving delta function. Changing to

polar coordinates, we then have

$$\Gamma = \frac{1}{2(2\pi)^5 m_A} \int \frac{|\vec{p}_X|^2 d|\vec{p}_X| d\Omega_X |\vec{p}_C|^2 d|\vec{p}_C| d\Omega_C}{8 E_X E_Y E_C} |\mathcal{M}|^2 \delta(m_A - E_X - E_Y - E_C) \ . \tag{C.4}$$

By Eq. (C.3), the choice for the axes with respect to which Ω_X and Ω_C are calculated is arbitrary. We choose the 3-axis to coincide with the direction of $\vec{p}_X$ so that

$$d\Omega_C = d\cos\theta_{XC} \ d\phi_C \ , \tag{C.5}$$

where θ_{XC} is the angle between $\vec{p}_C$ and $\vec{p}_X$. Exploiting the simple relation

$$E_i dE_i = |\vec{p}_i| d|\vec{p}_i| \tag{C.6}$$

and performing the trivial $d\Omega_X$ and $d\phi_C$ integrals, Eq. (C.4) reduces to

$$\Gamma = \frac{1}{(2\pi)^3 m_A} \int \frac{|\vec{p}_X||\vec{p}_C| dE_X dE_C d\cos\theta_{XC}}{8 E_Y} |\mathcal{M}|^2 \delta(m_A - E_X - E_Y - E_C) \ . \tag{C.7}$$

Note that the $d\cos\theta_{XC}$ integral is non-trivial, since E_Y is a function of $\cos\theta_{XC}$. That is,

$$E_Y = \sqrt{|\vec{p}_X + \vec{p}_C|^2 + m_Y^2} = \sqrt{m_X^2 + m_C^2 + m_Y^2 + 2|\vec{p}_X||\vec{p}_C|\cos\theta_{XC}} \ . \tag{C.8}$$

We are left with three integrations and one delta function. First, to conveniently encode the $[-1, 1]$ domain of the $\cos\theta_{XC}$ integral, we add a theta function factor, $\Theta(1 - \cos\theta_{XC}{}^2)$ and extend the $\cos\theta_{XC}$ integration limits to the entire real line. We now use the delta function to perform the integration over $d\cos\theta_{XC}$. From Eq. (C.8) observe that

$$\frac{dE_Y}{d\cos\theta_{XC}} = \frac{|\vec{p}_X||\vec{p}_C|}{\sqrt{m_X^2 + m_C^2 + m_Y^2 + 2|\vec{p}_X||\vec{p}_C|\cos\theta_{XC}}} = \frac{|\vec{p}_X||\vec{p}_C|}{E_Y} \ , \tag{C.9}$$

so that we may straightforwardly change variable from $\cos\theta_{XC}$ to E_Y and perform the final delta function integral. We end up with

$$\Gamma_{A\to X,Y,C} = \frac{1}{8(2\pi)^3 m_A} \int dE_X dE_C |\mathcal{M}|^2 \Theta(1 - \cos^2\theta_{XC}) \ . \tag{C.10}$$

Here $\cos\theta_{XC}$ is implicitly a function of $E_{X,C}$ and the masses.

We can now change variable from (E_X, E_C) to (s, s_1) using

$$E_X = \frac{m_A^2 + m_X^2 - s_1}{2m_A}, \qquad E_C = \frac{m_A^2 + m_C^2 - s}{2m_A} \qquad \Rightarrow \quad dE_X dE_C = \frac{ds ds_1}{4m_A^2} \ , \tag{C.11}$$

then from Eq. (C.10)

$$\frac{d\Gamma}{ds} = \frac{1}{32(2\pi)^3 m_A^3} \int ds_1 |\mathcal{M}|^2(s, s_1)\Theta(1 - \cos^2\theta_{XC}) \ . \tag{C.12}$$

In order to obtain the differential decay rate we need to perform just the s_1 integration. This integral can be performed once an explicit expression for $|\mathcal{M}|^2$ is given.

Before proceeding to consider the differential decay rates arising from different matrix elements, we still need to explicitly write down the limits of the s_1 integration due to the Θ function. In order to do so we must write $\cos\theta_{XC}$ as a function of (s, s_1) and then solve $\cos^2\theta_{XC} \leq 1$ for s_1. Define $s_2 = (p_X + p_C)^2$. Then

$$s_2 = (p_X + p_C)^2 = m_X^2 + m_C^2 + 2E_X E_C - 2|\vec{p}_X||\vec{p}_C|\cos\theta_{XC} \ . \tag{C.13}$$

Applying the identities (C.11), plus

$$|\vec{p}_i| = \sqrt{E_i^2 - m_i^2}, \qquad s + s_1 + s_2 = m_X^2 + m_C^2 + m_A^2 + m_Y^2 \ , \tag{C.14}$$

Eq. (C.13) becomes

$$\cos\theta_{XC} = \frac{2m_A^2(s + s_1 - m_Y^2 - m_A^2) + (m_A^2 + m_X^2 - s_1)(m_A^2 + m_C^2 - s)}{\sqrt{(m_A^2 + m_C^2 - s)^2 - 4m_A^2 m_C^2}\sqrt{(m_A^2 + m_X^2 - s_1)^2 - 4m_A^2 m_X^2}} \ . \tag{C.15}$$

The general solution for $\cos^2\theta_{XC} \leq 1$ in terms of s_1 is $s_{1_-} \leq s_1 \leq s_{1_+}$ with limits

$$s_{1_\pm} = \frac{m_A^2 + m_X^2 + m_Y^2 + m_C^2 - s}{2} + \frac{(m_Y^2 - m_X^2)(m_A^2 - m_C^2)}{2s} \\ \pm \frac{2}{s}\sqrt{\left[\left(\frac{m_A^2 + m_C^2 - s}{2}\right)^2 - m_A^2 m_C^2\right]\left[\left(\frac{m_Y^2 - m_X^2 + s}{2}\right)^2 - m_Y^2 s\right]} \ . \tag{C.16}$$

We now have our master formula for the differential decay rate

$$\frac{d\Gamma}{ds} = \frac{1}{32(2\pi)^3 m_A^3} \int_{s_{1-}}^{s_{1+}} ds_1 |\mathcal{M}|(s, s_1)^2 \ . \tag{C.17}$$

If the two leptons X and Y are massless, the integration limits reduce to

$$s_{1\pm} = \frac{m_A^2 + m_C^2 - s}{2} \pm \sqrt{\left(\frac{m_A^2 + m_C^2 - s}{2}\right)^2 - m_A^2 m_C^2} \ . \tag{C.18}$$

Defining a new variable $\eta \equiv 1 - s_1/m_B^2$, we immediately obtain the integration limits $\eta_\pm$ and the natural definition of ξ as written in Eq. (5.12) of the main text.

We now consider explicit examples and carry out the integral in (C.17) for the three cases considered in the main text.

C.1.1 ϕ^3 interaction

First consider the case in which all the particles involved are scalars with ϕ^3 vertices of the form

$$g_X \phi_A \phi_B \phi_X + g_Y \phi_C \phi_B \phi_Y \ . \tag{C.19}$$

To take into account the decay width Γ_B we use the Breit-Wigner approximation described in the main text (5.7). The matrix element is

$$|\mathcal{M}|^2_{\phi^3} = \frac{g_X^2 g_Y^2}{((p - p_X)^2 - m_B^2)^2 + m_B^2 \Gamma_B^2} = \frac{g_X^2 g_Y^2}{(s_1 - m_B^2)^2 + m_B^2 \Gamma_B^2} \ , \tag{C.20}$$

so the master formula (C.17) then becomes

$$\frac{d\Gamma}{ds} = \frac{g_X^2 g_Y^2}{32(2\pi)^3 m_A^3} \int_{s_{1-}}^{s_{1+}} ds_1 \frac{1}{(s_1 - m_B^2) + m_B^2 \Gamma_B^2} \ . \tag{C.21}$$

Using

$$\int ds_1 \frac{1}{(s_1 - m_B^2) + m_B^2 \Gamma_B^2} = \frac{1}{m_B \Gamma_B} \mathrm{Tan}^{-1}\left(\frac{s_1 - m_B^2}{m_B \Gamma_B}\right) \ , \tag{C.22}$$

we get the final result reported in the main text

$$\frac{d\Gamma}{ds} = \frac{g_X^2 g_Y^2}{32(2\pi)^3 m_A^3 m_B \Gamma_B}\left[\mathrm{Tan}^{-1}\left(\frac{m_B}{\Gamma_B}\eta_+\right) - \mathrm{Tan}^{-1}\left(\frac{m_B}{\Gamma_B}\eta_-\right)\right] , \tag{C.23}$$

where $\eta_\mp = 1 - s_{1_\pm}/m_B^2$ as defined in the main text (cf. Eq. (5.12)) .

C.1.2 Intermediate Scalar

We now move on to consider the decay in Fig. 5.1a. The corresponding Yukawa couplings are (Eq. (5.32))

$$\mathcal{L}_{\rm yuk}^{\rm s} = \bar{\psi}_A\big(g_L^X P_L + g_R^X P_R\big)\ell_X^\alpha U^{\alpha i *}\phi_B^i + \bar{\psi}_C\big(g_L^Y P_L + g_R^Y P_R\big)\ell_Y^\alpha U^{\alpha i *}\phi_B^i , \tag{C.24}$$

which include flavor mixing. We denote the amplitude for the jth B mass eigenstate as $\mathcal{M}_j^{\rm sc}$, and

$$\begin{aligned} i\mathcal{M}_j^{\rm sc} = {} & \bar{u}^\alpha(p_X)\big[g_L^X P_R + g_R^X P_L\big]u(p_A)\bar{u}(p_C)\big[g_L^Y P_L + g_R^Y P_R\big]v^\beta(p_Y) \\ & \times \frac{iU^{\alpha j}U^{\beta j *}}{(p_B^2 - m_j^2) + im_j\Gamma_j} . \end{aligned} \tag{C.25}$$

The total squared amplitude final involves both square and interference terms

$$|\mathcal{M}_{\rm Tot}^{\rm sc}|^2 = |\mathcal{M}_1^{\rm sc}|^2 + |\mathcal{M}_2^{\rm sc}|^2 + 2\mathrm{Re}\Big[\mathcal{M}_1^{\rm sc}(\mathcal{M}_2^{\rm sc})^*\Big] . \tag{C.26}$$

We focus first on the interference term. After computing the traces, we have

$$\begin{aligned} 2\mathrm{Re}\Big[\mathcal{M}_1^{\rm sc}(\mathcal{M}_2^{\rm sc})^*\Big] = {} & 2\Big[(g_L^X)^2 + (g_R^X)^2\Big]\Big[(g_L^Y)^2 + (g_R^Y)^2\Big]\mathrm{Re}[U_{\alpha i}U_{\beta j}U_{\alpha j}^* U_{\beta i}^*] \\ & \times \frac{\Big[(s_1 - m_1^2)(s_1 - m_2^2) + m_1 m_2 \Gamma_1 \Gamma_2\Big]}{\Big[(s_1 - m_1^2)^2 + m_1^2\Gamma_1^2\Big]\Big[(s_1 - m_2^2)^2 + m_2^2\Gamma_2^2\Big]}\mathcal{T}^{\rm sc} , \end{aligned} \tag{C.27}$$

$$\tag{C.28}$$

and

$$\mathcal{T}^{\rm sc} = 64(p_A \cdot p_X)(p_C \cdot p_Y) = 16(m_A^2 - s_1)(s_1 - m_C^2) \ . \tag{C.29}$$

Note that $s_1 = p_B^2$. The square terms $|\mathcal{M}_j^{\rm sc}|^2$ follow from Eq. (C.25)

$$|\mathcal{M}_j^{\rm sc}|^2 = 16\Big[(g_L^X)^2 + (g_R^X)^2\Big]\Big[(g_L^Y)^2 + (g_R^Y)^2\Big]|U^{\alpha j}|^2|U^{\beta j}|^2\frac{(m_A^2 - s_1)(s_1 - m_C^2)}{(s_1 - m_j^2)^2 + m_j^2\Gamma_j^2} \ . \tag{C.30}$$

The differential decay rate can be obtained plugging Eqs. (C.27) and (C.30) in the master formula (C.17). The final result is the sum of three integrations, involving the square terms and the interference one

$$\left.\frac{d\Gamma^{\alpha\beta}}{ds}\right|_{\rm sc} = \frac{\Big[(g_L^X)^2 + (g_R^X)^2\Big]\Big[(g_L^Y)^2 + (g_R^Y)^2\Big]}{(2\pi)^3 m_A^3}\left\{\sum_{j=1,2}\mathcal{I}_j + \mathcal{I}_{12}\right\} \ . \tag{C.31}$$

Here,

$$\begin{aligned}
\mathcal{I}_j &= |U^{\alpha j}|^2|U^{\beta j}|^2\int_{s_{1_}}^{s_{1+}} ds_1 \frac{(m_A^2 - s_1)(s_1 - m_C^2)}{(s_1 - m_j^2)^2 + m_j^2\Gamma_j^2} \\
&= m_j^2|U^{\alpha j}|^2|U^{\beta j}|^2\left[\frac{1 + (-)^j z}{1 + (-)^j y}\right]\left\{\left(\frac{s_0^j + \Gamma_j^2}{m_j^2}\right)\tan^{-1}\left[\frac{m_j}{\Gamma_j}\eta\right]\Bigg|_{\eta=\eta_-^j}^{\eta=\eta_+^j}\right. \\
&\qquad \left. + \frac{\Gamma_j}{m_j}\left[\left(\frac{m_A^2 + m_C^2}{2m_j^2} - 1\right)\log\left[\eta^2 + \left(\frac{\Gamma_j}{m_j}\right)^2\right] - \eta\right]\Bigg|_{\eta=\eta_-^j}^{\eta=\eta_+^j}\right\} \\
&\simeq |U^{\alpha j}|^2|U^{\beta j}|^2 s_0^j\left[\frac{1 + (-)^j z}{1 + (-)^j y}\right]\tan^{-1}\left[\frac{m_j}{\Gamma_j}\eta\right]\Bigg|_{\eta=\eta_-^j}^{\eta=\eta_+^j} \ ,
\end{aligned} \tag{C.32}$$

where m, z, y, and x are the oscillation parameters defined in Eqs. (5.27) and (5.28), $\eta_\mp^j \equiv 1 - s_{1_\pm}/m_j^2$,

$$s_0^j = \frac{(m_A^2 - m_j^2)(m_j^2 - m_C^2)}{m_j^2} \ , \tag{C.33}$$

and the approximation in Eq. (C.32) drops terms whose prefactors are suppressed by Γ_j/m_j.

The interference term is more involved. We report results to leading order in ϵ and we directly write the coefficients in terms of the oscillation parameters as in the main text. We have

$$\begin{aligned}\mathcal{I}_{12} &= 2\mathrm{Re}[U_{\alpha1}U^*_{\beta1}U^*_{\alpha2}U_{\beta2}]\int_{s_{1_-}}^{s_{1_+}} ds_1 \frac{\Big[(s_1-m_1^2)(s_1-m_2^2)+m_1m_2\Gamma_1\Gamma_2\Big]\mathcal{T}^{\rm sc}}{\Big[(s_1-m_1^2)^2+m_1^2\Gamma_1^2\Big]\Big[(s_1-m_2^2)^2+m_2^2\Gamma_2^2\Big]} \\ &= \frac{\mathrm{Re}[U_{\alpha1}U^*_{\beta1}U^*_{\alpha2}U_{\beta2}]m^2}{x^2+(1+yz)^2}\sum_{j=1,2}\left\{\mathcal{A}^j_{\rm sc}\tan^{-1}\left[\frac{m_j}{\Gamma_j}\eta\right]\Bigg|_{\eta=\eta^j_-}^{\eta=\eta^j_+}\right. \\ &\qquad \left. -\mathcal{B}^j_{\rm sc}\log\left[\eta^2+\left(\frac{\Gamma_j}{m_j}\right)^2\right]\Bigg|_{\eta=\eta^j_-}^{\eta=\eta^j_+}\right\}, \end{aligned} \tag{C.34}$$

where (at leading order in $\Gamma/m = 2z/x$)

$$\begin{aligned}\mathcal{A}^j_{\rm sc} &= \frac{m_A^2m^2(1-yz)(1-z^2)-m_A^2m_C^2(1+yz)+m_C^2m^2(1-yz)(1-z^2)}{m^4} \\ &\quad -\frac{m^4(1+(-)^jz)^3[1+(-)^jz(-3+3y+yz)]}{m^4}, \\ \mathcal{B}^j_{\rm sc} &= \pm\frac{x}{2}\frac{s_0^jm_j^2}{m^4}. \end{aligned} \tag{C.35}$$

These coefficients and $\mathcal{I}_{12}$ prefactors reduce to those in Eqs. (5.38) at leading order in z.

C.1.3 Intermediate Fermion

Finally, suppose the intermediate particles are fermions. The Yukawa couplings are as in Eq. (5.42)

$$\mathcal{L}^{\rm f}_{\rm yuk} = \bar\psi^i_B\big(g^X_LP_L+g^X_RP_R\big)U^{\alpha i*}\ell^\alpha_X\phi^\dagger_A + \bar\psi^i_B\big(g^Y_LP_L+g^Y_RP_R\big)U^{\alpha i*}\ell^\alpha_Y\phi^\dagger_C\,. \tag{C.36}$$

We denote the amplitude for the jth B mass eigenstate as $\mathcal{M}^{\rm f}_j$, and

$$i\mathcal{M}^{\rm f}_j = iU^{\alpha j}U^{\beta j*}\bar u^\alpha(p_X)\big[g^X_LP_R+g^X_RP_L\big]\frac{\not p_B+m_j-i\Gamma_j/2}{(p_B^2-m_j^2)+im_j\Gamma_j}\big[g^Y_LP_L+g^Y_RP_R\big]v^\beta(p_Y)\,. \tag{C.37}$$

Now, since A and C are scalars, the total helicity of the $|XY\rangle$ final state must be zero. Since X and Y are massless, spin-1/2 particles, if they have the same (opposite) chirality then they must have opposite (same) sign components of momentum in the angular momentum direction. These are the only options. As a result, the terms of the differential decay rate may depend only on a linear combination of $(g_L^X g_L^Y)^2$, $(g_R^X g_R^Y)^2$, $(g_R^X g_L^Y)^2$ and $(g_L^X g_R^Y)^2$, and the terms for the latter (former) two factors must have the same s dependence. Hence we may write the differential decay rate in the form (cf. Eqs. (5.43) and (5.47))

$$\left.\frac{d\Gamma^{\alpha\beta}}{ds}\right|_{\rm f} = \left[(g_L^X \tilde{g}_L^Y)^2 + (g_R^X \tilde{g}_R^Y)^2\right] \left.\frac{d\Gamma^{\alpha\beta}}{ds}\right|_{-} + \left[(g_L^X \tilde{g}_R^Y)^2 + (g_R^X \tilde{g}_L^Y)^2\right] \left.\frac{d\Gamma^{\alpha\beta}}{ds}\right|_{+} . \quad \text{(C.38)}$$

Here $d\Gamma/ds|_\pm$ are called the chiral decay rates for reasons explained in the main text, and each one of them has both square and interference contributions:

$$\left.\frac{d\Gamma^{\alpha\beta}}{ds}\right|_{\pm} = \left.\frac{d\Gamma_1^{\alpha\beta}}{ds}\right|_{\pm} + \left.\frac{d\Gamma_2^{\alpha\beta}}{ds}\right|_{\pm} + \left.\frac{d\Gamma_{12}^{\alpha\beta}}{ds}\right|_{\pm} . \quad \text{(C.39)}$$

For the sake of brevity, we introduce the following notation

$$g_+ = (g_L^X g_R^Y)^2 + (g_R^X g_L^Y)^2, \qquad g_- = (g_L^X g_L^Y)^2 + (g_R^X g_R^Y)^2 , \quad \text{(C.40)}$$

and simply report here all the integrands in terms of the variables of integration (s, s_1). The interference term is

$$\begin{aligned}\left.\mathcal{M}_{12}^{\rm f}\right|_+ =& \frac{32 g_+ {\rm Re}[U_{\alpha1} U_{\beta1}^* U_{\alpha2}^* U_{\beta2}]}{\left[(s_1 - m_1^2)^2 + m_1^2\Gamma_1^2\right]\left[(s_1 - m_2^2)^2 + m_2^2\Gamma_2^2\right]} \\ & \times \left\{ m_1 m_2 s \Big[(s_1 - m_1^2)(s_1 - m_2^2) + m_1 m_2 \Gamma_1 \Gamma_2\Big] \right. \\ & \left. + \frac{1}{2}\Big[(s_1 - m_2^2) m_1 \Gamma_1 - (s_1 - m_1^2) m_2 \Gamma_2\Big](m_1\Gamma_2 - m_2\Gamma_1) s \right\} ,\end{aligned} \quad \text{(C.41)}$$

$$\begin{aligned}\left.\mathcal{M}_{12}^{\rm f}\right|_- =& \frac{32 g_- {\rm Re}[U_{\alpha1} U_{\beta1}^* U_{\alpha2}^* U_{\beta2}]}{\left[(s_1 - m_1^2)^2 + m_1^2\Gamma_1^2\right]\left[(s_1 - m_2^2)^2 + m_2^2\Gamma_2^2\right]} \\ & \times \left[(m_A^2 - s_1)(s_1 - m_C^2) - s_1 s\right]\left[(s_1 - m_1^2)(s_1 - m_2^2) + m_1 m_2 \Gamma_1 \Gamma_2\right] .\end{aligned} \quad \text{(C.42)}$$

In contrast, the square terms are

$$|\mathcal{M}_j^{\rm f}|_+^2 = \frac{32\ g_+ |U^{\alpha j}|^2 |U^{\beta j}|^2 m_j^2 s}{\left[(s_1 - m_j^2)^2 + m_j^2 \Gamma_j^2\right]}\ , \tag{C.43}$$

$$|\mathcal{M}_j^{\rm f}|_-^2 = \frac{32\ g_- |U^{\alpha j}|^2 |U^{\beta j}|^2 \left[(m_A^2 - s_1)(s_1 - m_C^2) - s s_1\right]}{\left[(s_1 - m_j^2)^2 + m_j^2 \Gamma_j^2\right]}\ . \tag{C.44}$$

In order to obtain the final expression for $d\Gamma^{\alpha\beta}/ds\big|_{\rm f}$ we just need to perform the integrations over s_1 as in Eq. (C.17). At leading order in ϵ, the results are displayed in Eqs. (5.49) and (5.50), but the full coefficients of the interference terms (including terms to all z orders) are

$$\begin{aligned}
\mathcal{A}_+^j &= \frac{s}{m^2} \\
\mathcal{B}_+^j &= -(-)^j \frac{x}{2}\frac{s}{m^2}(1 - z^2) \\
\mathcal{A}_-^j &= \mathcal{A}_{\rm sc}^j - \frac{s}{m^2} \\
\mathcal{B}_-^j &= \mathcal{B}_{\rm sc}^j + (-)^j \frac{x}{2}\frac{s m_j^2}{m^4}\ .
\end{aligned} \tag{C.45}$$

with $\mathcal{A}_{\rm sc}^j$ and $\mathcal{A}_{\rm sc}^j$ defined in Eq. (C.35). Note that in the vectorial coupling case, the linear s dependence of the log coefficient terms cancel up to terms of order

$$\frac{xz}{x^2+1} \sim \epsilon \frac{x^2}{x^2+1} \leq \epsilon\ , \tag{C.46}$$

which are negligible, as expected.

APPENDIX D

SU(3) SUM RULES IN CHARM DECAYS

D.1 Abstract Sum Rule Generation

In this appendix, we show how to compute sum rules from the symmetries of the Hamiltonian H. Examining the structure of H in eqs. (6.15), note first that the **6** can be written in matrix form as $[\mathbf{6}]^i_j \equiv [\mathbf{6}]^{ij}$, i.e (dropping factors of 1/2 and overall signs)

$$[\mathbf{6}] = \begin{pmatrix} 0 & 0 & 0 \\ 0 & 1 & \lambda \\ 0 & \lambda & \lambda^2 \end{pmatrix} , \tag{D.1}$$

with tensor transformation law under a generator X

$$[\mathbf{6}]^i_j \to \{X[\mathbf{6}]\}^i_j + \{X[\mathbf{6}]^T\}^i_j \ . \tag{D.2}$$

This is clearly zero for $X = E^I_\pm$ and $E^D_\pm$, the raising/lowering operators (normalized to unity) of isospin and D-spin respectively. Similarly, defining the matrices $[\bar{\mathbf{15}}]_i$ via

$$([\bar{\mathbf{15}}]_i)^k_j \equiv [\bar{\mathbf{15}}]^k_{ij} \ , \tag{D.3}$$

then in matrix notation we may write the $\bar{\mathbf{15}}$ irrep as

$$[\bar{\mathbf{15}}]_1 = \begin{pmatrix} 0 & 0 & 0 \\ 0 & -\lambda & 1 \\ 0 & -\lambda^2 & \lambda \end{pmatrix} \qquad [\bar{\mathbf{15}}]_2 = \begin{pmatrix} 0 & 0 & 0 \\ -\lambda & 0 & 0 \\ -\lambda^2 & 0 & 0 \end{pmatrix} \qquad [\bar{\mathbf{15}}]_3 = \begin{pmatrix} 0 & 0 & 0 \\ 1 & 0 & 0 \\ \lambda & 0 & 0 \end{pmatrix} , \tag{D.4}$$

and by symmetry of the lower indices, the tensor transformation law under generator X is

$$[\bar{\mathbf{15}}]^k_{ij} \to 2\{[\bar{\mathbf{15}}]_{(i}X\}^k_{j)} - \{X[\bar{\mathbf{15}}]_i\}^k_j \ . \tag{D.5}$$

This is zero under the operator

$$T_- \equiv E_-^I + \lambda E_-^D = \begin{pmatrix} 0 & 0 & 0 \\ 1 & 0 & 0 \\ \lambda & 0 & 0 \end{pmatrix} \ . \tag{D.6}$$

Clearly both $\bar{\mathbf{3}}_{\boldsymbol{p}}$ and $\bar{\mathbf{3}}_{\boldsymbol{t}}$ have matrix form $\sim (\lambda^5 A^2, 0, 0)$, so that they are invariant under this operator too. Consequently, we deduce that the Hamiltonian itself is an invariant tensor under T_-. Furthermore, observe that the Hamiltonian is fully invariant under

$$S \equiv -\lambda H^U - \lambda^2 E_-^U + E_+^U = \begin{pmatrix} 0 & 0 & 0 \\ 0 & -\lambda & 1 \\ 0 & -\lambda^2 & \lambda \end{pmatrix} \ , \tag{D.7}$$

which is a linear combination of U-spin operators, and therefore must be QED charge preserving, too.

The invariance of H under these operators is related to the generation of sum rules for the amplitudes. As in the main text, a sum rule itself has the form

$$\mathcal{S}^{\alpha\beta\mu}(C_w)_{\alpha\beta\mu} = 0 \ . \tag{D.8}$$

The index μ here is a tensor index. To see this, note that that the meson tensor $(D_\mu)^i = \partial(D_3)^i/\partial D_\mu = \delta^i_\mu$. Then under an operator T,

$$T|D_\mu\rangle = |D_\alpha\rangle\langle D_\alpha|T|D_\mu\rangle = (D^\alpha)_j T^j_i (D_\mu)^i |D_\alpha\rangle = T^\alpha_\mu |D_\alpha\rangle \ . \tag{D.9}$$

Similarly for the out-state mesons we just have $\langle M_\alpha| = (M_\alpha)^\rho_\sigma \langle M^\rho_\sigma|$, where $\langle M^\rho_\sigma|$ are a normalized basis of the out-states. The completeness relation $\sum_\alpha \mathrm{Tr}\{AM^T_\alpha\}M_\alpha \equiv A - \mathbf{1}\mathrm{Tr}\{A\}$ and the tracelessness of T and M_α then implies

$$T\langle M_\alpha| = \mathrm{Tr}\big\{[T, M_\alpha]M^T_\beta\big\}\langle M_\beta| \equiv [T_8]^\beta_\alpha \langle M_\beta| \ , \tag{D.10}$$

so that we may treat α and β as indices in a basis transforming under the adjoint representation.

The key observation in generating sum rules abstractly is that provided $TH = 0$, then it follows that $TC_w = 0$ by eq. (6.8). Hence

$$T^{\rho\sigma\gamma}_{\alpha\beta\mu}[C_w]_{\rho\sigma\gamma} \equiv [T_8]^\gamma_\alpha [C_w]_{\gamma\beta\mu} + [T_8]^\gamma_\beta [C_w]_{\alpha\gamma\mu} + T^\gamma_\mu [C_w]_{\alpha\beta\gamma} = 0 \ . \tag{D.11}$$

This master formula permits us to compute sum rules without computing the Wigner-Eckart invariants: one need only select appropriate α, β, μ to generate a sum rule. As an example of the operation of this master formula, let us now consider $T = S$ or T_-, the two operators under which H is invariant. For $T = S$, we have in the $D \to P_8 P_8$ case

$$\langle M_\alpha| = \begin{pmatrix} \langle\pi^0| & \langle\eta_8| & \langle\pi^+| & \langle K^+| & \langle\pi^-| & \langle K^-| & \langle K^0| & \langle\bar{K}^0| \end{pmatrix}$$

$$[S_8]^\beta_\alpha = \begin{pmatrix} 0 & 0 & 0 & 0 & 0 & 0 & -\frac{\lambda^2}{\sqrt{2}} & -\frac{1}{\sqrt{2}} \\ 0 & 0 & 0 & 0 & 0 & 0 & \sqrt{\frac{3}{2}}\lambda^2 & \sqrt{\frac{3}{2}} \\ 0 & 0 & \lambda & \lambda^2 & 0 & 0 & 0 & 0 \\ 0 & 0 & -1 & -\lambda & 0 & 0 & 0 & 0 \\ 0 & 0 & 0 & 0 & -\lambda & 1 & 0 & 0 \\ 0 & 0 & 0 & 0 & -\lambda^2 & \lambda & 0 & 0 \\ \frac{1}{\sqrt{2}} & -\sqrt{\frac{3}{2}} & 0 & 0 & 0 & 0 & -2\lambda & 0 \\ \frac{\lambda^2}{\sqrt{2}} & -\sqrt{\frac{3}{2}}\lambda^2 & 0 & 0 & 0 & 0 & 0 & 2\lambda \end{pmatrix} . \tag{D.12}$$

The operator S does not change the electric charge of the states, so that provided each choice of α, β, μ corresponds to a QED preserving amplitude $D_\mu \to [P_8]_\alpha [P_8]_\beta$, then eq. (D.11) generates a sum-rule. For example, the linear combination of the choices $\{\alpha, \beta, \mu\} = \{K^+, \pi^-, D^0\}$ and $\{\alpha, \beta, \mu\} = \{K^-, \pi^+, D^0\}$ generates the U-

spin sum rule

$$
\begin{aligned}
0 &= S^{\rho\sigma\gamma}_{K^+\pi^-D^0}[C_w]_{\rho\sigma\gamma}/2\lambda^3 + S^{\rho\sigma\gamma}_{K^-\pi^+D^0}[C_w]_{\rho\sigma\gamma}/2\lambda \\
&= -\frac{[C_w]_{K^-K^+D^0}}{\lambda} + \frac{[C_w]_{\pi^-\pi^+D^0}}{\lambda} + [C_w]_{K^-\pi^+D^0} - \frac{[C_w]_{\pi^-K^+D^0}}{\lambda^2} \ . \qquad \text{(D.13)}
\end{aligned}
$$

Similarly, for the operator $T_- \equiv E^I_- + \lambda E^D_-$ one has

$$
[T_{-8}]^\beta_\alpha = \begin{pmatrix}
0 & 0 & -\sqrt{2} & -\frac{\lambda}{\sqrt{2}} & 0 & 0 & 0 & 0 \\
0 & 0 & 0 & -\sqrt{\frac{3}{2}}\lambda & 0 & 0 & 0 & 0 \\
0 & 0 & 0 & 0 & 0 & 0 & 0 & 0 \\
0 & 0 & 0 & 0 & 0 & 0 & 0 & 0 \\
\sqrt{2} & 0 & 0 & 0 & 0 & 0 & -\lambda & 0 \\
\frac{\lambda}{\sqrt{2}} & \sqrt{\frac{3}{2}}\lambda & 0 & 0 & 0 & 0 & 0 & -1 \\
0 & 0 & 0 & 1 & 0 & 0 & 0 & 0 \\
0 & 0 & \lambda & 0 & 0 & 0 & 0 & 0
\end{pmatrix} \ . \qquad \text{(D.14)}
$$

The operator T_- is a $\Delta Q = -1$ operator, so that eq. (D.11) produces a sum rule of QED preserving amplitudes for each choice of α, β, μ corresponding to a $\Delta Q = +1$ amplitude.

In order to produce the sum rules for our effective Hamiltonian (6.15), it is important to observe that not all QED preserving amplitudes can be produced by H. In particular, H can raise or lower U-spin by at most one unit, so that the $\Delta U = \pm 2$ amplitudes

$$
A_{D^0\to K^0K^0} \ , \qquad A_{D^0\to \bar{K}^0\bar{K}^0} \ , \qquad A_{D^+\to K^0K^+} \ , \qquad A_{D^+_s\to \bar{K}^0\pi^+} \ , \qquad \text{(D.15)}
$$

must be zero. Enforcing the zero value for these amplitudes, one obtains 21 linearly independent P_8P_8 sum-rules from the sum rule operators S and T_-, in the SU(3) flavor basis

i)

$$-3A_{D^0\to 2\eta_8} + A_{D^0\to 2\pi_0} - 4\sqrt{6}\lambda A_{D^0\to \eta_8\bar{K}^0} + 2A_{D^0\to K^0\bar{K}^0} = 0$$

ii)

$$\frac{3A_{D^0\to 2\eta_8}}{\sqrt{2}} + 3\sqrt{3}\lambda A_{D^0\to \eta_8\bar{K}^0} - \frac{3A_{D^0\to K^0\bar{K}^0}}{\sqrt{2}} - \frac{A_{D^+\to \bar{K}^0K^+}}{\sqrt{2}} + A_{D^+\to \pi_0\pi^+}$$
$$- \frac{\lambda A_{D_s^+\to \bar{K}^0K^+}}{\sqrt{2}} = 0$$

iii)

$$A_{D_s^+\to \pi_0\pi^+} = 0$$

iv)

$$3\sqrt{3}\lambda^2 A_{D^0\to \eta_8\bar{K}^0} + \frac{3A_{D^0\to 2\eta_8}\lambda}{\sqrt{2}} - \frac{3\lambda A_{D^0\to K^0\bar{K}^0}}{\sqrt{2}} - \frac{\lambda A_{D^+\to \bar{K}^0K^+}}{\sqrt{2}}$$
$$+ A_{D^+\to \pi_0K^+} = 0$$

v)

$$-\frac{3A_{D^0\to 2\eta_8}}{\sqrt{2}} - 3\sqrt{3}\lambda A_{D^0\to \eta_8\bar{K}^0} + \frac{3A_{D^0\to K^0\bar{K}^0}}{\sqrt{2}} + A_{D_s^+\to \pi_0K^+}$$
$$- \frac{\lambda A_{D_s^+\to \bar{K}^0K^+}}{\sqrt{2}} = 0$$

vi)

$$-\sqrt{3}A_{D^0\to 2\eta_8} + A_{D^0\to \eta_8\pi_0} - 2\sqrt{2}\lambda A_{D^0\to \eta_8\bar{K}^0} + \sqrt{3}A_{D^0\to K^0\bar{K}^0} = 0$$

vii)

$$\sqrt{3}\lambda^2 A_{D^0\to \eta_8\bar{K}^0} + A_{D^0\to K^0\pi_0} = 0$$

viii)

$$A_{D^0\to\pi_0\bar{K}^0} - \sqrt{3}A_{D^0\to\eta_8\bar{K}^0} = 0$$

ix)

$$-6A_{D^0\to 2\eta_8} - 7\sqrt{6}\lambda A_{D^0\to\eta_8\bar{K}^0} + 5A_{D^0\to K^0\bar{K}^0} + A_{D^0\to\pi^-\pi^+} + A_{D^+\to\bar{K}^0K^+}$$
$$+ \lambda A_{D_s^+\to\bar{K}^0K^+} = 0$$

x)

$$-3\sqrt{\frac{3}{2}}A_{D^0\to 2\eta_8} - 9\lambda A_{D^0\to\eta_8\bar{K}^0} + 3\sqrt{\frac{3}{2}}A_{D^0\to K^0\bar{K}^0} + \frac{A_{D^+\to\bar{K}^0K^+}}{\sqrt{6}} + A_{D^+\to\eta_8\pi^+}$$
$$+ \sqrt{\frac{3}{2}}\lambda A_{D_s^+\to\bar{K}^0K^+} = 0$$

xi)

$$-\frac{\sqrt{6}A_{D^0\to 2\eta_8}}{\lambda} - 6A_{D^0\to\eta_8\bar{K}^0} + \frac{\sqrt{6}A_{D^0\to K^0\bar{K}^0}}{\lambda} + \sqrt{\frac{2}{3}}\frac{A_{D^+\to\bar{K}^0K^+}}{\lambda}$$
$$+ A_{D_s^+\to\eta_8\pi^+} = 0$$

xii)

$$\lambda^2 A_{D_s^+\to\bar{K}^0K^+} + A_{D^+\to K^0\pi^+} = 0$$

xiii)

$$-6A_{D^0\to 2\eta_8} - 6\sqrt{6}\lambda A_{D^0\to\eta_8\bar{K}^0} + 6A_{D^0\to K^0\bar{K}^0} + A_{D^+\to\bar{K}^0K^+} + A_{D_s^+\to K^0\pi^+} = 0$$

xiv)

$$\frac{3A_{D^0\to 2\eta_8}}{\lambda} + 4\sqrt{6}A_{D^0\to\eta_8\bar{K}^0} - \frac{3A_{D^0\to K^0\bar{K}^0}}{\lambda} + A_{D^0\to K^-\pi^+} - \frac{A_{D^+\to\bar{K}^0K^+}}{\lambda}$$
$$- A_{D_s^+\to\bar{K}^0K^+} = 0$$

xv)

$$\frac{3A_{D^0\to 2\eta_8}}{\lambda} + 3\sqrt{6}A_{D^0\to\eta_8\bar{K}^0} - \frac{3A_{D^0\to K^0\bar{K}^0}}{\lambda} - \frac{A_{D^+\to\bar{K}^0K^+}}{\lambda} + A_{D^+\to\bar{K}^0\pi^+}$$

$$- A_{D_s^+\to\bar{K}^0K^+} = 0$$

xvi)

$$-4\sqrt{6}\lambda^2 A_{D^0\to\eta_8\bar{K}^0} + \lambda^2 A_{D_s^+\to\bar{K}^0K^+} - 3\lambda A_{D^0\to 2\eta_8} + 3\lambda A_{D^0\to K^0\bar{K}^0} + \lambda A_{D^+\to\bar{K}^0K^+}$$

$$+ A_{D^0\to\pi^-K^+} = 0$$

xvii)

$$-3\lambda^2 A_{D^0\to\eta_8\bar{K}^0} - \sqrt{\frac{3}{2}}\lambda A_{D^0\to 2\eta_8} + \sqrt{\frac{3}{2}}\lambda A_{D^0\to K^0\bar{K}^0} + \frac{\lambda A_{D^+\to\bar{K}^0K^+}}{\sqrt{6}}$$

$$+ A_{D^+\to\eta_8K^+} = 0$$

xviii)

$$-\sqrt{\frac{3}{2}}A_{D^0\to 2\eta_8} - 3\lambda A_{D^0\to\eta_8\bar{K}^0} + \sqrt{\frac{3}{2}}A_{D^0\to K^0\bar{K}^0} + \sqrt{\frac{2}{3}}A_{D^+\to\bar{K}^0K^+} + A_{D_s^+\to\eta_8K^+}$$

$$+ \sqrt{\frac{3}{2}}\lambda A_{D_s^+\to\bar{K}^0K^+} = 0$$

xix)

$$-3\sqrt{6}\lambda^2 A_{D^0\to\eta_8\bar{K}^0} + \lambda^2 A_{D_s^+\to\bar{K}^0K^+} - 3\lambda A_{D^0\to 2\eta_8} + 3\lambda A_{D^0\to K^0\bar{K}^0} + \lambda A_{D^+\to\bar{K}^0K^+}$$

$$+ A_{D_s^+\to K^0K^+} = 0$$

xx)

$$\sqrt{6}\lambda A_{D^0\to\eta_8\bar{K}^0} - A_{D^0\to K^0\bar{K}^0} + A_{D^0\to K^-K^+} - A_{D^+\to\bar{K}^0K^+} - \lambda A_{D_s^+\to\bar{K}^0K^+} = 0$$

xxi)

$$\lambda^2 A_{D^0\to\eta_8\bar{K}^0} + A_{D^0\to\eta_8 K^0} = 0 \ .$$

In the $D \to P_1 P_8$ case, we have final states $\langle \eta_1 M_\beta|$, where $\langle\eta_1|$ is an SU(3) singlet, so that the master formula (D.11) becomes

$$T^{\sigma\gamma}_{\beta\mu}[C_w]_{\eta_1\sigma\gamma} \equiv [T_8]^\gamma_\beta [C_w]_{\eta_1\gamma\mu} + T^\gamma_\mu [C_w]_{\eta_1\beta\gamma} = 0 \ . \tag{D.16}$$

Applying eq. (D.16) to all possible β,μ that correspond to QED-preserving $|\Delta U| < 2$ amplitudes, one further finds 5 linearly independent $P_1 P_8$ sum rules. In the SU(3) flavor basis these are

xxii)

$$-\frac{\sqrt{3}A_{D^0\to\eta\eta_1}}{\lambda} + \frac{A_{D^0\to\pi_0\eta_1}}{\lambda} - 2\sqrt{2}A_{D^0\to\bar{K}^0\eta_1} = 0$$

xxiii)

$$-\frac{2\sqrt{6}A_{D^0\to\eta\eta_1}}{\lambda} - 6A_{D^0\to\bar{K}^0\eta_1} + \frac{A_{D^+\to\pi^+\eta_1}}{\lambda} + \frac{A_{D_s^+\to K^+\eta'}}{\lambda} = 0$$

xxiv)

$$\frac{\sqrt{6}A_{D^0\to\eta\eta_1}}{\lambda} + 3A_{D^0\to\bar{K}^0\eta_1} - \frac{A_{D_s^+\to K^+\eta_1}}{\lambda} + A_{D_s^+\to\pi^+\eta_1} = 0$$

xxv)

$$-\frac{\sqrt{6}A_{D^0\to\eta\eta_1}}{\lambda} - 3A_{D^0\to\bar{K}^0\eta_1} + \frac{A_{D^+\to K^+\eta_1}}{\lambda^2} + \frac{A_{D_s^+\to K^+\eta_1}}{\lambda} = 0$$

xxvi)

$$\frac{A_{D^0\to K^0\eta_1}}{\lambda^2} + A_{D^0\to\bar{K}^0\eta_1} = 0 \ .$$

These 26 sum rules coincide precisely with those found by direct computation, and can be verified with by reference to the tables of Appendix D.2. Similar results can be obtained for the PV case. This method of computing sum rules applies only in the case that the invariants can be written in terms of the Hamiltonian (cf. eq. (6.8)) and there exist operators under which the Hamiltonian is invariant. Once we introduce the s-mass spurion then observe $T_- m_s$, $S m_s \neq 0$, so the above analysis fails at first order in the spurion, unless one finds an operator under which both H and m_s are invariants. Unfortunately, there does not seem to be such an operator available, so we are left with the option of just computing the invariants directly.

D.2 $D \to PP$ Invariants

D.2.1 $\mathcal{O}(1)$ Invariants

There are in principle seven linearly independent P_8P_8 Wigner-Eckart invariants at $\mathcal{O}(1)$ – i.e. zeroth order in the m_s or m_I spurion – four invariants for the P_1P_8 case and two for the P_1P_1 case. Due to the linear dependence of the two $\bar{\mathbf{3}}$ irreps, these are reduced respectively to five, two and one linearly independent invariants. Shown in Tables D.1 and D.2 below are the $\mathcal{O}(1)$ invariants for the P_1P_1, P_1P_8, and P_8P_8 amplitudes, labelled by $w = [^{\rm pp}_{xy}]^k_R$. Here x, y=1, 8 labels the P representations, R is the H irrep generating the invariant, and k indicates the kth such invariant. For convenience, we write only the invariant subscripts, so that

$$C_{[^{\rm pp}_{xy}]^k_R} = [^{\rm pp}_{xy}]^k_R \ . \tag{D.17}$$

It should be noted that the invariants in this paper are written in a basis different from that obtained by decomposing the final states into SU(3) irreps, and so they are not Clebsch-Gordan coefficients, but instead linear combinations of them. That is, in some approaches (see e.g. [200, 189]) one writes the PP final states $\mathbf{8} \otimes \mathbf{8} = \mathbf{1} \oplus \mathbf{8}_A \oplus \mathbf{8}_S \oplus \mathbf{10} \oplus \bar{\mathbf{10}} \oplus \mathbf{27}$, and then one deduces from the bosonic symmetry of the PP final state that e.g. the two linearly independent invariants arising from the $\bar{\mathbf{15}}$ are $\langle \mathbf{8}_S | \bar{\mathbf{15}} | \mathbf{3} \rangle$ and $\langle \mathbf{27} | \bar{\mathbf{15}} | \mathbf{3} \rangle$. We have taken a different approach: The invariants in this paper are obtained with respect to a basis of linearly independent SU(3) contractions of the initial and final states with the

Hamiltonian irrep of interest. For example, the PP $\mathcal{O}(1)$ invariants are explicitly

$$
\begin{gathered}
[{}^{\rm PP}_{88}]^{\bar{1}}_{\bar{\mathbf{3}}} = 3[M_P]^i_j[M_P]^j_i[\bar{\mathbf{3}}_{\boldsymbol{p}}]_k[D]^k/8 \ , \quad [{}^{\rm PP}_{88}]^{\bar{2}}_{\bar{\mathbf{3}}} = 3[M_P]^i_j[M_P]^j_k[\bar{\mathbf{3}}_{\boldsymbol{p}}]_i[D]^k/8 \ , \\
[{}^{\rm PP}_{88}]_{\mathbf{6}} = [M_P]^i_j[M_P]^k_i[\mathbf{6}]^{lj}[D]^m\varepsilon_{klm} \ , \\
[{}^{\rm PP}_{88}]^{\bar{1}}_{\bar{\mathbf{15}}} = [M_P]^i_j[M_P]^j_k[\bar{\mathbf{15}}]^k_{il}[D]^l \ , [{}^{\rm PP}_{88}]^{\bar{2}}_{\bar{\mathbf{15}}} = [M_P]^i_j[M_P]^k_l[\bar{\mathbf{15}}]^j_{ik}[D]^l \ , \\
[{}^{\rm PP}_{18}]_{\bar{\mathbf{3}}} = 3\eta_1[M_P]^j_i[\bar{\mathbf{3}}_{\boldsymbol{p}}]_j[D]^i/8 \ , \\
[{}^{\rm PP}_{18}]_{\mathbf{6}} = \eta_1[M_P]^i_j[\mathbf{6}]^{lj}[D]^m\varepsilon_{ilm} \ , \quad [{}^{\rm PP}_{18}]_{\bar{\mathbf{15}}} = \eta_1[M_P]^i_j[\bar{\mathbf{15}}]^j_{ik}[D]^k \ , \\
[{}^{\rm PP}_{11}]_{\bar{\mathbf{3}}} = 3\eta_1\eta_1[\bar{\mathbf{3}}_{\boldsymbol{p}}]_i[D]^i/8 \ .
\end{gathered}
\tag{D.18}
$$

These approaches are equivalent for the purposes of computing sum rules. We have adopted the latter approach, in part since we are unconcerned with the irrep in which each final state is embedded.

Of the 39 possible QED preserving amplitudes, only 34 are non-zero. The remaining five zero amplitudes are

$$
A_{D^0\to K^0K^0} \ , \qquad A_{D^0\to \bar{K}^0\bar{K}^0} \ , \qquad A_{D^+\to K^0K^+} \ , \qquad A_{D_s^+\to \bar{K}^0\pi^+} \ , \qquad A_{D_s^+\to \pi_0\pi^+} \ ,
\tag{D.19}
$$

and therefore are not shown in the tables. Of these, the first four are the $\Delta U = \pm 2$ amplitudes; the fifth amplitude is accidentally zero, as predicted in the sum rule (iii) of Appendix D.1.

ΔU	Ampl.	$[^{\rm PP}_{11}]_{\bar{\mathbf{3}}}$	$[^{\rm PP}_{18}]_{\bar{\mathbf{3}}}$	$[^{\rm PP}_{18}]_{\mathbf{6}}$	$[^{\rm PP}_{18}]_{\bar{\mathbf{15}}}$
0	$D^0 \to 2\eta_1$	$\frac{1}{4}\lambda^5 A^2$	0	0	0
0	$D^0 \to \eta_1\eta_8$	0	$\frac{\lambda^5 A^2}{8\sqrt{6}}$	$-\frac{\lambda}{2}\sqrt{\frac{3}{2}}$	$-\frac{\lambda}{2}\sqrt{\frac{3}{2}}$
1	$D^0 \to K^0\eta_1$	0	0	$-\frac{\lambda^2}{2}$	$-\frac{\lambda^2}{2}$
0	$D^0 \to \pi_0\eta_1$	0	$\frac{\lambda^5 A^2}{8\sqrt{2}}$	$\frac{\lambda}{2\sqrt{2}}$	$\frac{\lambda}{2\sqrt{2}}$
-1	$D^0 \to \eta_1\bar{K}^0$	0	0	$\frac{1}{2}$	$\frac{1}{2}$
1	$D^+ \to \eta_1 K^+$	0	0	$\frac{\lambda^2}{2}$	$-\frac{\lambda^2}{2}$
0	$D_s^+ \to \eta_1 K^+$	0	$\frac{\lambda^5 A^2}{8}$	$-\frac{\lambda}{2}$	$\frac{\lambda}{2}$
0	$D^+ \to \eta_1\pi^+$	0	$\frac{\lambda^5 A^2}{8}$	$\frac{\lambda}{2}$	$-\frac{\lambda}{2}$
-1	$D_s^+ \to \eta_1\pi^+$	0	0	$-\frac{1}{2}$	$\frac{1}{2}$

Table D.1: $D \to P_1P_1$ and $D \to P_1P_8$ $\mathcal{O}(1)$ invariants. A^2 is shorthand for $A^2(\rho - i\eta)$.

ΔU	Ampl.	$[{}^{pp}_{88}]^1_{\bar{\mathbf{3}}}$	$[{}^{pp}_{88}]^2_{\bar{\mathbf{3}}}$	$[{}^{pp}_{88}]_{\mathbf{6}}$	$[{}^{pp}_{88}]^1_{\overline{\mathbf{15}}}$	$[{}^{pp}_{88}]^2_{\overline{\mathbf{15}}}$
0	$D^0 \to \pi^-\pi^+$	0	$\frac{\lambda^5 A^2}{4}$	$-\frac{\lambda}{2}$	$-\lambda$	$-\frac{\lambda}{2}$
-1	$D^0 \to K^-\pi^+$	0	0	$\frac{1}{2}$	1	$\frac{1}{2}$
1	$D^0 \to \pi^- K^+$	0	0	$-\frac{\lambda^2}{2}$	$-\lambda^2$	$-\frac{\lambda^2}{2}$
0	$D^0 \to K^- K^+$	0	$\frac{\lambda^5 A^2}{4}$	$\frac{\lambda}{2}$	λ	$\frac{\lambda}{2}$
0	$D^0 \to 2\eta_8$	$-\frac{\lambda^5 A^2}{6}$	$\frac{\lambda^5 A^2}{4}$	$\frac{\lambda}{2}$	λ	$-\frac{\lambda}{2}$
1	$D^0 \to K^0\eta_8$	0	0	$\frac{\lambda^2}{2\sqrt{6}}$	$\frac{\lambda^2}{\sqrt{6}}$	$-\frac{\lambda^2}{2\sqrt{6}}$
-1	$D^0 \to \eta_8 \bar{K}^0$	0	0	$-\frac{1}{2\sqrt{6}}$	$-\frac{1}{\sqrt{6}}$	$\frac{1}{2\sqrt{6}}$
0	$D^0 \to K^0\bar{K}^0$	$-\frac{\lambda^5 A^2}{4}$	$\frac{\lambda^5 A^2}{4}$	0	0	0
0	$D^0 \to 2\pi_0$	0	$\frac{\lambda^5 A^2}{4}$	$-\frac{\lambda}{2}$	$-\lambda$	$\frac{\lambda}{2}$
0	$D^0 \to \pi_0\eta_8$	$\frac{\lambda^5 A^2}{4\sqrt{3}}$	0	$\frac{\lambda}{2\sqrt{3}}$	$\frac{\lambda}{\sqrt{3}}$	$-\frac{\lambda}{2\sqrt{3}}$
1	$D^0 \to K^0\pi_0$	0	0	$\frac{\lambda^2}{2\sqrt{2}}$	$\frac{\lambda^2}{\sqrt{2}}$	$-\frac{\lambda^2}{2\sqrt{2}}$
-1	$D^0 \to \pi_0\bar{K}^0$	0	0	$-\frac{1}{2\sqrt{2}}$	$-\frac{1}{\sqrt{2}}$	$\frac{1}{2\sqrt{2}}$
0	$D^+ \to \pi_0\pi^+$	0	0	0	0	$\frac{\lambda}{\sqrt{2}}$
1	$D^+ \to \pi_0 K^+$	0	0	$\frac{\lambda^2}{2\sqrt{2}}$	$-\frac{\lambda^2}{\sqrt{2}}$	$\frac{\lambda^2}{2\sqrt{2}}$
0	$D_s^+ \to \pi_0 K^+$	$\frac{\lambda^5 A^2}{4\sqrt{2}}$	0	$-\frac{\lambda}{2\sqrt{2}}$	$\frac{\lambda}{\sqrt{2}}$	$\frac{\lambda}{2\sqrt{2}}$
0	$D^+ \to \eta_8\pi^+$	$\frac{\lambda^5 A^2}{2\sqrt{6}}$	0	$\frac{\lambda}{\sqrt{6}}$	$-\sqrt{\frac{2}{3}}\lambda$	$-\sqrt{\frac{2}{3}}\lambda$
-1	$D_s^+ \to \eta_8\pi^+$	0	0	$-\frac{1}{\sqrt{6}}$	$\sqrt{\frac{2}{3}}$	$-\frac{1}{\sqrt{6}}$
1	$D^+ \to K^0\pi^+$	0	0	$\frac{\lambda^2}{2}$	$-\lambda^2$	$-\frac{\lambda^2}{2}$
0	$D_s^+ \to K^0\pi^+$	$\frac{\lambda^5 A^2}{4}$	0	$-\frac{\lambda}{2}$	λ	$-\frac{\lambda}{2}$
-1	$D^+ \to \bar{K}^0\pi^+$	0	0	0	0	1
1	$D^+ \to \eta_8 K^+$	0	0	$-\frac{\lambda^2}{2\sqrt{6}}$	$\frac{\lambda^2}{\sqrt{6}}$	$-\frac{\lambda^2}{2\sqrt{6}}$
0	$D_s^+ \to \eta_8 K^+$	$-\frac{\lambda^5 A^2}{4\sqrt{6}}$	0	$\frac{\lambda}{2\sqrt{6}}$	$-\frac{\lambda}{\sqrt{6}}$	$-\frac{5\lambda}{2\sqrt{6}}$
1	$D_s^+ \to K^0 K^+$	0	0	0	0	$-\lambda^2$
0	$D^+ \to \bar{K}^0 K^+$	$\frac{\lambda^5 A^2}{4}$	0	$\frac{\lambda}{2}$	$-\lambda$	$\frac{\lambda}{2}$
-1	$D_s^+ \to \bar{K}^0 K^+$	0	0	$-\frac{1}{2}$	1	$\frac{1}{2}$

Table D.2: $D \to P_8 P_8$ $\mathcal{O}(1)$ invariants. A^2 is shorthand for $A^2(\rho - i\eta)$.

D.2.2 Spurionic $\mathcal{O}(\varepsilon)$ Invariants

The invariants produced by Hm_s are shown in the following Tables D.3, D.4, D.5 and D.6. In this case, the number of invariants increases dramatically, so that for the sake of brevity we do not list the explicit contractions corresponding to each invariant. Each invariant is labelled as in the previous section, but with an extra s subscript.

ΔU	$\times\ \boldsymbol{\varepsilon}$	$[^{\rm PP}_{11}]_{\bar{\mathbf{3}}s}$	$[^{\rm PP}_{11}]_{\mathbf{6}s}$	$[^{\rm PP}_{11}]_{\bar{\mathbf{15}}s}$
0	$D^0 \to 2\eta_1$	$\frac{\Delta}{4}$	-3λ	-3λ

ΔU	$\times\ \boldsymbol{\varepsilon\Delta}$	$[^{\rm PP}_{18}]^1_{\bar{\mathbf{3}}s}$	$[^{\rm PP}_{18}]^2_{\bar{\mathbf{3}}s}$	$[^{\rm PP}_{18}]^3_{\bar{\mathbf{3}}s}$
0	$D^0 \to \pi_0\eta_1$	$\frac{1}{4\sqrt{2}}$	$\frac{1}{8\sqrt{2}}$	$\frac{1}{8\sqrt{2}}$
0	$D^0 \to \eta_1\eta_8$	$-\frac{1}{2\sqrt{6}}$	$\frac{1}{8\sqrt{6}}$	$\frac{1}{8\sqrt{6}}$
0	$D^+ \to \eta_1\pi^+$	$\frac{1}{4}$	$\frac{1}{8}$	$\frac{1}{8}$
0	$D_s^+ \to \eta_1 K^+$	$-\frac{1}{8}$	$\frac{1}{8}$	$-\frac{1}{4}$

ΔU	$\times\ \boldsymbol{\varepsilon}$	$[^{\rm PP}_{18}]^1_{\mathbf{6}s}$	$[^{\rm PP}_{18}]^2_{\mathbf{6}s}$	$[^{\rm PP}_{18}]^3_{\mathbf{6}s}$	$[^{\rm PP}_{18}]^1_{\bar{\mathbf{15}}s}$	$[^{\rm PP}_{18}]^2_{\bar{\mathbf{15}}s}$	$[^{\rm PP}_{18}]^3_{\bar{\mathbf{15}}s}$	$[^{\rm PP}_{18}]^4_{\bar{\mathbf{15}}s}$
0	$D^0 \to \pi_0\eta_1$	$\frac{\lambda}{2\sqrt{2}}$	$-\frac{\lambda}{\sqrt{2}}$	$-\frac{\lambda}{2\sqrt{2}}$	$-\frac{3\lambda}{2\sqrt{2}}$	$-\frac{\lambda}{\sqrt{2}}$	$-\frac{3\lambda}{2\sqrt{2}}$	$\frac{\lambda}{2\sqrt{2}}$
0	$D^0 \to \eta_1\eta_8$	$\frac{\lambda}{2}\sqrt{\frac{3}{2}}$	0	$\frac{\lambda}{2}\sqrt{\frac{3}{2}}$	$\frac{\lambda}{2}\sqrt{\frac{3}{2}}$	$-\sqrt{\frac{3}{2}}\lambda$	$-\frac{\lambda}{2}\sqrt{\frac{3}{2}}$	$\frac{\lambda}{2}\sqrt{\frac{3}{2}}$
1	$D^0 \to K^0\eta_1$	λ^2	λ^2	$\frac{\lambda^2}{2}$	0	$-\frac{\lambda^2}{2}$	0	$-\frac{\lambda^2}{2}$
-1	$D^0 \to \eta_1\bar{K}^0$	$\frac{1}{2}$	$\frac{1}{2}$	$-\frac{1}{2}$	$-\frac{3}{2}$	$\frac{1}{2}$	0	-1
0	$D^+ \to \eta_1\pi^+$	$\frac{\lambda}{2}$	$-\lambda$	$-\frac{\lambda}{2}$	$-\frac{3\lambda}{2}$	λ	$-\frac{3\lambda}{2}$	$-\frac{\lambda}{2}$
-1	$D_s^+ \to \eta_1\pi^+$	$-\frac{1}{2}$	$-\frac{1}{2}$	-1	$\frac{3}{2}$	-1	0	$\frac{1}{2}$
1	$D^+ \to \eta_1 K^+$	$-\lambda^2$	$-\lambda^2$	$-\frac{\lambda^2}{2}$	0	$-\frac{\lambda^2}{2}$	0	$-\frac{\lambda^2}{2}$
0	$D_s^+ \to \eta_1 K^+$	λ	$-\frac{\lambda}{2}$	$-\lambda$	0	$\frac{\lambda}{2}$	$-\frac{3\lambda}{2}$	$\frac{\lambda}{2}$

Table D.3: $D \to P_1P_1$ and $D \to P_1P_8$ invariants at first order in spurion. $\Delta = \lambda^5A^2(\rho - i\eta)$.

ΔU	$\times\ \varepsilon\boldsymbol{\Delta}$	$[^{\rm pp}_{88}]^1_{\bar{\mathbf{3}}s}$	$[^{\rm pp}_{88}]^2_{\bar{\mathbf{3}}s}$	$[^{\rm pp}_{88}]^3_{\bar{\mathbf{3}}s}$	$[^{\rm pp}_{88}]^4_{\bar{\mathbf{3}}s}$	$[^{\rm pp}_{88}]^5_{\bar{\mathbf{3}}s}$
0	$D^0 \to \pi^-\pi^+$	0	0	$\frac{1}{2}$	$\frac{1}{4}$	0
0	$D^0 \to K^-K^+$	0	0	$-\frac{1}{4}$	$\frac{1}{4}$	0
0	$D^0 \to 2\pi_0$	0	0	$\frac{1}{2}$	$\frac{1}{4}$	0
0	$D^0 \to \pi_0\eta_8$	$\frac{1}{4\sqrt{3}}$	$\frac{1}{4\sqrt{3}}$	0	0	$\frac{\sqrt{3}}{8}$
0	$D^0 \to 2\eta_8$	$-\frac{1}{6}$	$-\frac{1}{6}$	$-\frac{1}{2}$	$\frac{1}{4}$	$\frac{1}{4}$
0	$D^0 \to K^0\bar{K}^0$	$-\frac{1}{4}$	$-\frac{1}{4}$	$-\frac{1}{4}$	$\frac{1}{4}$	0
0	$D_s^+ \to \pi_0 K^+$	$\frac{1}{4\sqrt{2}}$	$-\frac{1}{2\sqrt{2}}$	0	0	0
0	$D^+ \to \eta_8\pi^+$	$\frac{1}{2\sqrt{6}}$	$\frac{1}{2\sqrt{6}}$	0	0	$\frac{\sqrt{\frac{3}{2}}}{4}$
0	$D_s^+ \to K^0\pi^+$	$\frac{1}{4}$	$-\frac{1}{2}$	0	0	0
0	$D_s^+ \to \eta_8 K^+$	$-\frac{1}{4\sqrt{6}}$	$\frac{1}{2\sqrt{6}}$	0	0	$\frac{\sqrt{\frac{3}{2}}}{4}$
0	$D^+ \to \bar{K}^0K^+$	$\frac{1}{4}$	$\frac{1}{4}$	0	0	0

Table D.4: $D \to P_8P_8$ invariants at first order in spurion, generated by $\bar{\mathbf{3}}$. $\Delta = \lambda^5A^2(\rho - i\eta)$.

ΔU	$\times\ \varepsilon$	$\left[{}^{\rm pp}_{88}\right]^1_{\mathbf{6}s}$	$\left[{}^{\rm pp}_{88}\right]^2_{\mathbf{6}s}$	$\left[{}^{\rm pp}_{88}\right]^3_{\mathbf{6}s}$	$\left[{}^{\rm pp}_{88}\right]^4_{\mathbf{6}s}$	$\left[{}^{\rm pp}_{88}\right]^5_{\mathbf{6}s}$	$\left[{}^{\rm pp}_{88}\right]^6_{\mathbf{6}s}$
0	$D^0 \to \pi^-\pi^+$	2λ	0	$-\frac{\lambda}{2}$	$-\lambda$	0	0
-1	$D^0 \to K^-\pi^+$	-2	0	$\frac{1}{2}$	$-\frac{1}{2}$	0	0
1	$D^0 \to \pi^-K^+$	$-\lambda^2$	0	λ^2	$-\lambda^2$	0	0
0	$D^0 \to K^-K^+$	λ	0	$-\lambda$	$-\frac{\lambda}{2}$	0	0
0	$D^0 \to 2\pi_0$	2λ	0	$-\frac{\lambda}{2}$	$-\lambda$	0	0
0	$D^0 \to \pi_0\eta_8$	$\frac{\lambda}{\sqrt{3}}$	$-\frac{\sqrt{3}\lambda}{2}$	$-\frac{\lambda}{\sqrt{3}}$	$-\frac{\lambda}{2\sqrt{3}}$	$\frac{\sqrt{3}\lambda}{2}$	$\frac{\sqrt{3}\lambda}{2}$
1	$D^0 \to K^0\pi_0$	$\frac{\lambda^2}{\sqrt{2}}$	0	$-\frac{\lambda^2}{\sqrt{2}}$	$\frac{\lambda^2}{\sqrt{2}}$	0	0
-1	$D^0 \to \pi_0\bar{K}^0$	$\sqrt{2}$	0	$-\frac{1}{2\sqrt{2}}$	$\frac{1}{2\sqrt{2}}$	0	$-\frac{3}{2\sqrt{2}}$
0	$D^0 \to 2\eta_8$	0	λ	$-\frac{\lambda}{2}$	0	-3λ	$-\lambda$
1	$D^0 \to K^0\eta_8$	$\frac{\lambda^2}{\sqrt{6}}$	0	$-\frac{\lambda^2}{\sqrt{6}}$	$\frac{\lambda^2}{\sqrt{6}}$	$-\sqrt{\frac{3}{2}}\lambda^2$	$-\sqrt{\frac{3}{2}}\lambda^2$
-1	$D^0 \to \eta_8\bar{K}^0$	$\sqrt{\frac{2}{3}}$	0	$-\frac{1}{2\sqrt{6}}$	$\frac{1}{2\sqrt{6}}$	$\sqrt{\frac{3}{2}}$	$\sqrt{\frac{3}{8}}$
0	$D^0 \to K^0\bar{K}^0$	0	$\frac{3\lambda}{2}$	0	0	0	$\frac{3\lambda}{2}$
1	$D^+ \to \pi_0K^+$	$\frac{\lambda^2}{\sqrt{2}}$	0	$-\frac{\lambda^2}{\sqrt{2}}$	$\frac{\lambda^2}{\sqrt{2}}$	0	0
0	$D_s^+ \to \pi_0K^+$	$-\frac{\lambda}{\sqrt{2}}$	$-\frac{3\lambda}{2\sqrt{2}}$	$-\frac{\lambda}{2\sqrt{2}}$	$-\frac{\lambda}{\sqrt{2}}$	0	0
0	$D^+ \to \eta_8\pi^+$	$\sqrt{\frac{2}{3}}\lambda$	$-\sqrt{\frac{3}{2}}\lambda$	$-\sqrt{\frac{2}{3}}\lambda$	$-\frac{\lambda}{\sqrt{6}}$	$\sqrt{\frac{3}{2}}\lambda$	$\sqrt{\frac{3}{2}}\lambda$
-1	$D_s^+ \to \eta_8\pi^+$	$-\sqrt{\frac{2}{3}}$	0	$-\frac{1}{\sqrt{6}}$	$\frac{1}{\sqrt{6}}$	$-\sqrt{\frac{3}{2}}$	0
1	$D^+ \to K^0\pi^+$	λ^2	0	$-\lambda^2$	λ^2	0	0
0	$D_s^+ \to K^0\pi^+$	$-\lambda$	$-\frac{3\lambda}{2}$	$-\frac{\lambda}{2}$	$-\lambda$	0	0
-1	$D^+ \to \bar{K}^0\pi^+$	0	0	0	0	0	$-\frac{3}{2}$
1	$D^+ \to \eta_8K^+$	$-\frac{\lambda^2}{\sqrt{6}}$	0	$\frac{\lambda^2}{\sqrt{6}}$	$-\frac{\lambda^2}{\sqrt{6}}$	$\sqrt{\frac{3}{2}}\lambda^2$	$\sqrt{\frac{3}{2}}\lambda^2$
0	$D_s^+ \to \eta_8K^+$	$\frac{\lambda}{\sqrt{6}}$	$\frac{\lambda}{2}\sqrt{\frac{3}{2}}$	$\frac{\lambda}{2\sqrt{6}}$	$\frac{\lambda}{\sqrt{6}}$	$-\sqrt{\frac{3}{2}}\lambda$	0
0	$D^+ \to \bar{K}^0K^+$	λ	$-\frac{3\lambda}{2}$	$-\lambda$	$-\frac{\lambda}{2}$	0	$-\frac{3\lambda}{2}$
-1	$D_s^+ \to \bar{K}^0K^+$	-1	0	$-\frac{1}{2}$	$\frac{1}{2}$	0	0

Table D.5: $D \to P_8P_8$ invariants at first order in spurion, generated by **6**.

ΔU	$\times\ \varepsilon$	$[^{pp}_{88}]^1_{\bar{\mathbf{15}}s}$	$[^{pp}_{88}]^2_{\bar{\mathbf{15}}s}$	$[^{pp}_{88}]^3_{\bar{\mathbf{15}}s}$	$[^{pp}_{88}]^4_{\bar{\mathbf{15}}s}$	$[^{pp}_{88}]^5_{\bar{\mathbf{15}}s}$	$[^{pp}_{88}]^6_{\bar{\mathbf{15}}s}$	$[^{pp}_{88}]^7_{\bar{\mathbf{15}}s}$	$[^{pp}_{88}]^8_{\bar{\mathbf{15}}s}$	$[^{pp}_{88}]^9_{\bar{\mathbf{15}}s}$
0	$D^0 \to \pi^-\pi^+$	0	2λ	$-\lambda$	2λ	$-\frac{\lambda}{2}$	λ	-3λ	$-\frac{\lambda}{2}$	$-\frac{\lambda}{2}$
-1	$D^0 \to K^-\pi^+$	0	-2	1	1	$\frac{1}{2}$	$\frac{1}{2}$	0	-1	$\frac{1}{2}$
1	$D^0 \to \pi^-K^+$	0	$-\lambda^2$	$-\lambda^2$	$2\lambda^2$	λ^2	λ^2	0	$-\frac{\lambda^2}{2}$	$-\frac{\lambda^2}{2}$
0	$D^0 \to K^-K^+$	0	λ	λ	λ	$-\lambda$	$\frac{\lambda}{2}$	-3λ	$-\lambda$	$\frac{\lambda}{2}$
0	$D^0 \to 2\eta_8$	2λ	0	λ	0	$-\frac{\lambda}{2}$	-2λ	-3λ	$-\frac{\lambda}{2}$	$-\frac{3\lambda}{2}$
1	$D^0 \to K^0\eta_8$	0	$\frac{\lambda^2}{\sqrt{6}}$	$\frac{\lambda^2}{\sqrt{6}}$	$-\sqrt{\frac{2}{3}}\lambda^2$	$-\frac{\lambda^2}{\sqrt{6}}$	$-\sqrt{\frac{2}{3}}\lambda^2$	0	$-\frac{\lambda^2}{2\sqrt{6}}$	$-\frac{5\lambda^2}{2\sqrt{6}}$
-1	$D^0 \to \eta_8\bar{K}^0$	0	$\sqrt{\frac{2}{3}}$	$-\frac{1}{\sqrt{6}}$	$-\frac{1}{\sqrt{6}}$	$\frac{5}{2\sqrt{6}}$	$\sqrt{\frac{2}{3}}$	0	$\frac{1}{2\sqrt{6}}$	$\frac{5}{2\sqrt{6}}$
0	$D^0 \to K^0\bar{K}^0$	3λ	0	0	0	$\frac{3\lambda}{2}$	0	-3λ	0	$\frac{3\lambda}{2}$
0	$D^0 \to 2\pi_0$	0	2λ	$-\lambda$	2λ	$-\frac{\lambda}{2}$	$-\lambda$	-3λ	$\frac{\lambda}{2}$	$-\frac{\lambda}{2}$
0	$D^0 \to \pi_0\eta_8$	$-\sqrt{3}\lambda$	$\frac{\lambda}{\sqrt{3}}$	$\frac{\lambda}{\sqrt{3}}$	$\frac{\lambda}{\sqrt{3}}$	$\frac{2\lambda}{\sqrt{3}}$	$\frac{5\lambda}{2\sqrt{3}}$	0	$-\frac{\lambda}{2\sqrt{3}}$	$\frac{\lambda}{2\sqrt{3}}$
1	$D^0 \to K^0\pi_0$	0	$\frac{\lambda^2}{\sqrt{2}}$	$\frac{\lambda^2}{\sqrt{2}}$	$-\sqrt{2}\lambda^2$	$\sqrt{2}\lambda^2$	$\frac{\lambda^2}{\sqrt{2}}$	0	$-\frac{\lambda^2}{2\sqrt{2}}$	$\frac{\lambda^2}{2\sqrt{2}}$
-1	$D^0 \to \pi_0\bar{K}^0$	0	$\sqrt{2}$	$-\frac{1}{\sqrt{2}}$	$-\frac{1}{\sqrt{2}}$	$-\frac{1}{2\sqrt{2}}$	$-\frac{1}{\sqrt{2}}$	0	$\frac{1}{2\sqrt{2}}$	$-\frac{1}{2\sqrt{2}}$
0	$D^+ \to \pi_0\pi^+$	0	0	0	0	0	$-\sqrt{2}\lambda$	0	$\frac{\lambda}{\sqrt{2}}$	0
1	$D^+ \to \pi_0K^+$	0	$-\frac{\lambda^2}{\sqrt{2}}$	$-\frac{\lambda^2}{\sqrt{2}}$	$\sqrt{2}\lambda^2$	$-\sqrt{2}\lambda^2$	$-\frac{\lambda^2}{\sqrt{2}}$	0	$\frac{\lambda^2}{2\sqrt{2}}$	$-\frac{\lambda^2}{2\sqrt{2}}$
0	$D_s^+ \to \pi_0K^+$	$-\frac{3\lambda}{\sqrt{2}}$	$\frac{\lambda}{\sqrt{2}}$	$-\sqrt{2}\lambda$	$-\sqrt{2}\lambda$	$\sqrt{2}\lambda$	$\frac{\lambda}{2\sqrt{2}}$	0	$\frac{\lambda}{2\sqrt{2}}$	$\frac{\lambda}{2\sqrt{2}}$
0	$D^+ \to \eta_8\pi^+$	$-\sqrt{6}\lambda$	$-\sqrt{\frac{2}{3}}\lambda$	$-\sqrt{\frac{2}{3}}\lambda$	$-\sqrt{\frac{2}{3}}\lambda$	$\sqrt{\frac{2}{3}}\lambda$	$\frac{\lambda}{\sqrt{6}}$	0	$-\sqrt{\frac{2}{3}}\lambda$	$-\frac{\lambda}{\sqrt{6}}$
-1	$D_s^+ \to \eta_8\pi^+$	0	$\sqrt{\frac{2}{3}}$	$-2\sqrt{\frac{2}{3}}$	$\sqrt{\frac{2}{3}}$	$-\sqrt{\frac{2}{3}}$	$-\frac{1}{\sqrt{6}}$	0	$\sqrt{\frac{2}{3}}$	$\frac{1}{\sqrt{6}}$
1	$D^+ \to K^0\pi^+$	0	$-\lambda^2$	$-\lambda^2$	$2\lambda^2$	λ^2	λ^2	0	$-\frac{\lambda^2}{2}$	$-\frac{\lambda^2}{2}$
0	$D_s^+ \to K^0\pi^+$	-3λ	λ	-2λ	-2λ	$-\lambda$	$-\frac{\lambda}{2}$	0	$-\frac{\lambda}{2}$	$\frac{\lambda}{2}$
-1	$D^+ \to \bar{K}^0\pi^+$	0	0	0	0	0	$-\frac{1}{2}$	0	$-\frac{1}{2}$	0
1	$D^+ \to \eta_8K^+$	0	$\frac{\lambda^2}{\sqrt{6}}$	$\frac{\lambda^2}{\sqrt{6}}$	$-\sqrt{\frac{2}{3}}\lambda^2$	$-\frac{\lambda^2}{\sqrt{6}}$	$-\sqrt{\frac{2}{3}}\lambda^2$	0	$-\frac{\lambda^2}{2\sqrt{6}}$	$-\frac{5\lambda^2}{2\sqrt{6}}$
0	$D_s^+ \to \eta_8K^+$	$\sqrt{\frac{3}{2}}\lambda$	$-\frac{\lambda}{\sqrt{6}}$	$\sqrt{\frac{2}{3}}\lambda$	$\sqrt{\frac{2}{3}}\lambda$	$\frac{\lambda}{\sqrt{6}}$	$-\frac{5\lambda}{2\sqrt{6}}$	0	$\frac{\lambda}{2\sqrt{6}}$	$\frac{5\lambda}{2\sqrt{6}}$
1	$D_s^+ \to K^0K^+$	0	0	0	0	0	$-\lambda^2$	0	$-\lambda^2$	0
0	$D^+ \to \bar{K}^0K^+$	-3λ	$-\lambda$	$-\lambda$	$-\lambda$	$-\frac{\lambda}{2}$	$\frac{\lambda}{2}$	0	$-\lambda$	λ
-1	$D_s^+ \to \bar{K}^0K^+$	0	1	-2	1	$\frac{1}{2}$	$\frac{1}{2}$	0	$\frac{1}{2}$	-1

Table D.6: $D \to P_8P_8$ invariants at first order in spurion, generated by $\bar{\mathbf{15}}$.

D.3 $D \to PV$ Invariants

D.3.1 $\mathcal{O}(1)$ Invariants

In the PV case, there are significantly more invariants for each irrep, since the invariants that are antisymmetric in the out-states are no longer zero. There are similarly twice as many amplitudes, simply because there are two ways to replace a P with a V in each. The $\mathcal{O}(1)$ – i.e. zeroth order in the m_s or m_I spurion – invariants are shown in Tables D.7, D.8 and D.9 below, for the P_1V_1, P_1V_8, V_1P_8 and P_8V_8 amplitudes. Similarly to Appendix D.2, each invariant is labelled by $[{}^{\text{pv}}_{xy}]^k_R$ as in eq. (D.17), where x, y=1, 8 labels the P and V representation respectively, R is the H representation as appropriate, and k indicates the kth such invariant.

ΔU	Ampl.	$[{}^{\text{pv}}_{11}]_{\bar{\mathbf{3}}}$	$[{}^{\text{pv}}_{18}]_{\bar{\mathbf{3}}}$	$[{}^{\text{pv}}_{18}]_{\mathbf{6}}$	$[{}^{\text{pv}}_{18}]_{\bar{\mathbf{15}}}$	$[{}^{\text{pv}}_{81}]_{\bar{\mathbf{3}}}$	$[{}^{\text{pv}}_{81}]_{\mathbf{6}}$	$[{}^{\text{pv}}_{81}]_{\bar{\mathbf{15}}}$
0	$D^0 \to \eta_1\phi_1$	$\frac{\Delta}{8}$	0	0	0	0	0	0
0	$D^0 \to \eta_1\omega_8$	0	$\frac{\Delta}{8\sqrt{6}}$	$-\frac{\lambda}{2}\sqrt{\frac{3}{2}}$	$-\frac{\lambda}{2}\sqrt{\frac{3}{2}}$	0	0	0
0	$D^0 \to \eta_1\rho_0$	0	$\frac{\Delta}{8\sqrt{2}}$	$\frac{\lambda}{2\sqrt{2}}$	$\frac{\lambda}{2\sqrt{2}}$	0	0	0
1	$D^0 \to \eta_1 K^{*0}$	0	0	$-\frac{\lambda^2}{2}$	$-\frac{\lambda^2}{2}$	0	0	0
−1	$D^0 \to \eta_1 \bar{K}^{*0}$	0	0	$\frac{1}{2}$	$\frac{1}{2}$	0	0	0
0	$D^0 \to \eta_8\phi_1$	0	0	0	0	$\frac{\Delta}{8\sqrt{6}}$	$-\frac{\lambda}{2}\sqrt{\frac{3}{2}}$	$-\frac{\lambda}{2}\sqrt{\frac{3}{2}}$
1	$D^0 \to K^0\phi_1$	0	0	0	0	0	$-\frac{\lambda^2}{2}$	$-\frac{\lambda^2}{2}$
0	$D^0 \to \pi_0\phi_1$	0	0	0	0	$\frac{\Delta}{8\sqrt{2}}$	$\frac{\lambda}{2\sqrt{2}}$	$\frac{\lambda}{2\sqrt{2}}$
−1	$D^0 \to \phi_1 \bar{K}^0$	0	0	0	0	0	$\frac{1}{2}$	$\frac{1}{2}$
0	$D^+ \to \eta_1\rho^+$	0	$\frac{\Delta}{8}$	$\frac{\lambda}{2}$	$-\frac{\lambda}{2}$	0	0	0
1	$D^+ \to \eta_1 K^{*+}$	0	0	$\frac{\lambda^2}{2}$	$-\frac{\lambda^2}{2}$	0	0	0
1	$D^+ \to \phi_1 K^+$	0	0	0	0	0	$\frac{\lambda^2}{2}$	$-\frac{\lambda^2}{2}$
0	$D^+ \to \phi_1\pi^+$	0	0	0	0	$\frac{\Delta}{8}$	$\frac{\lambda}{2}$	$-\frac{\lambda}{2}$
−1	$D_s^+ \to \eta_1\rho^+$	0	0	$-\frac{1}{2}$	$\frac{1}{2}$	0	0	0
0	$D_s^+ \to \eta_1 K^{*+}$	0	$\frac{\Delta}{8}$	$-\frac{\lambda}{2}$	$\frac{\lambda}{2}$	0	0	0
0	$D_s^+ \to \phi_1 K^+$	0	0	0	0	$\frac{\Delta}{8}$	$-\frac{\lambda}{2}$	$\frac{\lambda}{2}$
−1	$D_s^+ \to \phi_1\pi^+$	0	0	0	0	0	$-\frac{1}{2}$	$\frac{1}{2}$

Table D.7: $D \to P_1V_1$, $D \to P_1V_8$ and $D \to V_1P_8$ $\mathcal{O}(1)$ invariants. $\Delta = \lambda^5 A^2(\rho - i\eta)$.

ΔU	Ampl.	$[\mathrm{pv}]^1_{\bar{\mathbf{3}}}$	$[\mathrm{pv}]^2_{\bar{\mathbf{3}}}$	$[\mathrm{pv}]^3_{\bar{\mathbf{3}}}$	$[\mathrm{pv}]^1_{\mathbf{6}}$	$[\mathrm{pv}]^2_{\mathbf{6}}$	$[\mathrm{pv}]^3_{\mathbf{6}}$	$[\mathrm{pv}]^1_{\overline{\mathbf{15}}}$	$[\mathrm{pv}]^2_{\overline{\mathbf{15}}}$	$[\mathrm{pv}]^3_{\overline{\mathbf{15}}}$	$[\mathrm{pv}]^4_{\overline{\mathbf{15}}}$
0	$D^0 \to \eta_8\omega_8$	$-\frac{\Delta}{12}$	$\frac{\Delta}{8}$	$\frac{\Delta}{48}$	0	$\frac{\lambda}{4}$	$-\frac{\lambda}{4}$	$\frac{\lambda}{2}$	$\frac{\lambda}{4}$	$\frac{\lambda}{4}$	$-\frac{\lambda}{4}$
0	$D^0 \to \eta_8\rho_0$	$\frac{\Delta}{8\sqrt{3}}$	0	$\frac{\Delta}{16\sqrt{3}}$	$-\frac{\lambda}{2\sqrt{3}}$	$-\frac{\lambda}{4\sqrt{3}}$	$-\frac{\sqrt{3}\lambda}{4}$	$\frac{\lambda}{2\sqrt{3}}$	$\frac{5\lambda}{4\sqrt{3}}$	$\frac{\lambda}{4\sqrt{3}}$	$\frac{\lambda}{4\sqrt{3}}$
1	$D^0 \to \eta_8 K^{*0}$	0	0	0	$\frac{\lambda^2}{\sqrt{6}}$	$\frac{\lambda^2}{2\sqrt{6}}$	0	$\frac{\lambda^2}{2\sqrt{6}}$	$\frac{\lambda^2}{2\sqrt{6}}$	$-\frac{\lambda^2}{2\sqrt{6}}$	$-\frac{\lambda^2}{2\sqrt{6}}$
-1	$D^0 \to \eta_8 \bar{K}^{*0}$	0	0	0	$\frac{1}{2\sqrt{6}}$	$-\frac{1}{2\sqrt{6}}$	0	$-\frac{1}{2\sqrt{6}}$	$\frac{1}{\sqrt{6}}$	$-\frac{1}{\sqrt{6}}$	$\frac{1}{2\sqrt{6}}$
1	$D^0 \to K^0\omega_8$	0	0	0	$-\frac{\lambda^2}{\sqrt{6}}$	0	$-\frac{\lambda^2}{2\sqrt{6}}$	$\frac{\lambda^2}{2\sqrt{6}}$	0	$\frac{\lambda^2}{\sqrt{6}}$	0
1	$D^0 \to K^0\rho_0$	0	0	0	0	0	$-\frac{\lambda^2}{2\sqrt{2}}$	$\frac{\lambda^2}{2\sqrt{2}}$	$\frac{\lambda^2}{\sqrt{2}}$	0	0
0	$D^0 \to K^0\bar{K}^{*0}$	$-\frac{\Delta}{8}$	$\frac{\Delta}{8}$	0	$\frac{\lambda}{2}$	0	0	0	$\frac{\lambda}{2}$	$-\frac{\lambda}{2}$	0
0	$D^0 \to \pi_0\omega_8$	$\frac{\Delta}{8\sqrt{3}}$	0	$\frac{\Delta}{16\sqrt{3}}$	$\frac{\lambda}{2\sqrt{3}}$	$\frac{\sqrt{3}\lambda}{4}$	$\frac{\lambda}{4\sqrt{3}}$	$\frac{\lambda}{2\sqrt{3}}$	$-\frac{\sqrt{3}\lambda}{4}$	$\frac{\lambda}{4\sqrt{3}}$	$-\frac{\sqrt{3}\lambda}{4}$
0	$D^0 \to \pi_0\rho_0$	0	$\frac{\Delta}{8}$	$\frac{\Delta}{16}$	0	$-\frac{\lambda}{4}$	$\frac{\lambda}{4}$	$-\frac{\lambda}{2}$	$-\frac{\lambda}{4}$	$-\frac{\lambda}{4}$	$\frac{\lambda}{4}$
1	$D^0 \to \pi_0 K^{*0}$	0	0	0	0	$\frac{\lambda^2}{2\sqrt{2}}$	0	$\frac{\lambda^2}{2\sqrt{2}}$	$-\frac{\lambda^2}{2\sqrt{2}}$	$\frac{\lambda^2}{2\sqrt{2}}$	$-\frac{\lambda^2}{2\sqrt{2}}$
-1	$D^0 \to \pi_0 \bar{K}^{*0}$	0	0	0	$-\frac{1}{2\sqrt{2}}$	$-\frac{1}{2\sqrt{2}}$	0	$-\frac{1}{2\sqrt{2}}$	0	0	$\frac{1}{2\sqrt{2}}$
-1	$D^0 \to \omega_8 \bar{K}^0$	0	0	0	$-\frac{1}{2\sqrt{6}}$	0	$\frac{1}{2\sqrt{6}}$	$-\frac{1}{2\sqrt{6}}$	$-\sqrt{\frac{3}{8}}$	$\frac{1}{2\sqrt{6}}$	0
-1	$D^0 \to \rho_0 \bar{K}^0$	0	0	0	$\frac{1}{2\sqrt{2}}$	0	$\frac{1}{2\sqrt{2}}$	$-\frac{1}{2\sqrt{2}}$	$-\frac{1}{2\sqrt{2}}$	$-\frac{1}{2\sqrt{2}}$	0
0	$D^0 \to \bar{K}^0 K^{*0}$	$-\frac{\Delta}{8}$	$\frac{\Delta}{8}$	0	$-\frac{\lambda}{2}$	0	0	0	$-\frac{\lambda}{2}$	$\frac{\lambda}{2}$	0
-1	$D^0 \to K^-\rho^+$	0	0	0	0	$\frac{1}{2}$	0	$\frac{1}{2}$	$\frac{1}{2}$	$\frac{1}{2}$	$\frac{1}{2}$
0	$D^0 \to K^- K^{*+}$	0	$\frac{\Delta}{8}$	0	0	$\frac{\lambda}{2}$	0	$\frac{\lambda}{2}$	$\frac{\lambda}{2}$	$\frac{\lambda}{2}$	$\frac{\lambda}{2}$
0	$D^0 \to \pi^-\rho^+$	0	$\frac{\Delta}{8}$	0	0	$-\frac{\lambda}{2}$	0	$-\frac{\lambda}{2}$	$-\frac{\lambda}{2}$	$-\frac{\lambda}{2}$	$-\frac{\lambda}{2}$
1	$D^0 \to \pi^- K^{*+}$	0	0	0	0	$-\frac{\lambda^2}{2}$	0	$-\frac{\lambda^2}{2}$	$-\frac{\lambda^2}{2}$	$-\frac{\lambda^2}{2}$	$-\frac{\lambda^2}{2}$
1	$D^0 \to \rho^- K^+$	0	0	0	0	0	$\frac{\lambda^2}{2}$	$-\frac{\lambda^2}{2}$	0	0	0
0	$D^0 \to K^{*-} K^+$	0	$\frac{\Delta}{8}$	$\frac{\Delta}{8}$	0	0	$-\frac{\lambda}{2}$	$\frac{\lambda}{2}$	0	0	0
0	$D^0 \to \rho^-\pi^+$	0	$\frac{\Delta}{8}$	$\frac{\Delta}{8}$	0	0	$\frac{\lambda}{2}$	$-\frac{\lambda}{2}$	0	0	0
-1	$D^0 \to K^{*-}\pi^+$	0	0	0	0	0	$-\frac{1}{2}$	$\frac{1}{2}$	0	0	0

Table D.8: $D^0 \to P_8 V_8$ $\mathcal{O}(1)$ invariants. $\Delta = \lambda^5 A^2(\rho - i\eta)$.

ΔU	Ampl.	$[{}^{\rm pv}_{88}]^1_{\bar{\mathbf{3}}}$	$[{}^{\rm pv}_{88}]^2_{\bar{\mathbf{3}}}$	$[{}^{\rm pv}_{88}]^3_{\bar{\mathbf{3}}}$	$[{}^{\rm pv}_{88}]^1_{\mathbf{6}}$	$[{}^{\rm pv}_{88}]^2_{\mathbf{6}}$	$[{}^{\rm pv}_{88}]^3_{\mathbf{6}}$	$[{}^{\rm pv}_{88}]^1_{\mathbf{15}}$	$[{}^{\rm pv}_{88}]^2_{\mathbf{15}}$	$[{}^{\rm pv}_{88}]^3_{\mathbf{15}}$	$[{}^{\rm pv}_{88}]^4_{\mathbf{15}}$
0	$D^+ \to \eta_8 \rho^+$	$\frac{\Delta}{4\sqrt{6}}$	0	$\frac{\Delta}{8\sqrt{6}}$	$-\frac{\lambda}{\sqrt{6}}$	$-\frac{\lambda}{2\sqrt{6}}$	$-\frac{\lambda}{2}\sqrt{\frac{3}{2}}$	$-\frac{\lambda}{\sqrt{6}}$	$\frac{\lambda}{2\sqrt{6}}$	$-\frac{\lambda}{2\sqrt{6}}$	$-\frac{\lambda}{2\sqrt{6}}$
1	$D^+ \to \eta_8 K^{*+}$	0	0	0	$-\frac{\lambda^2}{\sqrt{6}}$	$-\frac{\lambda^2}{2\sqrt{6}}$	0	$\frac{\lambda^2}{2\sqrt{6}}$	$\frac{\lambda^2}{2\sqrt{6}}$	$-\frac{\lambda^2}{2\sqrt{6}}$	$-\frac{\lambda^2}{2\sqrt{6}}$
1	$D^+ \to K^0 \rho^+$	0	0	0	0	0	$-\frac{\lambda^2}{2}$	$-\frac{\lambda^2}{2}$	0	0	0
0	$D^+ \to \pi_0 \rho^+$	0	0	$\frac{\Delta}{8\sqrt{2}}$	0	$\frac{\lambda}{2\sqrt{2}}$	$\frac{\lambda}{2\sqrt{2}}$	0	$\frac{\lambda}{2\sqrt{2}}$	$-\frac{\lambda}{2\sqrt{2}}$	$\frac{\lambda}{2\sqrt{2}}$
1	$D^+ \to \pi_0 K^{*+}$	0	0	0	0	$\frac{\lambda^2}{2\sqrt{2}}$	0	$-\frac{\lambda^2}{2\sqrt{2}}$	$\frac{\lambda^2}{2\sqrt{2}}$	$-\frac{\lambda^2}{2\sqrt{2}}$	$\frac{\lambda^2}{2\sqrt{2}}$
-1	$D^+ \to \bar{K}^0 \rho^+$	0	0	0	$\frac{1}{2}$	$\frac{1}{2}$	$\frac{1}{2}$	0	0	0	$\frac{1}{2}$
0	$D^+ \to \bar{K}^0 K^{*+}$	$\frac{\Delta}{8}$	0	0	$\frac{\lambda}{2}$	$\frac{\lambda}{2}$	0	$-\frac{\lambda}{2}$	0	0	$\frac{\lambda}{2}$
1	$D^+ \to \omega_8 K^+$	0	0	0	$\frac{\lambda^2}{\sqrt{6}}$	0	$\frac{\lambda^2}{2\sqrt{6}}$	$\frac{\lambda^2}{2\sqrt{6}}$	0	$\frac{\lambda^2}{\sqrt{6}}$	0
1	$D^+ \to \rho_0 K^+$	0	0	0	0	0	$-\frac{\lambda^2}{2\sqrt{2}}$	$-\frac{\lambda^2}{2\sqrt{2}}$	$-\frac{\lambda^2}{\sqrt{2}}$	0	0
0	$D^+ \to \bar{K}^{*0} K^+$	$\frac{\Delta}{8}$	0	$\frac{\Delta}{8}$	$-\frac{\lambda}{2}$	0	$-\frac{\lambda}{2}$	$-\frac{\lambda}{2}$	$-\frac{\lambda}{2}$	$-\frac{\lambda}{2}$	0
0	$D^+ \to \omega_8 \pi^+$	$\frac{\Delta}{4\sqrt{6}}$	0	$\frac{\Delta}{8\sqrt{6}}$	$\frac{\lambda}{\sqrt{6}}$	$\frac{\lambda}{2}\sqrt{\frac{3}{2}}$	$\frac{\lambda}{2\sqrt{6}}$	$-\frac{\lambda}{\sqrt{6}}$	$-\frac{\lambda}{2}\sqrt{\frac{3}{2}}$	$-\frac{\lambda}{2\sqrt{6}}$	$-\frac{\lambda}{2}\sqrt{\frac{3}{2}}$
0	$D^+ \to \rho_0 \pi^+$	0	0	$-\frac{\Delta}{8\sqrt{2}}$	0	$-\frac{\lambda}{2\sqrt{2}}$	$-\frac{\lambda}{2\sqrt{2}}$	0	$-\frac{\lambda}{2\sqrt{2}}$	$\frac{\lambda}{2\sqrt{2}}$	$\frac{\lambda}{2\sqrt{2}}$
1	$D^+ \to K^{*0} \pi^+$	0	0	0	0	$\frac{\lambda^2}{2}$	0	$-\frac{\lambda^2}{2}$	$-\frac{\lambda^2}{2}$	$-\frac{\lambda^2}{2}$	$-\frac{\lambda^2}{2}$
-1	$D^+ \to \bar{K}^{*0} \pi^+$	0	0	0	$-\frac{1}{2}$	$-\frac{1}{2}$	$-\frac{1}{2}$	0	0	0	$\frac{1}{2}$
-1	$D_s^+ \to \eta_8 \rho^+$	0	0	0	$-\frac{1}{2\sqrt{6}}$	$-\frac{1}{\sqrt{6}}$	0	$\frac{1}{\sqrt{6}}$	$-\frac{1}{2\sqrt{6}}$	$\frac{1}{2\sqrt{6}}$	$-\frac{1}{\sqrt{6}}$
0	$D_s^+ \to \eta_8 K^{*+}$	$-\frac{\Delta}{8\sqrt{6}}$	0	$\frac{\Delta}{8\sqrt{6}}$	$-\frac{\lambda}{2\sqrt{6}}$	$-\frac{\lambda}{\sqrt{6}}$	$-\frac{\lambda}{2}\sqrt{\frac{3}{2}}$	$-\frac{\lambda}{2\sqrt{6}}$	$-\frac{\lambda}{2\sqrt{6}}$	$\frac{\lambda}{2\sqrt{6}}$	$-\frac{\lambda}{\sqrt{6}}$
0	$D_s^+ \to K^0 \rho^+$	$\frac{\Delta}{8}$	0	0	$-\frac{\lambda}{2}$	$-\frac{\lambda}{2}$	0	$\frac{\lambda}{2}$	0	0	$-\frac{\lambda}{2}$
1	$D_s^+ \to K^0 K^{*+}$	0	0	0	$-\frac{\lambda^2}{2}$	$-\frac{\lambda^2}{2}$	$-\frac{\lambda^2}{2}$	0	0	0	$-\frac{\lambda^2}{2}$
-1	$D_s^+ \to \pi_0 \rho^+$	0	0	0	$\frac{1}{2\sqrt{2}}$	0	0	0	$-\frac{1}{2\sqrt{2}}$	$\frac{1}{2\sqrt{2}}$	0
0	$D_s^+ \to \pi_0 K^{*+}$	$\frac{\Delta}{8\sqrt{2}}$	0	$\frac{\Delta}{8\sqrt{2}}$	$\frac{\lambda}{2\sqrt{2}}$	0	$\frac{\lambda}{2\sqrt{2}}$	$\frac{\lambda}{2\sqrt{2}}$	$-\frac{\lambda}{2\sqrt{2}}$	$\frac{\lambda}{2\sqrt{2}}$	0
-1	$D_s^+ \to \bar{K}^0 K^{*+}$	0	0	0	0	0	$\frac{1}{2}$	$\frac{1}{2}$	0	0	0
0	$D_s^+ \to \omega_8 K^+$	$-\frac{\Delta}{8\sqrt{6}}$	0	$-\frac{\Delta}{4\sqrt{6}}$	$\frac{\lambda}{2\sqrt{6}}$	$\frac{\lambda}{2}\sqrt{\frac{3}{2}}$	$\frac{\lambda}{\sqrt{6}}$	$-\frac{\lambda}{2\sqrt{6}}$	0	$-\frac{\lambda}{\sqrt{6}}$	$-\frac{\lambda}{2}\sqrt{\frac{3}{2}}$
0	$D_s^+ \to \rho_0 K^+$	$\frac{\Delta}{8\sqrt{2}}$	0	0	$-\frac{\lambda}{2\sqrt{2}}$	$-\frac{\lambda}{2\sqrt{2}}$	0	$\frac{\lambda}{2\sqrt{2}}$	$\frac{\lambda}{\sqrt{2}}$	0	$\frac{\lambda}{2\sqrt{2}}$
1	$D_s^+ \to K^{*0} K^+$	0	0	0	$\frac{\lambda^2}{2}$	$\frac{\lambda^2}{2}$	$\frac{\lambda^2}{2}$	0	0	0	$-\frac{\lambda^2}{2}$
-1	$D_s^+ \to \bar{K}^{*0} K^+$	0	0	0	0	$-\frac{1}{2}$	0	$\frac{1}{2}$	$\frac{1}{2}$	$\frac{1}{2}$	$\frac{1}{2}$
-1	$D_s^+ \to \omega_8 \pi^+$	0	0	0	$\frac{1}{2\sqrt{6}}$	0	$\frac{1}{\sqrt{6}}$	$\frac{1}{\sqrt{6}}$	$\sqrt{\frac{3}{8}}$	$\frac{1}{2\sqrt{6}}$	0
-1	$D_s^+ \to \rho_0 \pi^+$	0	0	0	$-\frac{1}{2\sqrt{2}}$	0	0	0	$\frac{1}{2\sqrt{2}}$	$-\frac{1}{2\sqrt{2}}$	0
0	$D_s^+ \to K^{*0} \pi^+$	$\frac{\Delta}{8}$	0	$\frac{\Delta}{8}$	$\frac{\lambda}{2}$	0	$\frac{\lambda}{2}$	$\frac{\lambda}{2}$	$\frac{\lambda}{2}$	$\frac{\lambda}{2}$	0

Table D.9: $D^+ \to P_8 V_8$ and $D_s^+ \to P_8 V_8$ $\mathcal{O}(1)$ invariants. $\Delta = \lambda^5 A^2(\rho - i\eta)$.

D.3.2 Spurionic $\mathcal{O}(\varepsilon)$ Invariants

We finally present the invariants produced by Hm_s for $D \to PV$, shown in Tables D.10 to D.15 following. Each invariant is labelled as in the previous section, but with an extra s subscript.

ΔU	$\times\ \boldsymbol{\varepsilon}$	$\begin{bmatrix}\text{PV}\\11\end{bmatrix}_{\bar{\mathbf{3}}s}$	$\begin{bmatrix}\text{PV}\\11\end{bmatrix}_{\mathbf{6}s}$	$\begin{bmatrix}\text{PV}\\11\end{bmatrix}_{\bar{\mathbf{15}}s}$
0	$D^0 \to \phi_1\eta_1$	$\frac{\Delta}{8}$	$-\frac{3\lambda}{2}$	$-\frac{3\lambda}{2}$

ΔU	$\times\ \boldsymbol{\varepsilon}$	$\begin{bmatrix}\text{PV}\\18\end{bmatrix}^1_{\bar{\mathbf{3}}s}$	$\begin{bmatrix}\text{PV}\\18\end{bmatrix}^2_{\bar{\mathbf{3}}s}$	$\begin{bmatrix}\text{PV}\\18\end{bmatrix}^3_{\bar{\mathbf{3}}s}$	$\begin{bmatrix}\text{PV}\\18\end{bmatrix}^1_{\mathbf{6}s}$	$\begin{bmatrix}\text{PV}\\18\end{bmatrix}^2_{\mathbf{6}s}$	$\begin{bmatrix}\text{PV}\\18\end{bmatrix}^3_{\mathbf{6}s}$	$\begin{bmatrix}\text{PV}\\18\end{bmatrix}^1_{\bar{\mathbf{15}}s}$	$\begin{bmatrix}\text{PV}\\18\end{bmatrix}^2_{\bar{\mathbf{15}}s}$	$\begin{bmatrix}\text{PV}\\18\end{bmatrix}^3_{\bar{\mathbf{15}}s}$	$\begin{bmatrix}\text{PV}\\18\end{bmatrix}^4_{\bar{\mathbf{15}}s}$
0	$D^0 \to \eta_1\omega_8$	$-\frac{\Delta}{2\sqrt{6}}$	$\frac{\Delta}{8\sqrt{6}}$	$\frac{\Delta}{8\sqrt{6}}$	$\frac{\lambda}{2}\sqrt{\frac{3}{2}}$	0	$\frac{\lambda}{2}\sqrt{\frac{3}{2}}$	$\frac{\lambda}{2}\sqrt{\frac{3}{2}}$	$-\sqrt{\frac{3}{2}}\lambda$	$-\frac{\lambda}{2}\sqrt{\frac{3}{2}}$	$\frac{\lambda}{2}\sqrt{\frac{3}{2}}$
0	$D^0 \to \eta_1\rho_0$	$\frac{\Delta}{4\sqrt{2}}$	$\frac{\Delta}{8\sqrt{2}}$	$\frac{\Delta}{8\sqrt{2}}$	$\frac{\lambda}{2\sqrt{2}}$	$-\frac{\lambda}{\sqrt{2}}$	$-\frac{\lambda}{2\sqrt{2}}$	$-\frac{3\lambda}{2\sqrt{2}}$	$-\frac{\lambda}{\sqrt{2}}$	$-\frac{3\lambda}{2\sqrt{2}}$	$\frac{\lambda}{2\sqrt{2}}$
1	$D^0 \to \eta_1 K^{*0}$	0	0	0	λ^2	λ^2	$\frac{\lambda^2}{2}$	0	$-\frac{\lambda^2}{2}$	0	$-\frac{\lambda^2}{2}$
-1	$D^0 \to \eta_1 \bar{K}^{*0}$	0	0	0	$\frac{1}{2}$	$\frac{1}{2}$	$-\frac{1}{2}$	$-\frac{3}{2}$	$\frac{1}{2}$	0	-1
0	$D^+ \to \eta_1\rho^+$	$\frac{\Delta}{4}$	$\frac{\Delta}{8}$	$\frac{\Delta}{8}$	$\frac{\lambda}{2}$	$-\lambda$	$-\frac{\lambda}{2}$	$-\frac{3\lambda}{2}$	λ	$-\frac{3\lambda}{2}$	$-\frac{\lambda}{2}$
1	$D^+ \to \eta_1 K^{*+}$	0	0	0	$-\lambda^2$	$-\lambda^2$	$-\frac{\lambda^2}{2}$	0	$-\frac{\lambda^2}{2}$	0	$-\frac{\lambda^2}{2}$
-1	$D_s^+ \to \eta_1\rho^+$	0	0	0	$-\frac{1}{2}$	$-\frac{1}{2}$	-1	$\frac{3}{2}$	-1	0	$\frac{1}{2}$
0	$D_s^+ \to \eta_1 K^{*+}$	$-\frac{\Delta}{8}$	$\frac{\Delta}{8}$	$-\frac{\Delta}{4}$	λ	$-\frac{\lambda}{2}$	$-\lambda$	0	$\frac{\lambda}{2}$	$-\frac{3\lambda}{2}$	$\frac{\lambda}{2}$

ΔU	$\times\ \boldsymbol{\varepsilon}$	$\begin{bmatrix}\text{PV}\\81\end{bmatrix}^1_{\bar{\mathbf{3}}s}$	$\begin{bmatrix}\text{PV}\\81\end{bmatrix}^2_{\bar{\mathbf{3}}s}$	$\begin{bmatrix}\text{PV}\\81\end{bmatrix}^3_{\bar{\mathbf{3}}s}$	$\begin{bmatrix}\text{PV}\\81\end{bmatrix}^1_{\mathbf{6}s}$	$\begin{bmatrix}\text{PV}\\81\end{bmatrix}^2_{\mathbf{6}s}$	$\begin{bmatrix}\text{PV}\\81\end{bmatrix}^3_{\mathbf{6}s}$	$\begin{bmatrix}\text{PV}\\81\end{bmatrix}^1_{\bar{\mathbf{15}}s}$	$\begin{bmatrix}\text{PV}\\81\end{bmatrix}^2_{\bar{\mathbf{15}}s}$	$\begin{bmatrix}\text{PV}\\81\end{bmatrix}^3_{\bar{\mathbf{15}}s}$	$\begin{bmatrix}\text{PV}\\81\end{bmatrix}^4_{\bar{\mathbf{15}}s}$
0	$D^0 \to \eta_8\phi_1$	$-\frac{\Delta}{2\sqrt{6}}$	$\frac{\Delta}{8\sqrt{6}}$	$\frac{\Delta}{8\sqrt{6}}$	$\frac{\lambda}{2}\sqrt{\frac{3}{2}}$	0	$\frac{\lambda}{2}\sqrt{\frac{3}{2}}$	$\frac{\lambda}{2}\sqrt{\frac{3}{2}}$	$-\sqrt{\frac{3}{2}}\lambda$	$-\frac{\lambda}{2}\sqrt{\frac{3}{2}}$	$\frac{\lambda}{2}\sqrt{\frac{3}{2}}$
1	$D^0 \to K^0\phi_1$	0	0	0	λ^2	λ^2	$\frac{\lambda^2}{2}$	0	$-\frac{\lambda^2}{2}$	0	$-\frac{\lambda^2}{2}$
0	$D^0 \to \pi_0\phi_1$	$\frac{\Delta}{4\sqrt{2}}$	$\frac{\Delta}{8\sqrt{2}}$	$\frac{\Delta}{8\sqrt{2}}$	$\frac{\lambda}{2\sqrt{2}}$	$-\frac{\lambda}{\sqrt{2}}$	$-\frac{\lambda}{2\sqrt{2}}$	$-\frac{3\lambda}{2\sqrt{2}}$	$-\frac{\lambda}{\sqrt{2}}$	$-\frac{3\lambda}{2\sqrt{2}}$	$\frac{\lambda}{2\sqrt{2}}$
-1	$D^0 \to \phi_1\bar{K}^0$	0	0	0	$\frac{1}{2}$	$\frac{1}{2}$	$-\frac{1}{2}$	$-\frac{3}{2}$	$\frac{1}{2}$	0	-1
1	$D^+ \to \phi_1 K^+$	0	0	0	$-\lambda^2$	$-\lambda^2$	$-\frac{\lambda^2}{2}$	0	$-\frac{\lambda^2}{2}$	0	$-\frac{\lambda^2}{2}$
0	$D^+ \to \phi_1\pi^+$	$\frac{\Delta}{4}$	$\frac{\Delta}{8}$	$\frac{\Delta}{8}$	$\frac{\lambda}{2}$	$-\lambda$	$-\frac{\lambda}{2}$	$-\frac{3\lambda}{2}$	λ	$-\frac{3\lambda}{2}$	$-\frac{\lambda}{2}$
0	$D_s^+ \to \phi_1 K^+$	$-\frac{\Delta}{8}$	$\frac{\Delta}{8}$	$-\frac{\Delta}{4}$	λ	$-\frac{\lambda}{2}$	$-\lambda$	0	$\frac{\lambda}{2}$	$-\frac{3\lambda}{2}$	$\frac{\lambda}{2}$
-1	$D_s^+ \to \phi_1\pi^+$	0	0	0	$-\frac{1}{2}$	$-\frac{1}{2}$	-1	$\frac{3}{2}$	-1	0	$\frac{1}{2}$

Table D.10: $D \to P_1V_1$, $D \to P_1V_8$ and $D \to P_8V_1$ $\mathcal{O}(\varepsilon)$ invariants. $\Delta = \lambda^5 A^2(\rho - i\eta)$.

ΔU	$\times\varepsilon\Delta$	$[\mathbf{\bar{3}}]^1_{\mathbf{8}8}$	$[\mathbf{\bar{3}}]^2_{\mathbf{8}8}$	$[\mathbf{\bar{3}}]^3_{\mathbf{8}8}$	$[\mathbf{\bar{3}}]^4_{\mathbf{8}8}$	$[\mathbf{\bar{3}}]^5_{\mathbf{8}8}$	$[\mathbf{\bar{3}}]^6_{\mathbf{8}8}$	$[\mathbf{\bar{3}}]^7_{\mathbf{8}8}$	$[\mathbf{\bar{3}}]^8_{\mathbf{8}8}$	$[\mathbf{\bar{3}}]^9_{\mathbf{8}8}$	$[\mathbf{\bar{3}}]^{10}_{\mathbf{8}8}$
0	$D^0 \to \eta_8\omega_8$	$-\frac{1}{12}$	$-\frac{1}{24}$	$-\frac{1}{12}$	$-\frac{1}{4}$	$-\frac{1}{12}$	$-\frac{1}{24}$	$\frac{1}{8}$	$\frac{1}{48}$	$\frac{1}{48}$	$\frac{1}{8}$
0	$D^0 \to \eta_8\rho_0$	$\frac{1}{8\sqrt{3}}$	$-\frac{1}{8\sqrt{3}}$	$\frac{1}{8\sqrt{3}}$	0	$-\frac{1}{4\sqrt{3}}$	$-\frac{1}{8\sqrt{3}}$	0	$\frac{1}{16\sqrt{3}}$	$\frac{1}{16\sqrt{3}}$	0
0	$D^0 \to K^0\bar{K}^{*0}$	$-\frac{1}{8}$	$\frac{1}{8}$	$-\frac{1}{8}$	$-\frac{1}{8}$	0	$-\frac{1}{4}$	$\frac{1}{8}$	0	0	0
0	$D^0 \to \pi_0\omega_8$	$\frac{1}{8\sqrt{3}}$	$\frac{1}{4\sqrt{3}}$	$\frac{1}{8\sqrt{3}}$	0	$\frac{1}{8\sqrt{3}}$	$\frac{1}{4\sqrt{3}}$	0	$\frac{1}{16\sqrt{3}}$	$\frac{1}{16\sqrt{3}}$	$\frac{\sqrt{3}}{8}$
0	$D^0 \to \pi_0\rho_0$	0	0	0	$\frac{1}{4}$	0	0	$\frac{1}{8}$	0	0	0
0	$D^0 \to \bar{K}^0K^{*0}$	$-\frac{1}{8}$	$-\frac{1}{4}$	$-\frac{1}{8}$	$-\frac{1}{8}$	0	0	$\frac{1}{8}$	0	0	0
0	$D^0 \to K^-K^{*+}$	0	0	0	$-\frac{1}{8}$	0	0	$\frac{1}{8}$	0	0	0
0	$D^0 \to \pi^-\rho^+$	0	0	0	$\frac{1}{4}$	0	0	$\frac{1}{8}$	0	0	0
0	$D^0 \to K^{*-}K^+$	0	0	0	$-\frac{1}{8}$	$-\frac{1}{8}$	0	$\frac{1}{8}$	$\frac{1}{8}$	$\frac{1}{8}$	0
0	$D^0 \to \rho^-\pi^+$	0	0	0	$\frac{1}{4}$	$\frac{1}{4}$	0	$\frac{1}{8}$	0	0	0
0	$D^+ \to \eta_8\rho^+$	$\frac{1}{4\sqrt{6}}$	$-\frac{1}{4\sqrt{6}}$	$\frac{1}{4\sqrt{6}}$	0	$-\frac{2\sqrt{6}}{4}$	$-\frac{1}{4\sqrt{6}}$	0	$\frac{8\sqrt{6}}{48}$	$\frac{8\sqrt{6}}{48}$	0
0	$D^+ \to \pi_0\rho^+$	0	0	0	0	$\frac{1}{4\sqrt{2}}$	0	0	$\frac{8\sqrt{2}}{48}$	$\frac{8\sqrt{2}}{48}$	0
0	$D^+ \to \bar{K}^0K^{*+}$	$\frac{1}{8}$	$\frac{1}{4}$	$\frac{1}{8}$	0	$-\frac{1}{8}$	$-\frac{1}{8}$	0	$\frac{1}{8}$	$\frac{1}{8}$	0
0	$D^+ \to \bar{K}^{*0}K^+$	$\frac{1}{8}$	$-\frac{1}{8}$	$\frac{1}{8}$	0	$\frac{1}{4}$	$\frac{1}{4}$	0	$\frac{1}{8}$	$\frac{1}{8}$	0
0	$D^+ \to \omega_8\pi^+$	$\frac{1}{4\sqrt{6}}$	$\frac{1}{2\sqrt{6}}$	$\frac{1}{4\sqrt{6}}$	0	$\frac{1}{4\sqrt{6}}$	$\frac{1}{2\sqrt{6}}$	0	$\frac{1}{8\sqrt{6}}$	$\frac{1}{8\sqrt{6}}$	$\frac{\sqrt{3}}{4}$
0	$D^+ \to \rho_0\pi^+$	0	0	0	0	$-\frac{1}{4\sqrt{2}}$	0	0	$\frac{1}{8\sqrt{2}}$	$\frac{1}{8\sqrt{2}}$	0
0	$D_s^+ \to \eta_8K^{*+}$	$-\frac{1}{8\sqrt{6}}$	$-\frac{1}{4\sqrt{6}}$	$\frac{1}{4\sqrt{6}}$	0	$-\frac{2\sqrt{6}}{4}$	$\frac{1}{2\sqrt{6}}$	0	$\frac{1}{8\sqrt{6}}$	$-\frac{1}{8\sqrt{6}}$	0
0	$D_s^+ \to K^0\rho^+$	$\frac{1}{8\sqrt{2}}$	$\frac{1}{4\sqrt{2}}$	$-\frac{1}{4\sqrt{2}}$	0	$\frac{1}{4\sqrt{2}}$	$-\frac{1}{8\sqrt{2}}$	0	$\frac{1}{8\sqrt{2}}$	$-\frac{1}{8\sqrt{2}}$	0
0	$D_s^+ \to \pi_0K^{*+}$	$\frac{1}{8\sqrt{2}}$	$\frac{1}{4\sqrt{2}}$	$-\frac{1}{4\sqrt{2}}$	0	$\frac{1}{4\sqrt{2}}$	$-\frac{1}{8\sqrt{2}}$	0	$\frac{1}{8\sqrt{2}}$	$-\frac{1}{8\sqrt{2}}$	0
0	$D_s^+ \to \omega_8K^+$	$-\frac{1}{8\sqrt{6}}$	$\frac{1}{8\sqrt{6}}$	$\frac{1}{4\sqrt{6}}$	0	$\frac{1}{4\sqrt{6}}$	$\frac{1}{8\sqrt{6}}$	0	$-\frac{1}{4\sqrt{6}}$	$\frac{1}{8\sqrt{6}}$	$\frac{\sqrt{3}}{4}$
0	$D_s^+ \to \rho_0K^+$	$\frac{1}{8\sqrt{2}}$	$-\frac{1}{8\sqrt{2}}$	$-\frac{1}{4\sqrt{2}}$	0	0	$-\frac{1}{8\sqrt{2}}$	0	0	$\frac{1}{8\sqrt{2}}$	0
0	$D_s^+ \to K^{*0}\pi^+$	$\frac{1}{8}$	$\frac{1}{4}$	$-\frac{1}{4}$	0	$\frac{1}{4}$	$-\frac{1}{8}$	0	$\frac{1}{8}$	$-\frac{1}{4\sqrt{2}}$	0

Table D.11: $D \to P_8V_8$ $\mathcal{O}(\varepsilon)$ invariants generated by $\bar{\mathbf{3}}$. $\Delta = \lambda^5 A^2(\rho - i\eta)$.

ΔU	$\times\ \varepsilon$	$[\mathrm{pv}]_{88}\mathbf{1}_s$	$[\mathrm{pv}]_{88}\mathbf{2}_s$	$[\mathrm{pv}]_{88}\mathbf{3}_s$	$[\mathrm{pv}]_{88}\mathbf{4}_s$	$[\mathrm{pv}]_{88}\mathbf{5}_s$	$[\mathrm{pv}]_{88}\mathbf{6}_s$	$[\mathrm{pv}]_{88}\mathbf{7}_s$	$[\mathrm{pv}]_{88}\mathbf{8}_s$	$[\mathrm{pv}]_{88}\mathbf{9}_s$	$[\mathrm{pv}]_{88}\mathbf{10}_s$	$[\mathrm{pv}]_{88}\mathbf{11}_s$	$[\mathrm{pv}]_{88}\mathbf{12}_s$
0	$D^0 \to \omega_8\eta_8$	0	0	$\frac{\lambda}{2}$	$-\frac{\lambda}{2}$	$-\frac{\lambda}{4}$	$-\frac{\lambda}{4}$	$\frac{\lambda}{4}$	0	0	0	$-\frac{3\lambda}{2}$	$-\frac{\lambda}{2}$
0	$D^0 \to \eta_8\rho_0$	$\frac{\lambda}{2\sqrt{3}}$	$-\frac{\lambda}{2\sqrt{3}}$	$-\frac{\lambda}{2\sqrt{3}}$	$\frac{\lambda}{\sqrt{3}}$	$-\frac{\lambda}{4\sqrt{3}}$	$-\frac{\lambda}{4\sqrt{3}}$	$\frac{\lambda}{4\sqrt{3}}$	$-\frac{\lambda}{2\sqrt{3}}$	$-\frac{\lambda}{2\sqrt{3}}$	$\frac{\lambda}{2\sqrt{3}}$	0	$\frac{\lambda}{2\sqrt{3}}$
1	$D^0 \to \eta_8\bar{K}^{*0}$	$\frac{\lambda^2}{2\sqrt{6}}$	$-\frac{\lambda^2}{2\sqrt{6}}$	$-\sqrt{\frac{2}{3}}\lambda^2$	$-\sqrt{\frac{2}{3}}\lambda^2$	$-\frac{\lambda^2}{\sqrt{6}}$	0	0	0	$\frac{\lambda^2}{\sqrt{6}}$	$-\frac{\lambda^2}{\sqrt{6}}$	0	$-\frac{\lambda^2}{\sqrt{6}}$
-1	$D^0 \to \eta_8\bar{K}^{*0}$	$\frac{1}{\sqrt{6}}$	$-\frac{1}{\sqrt{6}}$	$\frac{1}{2\sqrt{6}}$	$\frac{1}{\sqrt{6}}$	$-\frac{1}{2\sqrt{6}}$	0	0	0	$-\frac{1}{2\sqrt{6}}$	$-\frac{1}{2\sqrt{6}}$	0	$\frac{1}{\sqrt{6}}$
1	$D^0 \to \omega_8 K^0$	$\frac{\lambda^2}{2\sqrt{6}}$	$\frac{\lambda^2}{\sqrt{6}}$	$\sqrt{\frac{2}{3}}\lambda^2$	$\sqrt{\frac{2}{3}}\lambda^2$	0	0	0	$\frac{\lambda^2}{\sqrt{6}}$	$-\frac{\lambda^2}{\sqrt{6}}$	0	$-\sqrt{\frac{3}{2}}\lambda^2$	$-\sqrt{\frac{2}{3}}\lambda^2$
1	$D^0 \to K^0\rho_0$	$\frac{\lambda^2}{2\sqrt{2}}$	0	0	0	0	0	$\frac{\lambda^2}{\sqrt{2}}$	$\frac{\lambda^2}{\sqrt{2}}$	0	0	0	0
0	$D^0 \to K^0\bar{K}^{*0}$	0	$-\frac{\lambda}{2}$	$\frac{\lambda}{2}$	$-\lambda$	$-\frac{\sqrt{3}\lambda}{4}$	0	$-\frac{2\sqrt{6}}{\lambda^2}$	0	0	0	0	λ
0	$D^0 \to \omega_8\pi_0$	$\frac{\lambda}{2\sqrt{3}}$	$\frac{\lambda}{\sqrt{3}}$	$-\frac{\lambda}{\sqrt{3}}$	$\frac{\lambda}{2\sqrt{3}}$	$\frac{\lambda}{4\sqrt{3}}$	$\frac{\lambda}{4\sqrt{3}}$	$\frac{\lambda}{4\sqrt{3}}$	$\frac{\lambda}{2\sqrt{3}}$	$\frac{\lambda}{2\sqrt{3}}$	$\frac{\lambda}{2\sqrt{3}}$	$\frac{\sqrt{3}\lambda}{2}$	$\frac{\lambda}{\sqrt{3}}$
0	$D^0 \to \pi_0\rho_0$	$\frac{\lambda}{\sqrt{3}}$	$\frac{\lambda}{2\sqrt{3}}$	0	0	0	0	0	$-\frac{\lambda}{2\sqrt{3}}$	0	$\frac{\lambda}{2\sqrt{3}}$	0	0
1	$D^0 \to \pi_0 K^{*0}$	$\frac{\lambda^2}{2\sqrt{2}}$	$\frac{\lambda^2}{2\sqrt{2}}$	0	0	$-\frac{\lambda^2}{2\sqrt{2}}$	0	$\frac{\lambda^2}{\sqrt{2}}$	$\frac{\lambda^2}{\sqrt{2}}$	0	$-\frac{\lambda^2}{2\sqrt{2}}$	0	0
-1	$D^0 \to \pi_0\bar{K}^{*0}$	$\frac{1}{\sqrt{2}}$	0	$-\frac{1}{2\sqrt{2}}$	$-\frac{1}{2\sqrt{2}}$	$-\frac{\lambda^2}{2\sqrt{2}}$	0	0	0	$-\frac{1}{2\sqrt{2}}$	$-\frac{\lambda^2}{2\sqrt{2}}$	0	$-\frac{1}{\sqrt{2}}$
-1	$D^0 \to \omega_8\bar{K}^0$	$\frac{1}{\sqrt{6}}$	$\sqrt{\frac{2}{3}}$	$-\frac{1}{2\sqrt{6}}$	$-\frac{1}{2\sqrt{6}}$	0	$\frac{1}{2\sqrt{6}}$	$\frac{1}{2\sqrt{6}}$	$-\frac{1}{2\sqrt{6}}$	$-\frac{1}{2\sqrt{6}}$	0	$\sqrt{\frac{3}{2}}$	$\frac{1}{2\sqrt{6}}$
0	$D^0 \to \rho_0\bar{K}^0$	$\frac{1}{\sqrt{2}}$	$\frac{1}{\sqrt{2}}$	$\frac{1}{2\sqrt{2}}$	$\frac{1}{2\sqrt{2}}$	0	0	$\frac{1}{2\sqrt{2}}$	$\frac{1}{2\sqrt{2}}$	$-\frac{1}{2\sqrt{2}}$	0	0	$-\frac{1}{\sqrt{2}}$
0	$D^0 \to K^0\bar{K}^{*0}$	0	0	λ	$-\frac{\lambda}{2}$	0	0	0	0	$-\frac{\lambda}{2}$	0	0	$\frac{\lambda}{2}$
-1	$D^0 \to K^-\rho^+$	-1	-1	0	0	0	0	0	0	0	$\frac{1}{2}$	0	0
0	$D^0 \to K^-K^{*+}$	$\frac{\lambda}{2}$	$\frac{\lambda}{2}$	0	0	$-\frac{\lambda}{2}$	$\frac{1}{2}$	0	0	0	$\frac{\lambda}{2}$	0	0
0	$D^0 \to \pi^-\rho^+$	λ	λ	0	0	λ^2	0	0	0	0	λ	0	0
1	$D^0 \to \pi^-K^{*+}$	$-\frac{\lambda^2}{2}$	$-\frac{\lambda^2}{2}$	λ	λ	0	$-\lambda^2$	0	$-\lambda^2$	0	λ^2	0	0
1	$D^0 \to \rho^-K^+$	$\frac{\lambda^2}{2}$	$-\frac{\lambda^2}{2}$	λ	λ	0	$-\lambda^2$	λ	$-\frac{\lambda}{2}$	$-\frac{\lambda}{2}$	$\frac{\lambda}{2}$	0	0
0	$D^0 \to K^{*-}K^+$	$-\frac{\lambda^2}{2}$	$-\frac{\lambda^2}{2}$	0	0	0	0	$-\frac{\lambda}{2}$	$-\frac{\lambda}{2}$	0	0	0	0
0	$D^0 \to \rho^-\pi^+$	λ	λ	0	0	0	0	$\frac{\lambda}{2}$	λ	0	0	0	0
-1	$D^0 \to K^{*-}\pi^+$	-1	-1	0	0	0	0	$-\frac{1}{2}$	$-\frac{1}{2}$	0	0	0	0

Table D.12: $D^0 \to P_8V_8$ $\mathcal{O}(\varepsilon)$ invariants generated by **6**.

ΔU	$\times\ \boldsymbol{\varepsilon}$	$[\mathrm{PV}]^1_{88}\mathbf{6}_s$	$[\mathrm{PV}]^2_{88}\mathbf{6}_s$	$[\mathrm{PV}]^3_{88}\mathbf{6}_s$	$[\mathrm{PV}]^4_{88}\mathbf{6}_s$	$[\mathrm{PV}]^5_{88}\mathbf{6}_s$	$[\mathrm{PV}]^6_{88}\mathbf{6}_s$	$[\mathrm{PV}]^7_{88}\mathbf{6}_s$	$[\mathrm{PV}]^8_{88}\mathbf{6}_s$	$[\mathrm{PV}]^9_{88}\mathbf{6}_s$	$[\mathrm{PV}]^{10}_{88}\mathbf{6}_s$	$[\mathrm{PV}]^{11}_{88}\mathbf{6}_s$	$[\mathrm{PV}]^{12}_{88}\mathbf{6}_s$
0	$D^+ \to \eta_8 \rho^+$	$\frac{\lambda}{\sqrt{6}}$	$-\frac{\lambda}{\sqrt{6}}$	$-\frac{\lambda}{\sqrt{6}}$	$\sqrt{\frac{2}{3}}\lambda$	$-\frac{\lambda}{2\sqrt{6}}$	$-\frac{\lambda}{2}\sqrt{\frac{3}{2}}$	$\frac{\lambda}{2}\sqrt{\frac{3}{2}}$	0	$-\frac{\lambda}{\sqrt{6}}$	$\frac{\lambda}{\sqrt{6}}$	0	$\frac{\lambda}{\sqrt{6}}$
1	$D^+ \to \eta_8 K^{*+}$	$-\frac{\lambda^2}{2\sqrt{6}}$	$\frac{\lambda^2}{2\sqrt{6}}$	$\sqrt{\frac{2}{3}}\lambda^2$	$\sqrt{\frac{2}{3}}\lambda^2$	$\frac{\lambda^2}{\sqrt{6}}$	0	0	0	$-\frac{\lambda^2}{\sqrt{6}}$	$\frac{\lambda^2}{\sqrt{6}}$	0	$\frac{\lambda^2}{\sqrt{6}}$
1	$D^+ \to K^0 \rho^+$	$\frac{\lambda^2}{2}$	0	0	0	0	$-\frac{\lambda^2}{2\sqrt{2}}$	$\frac{\lambda^2}{2\sqrt{2}}$	$-\frac{\lambda}{\sqrt{2}}$	0	$-\frac{\lambda}{\sqrt{2}}$	0	0
0	$D^+ \to \pi_0 \rho^+$	0	$-\frac{\lambda^2}{2\sqrt{2}}$	0	0	$\frac{\lambda}{2\sqrt{2}}$	$\frac{\lambda}{2\sqrt{2}}$	0	0	$-\frac{1}{2}\lambda^2$	$\frac{1}{2}\lambda^2$	0	0
1	$D^+ \to \pi_0 K^{*+}$	$\frac{\lambda^2}{2\sqrt{2}}$	0	0	0	$-\frac{\lambda^2}{2\sqrt{2}}$	$\frac{1}{2}$	$\frac{1}{2}$	0	0	0	0	0
-1	$D^+ \to \bar{K}^0 \rho^+$	0	0	0	0	$\frac{\lambda}{2\sqrt{2}}$	0	0	0	0	0	0	0
0	$D^+ \to \bar{K}^0 K^{*+}$	$\frac{\lambda}{2}$	0	$\frac{1}{2}$	0	$-\frac{\lambda^2}{2\sqrt{2}}$	$\frac{1}{2}$	$\frac{1}{2}$	0	0	0	0	0
1	$D^+ \to \omega_8 K^{*+}$	$-\frac{\lambda^2}{2\sqrt{6}}$	$-\frac{\lambda^2}{\sqrt{6}}$	$-\frac{\lambda}{2}$	0	0	0	$-\frac{\lambda^2}{2\sqrt{6}}$	$-\frac{\lambda^2}{\sqrt{6}}$	$\frac{\lambda^2}{\sqrt{6}}$	$-\frac{\lambda^2}{2\sqrt{2}}$	$\sqrt{\frac{3}{2}}\lambda^2$	0
1	$D^+ \to \rho_0 K^{*+}$	$\frac{\lambda^2}{2\sqrt{2}}$	0	$-\sqrt{\frac{2}{3}}\lambda^2$	$-\sqrt{\frac{2}{3}}\lambda^2$	0	0	$-\frac{\lambda^2}{2\sqrt{2}}$	$-\frac{\lambda^2}{2\sqrt{2}}$	0	0	0	0
0	$D^+ \to \bar{K}^{*0} K^{*+}$	$\frac{\lambda}{2}$	0	0	$\frac{1}{2}\lambda$	$-\frac{\lambda}{2}\sqrt{\frac{3}{2}}$	0	$\frac{\lambda}{2}\sqrt{\frac{3}{2}}$	$-\frac{\lambda}{2}$	$-\frac{\lambda}{2}$	0	$\sqrt{\frac{3}{2}}\lambda$	$-\lambda$
0	$D^+ \to \omega_8 \pi^+$	$\frac{\lambda}{\sqrt{6}}$	$\sqrt{\frac{2}{3}}\lambda$	$-\sqrt{\frac{2}{3}}\lambda$	$\frac{\lambda}{\sqrt{6}}$	$-\frac{\lambda}{2\sqrt{6}}$	$-\frac{\lambda}{2\sqrt{6}}$	$\frac{\lambda}{2\sqrt{6}}$	$\frac{\lambda}{\sqrt{6}}$	$-\frac{\lambda}{2}$	0	$\sqrt{\frac{2}{3}}\lambda$	$\sqrt{\frac{2}{3}}\lambda$
0	$D^+ \to \rho_0 \pi^+$	0	$\frac{\lambda}{\sqrt{2}}$	0	0	$-\frac{\lambda}{2\sqrt{2}}$	$-\frac{\lambda}{2\sqrt{2}}$	$\frac{\lambda}{2\sqrt{2}}$	$\frac{\lambda}{\sqrt{2}}$	0	$\frac{\lambda}{\sqrt{2}}$	0	0
1	$D^+ \to K^{*0} \pi^+$	$\frac{\lambda^2}{2}$	0	0	0	$-\frac{1}{2}\lambda^2$	0	$-\frac{1}{2}\lambda^2$	0	0	$-\frac{1}{2}\lambda^2$	0	-1
-1	$D^+ \to \bar{K}^{*0} \pi^+$	$-\frac{1}{\sqrt{6}}$	$\frac{1}{\sqrt{6}}$	$-\frac{1}{2\sqrt{6}}$	$-\frac{1}{2\sqrt{6}}$	$-\frac{1}{2\sqrt{6}}$	$-\frac{1}{2}$	$-\frac{1}{2\sqrt{6}}$	$-\frac{1}{\sqrt{6}}$	$\frac{1}{\sqrt{6}}$	$-\frac{1}{2\sqrt{6}}$	$-\frac{1}{\sqrt{6}}$	$\frac{1}{2\sqrt{6}}$
-1	$D_s^+ \to \eta_8 \pi^+$	$-\frac{1}{\sqrt{6}}$	$-\frac{1}{\sqrt{6}}$	$\frac{1}{\sqrt{6}}$	$\frac{1}{\sqrt{6}}$	$\frac{1}{2\sqrt{6}}$	$\frac{1}{2\sqrt{6}}$	$-\frac{1}{2\sqrt{6}}$	$-\frac{1}{\sqrt{6}}$	$\frac{1}{\sqrt{6}}$	$\frac{1}{2\sqrt{6}}$	$-\frac{1}{\sqrt{6}}$	$-\frac{1}{2\sqrt{6}}$
0	$D_s^+ \to \eta_8 K^{*+}$	$\frac{\lambda}{2\sqrt{6}}$	$-\frac{\lambda}{2\sqrt{6}}$	$-\frac{\lambda}{2\sqrt{6}}$	$\frac{\lambda}{\sqrt{6}}$	$-\frac{\lambda}{2\sqrt{6}}$	$-\frac{\lambda}{2\sqrt{6}}$	$\frac{\lambda}{2\sqrt{6}}$	$\frac{\lambda}{\sqrt{6}}$	$-\frac{\lambda}{2\sqrt{6}}$	$\frac{\lambda}{\sqrt{6}}$	$-\frac{\lambda}{2\sqrt{6}}$	$\frac{\lambda}{2\sqrt{6}}$
1	$D_s^+ \to K^0 \rho^+$	$-\frac{\lambda}{2}$	$\frac{\lambda}{2\sqrt{2}}$	$\frac{\lambda}{2\sqrt{2}}$	$\frac{1}{2\sqrt{2}}\lambda$	$\frac{1}{2\sqrt{2}}\lambda$	$\frac{1}{2}\lambda^2$	$\frac{1}{2\sqrt{2}}\lambda$	$-\frac{1}{\sqrt{2}}\lambda$	$\frac{1}{2\sqrt{2}}\lambda$	$-\frac{1}{2\sqrt{2}}\lambda$	$\frac{1}{2\sqrt{2}}\lambda$	$\frac{1}{2\sqrt{2}}\lambda$
0	$D_s^+ \to \pi_0 \rho^+$	0	$-\frac{\lambda}{2\sqrt{2}}$	$-\frac{\lambda}{2\sqrt{2}}$	$-\frac{1}{2\sqrt{2}}\lambda$	$-\frac{1}{2\sqrt{2}}\lambda$	$-\frac{1}{2}\lambda^2$	$-\frac{1}{2\sqrt{2}}\lambda$	$\frac{1}{\sqrt{2}}\lambda$	$-\frac{1}{2\sqrt{2}}\lambda$	$\frac{1}{2\sqrt{2}}\lambda$	$-\frac{1}{2\sqrt{2}}\lambda$	$-\frac{1}{2\sqrt{2}}\lambda$
-1	$D_s^+ \to \pi_0 K^{*+}$	$-\frac{\lambda}{2\sqrt{2}}$	$\frac{\lambda}{2\sqrt{2}}$	$\frac{\lambda}{2\sqrt{2}}$	$-\frac{1}{2\sqrt{2}}\lambda$	$\frac{1}{2\sqrt{2}}\lambda$	$\frac{1}{2}\lambda^2$	$-\frac{1}{2\sqrt{2}}\lambda$	$-\frac{1}{\sqrt{2}}\lambda$	$\frac{1}{2\sqrt{2}}\lambda$	$-\frac{1}{2\sqrt{2}}\lambda$	$\frac{1}{2\sqrt{2}}\lambda$	$-\frac{1}{2\sqrt{2}}\lambda$
0	$D_s^+ \to \bar{K}^0 K^{*+}$	$-\frac{\lambda}{2}$	$\frac{\lambda}{2}$	$\frac{\lambda}{2}$	$-\frac{1}{2}\lambda$	$\frac{1}{2}\lambda$	$\frac{1}{2}\lambda^2$	$-\frac{1}{2}\lambda$	$-\frac{1}{\sqrt{2}}\lambda$	$\frac{1}{2}\lambda$	$-\frac{1}{2}\lambda$	$\frac{1}{2}\lambda$	$\frac{1}{2}\lambda$
-1	$D_s^+ \to \omega_8 \pi^+$	$\frac{\lambda}{2\sqrt{6}}$	$\frac{\lambda}{\sqrt{6}}$	$\frac{\lambda}{\sqrt{6}}$	$-\frac{\lambda}{\sqrt{6}}$	$-\frac{\lambda}{2}\sqrt{\frac{3}{2}}$	$-\sqrt{\frac{2}{3}}\lambda$	$-\sqrt{\frac{2}{3}}\lambda$	$\frac{\lambda}{\sqrt{6}}$	$-\frac{\lambda}{\sqrt{6}}$	$\frac{\lambda}{\sqrt{6}}$	$-\sqrt{\frac{3}{2}}\lambda$	$-\frac{\lambda}{2\sqrt{6}}$
0	$D_s^+ \to \rho_0 K^{*+}$	$-\frac{\lambda}{2\sqrt{2}}$	0	$-\frac{\lambda}{2\sqrt{2}}$	$\frac{\lambda}{\sqrt{2}}$	$-\frac{\lambda}{2\sqrt{2}}$	0	0	0	0	0	0	$\frac{\lambda}{2\sqrt{2}}$
1	$D_s^+ \to K^{*0} K^{*+}$	$-\frac{1}{2}$	0	$-\lambda^2$	$-\lambda^2$	$-\frac{1}{2}$	$-\lambda^2$	$-\lambda^2$	$-\lambda^2$	$-\lambda^2$	$-\frac{1}{2}\lambda^2$	0	$\frac{1}{2}\lambda^2$
-1	$D_s^+ \to \bar{K}^{*0} K^{*+}$	$-\frac{1}{2}$	$-\frac{1}{2}\sqrt{\frac{2}{3}}$	0	0	0	$-\sqrt{\frac{2}{3}}$	0	0	0	$-\frac{1}{2}\lambda^2$	0	0
-1	$D_s^+ \to \omega_8 \pi^+$	$-\frac{1}{\sqrt{6}}$	$-\sqrt{\frac{2}{3}}$	$\frac{1}{2\sqrt{6}}$	$\frac{1}{\sqrt{6}}$	$\frac{1}{2\sqrt{6}}$	$-\frac{1}{2}$	$\frac{1}{\sqrt{6}}$	$\frac{1}{\sqrt{6}}$	$-\frac{1}{\sqrt{6}}$	0	$-\sqrt{\frac{3}{2}}$	$-\frac{1}{2\sqrt{6}}$
-1	$D_s^+ \to \rho_0 \pi^+$	0	$-\frac{1}{\sqrt{2}}$	$-\frac{1}{2\sqrt{2}}$	$-\frac{1}{2\sqrt{2}}$	0	0	0	0	$-\frac{1}{\sqrt{2}}$	0	0	0
0	$D_s^+ \to K^{*0} \pi^+$	$-\frac{\lambda}{2}$	$-\frac{\lambda}{2}$	$-\lambda$	$\frac{\lambda}{2}$	0	$-\lambda$	$\frac{\lambda}{2}$	$-\lambda$	$-\lambda$	0	0	$-\frac{\lambda}{2}$

Table D.13: $D^+ \to P_8 V_8$ and $D_s^+ \to P_8 V_8$ $\mathcal{O}(\varepsilon)$ invariants generated by $\mathbf{6}$.

ΔU	$\times\ \varepsilon$	$\overline{88}_{15_s}^{PV\,1}$	$\overline{88}_{15_s}^{PV\,2}$	$\overline{88}_{15_s}^{PV\,3}$	$\overline{88}_{15_s}^{PV\,4}$	$\overline{88}_{15_s}^{PV\,5}$	$\overline{88}_{15_s}^{PV\,6}$	$\overline{88}_{15_s}^{PV\,7}$	$\overline{88}_{15_s}^{PV\,8}$	$\overline{88}_{15_s}^{PV\,9}$	$\overline{88}_{15_s}^{PV\,10}$	$\overline{88}_{15_s}^{PV\,11}$	$\overline{88}_{15_s}^{PV\,12}$	$\overline{88}_{15_s}^{PV\,13}$	$\overline{88}_{15_s}^{PV\,14}$	$\overline{88}_{15_s}^{PV\,15}$	$\overline{88}_{15_s}^{PV\,16}$	$\overline{88}_{15_s}^{PV\,17}$	$\overline{88}_{15_s}^{PV\,18}$
0	$D^0 \to \omega_8 \eta_8$	λ	$\frac{\lambda}{2}$	0	$\frac{\lambda}{2}$	$\frac{\lambda}{4}$	0	0	0	0	$-\frac{\lambda}{4}$	$-\frac{\lambda}{2}$	$-\lambda$	0	$-\frac{3\lambda}{2}$	$-\frac{\lambda}{4}$	$-\frac{\lambda}{4}$	0	$-\frac{3\lambda}{4}$
0	$D^0 \to \eta_8 \rho_0$	$-\frac{\sqrt{3}\lambda}{2}$	0	$\frac{\lambda}{2\sqrt{3}}$	$\frac{\lambda}{2\sqrt{3}}$	$\frac{\sqrt{3}\lambda}{4}$	$\frac{\lambda}{2\sqrt{3}}$	$\frac{\lambda}{2\sqrt{3}}$	$\sqrt{\frac{2}{3}}\lambda^2$	$\frac{\lambda}{2\sqrt{3}}$	$\frac{3\lambda}{4\sqrt{3}}$	$\frac{\lambda}{2\sqrt{3}}$	$\frac{\lambda}{\sqrt{3}}$	$-\frac{\lambda}{\sqrt{3}}$	0	$\frac{\sqrt{3}\lambda}{4}$	$\frac{\lambda}{4\sqrt{3}}$	$-\frac{\lambda}{4\sqrt{3}}$	$\frac{\lambda}{4\sqrt{3}}$
1	$D^0 \to \eta_8 K^{*0}$	0	0	$\frac{\lambda^2}{2\sqrt{6}}$	$\frac{\lambda^2}{2\sqrt{6}}$	0	$-\frac{\lambda^2}{\sqrt{6}}$	$-\frac{\lambda^2}{\sqrt{6}}$	$-\frac{\lambda^2}{\sqrt{6}}$	$\frac{\lambda^2}{2\sqrt{6}}$	$-\frac{\lambda^2}{\sqrt{6}}$	$-\frac{\lambda^2}{\sqrt{6}}$	$\sqrt{\frac{2}{3}}\lambda^2$	$-\frac{\lambda^2}{\sqrt{6}}$	0	0	$-\frac{\lambda^2}{2\sqrt{6}}$	$-\frac{\lambda^2}{2\sqrt{6}}$	$-\sqrt{\frac{2}{3}}\lambda^2$
-1	$D^0 \to \eta_8 \tilde{K}^{*0}$	0	$-\sqrt{\frac{3}{8}}$	$\frac{1}{\sqrt{6}}$	$-\frac{1}{2\sqrt{6}}$	0	$-\frac{1}{2\sqrt{6}}$	$-\frac{1}{2\sqrt{6}}$	$-\frac{1}{\sqrt{6}}$	$\frac{1}{\sqrt{6}}$	$\frac{1}{\sqrt{6}}$	$\frac{1}{\sqrt{6}}$	$\sqrt{\frac{2}{3}}$	$-\sqrt{\frac{2}{3}}$	0	0	$\sqrt{\frac{2}{3}}$	$\frac{1}{2\sqrt{6}}$	$\frac{1}{2\sqrt{6}}$
1	$D^0 \to \omega_8 \tilde{K}^0$	0	0	$\frac{\lambda^2}{2\sqrt{6}}$	$\frac{\lambda^2}{2\sqrt{6}}$	0	$\frac{\lambda^2}{2\sqrt{6}}$	$\frac{\lambda^2}{2\sqrt{6}}$	$\frac{\lambda^2}{\sqrt{6}}$	0	0	0	0	0	0	0	$\frac{\lambda^2}{\sqrt{6}}$	0	$-\frac{\lambda^2}{2\sqrt{6}}$
1	$D^0 \to K^0 \rho_0$	0	0	$\frac{\lambda^2}{2\sqrt{2}}$	$\frac{\lambda^2}{2\sqrt{2}}$	0	$\frac{\lambda^2}{2\sqrt{2}}$	0	$-\frac{\lambda^2}{\sqrt{2}}$	0	0	$-\sqrt{2}\lambda^2$	0	0	0	0	0	0	$\frac{\lambda^2}{2\sqrt{2}}$
0	$D^0 \to K^0 \tilde{K}^{*0}$	0	0	$\frac{\lambda}{2\sqrt{2}}$	0	0	$-\frac{\lambda}{\sqrt{3}}$	$-\frac{\lambda^2}{\sqrt{2}}$	$-\frac{\lambda}{2\sqrt{3}}$	$\frac{\lambda^2}{\sqrt{2}}$	$\frac{\lambda}{2}$	$\frac{\lambda^2}{\sqrt{2}}$	0	$-\frac{\lambda}{2}$	0	0	$-\frac{\lambda}{2}$	$\frac{\lambda^2}{\sqrt{2}}$	$\frac{\lambda}{2}$
0	$D^0 \to \omega_8 \pi_0$	$-\frac{\sqrt{3}\lambda}{2}$	$-\frac{\sqrt{3}\lambda}{2}$	$\frac{\lambda}{2\sqrt{3}}$	$\frac{\lambda}{2\sqrt{3}}$	$-\frac{\sqrt{3}\lambda}{4}$	$-\frac{\lambda}{\sqrt{3}}$	$\frac{\lambda}{2\sqrt{3}}$	$-\frac{\lambda}{2\sqrt{3}}$	0	$\frac{\sqrt{3}\lambda}{4}$	$-\lambda$	0	$\frac{\sqrt{3}\lambda}{2}$	$-\frac{3\lambda}{2}$	$-\frac{\sqrt{3}\lambda}{4}$	$-\frac{\lambda}{2}$	$\frac{\lambda}{4\sqrt{3}}$	$\frac{\lambda}{4\sqrt{3}}$
0	$D^0 \to \pi_0 \rho_0$	0	0	$\frac{\lambda^2}{2\sqrt{2}}$	$\frac{\lambda^2}{2\sqrt{2}}$	0	$-\frac{\lambda^2}{\sqrt{2}}$	$-\frac{\lambda^2}{\sqrt{2}}$	$\frac{\lambda^2}{\sqrt{2}}$	$-\frac{\lambda^2}{2\sqrt{2}}$	$\frac{\lambda^2}{\sqrt{2}}$	$\frac{\lambda^2}{\sqrt{2}}$	$-\frac{\lambda^2}{\sqrt{2}}$	$-\frac{\lambda^2}{2\sqrt{2}}$	0	0	0	$\frac{\lambda^2}{2\sqrt{2}}$	0
1	$D^0 \to \pi_0 \tilde{K}^{*0}$	0	0	$\frac{\lambda}{2\sqrt{2}}$	$-\frac{\lambda}{2\sqrt{2}}$	0	$-\frac{\lambda}{2\sqrt{2}}$	$-\frac{\lambda}{2\sqrt{2}}$	$-\frac{\lambda^2}{2\sqrt{2}}$	0	$\frac{\lambda}{4}$	$\frac{\lambda^2}{\sqrt{2}}$	$\frac{\lambda}{2}$	$-\frac{\lambda}{2}$	$-\frac{3\lambda}{2}$	$\frac{\lambda}{4}$	$\frac{\lambda}{4}$	$-\frac{\lambda^2}{2\sqrt{2}}$	$-\frac{\lambda}{4}$
-1	$D^0 \to \omega_8 \tilde{K}^0$	0	$\frac{3}{2\sqrt{2}}$	$\frac{1}{\sqrt{6}}$	$-\frac{1}{2\sqrt{6}}$	$-\sqrt{\frac{3}{8}}$	$-\frac{1}{2\sqrt{6}}$	$-\frac{1}{2\sqrt{6}}$	$\frac{1}{\sqrt{6}}$	$\frac{1}{2\sqrt{6}}$	$\sqrt{\frac{3}{8}}$	$\frac{1}{2\sqrt{6}}$	$-\frac{1}{2\sqrt{6}}$	$\frac{1}{\sqrt{6}}$	0	$\sqrt{\frac{3}{8}}$	$\frac{1}{2\sqrt{6}}$	$\frac{1}{2\sqrt{6}}$	$-\frac{1}{2\sqrt{6}}$
-1	$D^0 \to \rho_0 \tilde{K}^0$	0	$\sqrt{\frac{3}{8}}\frac{3}{2\sqrt{2}}$	$\frac{1}{\sqrt{6}}$	$-\frac{1}{2\sqrt{6}}$	$-\frac{3}{2\sqrt{2}}$	$-\frac{1}{2\sqrt{6}}$	$-\frac{1}{2\sqrt{6}}$	$-\frac{1}{2\sqrt{2}}$	$\frac{1}{2\sqrt{6}}$	$\sqrt{\frac{3}{8}}\frac{1}{2\sqrt{2}}$	$\frac{1}{2\sqrt{6}}$	$-\frac{1}{2\sqrt{2}}$	$\frac{1}{\sqrt{6}}$	0	$\frac{3}{2\sqrt{2}}$	$\frac{1}{2\sqrt{6}}$	$\frac{1}{2\sqrt{6}}$	$-\frac{1}{2\sqrt{2}}$
0	$D^0 \to K^0 \tilde{K}^{*0}$	$\frac{3\lambda}{2}$	0	$\frac{\lambda}{2}$	$\frac{\lambda}{2}$	0	$-\lambda$	$-\frac{\lambda}{2}$	$\frac{\lambda}{2}$	$\frac{\lambda}{2}$	$\frac{\lambda}{4}$	$\frac{\lambda}{2}$	$\frac{\lambda}{2}$	$-\frac{\lambda}{2}$	$-\frac{3\lambda}{2}$	$\frac{\lambda}{4}$	$\frac{\lambda}{4}$	$-\frac{\lambda}{2}$	$\frac{\lambda}{4}$
-1	$D^0 \to K^- \rho^+$	0	0	-1	$\frac{1}{2}$	0	$\frac{1}{2}$	$\frac{1}{2}$	$\frac{1}{2}$	-1	$-\frac{1}{2}$	$\frac{1}{2}$	$\frac{1}{2}$	$-\frac{1}{2}$	$\frac{3\lambda}{2}$	$-\frac{1}{4}$	$-\frac{1}{4}$	$\frac{1}{2}$	$\frac{1}{4}$
0	$D^0 \to K^- K^{*+}$	0	0	$\frac{\lambda}{2}$	$-\lambda$	0	$-\frac{\lambda}{2}$	$\frac{\lambda}{2}$	$\frac{\lambda}{2}$	$\frac{\lambda}{2}$	$-\frac{\lambda}{2}$	$\frac{\lambda}{2}$	$\frac{\lambda}{2}$	$-\frac{\lambda}{2}$	$-\frac{3\lambda}{2}$	$\frac{\lambda}{4}$	$\frac{\lambda}{4}$	$-\frac{\lambda}{2}$	$\frac{\lambda}{4}$
0	$D^0 \to \pi^- \rho^+$	0	0	$-\frac{\lambda}{2}$	λ	0	$-\frac{\lambda}{2}$	$-\frac{\lambda}{2}$	$-\frac{\lambda}{2}$	λ^2	$-\frac{\lambda}{2}$	$-\frac{\lambda}{2}$	$\frac{\lambda}{2}$	$\frac{\lambda}{2}$	$\frac{3\lambda}{2}$	$-\frac{\lambda}{4}$	$-\frac{\lambda}{4}$	$\frac{\lambda}{2}$	$-\frac{\lambda}{4}$
1	$D^0 \to \pi^- K^{*+}$	0	0	$-\frac{\lambda^2}{2}$	$\frac{\lambda^2}{2}$	0	$\frac{\lambda^2}{2}$	$\frac{\lambda^2}{2}$	$\frac{\lambda^2}{2}$	λ^2	$\frac{\lambda^2}{2}$	$\frac{\lambda^2}{2}$	$-\frac{\lambda^2}{2}$	$-\frac{\lambda^2}{2}$	$-\frac{3\lambda^2}{2}$	$\frac{\lambda^2}{4}$	$\frac{\lambda^2}{4}$	$-\frac{\lambda^2}{2}$	$\frac{\lambda^2}{4}$
1	$D^0 \to \rho^- K^+$	0	0	$\frac{\lambda^2}{2}$	$-\frac{\lambda^2}{2}$	0	$-\frac{\lambda^2}{2}$	$-\frac{\lambda^2}{2}$	$-\frac{\lambda^2}{2}$	λ^2	$-\frac{\lambda^2}{2}$	$-\frac{\lambda^2}{2}$	$\frac{\lambda^2}{2}$	$\frac{\lambda^2}{2}$	$\frac{3\lambda^2}{2}$	$-\frac{\lambda^2}{4}$	$-\frac{\lambda^2}{4}$	$\frac{\lambda^2}{2}$	$-\frac{\lambda^2}{4}$
0	$D^0 \to K^- K^{*+}$	0	0	$-\frac{\lambda}{2}$	$\frac{\lambda}{2}$	0	$\frac{\lambda}{2}$	$\frac{\lambda}{2}$	$\frac{\lambda}{2}$	$-\frac{\lambda^2}{2}$	$\frac{\lambda}{2}$	$\frac{\lambda}{2}$	$-\frac{\lambda}{2}$	$-\frac{\lambda}{2}$	$\frac{3\lambda}{2}$	$-\frac{\lambda}{4}$	$-\frac{\lambda}{4}$	$\frac{\lambda}{2}$	$-\frac{\lambda}{4}$
0	$D^0 \to \pi^- \rho^+$	0	0	$\frac{\lambda^2}{2}$	$-\frac{\lambda^2}{2}$	0	$\frac{\lambda^2}{2}$	$\frac{\lambda^2}{2}$	$\frac{\lambda^2}{2}$	$-\lambda^2$	$\frac{\lambda^2}{2}$	$\frac{\lambda^2}{2}$	$-\frac{\lambda^2}{2}$	$-\frac{\lambda^2}{2}$	$-\frac{3\lambda^2}{2}$	$\frac{\lambda^2}{4}$	$\frac{\lambda^2}{4}$	$-\frac{\lambda^2}{2}$	$\frac{\lambda^2}{4}$
-1	$D^0 \to \rho^- \pi^+$	0	0	$-\frac{\lambda}{2}$	$\frac{\lambda}{2}$	0	$\frac{\lambda}{2}$	$\frac{\lambda}{2}$	$\frac{\lambda}{2}$	$-\lambda^2$	$\frac{\lambda}{2}$	$\frac{\lambda}{2}$	$-\frac{\lambda}{2}$	$-\frac{\lambda}{2}$	$\frac{3\lambda}{2}$	$-\frac{\lambda}{4}$	$-\frac{\lambda}{4}$	$\frac{\lambda}{2}$	$-\frac{\lambda}{4}$
-1	$D^0 \to K^+ \pi^+$	0	0	$\frac{\lambda}{2}$	$-\frac{\lambda}{2}$	0	$-\frac{\lambda}{2}$	$-\frac{\lambda}{2}$	$-\frac{\lambda}{2}$	λ^2	$-\frac{\lambda}{2}$	$-\frac{\lambda}{2}$	$\frac{\lambda}{2}$	$\frac{\lambda}{2}$	$-\frac{3\lambda}{2}$	$\frac{\lambda}{4}$	$\frac{\lambda}{4}$	$-\frac{\lambda}{2}$	$\frac{\lambda}{4}$
-1	$D^0 \to K^{*+} \pi^+$	0	0	$\frac{\lambda}{2}$	$-\frac{\lambda}{2}$	0	$-\frac{\lambda}{2}$	$-\frac{\lambda}{2}$	$-\frac{\lambda}{2}$	λ^2	$-\frac{\lambda}{2}$	$-\frac{\lambda}{2}$	$\frac{\lambda}{2}$	$\frac{\lambda}{2}$	$-\frac{3\lambda}{2}$	$\frac{\lambda}{4}$	$\frac{\lambda}{4}$	$-\frac{\lambda}{2}$	$\frac{\lambda}{4}$

Table D.14: $D^0 \to P_8 V_8$ $\mathcal{O}(\varepsilon)$ invariants generated by $\bar{\mathbf{15}}$.

ΔU	$\times\ \varepsilon$	$[\mathrm{PV}]^1_{\mathbf{88}}\,\bar{\mathbf{15}}_{\mathbf{s}}$	$[\mathrm{PV}]^2_{\mathbf{88}}\,\bar{\mathbf{15}}_{\mathbf{s}}$	$[\mathrm{PV}]^3_{\mathbf{88}}\,\bar{\mathbf{15}}_{\mathbf{s}}$	$[\mathrm{PV}]^4_{\mathbf{88}}\,\bar{\mathbf{15}}_{\mathbf{s}}$	$[\mathrm{PV}]^5_{\mathbf{88}}\,\bar{\mathbf{15}}_{\mathbf{s}}$	$[\mathrm{PV}]^6_{\mathbf{88}}\,\bar{\mathbf{15}}_{\mathbf{s}}$	$[\mathrm{PV}]^7_{\mathbf{88}}\,\bar{\mathbf{15}}_{\mathbf{s}}$	$[\mathrm{PV}]^8_{\mathbf{88}}\,\bar{\mathbf{15}}_{\mathbf{s}}$	$[\mathrm{PV}]^9_{\mathbf{88}}\,\bar{\mathbf{15}}_{\mathbf{s}}$	$[\mathrm{PV}]^{10}_{\mathbf{88}}\,\bar{\mathbf{15}}_{\mathbf{s}}$	$[\mathrm{PV}]^{11}_{\mathbf{88}}\,\bar{\mathbf{15}}_{\mathbf{s}}$	$[\mathrm{PV}]^{12}_{\mathbf{88}}\,\bar{\mathbf{15}}_{\mathbf{s}}$	$[\mathrm{PV}]^{13}_{\mathbf{88}}\,\bar{\mathbf{15}}_{\mathbf{s}}$	$[\mathrm{PV}]^{14}_{\mathbf{88}}\,\bar{\mathbf{15}}_{\mathbf{s}}$	$[\mathrm{PV}]^{15}_{\mathbf{88}}\,\bar{\mathbf{15}}_{\mathbf{s}}$	$[\mathrm{PV}]^{16}_{\mathbf{88}}\,\bar{\mathbf{15}}_{\mathbf{s}}$	$[\mathrm{PV}]^{17}_{\mathbf{88}}\,\bar{\mathbf{15}}_{\mathbf{s}}$	$[\mathrm{PV}]^{18}_{\mathbf{88}}\,\bar{\mathbf{15}}_{\mathbf{s}}$
0	$D^+ \to \eta_8 \rho^+$	$-\sqrt{\frac{3}{2}}\lambda$	0	$-\frac{\lambda}{\sqrt{6}}$	$-\frac{\lambda}{\sqrt{6}}$	$\frac{\lambda}{2}\sqrt{\frac{3}{2}}$	$-\frac{\lambda}{\sqrt{6}}$	$-\frac{\lambda}{\sqrt{6}}$	$-\sqrt{\frac{2}{3}}\lambda$	$-\frac{\lambda}{2\sqrt{6}}$	$\frac{\lambda}{2\sqrt{6}}$	$-\sqrt{\frac{2}{3}}\lambda$	$\sqrt{\frac{2}{3}}\lambda$	0	0	$-\frac{\lambda}{2}\sqrt{\frac{3}{2}}$	$-\frac{\lambda}{2\sqrt{6}}$	$-\frac{\lambda}{2\sqrt{6}}$	$-\frac{\lambda}{2\sqrt{6}}$
1	$D^+ \to \eta_8 K^{*+}$	0	0	$-\frac{\lambda^2}{2\sqrt{6}}$	$-\frac{\lambda^2}{2\sqrt{6}}$	0	$-\frac{\lambda^2}{\sqrt{6}}$	$-\frac{\lambda^2}{\sqrt{6}}$	$-\sqrt{\frac{2}{3}}\lambda^2$	0	$\frac{\lambda^2}{2\sqrt{6}}$	$-\frac{\lambda^2}{\sqrt{6}}$	$-\sqrt{\frac{2}{3}}\lambda^2$	0	0	$-\frac{\lambda^2}{2\sqrt{6}}$	$-\frac{\lambda^2}{2\sqrt{6}}$	$-\frac{\lambda^2}{2\sqrt{6}}$	$-\sqrt{\frac{2}{3}}\lambda^2$
1	$D^+ \to K^0 \rho^+$	0	0	$\frac{\lambda^2}{2\sqrt{6}}$	$-\frac{\lambda^2}{2}$	0	$-\frac{\lambda^2}{2}$	$\frac{\lambda^2}{\sqrt{6}}$	$\frac{\lambda^2}{\sqrt{3}}$	$\frac{\lambda^2}{2\sqrt{6}}$	$-\frac{\lambda^2}{2\sqrt{6}}$	$\frac{\lambda^2}{\sqrt{3}}$	$\frac{\lambda^2}{\sqrt{3}}$	$\frac{\lambda^2}{2}$	0	$\frac{\lambda^2}{2\sqrt{6}}$	$\frac{\lambda^2}{2\sqrt{6}}$	$\frac{\lambda^2}{\sqrt{6}}$	0
0	$D^+ \to \pi_0 \rho^+$	0	0	$-\frac{\lambda^2}{2}$	0	0	$\frac{\lambda^2}{\sqrt{2}}$	$\frac{\lambda^2}{\sqrt{2}}$	0	$\frac{\lambda^2}{2\sqrt{2}}$	$-\frac{\lambda^2}{2\sqrt{2}}$	0	0	0	0	$-\frac{\lambda^2}{2\sqrt{2}}$	$-\frac{\lambda^2}{2\sqrt{2}}$	$-\frac{\lambda^2}{2\sqrt{2}}$	0
1	$D^+ \to \pi_0 K^{*+}$	0	0	$-\frac{\lambda^2}{2\sqrt{2}}$	$-\frac{\lambda^2}{2\sqrt{2}}$	0	$\frac{\lambda^2}{\sqrt{2}}$	$-\frac{\lambda^2}{2\sqrt{2}}$	0	$-\frac{\lambda^2}{2\sqrt{2}}$	$\frac{\lambda^2}{2\sqrt{2}}$	0	0	0	0	$\frac{\lambda^2}{2\sqrt{2}}$	$\frac{\lambda^2}{2\sqrt{2}}$	$\frac{\lambda^2}{2\sqrt{2}}$	0
−1	$D^+ \to K^0 \rho^+$	0	$-\frac{3}{2}$	$-\frac{\lambda}{\sqrt{6}}$	$-\frac{\lambda}{\sqrt{6}}$	$-\frac{3\lambda}{2\sqrt{2}}$	$-\frac{\lambda}{\sqrt{6}}$	$-\frac{\lambda}{\sqrt{6}}$	$-\sqrt{\frac{2}{3}}\lambda$	$-\frac{\lambda}{2\sqrt{6}}$	$\frac{\lambda}{2\sqrt{6}}$	$-\frac{\lambda}{\sqrt{6}}$	$-\sqrt{\frac{2}{3}}\lambda$	$-\frac{\lambda}{\sqrt{6}}$	$-\frac{\lambda}{2}\sqrt{\frac{3}{2}}$	$-\frac{\lambda}{2\sqrt{6}}$	$-\frac{\lambda}{2\sqrt{6}}$	$-\frac{\lambda}{2\sqrt{6}}$	$-\frac{\lambda}{\sqrt{6}}$
0	$D^+ \to K^{*0} K^+$	0	$-\frac{3\lambda}{2}$	$-\frac{\lambda^2}{2\sqrt{6}}$	$-\frac{\lambda^2}{2\sqrt{6}}$	0	$-\frac{\lambda^2}{2\sqrt{2}}$	$-\frac{\lambda^2}{2\sqrt{6}}$	$-\frac{\lambda^2}{2}$	$-\frac{\lambda^2}{2\sqrt{6}}$	$\frac{\lambda^2}{2\sqrt{6}}$	$-\frac{\lambda^2}{2\sqrt{2}}$	$-\frac{\lambda^2}{2}$	$-\frac{\lambda^2}{2\sqrt{6}}$	$-\frac{\lambda^2}{2\sqrt{6}}$	$-\frac{\lambda^2}{2\sqrt{6}}$	$-\frac{\lambda^2}{2\sqrt{6}}$	$-\frac{\lambda^2}{2\sqrt{6}}$	$-\frac{\lambda^2}{2\sqrt{6}}$
1	$D^+ \to \omega_8 K^+$	0	0	$-\frac{\lambda}{\sqrt{6}}$	$-\frac{\lambda}{\sqrt{6}}$	0	$-\frac{\lambda}{\sqrt{6}}$	$-\frac{\lambda}{\sqrt{6}}$	0	$\frac{\lambda}{\sqrt{6}}$	$-\frac{\lambda}{\sqrt{6}}$	$\frac{\lambda}{\sqrt{6}}$	0	$\frac{\lambda}{\sqrt{6}}$	$\frac{\lambda}{\sqrt{6}}$	$\frac{\lambda}{\sqrt{6}}$	$\frac{\lambda}{\sqrt{6}}$	$\frac{\lambda}{\sqrt{6}}$	$\frac{\lambda}{\sqrt{6}}$
1	$D^+ \to \rho_0 K^+$	0	$-\frac{3\lambda}{2\sqrt{2}}$	$-\frac{\lambda^2}{2\sqrt{2}}$	$-\frac{\lambda^2}{2\sqrt{2}}$	0	$-\frac{\lambda^2}{2\sqrt{2}}$	$-\frac{\lambda^2}{2\sqrt{2}}$	0	$-\frac{\lambda^2}{2\sqrt{2}}$	$\frac{\lambda^2}{2\sqrt{2}}$	$-\frac{\lambda^2}{2\sqrt{2}}$	0	$-\frac{\lambda^2}{2\sqrt{2}}$	$-\frac{\lambda^2}{2\sqrt{2}}$	$-\frac{\lambda^2}{2\sqrt{2}}$	$-\frac{\lambda^2}{2\sqrt{2}}$	$-\frac{\lambda^2}{2\sqrt{2}}$	0
0	$D^+ \to K^{*0} K^+$	0	0	$-\frac{\lambda}{\sqrt{6}}$	$-\frac{\lambda}{\sqrt{6}}$	0	$-\frac{\lambda}{\sqrt{6}}$	$-\frac{\lambda}{\sqrt{6}}$	0	$\frac{\lambda}{\sqrt{6}}$	$-\frac{\lambda}{\sqrt{6}}$	$\frac{\lambda}{\sqrt{6}}$	0	$\frac{\lambda}{\sqrt{6}}$	$\frac{\lambda}{\sqrt{6}}$	$\frac{\lambda}{\sqrt{6}}$	$\frac{\lambda}{\sqrt{6}}$	$\frac{\lambda}{\sqrt{6}}$	$\frac{\lambda}{\sqrt{6}}$
0	$D^+ \to \omega_8 \pi^+$	0	$-\sqrt{\frac{3}{2}}\lambda$	$-\frac{\lambda}{\sqrt{6}}$	$-\frac{\lambda}{\sqrt{6}}$	$-\frac{3\lambda}{2\sqrt{2}}$	$-\frac{\lambda}{\sqrt{6}}$	$-\frac{\lambda}{\sqrt{6}}$	$-\sqrt{\frac{2}{3}}\lambda$	$-\frac{\lambda}{2\sqrt{6}}$	$\frac{\lambda}{2\sqrt{6}}$	$-\frac{\lambda}{\sqrt{6}}$	$-\sqrt{\frac{2}{3}}\lambda$	$-\frac{\lambda}{\sqrt{6}}$	$-\frac{\lambda}{2}\sqrt{\frac{3}{2}}$	$-\frac{\lambda}{2\sqrt{6}}$	$-\frac{\lambda}{2\sqrt{6}}$	$-\frac{\lambda}{2\sqrt{6}}$	$-\frac{\lambda}{\sqrt{6}}$
0	$D^+ \to \rho_0 \pi^+$	0	0	0	0	$-\frac{3\lambda}{2\sqrt{2}}$	0	0	0	0	0	0	0	0	$-\frac{3\lambda}{2}$	0	0	0	0
1	$D^+ \to K^{*0} \pi^+$	0	0	$-\frac{\lambda^2}{2}$	$-\frac{\lambda^2}{2}$	$\frac{3}{2}$	λ^2	0	$\frac{\lambda^2}{\sqrt{6}}$	$-\frac{\lambda^2}{2\sqrt{6}}$	$\frac{\lambda^2}{2\sqrt{6}}$	λ^2	$\frac{\lambda^2}{\sqrt{6}}$	$\frac{\lambda^2}{\sqrt{6}}$	$-\frac{3\lambda}{2\sqrt{2}}$	$-\frac{\lambda^2}{2\sqrt{6}}$	$-\frac{\lambda^2}{2\sqrt{6}}$	$-\frac{\lambda^2}{2\sqrt{6}}$	$-\frac{\lambda^2}{2\sqrt{6}}$
−1	$D^+ \to \bar{K}^{*0} \pi^+$	$\frac{3}{2}$	$\sqrt{\frac{3}{8}}$	$\frac{\lambda^2}{2\sqrt{6}}$	$\frac{\lambda^2}{2\sqrt{6}}$	0	$\frac{\lambda^2}{\sqrt{6}}$	$\frac{\lambda^2}{\sqrt{6}}$	$\sqrt{\frac{2}{3}}\lambda^2$	$\frac{\lambda^2}{2\sqrt{6}}$	$-\frac{\lambda^2}{2\sqrt{6}}$	$\frac{\lambda^2}{\sqrt{6}}$	$\sqrt{\frac{2}{3}}\lambda^2$	$\frac{\lambda^2}{2\sqrt{6}}$	$\frac{\lambda^2}{2\sqrt{6}}$	$\frac{\lambda^2}{2\sqrt{6}}$	$\frac{\lambda^2}{2\sqrt{6}}$	$\frac{\lambda^2}{2\sqrt{6}}$	$\frac{\lambda^2}{2\sqrt{6}}$
0	$D_s^+ \to \eta_8 K^{*+}$	0	$\sqrt{\frac{3}{8}}\lambda$	$\frac{\lambda}{2\sqrt{6}}$	$\frac{\lambda}{2\sqrt{6}}$	0	$\frac{\lambda}{\sqrt{6}}$	$\frac{\lambda}{\sqrt{6}}$	$\sqrt{\frac{2}{3}}\lambda$	$\frac{\lambda}{2\sqrt{6}}$	$-\frac{\lambda}{2\sqrt{6}}$	$\frac{\lambda}{\sqrt{6}}$	$\sqrt{\frac{2}{3}}\lambda$	$\frac{\lambda}{\sqrt{6}}$	$\frac{\lambda}{2\sqrt{6}}$	$\frac{\lambda}{2\sqrt{6}}$	$\frac{\lambda}{2\sqrt{6}}$	$\frac{\lambda}{2\sqrt{6}}$	$\sqrt{\frac{2}{3}}\lambda$
1	$D_s^+ \to \eta_8 K^{*+}$	$\frac{\lambda}{2}\sqrt{\frac{3}{2}}$	$\sqrt{\frac{3}{8}}\lambda$	$\frac{\lambda^2}{2\sqrt{6}}$	$\frac{\lambda^2}{2\sqrt{6}}$	0	$\frac{\lambda^2}{\sqrt{6}}$	$\frac{\lambda^2}{\sqrt{6}}$	$\sqrt{\frac{2}{3}}\lambda^2$	$\frac{\lambda^2}{2\sqrt{6}}$	$-\frac{\lambda^2}{2\sqrt{6}}$	$\frac{\lambda^2}{\sqrt{6}}$	$\sqrt{\frac{2}{3}}\lambda^2$	$\frac{\lambda^2}{2\sqrt{6}}$	$\frac{\lambda^2}{2\sqrt{6}}$	$\frac{\lambda^2}{2\sqrt{6}}$	$\frac{\lambda^2}{2\sqrt{6}}$	$\frac{\lambda^2}{2\sqrt{6}}$	$\frac{\lambda^2}{2\sqrt{6}}$
0	$D_s^+ \to K^0 \rho^+$	$-\frac{3\lambda}{2\sqrt{2}}$	$-\frac{3\lambda}{2\sqrt{2}}$	0	0	0	0	0	0	0	0	0	0	0	0	0	0	0	0
−1	$D_s^+ \to \pi_0 K^{*+}$	0	0	$-\frac{\lambda}{2\sqrt{6}}$	$-\frac{\lambda}{2\sqrt{6}}$	0	$-\frac{\lambda}{\sqrt{6}}$	$-\frac{\lambda}{\sqrt{6}}$	0	$\frac{\lambda}{2\sqrt{6}}$	$-\frac{\lambda}{2\sqrt{6}}$	$\frac{\lambda}{\sqrt{6}}$	0	$\frac{\lambda}{2\sqrt{6}}$	$\frac{\lambda}{2\sqrt{6}}$	$\frac{\lambda}{2\sqrt{6}}$	$\frac{\lambda}{2\sqrt{6}}$	$\frac{\lambda}{2\sqrt{6}}$	$\frac{\lambda}{2\sqrt{6}}$
1	$D_s^+ \to \pi_0 K^{*+}$	0	$-\frac{3\lambda}{2\sqrt{2}}$	$\frac{\lambda}{2\sqrt{2}}$	$\frac{\lambda}{2\sqrt{2}}$	0	$\frac{\lambda}{\sqrt{2}}$	$\frac{\lambda}{\sqrt{2}}$	0	$-\frac{\lambda}{2\sqrt{2}}$	$\frac{\lambda}{2\sqrt{2}}$	$-\frac{\lambda}{\sqrt{2}}$	0	$-\frac{\lambda}{2\sqrt{2}}$	$-\frac{\lambda}{2\sqrt{2}}$	$-\frac{\lambda}{2\sqrt{2}}$	$-\frac{\lambda}{2\sqrt{2}}$	$-\frac{\lambda}{2\sqrt{2}}$	0
−1	$D_s^+ \to \bar{K}^0 K^{*+}$	0	0	$-\frac{\lambda}{2\sqrt{6}}$	$-\frac{\lambda}{2\sqrt{6}}$	0	$-\frac{\lambda}{\sqrt{6}}$	$-\frac{\lambda}{\sqrt{6}}$	0	$\frac{\lambda}{2\sqrt{6}}$	$-\frac{\lambda}{2\sqrt{6}}$	$\frac{\lambda}{\sqrt{6}}$	0	$\frac{\lambda}{2\sqrt{6}}$	$\frac{\lambda}{2\sqrt{6}}$	$\frac{\lambda}{2\sqrt{6}}$	$\frac{\lambda}{2\sqrt{6}}$	$\frac{\lambda}{2\sqrt{6}}$	$\frac{\lambda}{2\sqrt{6}}$
0	$D_s^+ \to \omega_8 K^+$	$\frac{\lambda}{2}\sqrt{\frac{3}{2}}$	0	$-\frac{\lambda}{2\sqrt{6}}$	$-\frac{\lambda}{2\sqrt{6}}$	0	$-\frac{\lambda}{\sqrt{6}}$	$-\frac{\lambda}{\sqrt{6}}$	0	$-\frac{\lambda}{2\sqrt{6}}$	$\frac{\lambda}{2\sqrt{6}}$	$-\frac{\lambda}{\sqrt{6}}$	0	$-\frac{\lambda}{2\sqrt{6}}$	$-\frac{\lambda}{2\sqrt{6}}$	$-\frac{\lambda}{2\sqrt{6}}$	$-\frac{\lambda}{2\sqrt{6}}$	$-\frac{\lambda}{2\sqrt{6}}$	$-\frac{\lambda}{2\sqrt{6}}$
0	$D_s^+ \to \rho_0 K^+$	$-\frac{3\lambda}{2\sqrt{2}}$	0	$\frac{\lambda}{2\sqrt{2}}$	$\frac{\lambda}{2\sqrt{2}}$	0	$\frac{\lambda}{\sqrt{2}}$	$\frac{\lambda}{\sqrt{2}}$	0	$-\frac{\lambda}{2\sqrt{2}}$	$\frac{\lambda}{2\sqrt{2}}$	$-\frac{\lambda}{\sqrt{2}}$	0	$-\frac{\lambda}{2\sqrt{2}}$	$-\frac{\lambda}{2\sqrt{2}}$	$-\frac{\lambda}{2\sqrt{2}}$	$-\frac{\lambda}{2\sqrt{2}}$	$-\frac{\lambda}{2\sqrt{2}}$	0
1	$D_s^+ \to K^{*0} K^+$	0	0	$\frac{\lambda}{2\sqrt{6}}$	$\frac{\lambda}{2\sqrt{6}}$	0	$\frac{\lambda}{\sqrt{6}}$	$\frac{\lambda}{\sqrt{6}}$	0	$-\frac{\lambda}{2\sqrt{6}}$	$\frac{\lambda}{2\sqrt{6}}$	$-\frac{\lambda}{\sqrt{6}}$	0	$-\frac{\lambda}{2\sqrt{6}}$	$-\frac{\lambda}{2\sqrt{6}}$	$-\frac{\lambda}{2\sqrt{6}}$	$-\frac{\lambda}{2\sqrt{6}}$	$-\frac{\lambda}{2\sqrt{6}}$	$-\frac{\lambda}{2\sqrt{6}}$
−1	$D_s^+ \to \bar{K}^{*0} K^+$	$-\frac{1}{2}$	$-\frac{1}{\sqrt{6}}$	$\frac{1}{2}$	$\frac{1}{2}$	0	$\frac{1}{2}$	$\frac{1}{2}$	$\frac{1}{\sqrt{6}}$	$\frac{1}{2}$	$-\frac{1}{2}$	$\frac{1}{2}$	$\frac{1}{\sqrt{6}}$	$\frac{1}{2}$	$\frac{1}{2}$	$\frac{1}{2}$	$\frac{1}{2}$	$\frac{1}{2}$	$\frac{1}{\sqrt{6}}$
−1	$D_s^+ \to \omega_8 \pi^+$	0	$-\sqrt{\frac{3}{8}}$	$\frac{1}{\sqrt{6}}$	$\frac{1}{\sqrt{6}}$	0	$-\sqrt{\frac{2}{3}}$	$-\sqrt{\frac{2}{3}}$	$-\frac{1}{\sqrt{6}}$	$\frac{1}{\sqrt{6}}$	$-\frac{1}{\sqrt{6}}$	$-\sqrt{\frac{2}{3}}$	$-\frac{1}{\sqrt{6}}$	$\frac{1}{\sqrt{6}}$	$\frac{1}{\sqrt{6}}$	$\frac{1}{\sqrt{6}}$	$\frac{1}{\sqrt{6}}$	$\frac{1}{\sqrt{6}}$	$-\frac{1}{\sqrt{6}}$
0	$D_s^+ \to \rho_0 \pi^+$	$-\frac{3\lambda}{2\sqrt{2}}$	$-\frac{3\lambda}{2\sqrt{2}}$	0	0	$-\frac{3\lambda}{2\sqrt{2}}$	0	0	0	0	0	0	0	0	$-\frac{3\lambda}{2}$	0	0	0	0
1	$D_s^+ \to K^{*0} K^+$	0	0	$\frac{\lambda^2}{2\sqrt{6}}$	$\frac{\lambda^2}{2\sqrt{6}}$	0	$\frac{\lambda^2}{\sqrt{6}}$	$\frac{\lambda^2}{\sqrt{6}}$	$\sqrt{\frac{2}{3}}\lambda^2$	$\frac{\lambda^2}{2\sqrt{6}}$	$-\frac{\lambda^2}{2\sqrt{6}}$	$\frac{\lambda^2}{\sqrt{6}}$	$\sqrt{\frac{2}{3}}\lambda^2$	$\frac{\lambda^2}{2\sqrt{6}}$	$\frac{\lambda^2}{2\sqrt{6}}$	$\frac{\lambda^2}{2\sqrt{6}}$	$\frac{\lambda^2}{2\sqrt{6}}$	$\frac{\lambda^2}{2\sqrt{6}}$	$\frac{\lambda^2}{2\sqrt{6}}$
−1	$D_s^+ \to \bar{K}^{*0} K^+$	$\frac{1}{2}$	$\frac{1}{\sqrt{6}}$	$\frac{1}{2}$	$\frac{1}{2}$	0	$\frac{1}{2}$	$\frac{1}{2}$	$\frac{1}{\sqrt{6}}$	$\frac{1}{2}$	$-\frac{1}{2}$	$\frac{1}{2}$	$\frac{1}{\sqrt{6}}$	$\frac{1}{2}$	$\frac{1}{2}$	$\frac{1}{2}$	$\frac{1}{2}$	$\frac{1}{2}$	$\frac{1}{\sqrt{6}}$
−1	$D_s^+ \to \omega_8 \pi^+$	0	$-\sqrt{\frac{3}{8}}$	$\frac{1}{\sqrt{6}}$	$\frac{1}{\sqrt{6}}$	0	$-\sqrt{\frac{2}{3}}$	$-\sqrt{\frac{2}{3}}$	$-\frac{1}{\sqrt{6}}$	$\frac{1}{\sqrt{6}}$	$-\frac{1}{\sqrt{6}}$	$-\sqrt{\frac{2}{3}}$	$-\frac{1}{\sqrt{6}}$	$\frac{1}{\sqrt{6}}$	$\frac{1}{\sqrt{6}}$	$\frac{1}{\sqrt{6}}$	$\frac{1}{\sqrt{6}}$	$\frac{1}{\sqrt{6}}$	$-\frac{1}{\sqrt{6}}$
0	$D_s^+ \to \rho_0 \pi^+$	$-\frac{3\lambda}{2\sqrt{2}}$	$-\frac{3\lambda}{2\sqrt{2}}$	0	0	$-\frac{3\lambda}{2\sqrt{2}}$	0	0	0	0	0	0	0	0	$-\frac{3\lambda}{2}$	0	0	0	0

Table D.15: $D^+ \to P_8 V_8$ and $D_s^+ \to P_8 V_8$ $\mathcal{O}(\varepsilon)$ invariants generated by $\bar{\mathbf{15}}$.

REFERENCES

[1] **ATLAS Collaboration** Collaboration, G. Aad *et al.*, "Observation of a new particle in the search for the Standard Model Higgs boson with the ATLAS detector at the LHC," *Phys.Lett.* **B716** (2012) 1–29, arXiv:1207.7214 [hep-ex].

[2] **CMS Collaboration** Collaboration, S. Chatrchyan *et al.*, "Observation of a new boson at a mass of 125 GeV with the CMS experiment at the LHC," *Phys.Lett.* **B716** (2012) 30–61, arXiv:1207.7235 [hep-ex].

[3] **Particle Data Group** Collaboration, J. Beringer *et al.*, "The review of particle physics," *Phys Rev D* **86** (2012) 010001.

[4] N. Arkani-Hamed and Y. Grossman, "Light active and sterile neutrinos from compositeness," *Phys. Lett.* **B459** (1999) 179, hep-ph/9806223.

[5] **Planck Collaboration** Collaboration, P. Ade *et al.*, "Planck 2013 results. I. Overview of products and scientific results," arXiv:1303.5062 [astro-ph.CO].

[6] **LHCb collaboration** Collaboration, R. Aaij *et al.*, "Search for direct CP violation in $D^0 \to h^- h^+$ modes using semileptonic B decays," arXiv:1303.2614 [hep-ex].

[7] R. D. Peccei, "Composite models of quarks and leptons," in *Gauge Theories of the Eighties*, vol. 181, p. 355. Springer Berlin, 1983.

[8] M. E. Peskin, "Compositeness of quarks and leptons," in *Proceedings of the International Symposium on Lepton and Photon Interactions at High Energies*, W. Pfiel, ed., p. 880. Physikalisches Insitut, Unversität Bonn, 1981.

[9] S. Dimopoulos, S. Raby, and L. Susskind, "Light composite fermions," *Nucl. Phys. B* **173** no. 2, (1980) 208.

[10] S. Raby, S. Dimopoulos, and L. Susskind, "Tumbling gauge theories," *Nucl. Phys. B* **169** (1980) 373.

[11] O. Napoly, "On the validity of the complementarity principle for dynamically broken gauge theories," *Nucl. Phys. B* **198** (1982) 119.

[12] Y. Grossman and Y. Tsai, "Leptogenesis with composite neutrinos," *JHEP* **12** (2008) 016, arXiv: 0811.0871.

[13] T. Okui, "Searching for composite neutrinos in the cosmic microwave background," *JHEP* **09** (2005) 017, hep-ph/0405083.

[14] P. Langacker, "A mechanism for ordinary-sterile neutrino mixing," *Phys. Rev. D* **58** (1998) 093017, arXiv:hep-ph/9805281.

[15] D. A. Demir, L. L. Everett, and P. Langacker, "Dirac neutrino masses from generalized supersymmetry breaking," *Phys. Rev. Lett.* **100** no. 9, (2008) 091804.

[16] G. Marshall, M. McCaskey, and M. Sher, "A Supersymmetric Model with Dirac Neutrino Masses," *Phys. Rev. D* **81** (2010) 053006, arXiv:0912.1599.

[17] S. Abel, A. Dedes, and K. Tamvakis, "Naturally small Dirac neutrino masses in supergravity," *Phys. Rev. D* **71** (2005) 033003, arXiv:hep-ph/0402287.

[18] Y. Grossman and M. Neubert, "Neutrino masses and mixings in non-factorizable geometry," *Phys. Lett.* **B474** (2000) 361, hep-ph/9912408.

[19] N. Arkani-Hamed, S. Dimopoulos, G. Dvali, and J. March-Russell, "Neutrino masses from large extra dimensions," *Phys. Rev. D* **65** no. 2, (Dec, 2001) 024032.

[20] K. R. Dienes, E. Dudas, and T. Gherghetta, "Light neutrinos without heavy mass scales: A higher- dimensional seesaw mechanism," *Nucl. Phys.* **B557** (1999) 25, arXiv:hep-ph/9811428.

[21] P. Q. Hung, "A new mechanism for a naturally small Dirac neutrino mass," *Phys. Rev. D* **67** (2003) 095011, arXiv:hep-ph/0210131.

[22] T. Gherghetta, "Dirac neutrino masses with Planck scale lepton number violation," *Phys. Rev. Lett.* **92** (2004) 161601, hep-ph/0312392.

[23] H. Davoudiasl, R. Kitano, G. D. Kribs, and H. Murayama, "Models of neutrino mass with a low cutoff scale," *Phys. Rev. D* **71** (2005) 113004, arXiv:hep-ph/0502176.

[24] L. M. Krauss and F. Wilczek, "Discrete gauge symmetry in continuum theories," *Phys. Rev. Lett.* **62** no. 11, (Mar, 1989) 1221.

[25] I. Gogoladze and A. Perez-Lorenzana, "Small Dirac neutrino masses and R-parity from anomalous U(1) symmetry," *Phys. Rev. D* **65** (2002) 095011, arXiv:hep-ph/0112034.

[26] M.-C. Chen, A. de Gouvêa, and B. A. Dobrescu, "Gauge trimming of neutrino masses," *Phys. Rev. D* **75** no. 5, (2007) 055009.

[27] G. von Gersdorff and M. Quiros, "Conformal Neutrinos: an Alternative to the See-saw Mechanism," *Phys. Lett.* **B678** (2009) 317–321, arXiv:0901.0006 [hep-ph].

[28] G. 't Hooft, "Naturalness, chiral symmetry, and spontaneous chiral symmetry breaking," in *Recent developments in gauge theories*. Plenum Press, 1980.

[29] S. Weinberg, *The Quantum Theory of Fields: Volume II*. Cambridge University Press, 1996.

[30] C. T. Hill and E. H. Simmons, "Strong dynamics and electroweak symmetry breaking," *Phys. Rept.* **381** (2003) 235–402, arXiv:hep-ph/0203079.

[31] C. Amsler et al. (Particle Data Group), "Review of particle physics," *Phys. Lett.* **B667** (2008) 1.

[32] S. Dodelson and L. M. Widrow, "Sterile Neutrinos as Dark Matter," *Phys. Rev. Lett.* **72** (1994) 17–20, arXiv:hep-ph/9303287.

[33] T. Asaka, S. Blanchet, and M. Shaposhnikov, "The [nu]msm, dark matter and neutrino masses," *Phys. Lett.* **B631** no. 4, (2005) 151.

[34] T. Asaka, M. Shaposhnikov, and A. Kusenko, "Opening a new window for warm dark matter," *Phys. Lett.* **B638** (2006) 401, arXiv:hep-ph/0602150.

[35] A. Kusenko, "Sterile neutrinos: The Dark side of the light fermions," *Phys.Rept.* **481** (2009) 1–28, arXiv:0906.2968 [hep-ph].

[36] M. Loewenstein and A. Kusenko, "Dark Matter Search Using Chandra Observations of Willman 1, and a Spectral Feature Consistent with a

Decay Line of a 5 keV Sterile Neutrino," *Astrophys. J.* **714** (2010) 652, arXiv:0912.0552 [astro-ph.HE].

[37] L. J. Hall, K. Jedamzik, J. March-Russell, and S. M. West, "Freeze-In Production of FIMP Dark Matter," *JHEP* **1003** (2010) 080, arXiv:0911.1120 [hep-ph].

[38] S. Antusch, C. Biggio, E. Fernandez-Martinez, M. B. Gavela, and J. Lopez-Pavon, "Unitarity of the Leptonic Mixing Matrix," *JHEP* **10** (2006) 084, arXiv:hep-ph/0607020.

[39] C. Giunti, C. W. Kim, and U. W. Lee, "Remarks on the weak states of neutrinos," *Phys. Rev. D* **45** no. 7, (Apr, 1992) 2414.

[40] P. Langacker and D. London, "Lepton-number violation and massless nonorthogonal neutrinos," *Phys. Rev. D* **38** no. 3, (Aug, 1988) 907.

[41] K. A. Olive and M. S. Turner, "Cosmological bounds on the masses of stable, right-handed neutrinos," *Phys. Rev. D* **25** (Jan, 1982) 213–216. http://link.aps.org/doi/10.1103/PhysRevD.25.213.

[42] S. Dodelson and L. M. Widrow, "Sterile neutrinos as dark matter," *Phys. Rev. Lett.* **72** (Jan, 1994) 17–20. http://link.aps.org/doi/10.1103/PhysRevLett.72.17.

[43] X.-D. Shi and G. M. Fuller, "A New dark matter candidate: Nonthermal sterile neutrinos," *Phys.Rev.Lett.* **82** (1999) 2832–2835, arXiv:astro-ph/9810076 [astro-ph].

[44] K. Abazajian, G. M. Fuller, and M. Patel, "Sterile neutrino hot, warm, and cold dark matter," *Phys. Rev. D* **64** (May, 2001) 023501. http://link.aps.org/doi/10.1103/PhysRevD.64.023501.

[45] A. Dolgov and S. Hansen, "Massive sterile neutrinos as warm dark matter," *Astropart.Phys.* **16** (2002) 339–344, arXiv:hep-ph/0009083 [hep-ph].

[46] P. L. Biermann and A. Kusenko, "Relic keV sterile neutrinos and reionization," *Phys.Rev.Lett.* **96** (2006) 091301, arXiv:astro-ph/0601004 [astro-ph].

[47] A. Boyarsky, A. Neronov, O. Ruchayskiy, M. Shaposhnikov, and

I. Tkachev, "Where to find a dark matter sterile neutrino?," *Phys.Rev.Lett.* **97** (2006) 261302, arXiv:astro-ph/0603660 [astro-ph].

[48] D. Boyanovsky and C. Ho, "Sterile neutrino production via active-sterile oscillations: The Quantum Zeno effect," *JHEP* **0707** (2007) 030, arXiv:hep-ph/0612092 [hep-ph].

[49] T. Asaka, M. Shaposhnikov, and M. Laine, "Lightest sterile neutrino abundance within the œ msm," *Journal of High Energy Physics* **2007** no. 01, (2007) 091. http://stacks.iop.org/1126-6708/2007/i=01/a=091.

[50] D. Aristizabal Sierra, J. Kubo, D. Restrepo, D. Suematsu, and O. Zapata, "Radiative seesaw: Warm dark matter, collider and lepton flavour violating signals," *Phys.Rev.* **D79** (2009) 013011, arXiv:0808.3340 [hep-ph].

[51] M. Laine and M. Shaposhnikov, "Sterile neutrino dark matter as a consequence of nuMSM-induced lepton asymmetry," *JCAP* **0806** (2008) 031, arXiv:0804.4543 [hep-ph].

[52] J. Wu, C.-M. Ho, and D. Boyanovsky, "Sterile neutrinos produced near the EW scale. I. Mixing angles, MSW resonances and production rates," *Phys.Rev.* **D80** (2009) 103511, arXiv:0902.4278 [hep-ph].

[53] G. B. Gelmini, E. Osoba, and S. Palomares-Ruiz, "Inert-Sterile Neutrino: Cold or Warm Dark Matter Candidate," *Phys.Rev.* **D81** (2010) 063529, arXiv:0912.2478 [hep-ph].

[54] A. Boyarsky, O. Ruchayskiy, and M. Shaposhnikov, "The Role of sterile neutrinos in cosmology and astrophysics," *Ann.Rev.Nucl.Part.Sci.* **59** (2009) 191–214, arXiv:0901.0011 [hep-ph].

[55] H. de Vega and N. Sanchez, "Model independent analysis of dark matter points to a particle mass at the keV scale," *Mon.Not.Roy.Astron.Soc.* **404** (2010) 885, arXiv:0901.0922 [astro-ph.CO].

[56] H. de Vega, P. Salucci, and N. Sanchez, "The mass of the dark matter particle from theory and observations," *New Astron.* **17** (2012) 653–666, arXiv:1004.1908 [astro-ph.CO].

[57] H. de Vega and N. Sanchez, "Warm dark matter in the galaxies:theoretical

and observational progresses. Highlights and conclusions of the chalonge meudon workshop 2011," arXiv:1109.3187 [astro-ph.CO].

[58] T. Araki and Y. Li, "Q_6 flavor symmetry model for the extension of the minimal standard model by three right-handed sterile neutrinos," *Phys.Rev.* **D85** (2012) 065016, arXiv:1112.5819 [hep-ph].

[59] C.-S. Chen and R. Takahashi, "Hierarchically Acting Sterile Neutrinos," arXiv:1112.2102 [hep-ph].

[60] A. Merle and V. Niro, "Deriving Models for keV sterile Neutrino Dark Matter with the Froggatt-Nielsen mechanism," *JCAP* **1107** (2011) 023, arXiv:1105.5136 [hep-ph].

[61] C.-Q. Geng and R. Takahashi, "Magnetic dipole moment and keV neutrino dark matter," *Phys.Lett.* **B710** (2012) 324–327, arXiv:1201.1534 [hep-ph].

[62] P. Bode, J. P. Ostriker, and N. Turok, "Halo formation in warm dark matter models," *Astrophys.J.* **556** (2001) 93–107, arXiv:astro-ph/0010389 [astro-ph].

[63] J. Zavala, Y. Jing, A. Faltenbacher, G. Yepes, Y. Hoffman, *et al.*, "The velocity function in the local environment from LCDM and LWDM constrained simulations," *Astrophys.J.* **700** (2009) 1779–1793, arXiv:0906.0585 [astro-ph.CO].

[64] A. Kusenko and G. Segre, "Neutral current induced neutrino oscillations in a supernova," *Phys.Lett.* **B396** (1997) 197–200, arXiv:hep-ph/9701311 [hep-ph].

[65] A. Boyarsky, D. Iakubovskyi, O. Ruchayskiy, and V. Savchenko, "Constraints on decaying Dark Matter from XMM-Newton observations of M31," *Mon.Not.Roy.Astron.Soc.* **387** (2008) 1361, arXiv:0709.2301 [astro-ph].

[66] A. Boyarsky, J. Lesgourgues, O. Ruchayskiy, and M. Viel, "Lyman-alpha constraints on warm and on warm-plus-cold dark matter models," *JCAP* **0905** (2009) 012, arXiv:0812.0010 [astro-ph].

[67] S. Das and K. Sigurdson, "Cosmological Limits on Hidden Sector Dark

Matter," *Phys.Rev.* **D85** (2012) 063510, arXiv:1012.4458 [astro-ph.CO].

[68] C. R. Watson, Z. Li, and N. K. Polley, "Constraining Sterile Neutrino Warm Dark Matter with Chandra Observations of the Andromeda Galaxy," arXiv:1111.4217 [astro-ph.CO].

[69] M. Shaposhnikov and I. Tkachev, "The nuMSM, inflation, and dark matter," *Phys.Lett.* **B639** (2006) 414–417, arXiv:hep-ph/0604236 [hep-ph].

[70] A. Anisimov, Y. Bartocci, and F. L. Bezrukov, "Inflaton mass in the nuMSM inflation," *Phys.Lett.* **B671** (2009) 211–215, arXiv:0809.1097 [hep-ph].

[71] F. Bezrukov, H. Hettmansperger, and M. Lindner, "kev sterile neutrino dark matter in gauge extensions of the standard model," *Phys. Rev. D* **81** (Apr, 2010) 085032.

[72] W. Liao, "keV scale ν_R dark matter and its detection in β decay experiment," *Phys.Rev.* **D82** (2010) 073001, arXiv:1005.3351 [hep-ph].

[73] A. Boyarsky, J. Nevalainen, and O. Ruchayskiy, "Constraints on the parameters of radiatively decaying dark matter from the dark matter halo of the Milky Way and Ursa Minor," *Astron.Astrophys.* **471** (2007) 51–57, arXiv:astro-ph/0610961 [astro-ph].

[74] A. Boyarsky, A. Neronov, O. Ruchayskiy, and M. Shaposhnikov, "Restrictions on parameters of sterile neutrino dark matter from observations of galaxy clusters," *Phys. Rev. D* **74** (Nov, 2006) 103506. http://link.aps.org/doi/10.1103/PhysRevD.74.103506.

[75] K. L. McDonald, "Light Neutrinos from a Mini-Seesaw Mechanism in Warped Space," *Phys.Lett.* **B696** (2011) 266–272, arXiv:1010.2659 [hep-ph].

[76] M. Duerr, D. P. George, and K. L. McDonald, "Neutrino Mass and $\mu \to e + \gamma$ from a Mini-Seesaw," *JHEP* **1107** (2011) 103, arXiv:1105.0593 [hep-ph].

[77] E. Farhi and L. Susskind, "Technicolour," *Phys. Rept.* **74** no. 3, (1981) 277.

[78] Y. Grossman and D. J. Robinson, "Composite Dirac Neutrinos," *JHEP* **1101** (2011) 132, arXiv:1009.2781 [hep-ph].

[79] R. Hundi and S. Roy, "Constraints on composite Dirac neutrinos from observations of galaxy clusters," *Phys.Lett.* **B702** (2011) 228–234, arXiv:1105.0291 [hep-ph].

[80] M. Loewenstein and A. Kusenko, "Dark Matter Search Using XMM-Newton Observations of Willman 1," *Astrophys.J.* **751** (2012) 82, arXiv:1203.5229 [astro-ph.CO].

[81] A. Rajaraman, W. Shepherd, T. M. Tait, and A. M. Wijangco, "Lhc bounds on interactions of dark matter," 1108.1196v1. http://arxiv.org/abs/1108.1196v1.

[82] P. J. Fox, R. Harnik, J. Kopp, and Y. Tsai, "Missing energy signatures of dark matter at the lhc," 1109.4398v1. http://arxiv.org/abs/1109.4398v1.

[83] U. Seljak, A. Makarov, P. McDonald, and H. Trac, "Can sterile neutrinos be the dark matter?," *Phys.Rev.Lett.* **97** (2006) 191303, arXiv:astro-ph/0602430 [astro-ph].

[84] A. Kusenko, "Sterile neutrinos, dark matter, and the pulsar velocities in models with a Higgs singlet," *Phys.Rev.Lett.* **97** (2006) 241301, arXiv:hep-ph/0609081 [hep-ph].

[85] K. Petraki and A. Kusenko, "Dark-matter sterile neutrinos in models with a gauge singlet in the Higgs sector," *Phys.Rev.* **D77** (2008) 065014, arXiv:0711.4646 [hep-ph].

[86] T. DeGrand and K. Kajantie, "Supercooling, entropy production, and bubble kinetics in the quark-hadron phase transition in the early universe," *Phys. Lett. B* **147** no. 4, (1984) 273 – 278.

[87] T. Csorgo and L. Csernai, "Quark - gluon plasma freezeout from a supercooled state?," *Phys.Lett.* **B333** (1994) 494–499, arXiv:hep-ph/9406365 [hep-ph].

[88] **WMAP Collaboration** Collaboration, E. Komatsu *et al.*, "Seven-Year Wilkinson Microwave Anisotropy Probe (WMAP) Observations:

Cosmological Interpretation," *Astrophys.J.Suppl.* **192** (2011) 18, arXiv:1001.4538 [astro-ph.CO].

[89] B. Benson, T. de Haan, J. Dudley, C. Reichardt, K. Aird, *et al.*, "Cosmological Constraints from Sunyaev-Zel'dovich-Selected Clusters with X-ray Observations in the First 178 Square Degrees of the South Pole Telescope Survey," arXiv:1112.5435 [astro-ph.CO].

[90] B. Pontecorvo, "Neutrino experiments and the problem of conservation of leptonic charge," *Sov. Phys. JETP* **26** (1968) 984.

[91] S. M. Bilenky and B. Pontecorvo, "Lepton mixing and neutrino oscillations," *Phys. Rept.* **41** no. 4, (1978) 225.

[92] B. Kayser, "On the quantum mechanics of neutrino oscillation," *Phys. Rev. D* **24** no. 1, (1981) 110.

[93] C. Giunti, C. W. Kim, and U. W. Lee, "When do neutrinos really oscillate? quantum mechanics of neutrino oscillations," *Phys. Rev. D* **44** no. 11, (1991) 3635.

[94] C. Giunti, C. W. Kim, and U. W. Lee, "Remarks on the weak states of neutrinos," *Phys. Rev. D* **45** no. 7, (Apr, 1992) 2414.

[95] H. J. Lipkin, "Theories of non-experiments in coherent decays of neutral mesons," *Phys. Lett. B* **348** (1995) 604.

[96] K. Kiers, S. Nussinov, and N. Weiss, "Coherence effects in neutrino oscillations," *Phys. Rev.* **D53** (1996) 537, arXiv:hep-ph/9506271.

[97] Y. Grossman and H. J. Lipkin, "Flavor oscillations from a spatially localized source: A simple general treatment," *Phys. Rev.* **D55** (1997) 2760, arXiv:hep-ph/9607201.

[98] H. J. Lipkin, "Quantum mechanics of neutrino oscillations: Hand waving for pedestrians," 1999.

[99] C. Giunti and C. W. Kim, "Quantum mechanics of neutrino oscillations," *Found. Phys. Lett.* **14** (2001) 213, arXiv:hep-ph/0011074.

[100] C. Giunti, "Neutrino wave packets in quantum field theory," *JHEP* **11** (2002) 017, arXiv:hep-ph/0205014.

[101] M. Beuthe, "Towards a unique formula for neutrino oscillations in vacuum," *Phys. Rev.* **D66** (2002) 013003, arXiv:hep-ph/0202068.

[102] S. M. Bilenky, F. von Feilitzsch, and W. Potzel, "Neutrino oscillations and uncertainty relations," 2011.

[103] J. Rich, "Quantum mechanics of neutrino oscillations," *Phys. Rev. D* **48** no. 9, (Nov, 1993) 4318.

[104] C. Giunti, C. W. Kim, J. A. Lee, and U. W. Lee, "On the treatment of neutrino oscillations without resort to weak eigenstates," *Phys. Rev.* **D48** (1993) 4310–4317, arXiv:hep-ph/9305276.

[105] W. Grimus and P. Stockinger, "Real Oscillations of Virtual Neutrinos," *Phys. Rev.* **D54** (1996) 3414–3419, arXiv:hep-ph/9603430.

[106] C. Giunti, C. W. Kim, and U. W. Lee, "When do neutrinos cease to oscillate?," *Phys. Lett.* **B421** (1998) 237–244, arXiv:hep-ph/9709494.

[107] J. Campagne, "Neutrino oscillations from pion decay in flight," *Phys. Lett. B* **400** (1997) 135.

[108] W. Grimus, P. Stockinger, and S. Mohanty, "Field-theoretical approach to coherence in neutrino oscillations," *Phys. Rev. D* **59** no. 1, (1998) 013011.

[109] A. Ioannisian and A. Pilaftsis, "Neutrino oscillations in space within a solvable model," *Phys. Rev. D* **59** no. 5, (1999) 053003.

[110] P. Stockinger, "Introduction to a field-theoretical treatment of neutrino oscillations," *Pramana* **54** (2000) 203–214.

[111] I. Yu. Kobzarev, B. V. Martem'yanov, L. B. Okun, and M. G. Shchepkin, "Sum rules in neutrino oscillations," *Sov. J. Nucl. Phys.* **35** no. 5, (1982) 708.

[112] E. Alfinito, M. Blasone, A. Iorio, and G. Vitiello, "Squeezed neutrino oscillations in quantum field theory," *Physics Letters B* **362** no. 1, (1995) 91.

[113] M. Blasone, P. A. Henning, and G. Vitiello, "The exact formula for neutrino oscillations," *Phys. Lett. B* **451** (1999) 140.

[114] M. Binger and C.-R. Ji, "Quantum field theory of meson mixing," *Phys. Rev.* **D60** (1999) 056005, arXiv:hep-ph/9901407.

[115] M. Blasone, A. Capolupo, O. Romei, and G. Vitiello, "Quantum field theory of boson mixing," *Phys. Rev.* **D63** (2001) 125015, arXiv:hep-ph/0102048.

[116] M. Blasone, A. Capolupo, and G. Vitiello, "Quantum field theory of three flavor neutrino mixing and oscillations with CP violation," *Phys. Rev.* **D66** (2002) 025033, arXiv:hep-th/0204184.

[117] Y. F. Li and Q. Y. Liu, "A paradox on quantum field theory of neutrino mixing and oscillations," *JHEP* **10** (2006) 048, arXiv:hep-ph/0604069.

[118] A. G. Cohen, S. L. Glashow, and Z. Ligeti, "Disentangling neutrino oscillations," *Phys. Lett. B* **678** no. 2, (2009) 191.

[119] B. D. Keister and W. N. Polyzou, "Relativistic quantum theories and neutrino oscillations," *Phys. Scr.* **81** (2010) 055102.

[120] M. Dvornikov, "Field theory description of neutrino oscillations," 2010.

[121] K. Nakamura *et al.* (Particle Data Group), "2010 review of particle physics," *J. Phys. G* **37** (2010) 075021.

[122] M. Beuthe, "Oscillations of neutrinos and mesons in quantum field theory," *Phys. Rept.* **375** (2003) 105–218, arXiv:hep-ph/0109119.

[123] E. K. Akhmedov and J. Kopp, "Neutrino oscillations: Quantum mechanics vs. quantum field theory," *JHEP* **04** (2010) 008, arXiv:1001.4815 [hep-ph].

[124] G. C. Branco, L. Lavoura, and J. P. Silva, *CP Violation*. Oxford University Press, 1999.

[125] I. I. Bigi and A. I. Sanda, *CP Violation*. Cambridge University Press, 2009.

[126] S. Weinberg, *The Quantum Theory of Fields Vol II*. Cambridge University Press, 1996.

[127] J. Zinn-Justin, *Quantum Field Theory and Critical Phenomena*. Oxford University Press, 2002.

[128] Y. Grossman, M. Martone, and J. P. Silva *in preparation* (2011) .

[129] A. Pilaftisis, "Resonant cp violation induced by particle mixing in transition amplitudes," *Nucl. Phys. B* **504** (1997) 61–107, arXiv:hep-ph/9702393.

[130] H.-J. He, N. Polonsky, and S.-F. Su, "Extra families, higgs spectrum and oblique corrections," *Phys. Rev. D* **64** no. 053004, (2001) , arXiv:hep-ph/0102144.

[131] G. D. Kribs, T. Plehn, M. Spannowsky, and T. M. P. Tait, "Four generations and higgs physics," *Phys. Rev. D* **76** no. 075016, (2007) , arXiv:hep-ph/0706.3718.

[132] P. Q. Hung and M. Sher, "Experimental constraints on fourth quark masses," *Phys. Rev. D* **77** no. 037302, (2008) , arXiv:hep-ph/0711.4353.

[133] B. C. Allanach, C. G. Lester, M. A. Parker, and B. R. Webber, "Measuring sparticle masses in non-universal string inspired models at the lhc," *JHEP* **09** (2000) 004, arXiv:hep-ph/0007009.

[134] I. Hinchliffe, F. E. Paige, M. P. Shapiro, J. Soderqvist, and W. Yao, "Precision susy measurements at cern lhc," *Phys. Rev. D* **55** (1997) 5520–5540, arXiv:hep-ph/9610544.

[135] P. Meade and M. Reece, "Two partners at the lhc: Spin and mass measurement," *Phys. Rev. D* **74** (2006) 015010, arXiv:hep-ph/0601124.

[136] B. K. Gjelsten, D. J. Miller, P. Osland, and A. R. Raklev, "Mass determination in cascade decays using shape formulas," *AIP Conf. Proc.* **903** (2007) 257–260, arXiv:hep-ph/0611259.

[137] M. Burns, K. T. Matchev, and M. Park, "Using kinematic boundary lines for particles mass measurements and disambiguation in susy-like events with missing energy," *JHEP* **05** (2009) 094, arXiv:0903.4371 [hep-ph].

[138] C. G. Lester, M. A. Parker, and M. J. White, "Three body kinematic endpoints in susy models with non-universal higgs masses," *JHEP* **10** (2007) 051, arXiv:hep-ph/0609298.

[139] G. W. et al., "Physics interplay of the lhc and the ilc," *Phys. Rept.* **426** (2006) 47–358, arXiv:hep-ph/0410364.

[140] A. J. Barr and C. G. Lester, "A review of the mass measurement techiniques proposed for the large hadron collider," *J. Phys. G* **37** (2010) 123001, arXiv:1004.2732 [hep-ph].

[141] B. K. Gjelsten, D. J. Miller, and P. Osland, "Measurement of susy masses via cascade decays for sps 1a," *JHEP* **12** (2004) 003, arXiv:hep-ph/0410303.

[142] B. K. Gjelsten, D. J. Miller, and P. Osland, "Measurement of the gluino mass via cascade decays for sps 1a," *JHEP* **06** (2005) 015, arXiv:hep-ph/0501033.

[143] B. K. Gjelsten, D. J. Miller, P. Osland, and A. R. Raklev, "Mass determination in cascade decays using shape formulas," *AIP Conf. Proc.* **903** (2007) 257–260, arXiv:hep-ph/0611259.

[144] C. G. Lester, M. A. Parker, and M. J. White, "Determing susy model parameters and masses at the lhc using cross-sections, kinematic edges and other observables," *JHEP* **01** (2006) 080, arXiv:hep-ph/0508143.

[145] F. E. Paige, "Determining susy particle masses at lhc," arXiv:hep-ph/9609373.

[146] D. J. Miller, P. Osland, and A. R. Raklev, "Invariant mass distributions in cascade decays," *JHEP* **03** (2006) 034, arXiv:hep-ph/0510356.

[147] N. Arkani-Hamed, H.-C. Cheng, J. L. Feng, and L. J. Hall, "Probing Lepton Flavor Violation at Future Colliders," *Phys. Rev. Lett.* **77** (1996) 1937–1940, arXiv:hep-ph/9603431.

[148] N. Arkani-Hamed, J. L. Feng, L. J. Hall, and H.-C. Cheng, "CP violation from slepton oscillations at the LHC and NLC," *Nucl. Phys.* **B505** (1997) 3, arXiv:hep-ph/9704205.

[149] J. Hisano, R. Kitano, and M. M. Nojiri, "Slepton oscillation at large hadron collider," *Phys.Rev.* **D65** (2002) 116002, arXiv:hep-ph/0202129 [hep-ph].

[150] J. L. Feng, C. G. Lester, Y. Nir, and Y. Shadmi, "The Standard Model and Supersymmetric Flavor Puzzles at the Large Hadron Collider," *Phys. Rev.* **D77** (2008) 076002, arXiv:0712.0674 [hep-ph].

[151] G. Hiller, Y. Hochberg, and Y. Nir, "Flavor Changing Processes in Supersymmetric Models with Hybrid Gauge- and Gravity-Mediation," *JHEP* **03** (2009) 115, arXiv:0812.0511 [hep-ph].

[152] K. Agashe and M. Graesser, "Signals of supersymmetric lepton flavor violation at the CERN LHC," *Phys.Rev.* **D61** (2000) 075008, arXiv:hep-ph/9904422 [hep-ph].

[153] I. Hinchliffe and F. Paige, "Lepton flavor violation at the CERN LHC," *Phys.Rev.* **D63** (2001) 115006, arXiv:hep-ph/0010086 [hep-ph].

[154] R. Kitano, "A Clean Slepton Mixing Signal at the LHC," *JHEP* **0803** (2008) 023, arXiv:0801.3486 [hep-ph].

[155] J. L. Feng, S. T. French, C. G. Lester, Y. Nir, and Y. Shadmi, "The Shifted Peak: Resolving Nearly Degenerate Particles at the LHC," *Phys.Rev.* **D80** (2009) 114004, arXiv:0906.4215 [hep-ph].

[156] J. L. Feng, S. T. French, I. Galon, C. G. Lester, Y. Nir, *et al.*, "Measuring Slepton Masses and Mixings at the LHC," *JHEP* **1001** (2010) 047, arXiv:0910.1618 [hep-ph].

[157] I. Galon and Y. Shadmi, "Kinematic Edges with Flavor Splitting and Mixing," arXiv:1108.2220 [hep-ph].

[158] L.-T. Wang and I. Yavin, "A Review of Spin Determination at the LHC," *Int. J. Mod. Phys.* **A23** (2008) 4647, arXiv:0802.2726 [hep-ph].

[159] A. M. Badalyan, L. P. Kok, M. I. Polikarpov, and Y. A. Simonov, "Resonances in coupled channels in nuclear and particle physics," *Physics Reports* **82** no. 2, (1982) 31.

[160] S. U. Chung, J. Brose, R. Hackmann, E. Klempt, S. Spanier, and C. Strassburger, "Partial wave analysis in k-matrix formalism," *Annalen der Physik* **507** no. 5, (1995) 404.

[161] **CDF Collaboration** Collaboration, T. Aaltonen *et al.*, "Measurement of *cp*-violating asymmetries in $D^0 \to \pi^+\pi^-$ and $D^0 \to k^+k^-$ decays at cdf," *Phys. Rev. D* **85** (Jan, 2012) 012009.

[162] **CDF Collaboration** Collaboration, T. Aaltonen *et al.*, "Measurement of

the difference in *cp*-violating asymmetries in $D^0 \to k^+k^-$ and $D^0 \to \pi^+\pi^-$ decays at cdf," *Phys. Rev. Lett.* **109** (Sep, 2012) 111801.

[163] **LHCb Collaboration** Collaboration, R. Aaij *et al.*, "Evidence for CP violation in time-integrated $D^0 \to h^-h^+$ decay rates," *Phys.Rev.Lett.* **108** (2012) 111602, arXiv:1112.0938 [hep-ex].

[164] **Belle Collaboration** Collaboration, M. Staric *et al.*, "Measurement of CP asymmetry in Cabibbo suppressed D^0 decays," *Phys.Lett.* **B670** (2008) 190–195, arXiv:0807.0148 [hep-ex].

[165] **Belle Collaboration** Collaboration, M. Staric *et al.*, "Evidence for D^0 - $\bar{D}^0$ Mixing," *Phys.Rev.Lett.* **98** (2007) 211803, arXiv:hep-ex/0703036 [hep-ex].

[166] **BABAR Collaboration** Collaboration, B. Aubert *et al.*, "Measurement of D^0 - $\bar{D}^0$ mixing using the ratio of lifetimes for the decays $D^0 \to K^-\pi^+$, K^-K^+, and $\pi^-\pi^+$," *Phys.Rev.* **D78** (2008) 011105, arXiv:0712.2249 [hep-ex].

[167] **BaBar Collaboration** Collaboration, B. Aubert *et al.*, "Search for CP violation in the decays $D^0 \to K^-K^+$ and $D^0 \to \pi^-\pi^+$," *Phys.Rev.Lett.* **100** (2008) 061803, arXiv:0709.2715 [hep-ex].

[168] K. Wang and G. Zhu, "Can Up FCNC solve the ΔA_{CP} puzzle?," *Phys.Lett.* **B709** (2012) 362–365, arXiv:1111.5196 [hep-ph].

[169] C.-H. Chen, C.-Q. Geng, and W. Wang, "CP violation in $D^0 \to (K^-K^+, \pi^-\pi^+)$ from diquarks," *Phys.Rev.* **D85** (2012) 077702, arXiv:1202.3300 [hep-ph].

[170] G. F. Giudice, G. Isidori, and P. Paradisi, "Direct CP violation in charm and flavor mixing beyond the SM," *JHEP* **1204** (2012) 060, arXiv:1201.6204 [hep-ph].

[171] **LHCb collaboration** Collaboration, I. Bediaga *et al.*, "Implications of LHCb measurements and future prospects," arXiv:1208.3355 [hep-ex].

[172] G. Isidori, J. F. Kamenik, Z. Ligeti, and G. Perez, "Implications of the LHCb Evidence for Charm CP Violation," *Phys.Lett.* **B711** (2012) 46–51, arXiv:1111.4987 [hep-ph].

[173] X. Chang, M.-K. Du, C. Liu, J.-S. Lu, and S. Yang, "LHCb $\triangle A_{CP}$ of D Meson and R-Parity Violation," arXiv:1201.2565 [hep-ph].

[174] Y. Grossman, A. L. Kagan, and Y. Nir, "New physics and CP violation in singly Cabibbo suppressed D decays," *Phys.Rev.* **D75** (2007) 036008, arXiv:hep-ph/0609178 [hep-ph].

[175] W. Altmannshofer, R. Primulando, C.-T. Yu, and F. Yu, "New Physics Models of Direct CP Violation in Charm Decays," *JHEP* **1204** (2012) 049, arXiv:1202.2866 [hep-ph].

[176] Y. Hochberg and Y. Nir, "Relating direct CP violation in D decays and the forward-backward asymmetry in $t\bar{t}$ production," *Phys.Rev.Lett.* **108** (2012) 261601, arXiv:1112.5268 [hep-ph].

[177] T. Feldmann, S. Nandi, and A. Soni, "Repercussions of Flavour Symmetry Breaking on CP Violation in D-Meson Decays," *JHEP* **1206** (2012) 007, arXiv:1202.3795 [hep-ph].

[178] G. Isidori and J. F. Kamenik, "Shedding light on CP violation in the charm system via D to V gamma decays," arXiv:1205.3164 [hep-ph].

[179] Y. Grossman, A. L. Kagan, and J. Zupan, "Testing for new physics in singly Cabibbo suppressed D decays," *Phys.Rev.* **D85** (2012) 114036, arXiv:1204.3557 [hep-ph].

[180] M. Golden and B. Grinstein, "Enhanced cp violations in hadronic charm decays," *Physics Letters B* **222** no. 3–4, (1989) 501 – 506.

[181] F. Buccella, M. Lusignoli, G. Miele, A. Pugliese, and P. Santorelli, "Nonleptonic weak decays of charmed mesons," *Phys.Rev.* **D51** (1995) 3478–3486, arXiv:hep-ph/9411286 [hep-ph].

[182] J. Brod, Y. Grossman, A. L. Kagan, and J. Zupan, "A consistent picture for large penguins in $D \to pi^+pi^-$, K^+K^-," arXiv:1203.6659 [hep-ph].

[183] H.-n. Li, C.-D. Lu, and F.-S. Yu, "Branching ratios and direct CP asymmetries in $D \to PP$ decays," *Phys.Rev.* **D86** (2012) 036012, arXiv:1203.3120 [hep-ph].

[184] E. Franco, S. Mishima, and L. Silvestrini, "The Standard Model confronts

CP violation in $D^0 \to \pi^+\pi^-$ and $D^0 \to K^+K^-$," *JHEP* **1205** (2012) 140, arXiv:1203.3131 [hep-ph].

[185] D. Pirtskhalava and P. Uttayarat, "CP Violation and Flavor SU(3) Breaking in D-meson Decays," *Phys.Lett.* **B712** (2012) 81–86, arXiv:1112.5451 [hep-ph].

[186] B. Bhattacharya, M. Gronau, and J. L. Rosner, "Direct CP Violation in D Decays in view of LHCb and CDF Results," arXiv:1207.0761 [hep-ph].

[187] H.-Y. Cheng and C.-W. Chiang, "SU(3) symmetry breaking and CP violation in $D \to PP$ decays," arXiv:1205.0580 [hep-ph].

[188] G. Hiller, M. Jung, and S. Schacht, "SU(3)-Flavor Anatomy of Non-Leptonic Charm Decays," arXiv:1211.3734 [hep-ph].

[189] M. J. Savage, "Su(3) violations in the nonleptonic decay of charmed hadrons," *Physics Letters B* **257** no. 3–4, (1991) 414 – 418.

[190] K. Waikwok and S. Rosen, "Minimal breaking of flavor su (3) in nonleptonic charm decay," *Physics Letters B* **298** no. 3–4, (1993) 413.

[191] I. Hinchliffe and T. A. Kaeding, "Nonleptonic two-body decays of D mesons in broken SU(3)," *Phys.Rev.* **D54** (1996) 914–928, arXiv:hep-ph/9502275 [hep-ph].

[192] A. J. Buras, "Weak Hamiltonian, CP violation and rare decays," arXiv:hep-ph/9806471 [hep-ph].

[193] M. Gronau, Y. Grossman, G. Raz, and J. L. Rosner, "Suppression of flavor symmetry breaking in B decay sum rules," *Phys.Lett.* **B635** (2006) 207–212, arXiv:hep-ph/0601129 [hep-ph].

[194] C. Thomas, "Composition of the Pseudoscalar Eta and Eta' Mesons," *JHEP* **0710** (2007) 026, arXiv:0705.1500 [hep-ph].

[195] F. Ambrosino, A. Antonelli, M. Antonelli, F. Archilli, P. Beltrame, *et al.*, "A Global fit to determine the pseudoscalar mixing angle and the gluonium content of the eta-prime meson," *JHEP* **0907** (2009) 105, arXiv:0906.3819 [hep-ph].

[196] F.-G. Cao, "Determination of the η-η' mixing angle," *Phys.Rev.* **D85** (2012) 057501, arXiv:1202.6075 [hep-ph].

[197] J. L. Rosner and D. A. Suprun, "Measuring the relative strong phase in $D0 \to K^{*+}K^-$ and $D0 \to K^{*-}K^+$ decays," *Phys.Rev.* **D68** (2003) 054010, arXiv:hep-ph/0303117 [hep-ph].

[198] M. E. Peskin and D. V. Schroeder, *An Introduction to Quantum Field Theory*. Addison-Wesley Publishing Company, 1996.

[199] S. Weinberg, *The Quantum Theory of Fields Vol I*. Cambridge University Press, 1996.

[200] C. Quigg, "Charmed meson decays and the structure of the charged weak current," *Zeit. Phys. C* **4** (1980) 55–62.